Exploring the role of sortilin related receptor 1 in glioblastoma

by

Lydia Jones

A thesis submitted in partial fulfilment for the requirements for the degree of Doctor of Philosophy at the University of Central Lancashire

May 2024

RESEARCH STUDENT DECLARATION FORM

Type of Award **Doctor of Philosophy**

School **Pharmacy & Biomedical Sciences**

1. Concurrent registration for two or more academic awards

I declare that while registered as a candidate for the research degree, I have not been a registered candidate or enrolled student for another award of the University or other academic or professional institution

2. Material submitted for another award

I declare that no material contained in the thesis has been used in any other submission for an academic award and is solely my own work

3. Collaboration

Where a candidate's research programme is part of a collaborative project, the thesis must indicate in addition clearly the candidate's individual contribution and the extent of the collaboration. Please state below:

N/A

4. Use of a Proof-reader

No proof-reading service was used in the compilation of this thesis.

Signature of Candidate: 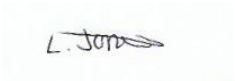

Print name: Lydia Jones

Abstract

An inverse comorbidity exists between neurodegenerative diseases like Alzheimer's disease and Parkinson's disease and various cancers. Likely due to occupying opposite ends of the same spectrum; neurodegeneration causing premature cell death and cancer driving uncontrolled cell proliferation. Alzheimer's disease offers greatest protection against lung cancer but, surprisingly, the impact Alzheimer's disease may have on brain cancers has not been fully investigated. This thesis will explore the role of the Alzheimer's disease risk factor protein sortilin related receptor 1 (SorL1) in glioblastoma, the gravest and most common primary brain tumour. SorL1 binds to the amyloid precursor protein to regulate trafficking to the early and late endosomes for cleavage into amyloid beta (Aβ) peptides. In Alzheimer's disease, SorL1 expression is reduced, increasing Aβ secretion and contributing to the characteristic extracellular amyloid plaques. SorL1 has previously been implicated in peripheral cancers including breast and leukaemia but has never been investigated in glioblastoma. This thesis explores the expression and function of SorL1 in glioblastoma and downstream effects on Aβ40 (most abundant species of Aβ) and Aβ42 (the more aggregate prone species commonly found in Alzheimer's disease).

Expression of SorL1 in immortalised cell lines (U87MG, 1321N1 and SVGp12) and primary cells (patient derived (PD) 301, PD304 and normal human astrocytes (NHA)), and subsequent expression of Aβ40 and Aβ42 was determined through combinations of immunofluorescence, western blot and ELISA. Secretion of SorL1 into spent medium of PD301, PD304 and NHA cells and in mouse serum from glioblastoma tumour bearing mice was investigated. The contribution SorL1 makes to cell function in glioblastoma was achieved by transiently transfecting PD301 and PD304 cells with siRNA vectors to knock down SorL1. Following confirmation of SorL1 knock down by western blot and immunofluorescence, cell proliferation, viability, migration and impact on amyloid processing was determined.

SorL1 was found to be more highly expressed in glioblastoma cells (U87MG, PD301 and PD304) than control cell counterparts (SVGp12 and NHA) with concomitant reduction in Aβ42 expression in PD301 and PD304 cells compared to NHA cells. Expression of Aβ40 was similar between PD301, PD304 and NHA cells. Furthermore, secretion of SorL1 from PD cells into medium was significantly reduced compared to NHA cells. SorL1 in mouse serum did not change during progression of tumour or between tumour bearing mice or mice following sham surgery. Successful transfection of siRNA against SorL1 in PD301 and PD304 cells knocked down SorL1 by approximately 50%. SorL1 siRNA transfected cells had increased Aβ40 and Aβ42 expression and SorL1 knock down reduced proliferation and migration of glioblastoma cells.

Findings here suggest SorL1 remains functional to drive APP processing away from Aβ42 production in glioblastoma and reducing SorL1 activity may be a potential therapeutic strategy for glioblastoma in the future.

Table of Contents

List of Figures……11

List of Tables……15

List of Abbreviations……16

Acknowledgements……18

1 Chapter 1 – Introduction……20

1.1 Comorbidity between Diseases……20

1.1.1 Cancer and Central Nervous System Diseases……20

1.1.2 Comorbidity between Cancer and Alzheimer's Disease……21

1.1.2.1 P53 Role in Comorbidity between Alzheimer's Disease and Cancer……23

1.2 Alzheimer's Disease……24

1.2.1 Alzheimer's Disease Incidence and Diagnosis……24

1.2.2 Pathological Progression of Alzheimer's disease……25

1.2.3 Established and Emerging Risk Genes of Alzheimer's Disease……26

1.2.4 Sortilin Related Receptor 1……27

1.2.4.1 SorL1 Function within the Cell……28

1.2.4.2 SorL1 and Alzheimer's Disease……31

1.2.4.3 SorL1 and Cancer……32

1.2.5 Amyloid Precursor Protein……33

1.2.6 Amyloidogenic Pathway vs Non-amyloidogenic Pathway……34

1.2.7 Amyloid Cascade Hypothesis……36

1.2.8 Amyloid Beta……38

1.2.8.1 Amyloid Beta Sealing Leaks in the Blood Brain Barrier……39

1.2.8.2 Amyloid Beta Regulating Synaptic Function……40

1.2.8.3 Amyloid Beta Having Antimicrobial Properties……41

1.2.8.4 Amyloid Beta and Cancer……41

1.3 Cancer 43
1.3.1 Glioma Brain Tumours 45
1.3.1.1 Glioblastoma Brain Tumours 46
1.3.1.1.1 Clinical Presentation of Glioblastomas 46
1.3.1.1.2 Risk Factors of Glioblastoma 47
1.3.1.1.3 Current Treatments of Glioblastoma 47
1.3.2 Comorbidity Between Glioma and Alzheimer's Disease 48
1.3.3 Interactions Between Glioma and Amyloid Beta 49
1.4 Aims and Objectives 51
2 Chapter 2 – Methods 53
2.1 Bioinformatics 53
2.2 Cell Culture 53
2.2.1 Media 54
2.2.2 Passaging 54
2.2.3 Cryopreserving 55
2.2.4 Cell Counting 56
2.2.5 Growth Curves 57
2.3 Immunocytochemistry 57
2.3.1 Seeding Cells 57
2.3.2 Fixation 57
2.3.3 Staining 58
2.4 Fluorescent Microscopy 59
2.4.1 Deconvolution Microscopy 59
2.4.2 Confocal Microscopy 60
2.4.3 Image J Analysis 60
2.4.4 Statistical Analysis 60
2.5 Glioblastoma orthotopic xenograft in mice 61
2.6 Western Blotting 62

2.6.1 Cell Lysate Preparation 62
2.6.2 Cell Medium Collection 63
2.6.3 SDS-PAGE Gels 63
2.6.4 Western Buffers 65
2.6.5 SDS-PAGE Gel Electrophoresis and Transfer 66
2.6.6 Staining 66
2.6.7 Imaging 68
2.6.8 Image Analysis 68
2.6.9 Statistical Analysis 69
2.7 ELISA 69
2.8 Transient Transfections 69
2.8.1 Plasmids 70
2.8.2 Bacterial Reagents 71
2.8.3 Bacterial Transformation 72
2.8.4 Plasmid Purification 73
2.8.5 NanoDrop 73
2.8.6 Transfections 73
2.8.7 Puromycin Kill Curve 74
2.9 Knock Down of SorL1 75
2.9.1 Staining 75
2.9.2 Western blotting 75
2.10 Functional Studies 75
2.10.1 MTS Assay 75
2.10.2 Statistical Analysis 76
2.10.3 Scratch Assay 77
2.10.4 Statistical Analysis 77
3 Chapter 3 – Expression of SorL1, Aβ40 and Aβ42 in Glioblastoma Cells 80

3.1 Background 80
3.1.1 Aβ Expression.....80
3.1.2 SorL1 Expression 81
3.2 Results – Expression 82
3.2.1 Characterising Glioblastoma Cell Growth 82
3.2.2 Expression of Aβ40, Aβ42 and SorL1 in Immortalised Cell Lines.....87
3.2.2.1 Immunocytochemical Expression of Aβ40 in Cell Lines..... 87
3.2.2.2 Immunocytochemical Expression of Aβ42 in Cell Lines..... 91
3.2.2.3 Immunocytochemical Expression of SorL1 in Cell Lines..... 95
3.2.2.4 Quantification of SorL1 Protein in Cell Lines 99
3.2.2.5 Expression of SorL1 using Bioinformatics 100
3.2.3 Expression of Aβ40, Aβ42 and SorL1 in Patient Derived Primary Cells.....103
3.2.3.1 Expression of SorL1 in Primary Cells..... 104
3.2.3.2 Expression of Aβ40 in Primary Cells..... 107
3.2.3.3 Expression of Aβ42 in Primary Cells..... 110
3.3 Discussion 113
3.3.1 Cell Line vs Patient Derived.....113
3.3.2 Growth Curve Troubleshooting.....114
3.3.3 Relative Expression of SorL1 to the Stage of Cancer 115
3.3.4 Relative Expression of Aβ40 and Aβ42 in Glioma.....116
4 Chapter 4 – Secretion of SorL1 119
4.1 Background 119
4.1.1 Synthesis of SorL1 119
4.1.2 Secretion of Soluble SorL1 119
4.1.3 Diagnostic Properties 121
4.2 Results – Secretion 122
4.2.1 SorL1 Secretion in Medium.....122

4.2.2 SorL1 Secretion in Mouse Serum 124

4.3 Discussion 131

4.3.1 Decreased Secretion of Soluble SorL1 in Glioblastoma Medium 131

4.3.2 Serum from Mice Implanted with Glioblastoma has no Difference in Soluble SorL1 133

5 Chapter 5 – Knock Down Model of SorL1 in PD301 and PD304 Cells 136

5.1 Background 136

5.1.1 Gene Silencing Systems – RNAi vs CRISPR 136

5.1.2 SorL1 Mutations in Alzheimer's Disease 137

5.1.3 Knock Down Model of SorL1 in Cancer 138

5.1.4 Gene Silencing siRNAs Chosen 138

5.2 Results – Developing a Knock Down Model of SorL1 .. 139

5.2.1 Optimising Transient Transfection of PD301 and PD304 Cells 140

5.2.2 Transfection with SorL1 siRNA Knocks Down SorL1 145

5.3 Discussion 157

6 Chapter 6 – Functional Effects due to SorL1 Knock Down 160

6.1 Background 160

6.1.1 Function of SorL1 160

6.1.2 Functional Implications when SorL1 Protein is Knocked Down or Reduced 162

6.2 Results – Functional Effects 163

6.2.1 Functional Effect of SorL1 Knock Down in PD301 and PD304 Cells: Aβ40 Expression 163

6.2.2 Functional Effect of SorL1 Knock Down in PD301 and PD304 Cells: Aβ42 Expression 171
6.2.3 Functional Effect of SorL1 Knock Down in PD301 and PD304 Cells: Proliferation and Viability.....179
6.2.4 Functional Effect of SorL1 Knock Down in PD301 and PD304 Cells: Migration 183
6.3 Discussion 192
6.3.1 SorL1 Knock Down Likely Increases Expression of Amyloid Beta.....192
6.3.2 SorL1 Knock Down has Detrimental Effect on Glioma Cell Function.....194
6.3.3 Functional Effects on the Different Patient Derived Cells.....196
7 Chapter 7 – General Discussion 199
7.1 SorL1 as a Therapeutic Target..... 199
7.1.1 SorL1 as a Therapeutic Adjunct 200
7.2 Mechanisms of SorL1..... 202
7.3 Using SorL1 as a Diagnostic Tool 205
7.4 Future Work 207
8 Appendices.....210
8.1 Appendix 1 – Full Blots from Westerns..... 210
8.2 Appendix 2 – Optimisation of Transfection 215
8.3 Appendix 3 – Characterisation of Antibody for Aβ40 and Aβ42. 216
8.4 Appendix 4 – Standard Curves for ELISA 220
9 References.....224

List of Figures

Figure 1.1 – Structure and binding sites of SorL1. 28
Figure 1.2 – SorL1 sorting of APP. 30
Figure 1.3 – Trafficking of APP around the cell. 34
Figure 1.4 – Cleavage of APP through amyloidogenic and non-amyloidogenic pathways. 36
Figure 1.5 – General structures of Aβ monomer, fibril and oligomers. 39
Figure 1.6 – Hallmarks of cancer. 44
Figure 1.7 – Flowchart to classify glioma tumours on histological and molecular features. 46
Figure 2.1 – Haemocytometer grid. 56
Figure 2.2 – pLenti-siRNA-GFP vector maps. 71
Figure 3.1 – Growth analysis for human cell lines. 84
Figure 3.2 – Growth analysis for primary cells. 86
Figure 3.3 – Aβ40 expression in U87MG cells. 88
Figure 3.4 – Aβ40 expression in 1321N1 cells. 89
Figure 3.5 – Aβ40 expression in SVGp12 cells. 90
Figure 3.6 – Aβ42 expression in U87MG cells. 92
Figure 3.7 – Aβ42 expression in 1321N1 cells. 93
Figure 3.8 – Aβ42 expression in SVGp12 cells. 94
Figure 3.9 – SorL1 expression in U87MG cells. 96
Figure 3.10 – SorL1 expression in 1321N1 cells. 97
Figure 3.11 – SorL1 expression in SVGp12 cells. 98
Figure 3.12 – SorL1 expression in U87MG, 1321N1 and SVGp12 lysates. 99
Figure 3.13 – Significantly higher SorL1 expression in U87MG cells than 1321N1 and SVGp12 cells. 100
Figure 3.14 – Heat map of SorL1 protein in glioblastoma and lower-grade glioma. 101
Figure 3.15 – Alteration frequency of SorL1 in lower grade glioma and glioblastoma. 102
Figure 3.16 – Survival Curve of glioblastoma and lower grade glioma studies with altered SorL1 expression compared to unaltered group. 103
Figure 3.17 – SorL1 expression in PD301, PD304 and NHA cell lysates. 104
Figure 3.18 – Significantly higher SorL1 expression in PD301 and PD304 cells than NHA cells. 105
Figure 3.19 – Immunofluorescence confirms SorL1 expression in PD301, PD304 and NHA cells. 106
Figure 3.20 – Corrected total cell fluorescence of SorL1 expression is increased in PD301 and PD304 cells. 107
Figure 3.21 – Immunofluorescence confirms Aβ40 expression in PD301, PD304 and NHA cells. 108

Figure 3.22 – Corrected total cell fluorescence of Aβ40 expression in PD301, PD304 and NHA cells 109
Figure 3.23 - Aβ40 expression in PD301, PD304 and NHA cells..... 110
Figure 3.24 – Immunofluorescence confirms Aβ42 expression in PD301, PD304 and NHA cells. 111
Figure 3.25 – Corrected total cell fluorescence of Aβ42 expression is decreased in PD301 and PD304 cells...... 112
Figure 3.26 - Aβ42 expression in decreased in PD301 and PD304 cells.... 113
Figure 4.1 – Structure of SorL1...... 120
Figure 4.2 – Western blot of PD301, PD304 and NHA cell medium using SorL1 antibody. 123
Figure 4.3 – Soluble SorL1 secretion in PD301, PD304 and NHA cell medium. 124
Figure 4.4 – Western blot of serum from weekly bleeds from mice implanted with U87MG cells and sham mice with SorL1 antibody. 126
Figure 4.5 – Soluble SorL1 secretion in serum from weekly bleeds of mice implanted with U87MG cells...... 127
Figure 4.6 – Soluble SorL1 secretion in serum from weekly bleeds of sham mice. 128
Figure 4.7 – Mean sSorL1 secretion comparing serum from glioblastoma and sham mice over weekly bleeds...... 129
Figure 4.8 – Western blot of serum from terminal bleeds from mice implanted with U87MG cells and sham mice with SorL1 antibody. 130
Figure 4.9 – Soluble SorL1 secretion comparing serum from terminal bleeds from glioblastoma and sham mice...... 131
Figure 5.1 – Transfection success in PD301 cells. 142
Figure 5.2 – Transfection success in PD304 cells. 144
Figure 5.3 – Puromycin kill curve...... 145
Figure 5.4 – Fluorescence of SorL1 is reduced in PD301 cells transfected with SorL1 siRNA vector...... 146
Figure 5.5 – Corrected total cell fluorescence of SorL1 expression is reduced in PD301 cells transfected with SorL1 siRNA vector...... 148
Figure 5.6 – SorL1 expression is reduced in PD301 cells transfected with SorL1 siRNA vector...... 149
Figure 5.7 – Reduction of SorL1 expression in PD301 cells transfected with SorL1 siRNA vector...... 150
Figure 5.8 – Fluorescence of SorL1 is reduced in PD304 cells transfected with SorL1 siRNA vector...... 152
Figure 5.9 – Corrected total cell fluorescence of SorL1 expression is reduced in PD304 cells transfected with SorL1 siRNA vector...... 153
Figure 5.10 – SorL1 expression is reduced in PD301 cells transfected with SorL1 siRNA vector...... 155

Figure 5.11 – Reduction of SorL1 expression in PD304 cells transfected with SorL1 siRNA vector. 156
Figure 6.1 – SorL1 trafficking around the cell. 161
Figure 6.2 – Immunofluorescence of Aβ40 in SorL1 siRNA transfected PD301 cells. 164
Figure 6.3– Corrected total cell fluorescence of Aβ40 expression is increased in SorL1 knock down PD301 cells. 165
Figure 6.4 – Immunofluorescence of Aβ40 in SorL1 siRNA transfected PD304 cells. 166
Figure 6.5 – Corrected total cell fluorescence of Aβ40 expression is increased in SorL1 knock down PD304 cells. 168
Figure 6.6 – Aβ40 expression in SorL1 knock down PD301 cells. 170
Figure 6.7 – Aβ40 expression in SorL1 knock down PD304 cells. 171
Figure 6.8 – Immunofluorescence of Aβ42 in SorL1 siRNA transfected PD301 cells. 173
Figure 6.9 – Corrected total cell fluorescence of Aβ42 expression is increased in SorL1 knock down PD301 cells. 174
Figure 6.10 – Immunofluorescence of Aβ42 in SorL1 siRNA transfected PD304 cells. 175
Figure 6.11 – Corrected total cell fluorescence of Aβ42 expression is increased in SorL1 knock down PD304 cells. 177
Figure 6.12 – Aβ42 expression SorL1 knock down PD301 cells. 178
Figure 6.13 – Aβ42 expression SorL1 knock down PD304 cells. 179
Figure 6.14 – Proliferation rate of PD301 cells transfected with SorL1 siRNA vector. 180
Figure 6.15 – Percentage cell viability of PD301 cells transfected with SorL1 siRNA vector. 181
Figure 6.16 – Proliferation rate of PD304 cells transfected with SorL1 siRNA vector. 182
Figure 6.17 – Percentage cell viability of PD304 cells transfected with SorL1 siRNA vector. 183
Figure 6.18 – Representative images of scratch assay on PD301 cells. 185
Figure 6.19 – Representative images of scratch assay on PD304 cells. 186
Figure 6.20 – Percentage wound closure of PD301 cells transfected with SorL1 siRNA vector. 188
Figure 6.21 – Rate of cell migration of PD301 cells transfected with SorL1 siRNA vector. 190
Figure 6.22 – Percentage wound closure of PD304 cells transfected with SorL1 siRNA vector. 191
Figure 6.23 – Rate of cell migration of PD304 cells transfected with SorL1 siRNA vector. 192
Figure A1.1 – SorL1 expression in U87MG, 1321N1 and SVGp12 lysates. 211
Figure A1.2 – SorL1 expression in PD301, PD304 and NHA lysates. 212

Figure A1.3 – Soluble SorL1 expression in PD301, PD304 and NHA cell medium......213
Figure A1.4 – Soluble SorL1 expression in mouse serum taken weekly from mice implanted with glioblastoma and sham mice......213
Figure A1.5 – Soluble SorL1 expression in mouse serum taken from terminal bleeds mice implanted with glioblastoma and sham mice......214
Figure A1.6 – SorL1 expression in PD301 cell conditions......215
Figure A1.7 – SorL1 expression in PD304 cell conditions......215
Figure A3.1 – Aβ40 expression in PD301 cells.....218
Figure A3.2 – Aβ40 expression in PD304 cells.....219
***Figure A3.3* – Aβ42 expression in PD301 cells**.....220
***Figure A3.4* – Aβ42 expression in PD304 cells**.....221
Figure A4.1 – Standard curve for Aβ40 ELISA......222
Figure A4.2 – Standard curve for Aβ42 ELISA......223

List of Tables

Table 2.1 – Cell Lines. 53
Table 2.2 – Primary antibodies used for immunocytochemistry. 58
Table 2.3 – Secondary antibodies used for immunocytochemistry. 59
Table 2.4 – Components to make up x2 gels. 64
Table 2.5 – Primary antibodies used for western blotting. 67
Table 2.6 – Secondary HRP antibodies used for Western blotting. 67
Table 2.7 – Plasmids 70
Table 5.1 – Optimal ratio of transfection reagents for PD301 cells. 141
Table 5.2 – Optimal ratio of transfection reagents for PD304 cells. 143
Table A2.1 – Optimisation of ratio for transfection reagents for PD301 cells……215
Table A2.2 – Optimisation of ratio for transfection reagents for PD304 cells……216

List of Abbreviations

SorL1	Sortilin related receptor 1
Aβ	Amyloid beta
APP	Amyloid precursor protein
U87MG	Stage IV glioblastoma cell line
1321N1	Stage II astrocytoma cell line
SVGp12	Foetal astrocytes cell line
PD	Patient derived
NHA	Normal human astrocytes
CNS	Central nervous system
MCF-7	Breast cancer cell line
PET	Positron emission tomography
MRI	Magnetic resonance imaging
CT	Computed tomography
BACE1	β-site amyloid precursor protein cleaving enzyme 1
sAPPβ	soluble APPβ
AICD	APP intracellular domain
ADAM	A Disintegrin and Metalloprotease
TACE	Tumour necrosis factor-A Converting Enzyme
sAPPα	soluble APPα
CTFα	C-terminal APP fragment
P3	Truncated Aβ
PSEN1	Presenilin 1
PSEN2	Presenilin 2
EOAD	Early onset Alzheimer's disease
LOAD	Late onset Alzheimer's disease
ApoE	Apolipoprotein E
VPS10	Vacuolar protein sorting 10
LDLR	Low-density lipoprotein receptor
FN-type	Fibronectin-type
TMD	Transmembrane domain

EGF	Epidermal growth factor
ICD	Cytosolic domain
sSorL1	Soluble SorL1
GGA	Gamma-adaptin ear homology domain, ARF-interacting
AP1/AP2	Clathrin adaptor proteins
PACS1	Phosphofurin acidic cluster sorting protein 1
ALP1/ALP2	APP-like proteins
ER	Endoplasmic reticulum
TGN	Trans Golgi network
WHO	World Health Organisation
TTF	Tumour treating fields
MGMT	O^6-methylguanine-DNA methyltransferase
CSF	Cerebrospinal fluid
IDH	Isocitrate dehydrogenase
siRNA	Small interfering RNA
CAD	Cationic amphiphilic drug
uPAR	Urokinase-type plasminogen activator receptor

Acknowledgements

I would first like to thank my supervisor Dr Chris Smith for all of your support. I am so honoured to be your first PhD student and want to thank you for pushing me to become the independent researcher I am today!

I would also like to give a huge thanks to my other supervisors, both past and present, Dr Izabela Stasik, Dr Vicky Jones and Dr Lisa Shaw for all your help over the past few years.

Naturally I want to thank everyone from the faculty that have helped me over the course of my PhD, but special thanks go to Dr Jane Alder and Dr Julie Burrow for all the guidance you have given me.

A massive shout out to the charity that has made all of this possible, BK's Heroes. Without your kind donations this thesis would not exist. Fiona, Dave and all the BK's Heroes family, thank you so much for welcoming me in.

I would also like to thank everyone that have come and gone in Darwin office DB120, for all the laughter, venting and support.

Klaudia, my caffeine queen! I honestly don't think I could have made it without you. We've laughed and cried, you've been my other half at the university.

I would also like to give a huge thanks to my mum, dad and brother Zak. Thank you all for believing in me. I appreciate you all so much for always encouraging and supporting me in every way.

Finally, I would like to thank my best friend and boyfriend James for all his love and encouragement. James, you have had to endure all my stress these past couple of months, I bet you're relieved it's all over!

Chapter 1

Introduction

1 Chapter 1 – Introduction

This thesis is to explore the role of SorL1 in glioblastoma. Previously, SorL1 protein expression has been most thoroughly investigated in Alzheimer's disease, however, it has not been explored extensively in cancer. This project arose from the inverse comorbidity seen between Alzheimer's disease and cancer reported in the literature, and so, this thesis has investigated proteins heavily involved with Alzheimer's disease in glioblastoma tumour cells.

1.1 Comorbidity between Diseases

1.1.1 Cancer and Central Nervous System Diseases

Epidemiological studies investigating the relationship between central nervous system (CNS) diseases as a collective, and cancers as a whole, suggest an inverse correlation (Driver, 2014). Meta-analyses and systematic review of 50 studies including more than 570,000 individuals between eight cancers (brain, breast, colorectal, lung, prostate, leukaemia, melanoma and testicular) and eight CNS disorders (Alzheimer's disease, Parkinson's disease, Huntington's disease, amyotrophic lateral sclerosis, Down's syndrome, multiple sclerosis, schizophrenia and autism spectrum disorders) was conducted (Catalá-López *et al.,* 2014). A systematic review was carried out to methodically review literature published that reported cancer comorbidity in patients with CNS disorders with an estimate of association with measures of variation (e.g. relative risk with confidence intervals). Overall and cancer-site specific meta-analyses statistically analysed and combined results from the multiple studies that met the eligible criteria. Results from meta-analyses were controlled during analysis using a random-effects model, which considers within-study and between-study variation incorporating differences of effects into overall analysis, and a fixed-effects model was used when effects of studies were reported according to sex or multiple regions of a country (Catalá-López *et al.,* 2014). Meta-analysis of another study also controlled for sex, but also age and year of diagnosis of either cancer or Alzheimer's disease during the observation period (Musicco *et al.,* 2013). Further nested-case control

observational studies investigated neurodegenerative diseases of Parkinson's disease and Alzheimer's disease comorbidity with either smoking related cancers or non-smoking related cancers (Driver, 2014; Driver *et al.,* 2012). Each dementia case was matched to controls of age and sex who were dementia free at the time of the dementia diagnosis (index date) and also free of cancer as of the index date, and following 5 years, models were subsequently adjusted for tobacco use and body mass index (Driver, 2014; Driver *et al.,* 2012).

Meta-analyses investigating comorbidity of CNS disorders revealed individuals with CNS disorders had an 8% risk reduction of developing cancer (Catalá-López *et al.,* 2014). It could be considered that cancer and neurodegeneration have opposing mechanisms, with cancer cells being resistant to cell death while premature cell death occurs in neurodegenerative disorders (Plun-Favreau *et al.,* 2010). Therefore the observation that the subgroup of neurodegenerative diseases had a greater reduction of co-occurrence at 20% collectively may not be unexpected (Catalá-López *et al.,* 2014). While individually multiple sclerosis, Parkinson's disease and Huntington's disease saw reduced co-occurrence of 9%, 17% and 47% respectively, the greatest of all was Alzheimer's disease that had reduced co-occurrence of 68% (Catalá-López *et al.,* 2014).

1.1.2 Comorbidity between Cancer and Alzheimer's Disease

Both Alzheimer's disease and cancer occurrence increases with age and consequently, it would be thought that both conditions would be seen within the same individual in the aging population (Musicco *et al.,* 2013). However, this expected comorbidity is not the case and was first noticed in the early 1990s when autopsies revealed a significant difference in the prevalence of Alzheimer's disease between patients with and without cancer (Tirumalasetti *et al.,* 1991; Thorpe *et al.,*1994).

Longitudinal and cross-over epidemiological studies have confirmed the inverse relationship between Alzheimer's disease and various cancers. The risk of a patient developing cancer when already presenting with Alzheimer's disease is

significantly reduced, and the reverse is true as patients with a history of cancer had a reduced risk of Alzheimer's disease (Roe *et al.,* 2005, Roe *et al.,* 2010). Further literature supported this inverse correlation as a later study found Alzheimer's disease patients had a 50% reduced risk of cancer and cancer patients had a 35% reduced risk of developing Alzheimer's disease (Musicco *et al.,* 2013). Alzheimer's disease has been strongly inversely correlated with individual cancers, specifically lung as Alzheimer's disease had the lowest risk in survivors of smoking related cancers compared to cancers not related to smoking (Driver *et al.,* 2012*)*. Further studies found a significantly reduced risk of developing lung cancer in Taiwanese male Alzheimer's disease patients, and similar results were also true for Caucasian adults (Roe *et al.,*2010; Ou *et al.,*2013). A large cohort in Korea also showed Alzheimer's disease patients has a significantly reduced chance of developing overall malignancy as well as developing any of the 10 site-specific cancers investigated (Kang *et al.,* 2023). Out of the 10 site-specific cancers, pancreatic cancer showed the strongest inverse correlation with Alzheimer's disease, followed by hepatic, gastric, kidney, lung, thyroid, colorectal, gallbladder and biliary, hematologic malignancy and finally bladder cancers (Kang *et al.,* 2023).

Further investigations have occurred in breast cancer, as a protective mechanism has been implied between the characteristic Alzheimer's disease proteins and breast cancer. Amyloid beta (Aβ) peptide, characteristically found in Alzheimer's disease, was found to inhibit tumour cell proliferation in breast cancer cells (Zhao *et al.,* 2009). In addition to the Aβ peptide, a fragment has also been found to potently supress breast tumour growth *in vivo*, however, *in vitro*, it was unable to inhibit MCF-7 cells (breast cancer cell line), therefore suggesting there is no direct anti-proliferative effects and more likely inhibits tumour growth through anti-angiogenic properties (Paris *et al.,* 2010).

The mechanism behind this inverse comorbidity between cancer and Alzheimer's disease remains elusive and may be biological or due to drug treatments for either disease. A pharmacological hypothesis however is not sustained by the observation that Alzheimer's disease treatments, with either acetylcholine esterase

inhibitors or memantine, are not ubiquitous and are usually only for a finite period, limiting ability to influence progression of a different biological process (Lanni *et al.,* 2021). Conversely, while Alzheimer's disease treatment options are very limited, cancer treatments are more personalised and have a myriad of targets thereby limiting the likelihood of a common pharmacological mechanism. Therefore, it seems a more likely that a common biological mechanism underlies the inverse comorbidity between cancer and Alzheimer's disease. Analysis of processes and pathways show dysregulation in opposite directions for lung cancer and Alzheimer's disease, therefore supporting the inverse comorbidity observed in the epidemiological studies (Driver *et al.,* 2012; Sánchez-Valle *et al.,* 2017). There is a growing amount of literature exploring the genes, proteins and pathways that are dysregulated in both Alzheimer's disease and cancer, and often this dysregulation occurs in opposite directions (Houck *et al.,* 2018).

1.1.2.1 P53 Role in Comorbidity between Alzheimer's Disease and Cancer

P53 is one such protein that has been investigated with the association of cancer and Alzheimer's disease. The protein p53 was discovered in 1979 and has been heavily studied within oncology and cancer biology (Borrero and El-Deiry, 2021). P53 is encoded by the gene *TP53.* The gene is involved in the protection of DNA integrity of the cell as well as development, aging and differentiation of the cell (Jain and Barton, 2018). Whereas, the protein it encodes, p53, is a transcription factor normally protecting the cell following cellular stress signals (Borrero and El-Deiry, 2021). The protein concentration of p53 is kept low within the cell and regulated by a negative feedback loop, so if the cell was to receive a stressor stimulus, for example, DNA damage, oxidative stress or oncogene activation, p53 initiates a cascade of cellular responses that include cell arrest, metabolic adaption or apoptosis (Hashimoto *et al.,* 2019; Wolfrum *et al.,* 2022). Mutations in *TP53*, the most commonly mutated gene in cancer, mutates p53 and due to its role being key to cell cycle regulation, loss of function causes cells to uncontrollably proliferate (Borrero and El-Deiry, 2021; Houck *et al.,* 2018). However, p53 has also been studied in Alzheimer's disease, as elevated levels of p53 was initially observed implying the protein has a key role in the development of

neurodegenerative diseases (Chang *et al.,* 2012). P53 within the CNS has the ability to induce tau aggregation and neurofibrillary tangles (characteristics of Alzheimer's disease) when activated (Nelson and Xu, 2023). There are theories as to why p53 activation occurs in Alzheimer's disease, one such theory is the accumulation of Aβ triggering increased levels of pro-apoptotic proteins and therefore stimulating p53 and cell death (Troy *et al.,* 2000). Another study found formation of p53 oligomers and fibrils in the Alzheimer's disease brain co-localised with tau protein, and therefore theorised the aggregation of p53 leads to dispersal of the endogenous protein in neurones triggering their apoptosis (Farmer *et al.,* 2020).

Therefore, when exploring the inverse relationship between Alzheimer's disease and cancer, it is understandable why p53 has been investigated; as p53 loses function in cancers so cells resist cell death and proliferation occurs, compared to an upregulation being seen in Alzheimer's disease causing a stress response and neuronal death due to apoptotic effects (Behrens *et al.,* 2009; Plun-Favreau *et al.,* 2010).

1.2 Alzheimer's Disease

Alzheimer's disease (named after German psychiatrist Alois Alzheimer) is the most common form of dementia characterised by progressive loss of cognition and memory (Breijyeh and Karaman, 2020; Zhao *et al.,* 2009). The most recent report conducted in the United Kingdom in 2019 by the Alzheimer's Society found approximately 900,000 people are living with dementia and is projected to rise to 1.6 million by 2040 (Alzheimer's Society, 2023). Alzheimer's disease accounts for approximately two-thirds of dementia cases of individuals 65 years or older (Huang *et al.,* 2020; Kumar *et al.,* 2023).

1.2.1 Alzheimer's Disease Incidence and Diagnosis

Alzheimer's disease can either be familial, accounting for 5% of all cases, or sporadic accounting for the remaining 95% (Zhou and Wang, 2011). Furthermore,

while Alzheimer's disease is predominantly seen in the elderly, known as late onset Alzheimer's disease (LOAD), onset of Alzheimer's disease can occur before the age of 65 known as early onset Alzheimer's disease (EOAD), and accounts for less than 10% of patients (Kumar *et al.,* 2023).

A clinical diagnosis of Alzheimer's disease is made following neurological examination with cognitive function tests alongside medical and family histories. If done, brain imaging using either positron emission tomography (PET) or magnetic resonance imaging (MRI) scans can reveal structural abnormalities and indicate how far the disease has progressed (Barthel *et al.,* 2011; Kumar *et al.,* 2023; Sharma and Singh, 2016). There has been a clinical need for a quantitative diagnostic biomarker for many years. Recent candidates include vitamin B12 levels in the blood as some studies have associated a deficiency with neurologic problems, increasing the risk of Alzheimer's disease (Jatoi *et al.,* 2020; Cho *et al.,* 2018).

Clinical diagnosis of Alzheimer's disease is not however completely accurate as Alzheimer's disease can only be definitively diagnosed following examination of the brain's morphological and pathological changes at post-mortem (Barthel *et al.,* 2011). Studies comparing an Alzheimer's disease post-mortem diagnosis to the clinical diagnosis prior to death, found a clinical accuracy of 77% (Sabbagh *et al.,* 2017). Alzheimer's disease is diagnosed when autopsy definitively reveals characteristic amyloid beta (Aβ) plaques and tau neurofibrillary tangles with associated atrophy of brain tissue, specifically in the hippocampal area of the brain (Perl, 2010).

1.2.2 Pathological Progression of Alzheimer's disease

There are three main stages in the pathological progression of Alzheimer's disease (Gustaw-Rothenberg *et al.,* 2010). Initially the pre-clinical or pre-symptomatic stage can last for several years (De-Paula *et al.,* 2012). It is characterised by early pathological changes in the brain resulting in very minor cognitive symptoms or can be completely asymptomatic with no functional impairment in daily activities

and so no obvious clinical signs of Alzheimer's disease (Kumar *et al.,* 2023; Dubois *et al.,* 2016). The second stage is mild cognitive impairment, considered when cognitive abilities become compromised, however, is not severe enough to effect daily function of life (Wattmo *et al.,* 2016). Patients in the mild cognitive impairment stage progress to dementia at a rate of approximately 10% per year (Kumar *et al.,* 2023). Diagnosis of dementia is the final stage of the pathological progression of Alzheimer's disease due to significant functional and cognitive impairments (Awasthi *et al.,* 2016). Patients lose their memory leading to confusion about their location and confusion communicating; some also lose their circadian brain pattern meaning sleep is dysregulated, and disruptive behaviours occur in approximately 50% of all Alzheimer's disease patients (Kumar *et al.,* 2023). At this stage, the brain has a significant accumulation of Aβ plaques and neurofibrillary tangles specifically in the cerebral cortex (Breijyeh and Karaman, 2020; De-Paula *et al.,* 2012)

It is difficult to diagnose the pre-clinical stage of Alzheimer's disease as symptoms very rarely show during this early stage, occurring over a 10 or 20 year period before the onset of the disease can be seen in the neuropathology of Alzheimer's disease patients (Sharma and Singh, 2016).

1.2.3 Established and Emerging Risk Genes of Alzheimer's Disease

The majority of known risk genes of Alzheimer's disease are due to dominant genes found in familial EOAD cases. Almost all of EOAD cases can be narrowed down to mutations in three genes. These are amyloid precursor protein (*APP*), presenilin 1 (*PSEN1*) and presenilin 2 (*PSEN2*) (Rovelet-Lecrux *et al.,* 2021). Missense mutations in all three of these genes increase the production of Aβ42 throughout life which is the more aggregate prone form of the peptide, which triggers Alzheimer's disease as suggested by the amyloid cascade hypothesis (Selkoe and Hardy, 2016) .

Currently, the strongest established genetic risk for LOAD is the Apolipoprotein E (*APOE*) gene (Hunsberger *et al.,* 2019; Robinson and Bishop, 2002). The *APOE*

gene encodes a protein that has an essential role in lipid metabolism and also Aβ metabolism and clearance (Mahley, 1988; Kanekiyo *et al.,* 2014). Specifically the ε4 allele has been shown as a risk factor for both EOAD and LOAD as homozygous *APOE4* genetic carriers are 15 times more likely to develop Alzheimer's disease (Hunsberger *et al.,* 2019). Due to the function of APOE clearing Aβ, failure of Aβ clearance mechanisms due to mutations to the ε4 allele, creates a gradual accumulation of Aβ42 within the brain leading to Alzheimer's disease (Selkoe and Hardy, 2016)

However, emerging at risk genes have been found through whole exome and genome sequencing that have been linked not only the familial and EOAD cases but also sporadic and LOAD cases namely *TREM2, ABCA7* and *SORL1* (Guerreiro *et al.,* 2013; Steinberg *et al.,* 2015; Nicolas *et al.,* 2016; Rovelet-Lecrux *et al.,* 2021; Campion *et al.,* 2019). The proteins encoded by these genes are implicated in functions within the immune and lipid transport systems, and all three have been linked with an increased risk of Alzheimer's disease (Bellenguez *et al.,* 2017).

1.2.4 Sortilin Related Receptor 1

Sortilin related receptor 1 (*SORL1*) also known as *SORLA* or *LR11* is a gene located on chromosome 11 encoding a transmembrane protein approximately 250kDa (Andersen *et al.,* 2005; Barthelson *et al.,* 2020; Nicolas *et al.,* 2016). SorL1 is a multifunctional sorting receptor, expressed throughout the body, with especially high levels in the CNS, particularly within neurones in the hippocampus and within nuclei in the brain stem and Purkinje cells (Motoi *et al.,* 1999).

The multifunctional SorL1 protein has a complex structure made up of multiple functional domains. Initially, the pro-peptide is cleaved in the Golgi, to release the functional protein (Nielsen *et al.,* 2007). Based on the structure of SorL1, the protein can be regarded as a member of the vacuolar protein sorting 10 (VPS10) proteins, and low-density lipoprotein receptor (LDLR) families due to the multiple class A and class B repeats responsible for binding a broad set of ligands (Jacobsen *et al.,* 2001; Nielsen *et al.,* 2007). The fibronectin-type (FN-type)

repeats are further found in neural cell adhesion molecules (Jacobsen *et al.,* 2001). Also part of structure is an epidermal growth factor-like (EGF-like) domain (Barthelson *et al.,* 2020). The transmembrane domain (TMD) of SorL1 is where SorL1 is cleaved to extracellularly release soluble SorL1 (sSorL1). The cytosolic domain (ICD) contains multiple binding sites for cytosolic adaptors, for example Golgi-localising Gamma-adaptin ear homology domain ARF-interacting (GGA) proteins, clathrin adaptor proteins (AP1/AP2) and phosphofurin acidic cluster sorting protein 1 (PACS1), proteins that direct SorL1 between the Golgi and endosomes and cell surface (Barthelson *et al.,* 2020; Schmidt *et al.,* 2007) (Figure 1.1).

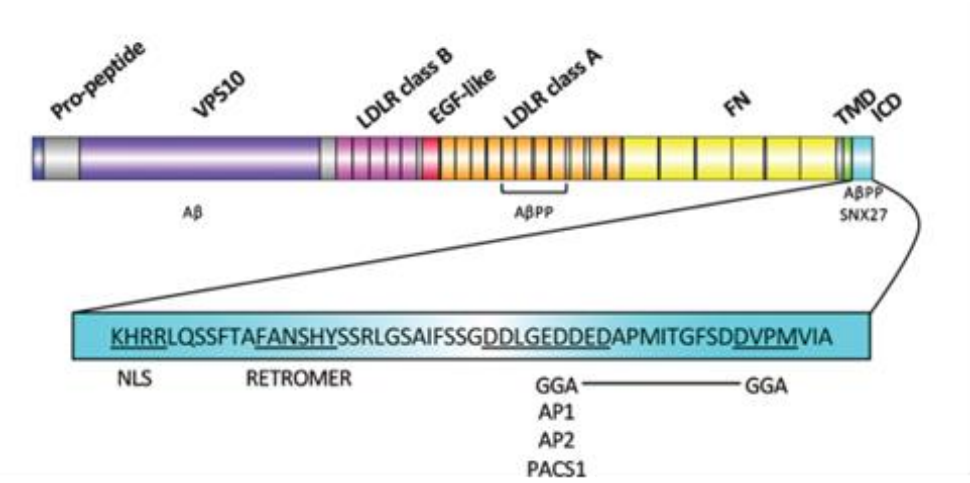

Figure 1.1 – Structure and binding sites of SorL1.

Structure includes a pro-peptide, VSP10 domain, LDLR class B repeats, an EGF-like domain, LDLR class A repeats, FN type repeats, a transmembrane region (TMD) and cytosolic domain (ICD). Binding sites are also shown for various proteins (Barthelson et al., 2020).

1.2.4.1 SorL1 Function within the Cell

The role of SorL1 was initially found to be involved with intracellular trafficking and lipoprotein metabolism in neurones (Motoi *et al.,* 1999). However, knowledge of SorL1 function within the cell has since been expanded. SorL1 binds directly to the amyloid precursor protein (APP) shuttling between the Golgi and endosomes,

controlling the route taken either into endocytic or recycling pathways or to the cell surface (Schmidt *et al.,* 2017; Rovelet-Lecrux *et al.,* 2021; Lee *et al.,* 2008; Andersen *et al.,* 2005; Herskowitz *et al.,* 2012).

SorL1 is a multifunctional sorting receptor that traffics APP within cell (Offe *et al.,* 2006). It is hypothesised one such function of SorL1 is it acts as a retention factor for APP, blocking APP from entering the secretory pathway (Figure 1.2A). The inhibition of this pathway leads to a reduction of APP sent to the cell surface to be cleaved in the non-amyloidogenic pathway (Andersen *et al.,* 2005; Offe *et al.,* 2006; Schmidt *et al.,* 2007). APP prefers to oligomerise creating APP homodimers however, SorL1 is also hypothesised to bind to APP to block dimerization and shifts the mode of secretase action to the monomer variant (Figure 1.2A) (Schmidt *et al.,* 2012; Willnow and Andersen, 2013). Naturally, approximately 30-50% of APP molecules are homodimers, and when APP is dimerised, it has been found there is a seven fold increase in total Aβ production (Munter *et al.,* 2007; Scheuermann *et al.,* 2001). As such the nature of APP dimerization has been considered to be potentially necessary for APP to leave the Golgi (Willnow and Andersen, 2013).

Further functions of SorL1 involve regulating the sorting of APP. The trafficking and positioning of APP for cleavage is carried out by the SorL1 protein. However, cytosolic adaptors GGA, AP1/AP2 and PACS1 have also been found necessary for intracellular trafficking; Section 1.2.4 (Barthelson *et al.,* 2020; Nielsen *et al.,* 2007). SorL1 transports APP to the early endosomes from the Golgi and either retrogrades APP back to the Golgi or blocks the protein from continuing to the late endosomes (Nielsen *et al.,* 2007; Schmidt *et al.,* 2017) (Figure 1.2B). Therefore, this controls the rate at which APP enters the amyloidogenic pathway being cleaved by β-secretase and γ-secretase (Willnow and Andersen, 2013). Consequently, the rate at which APP arrives at the early and late endosomes controls the amount of Aβ produced (Andersen *et al.,* 2005; Monti and Andersen, 2017).

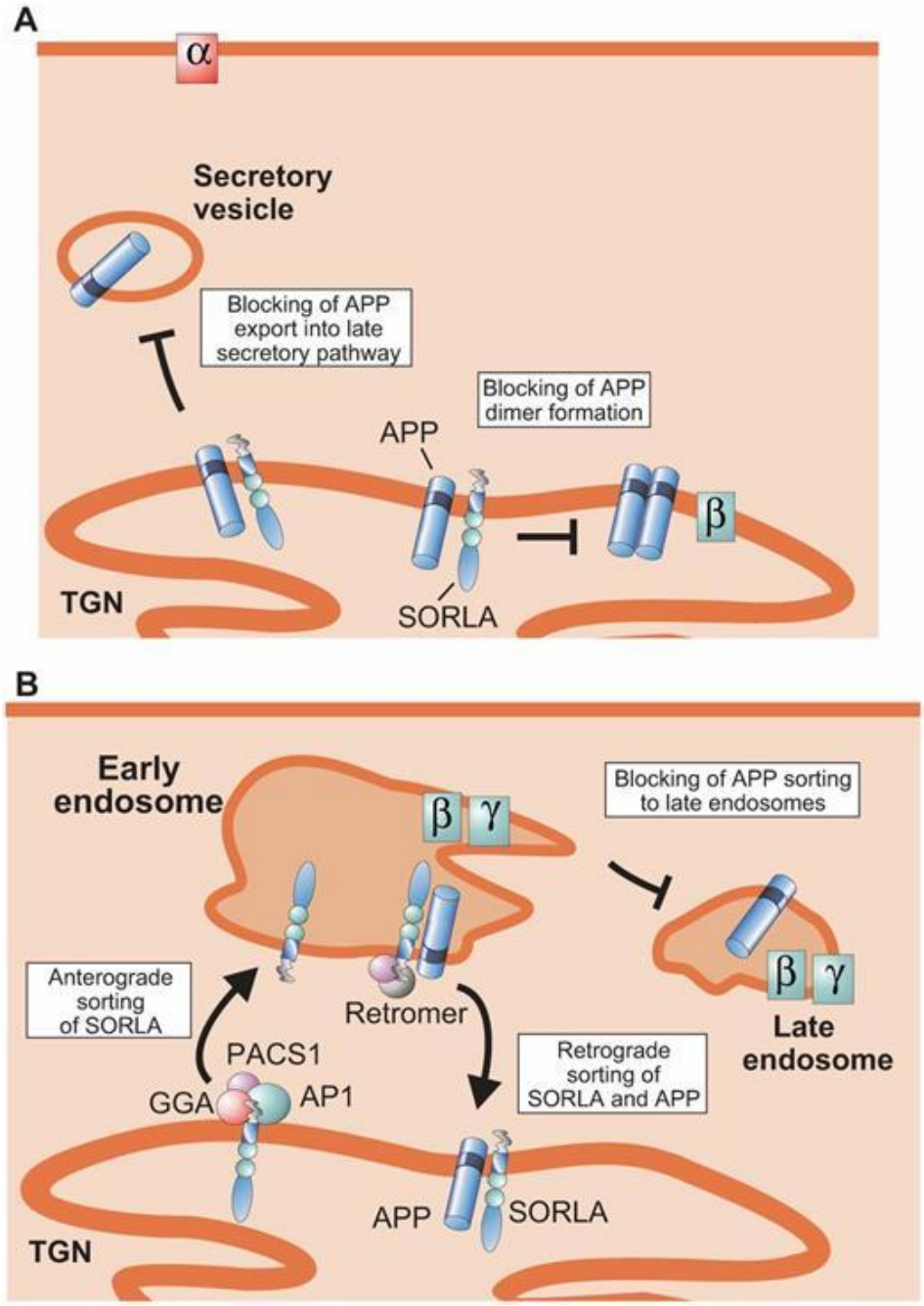

Figure 1.2 – SorL1 sorting of APP.

SorL1 acting as a retention factor, binding to APP blocking dimer formation within the Golgi (TGN) and retaining APP in the Golgi blocking APP export to secretory pathway to be cleaved by α-secretase (α) (A). SorL1 acting as a sorting protein, shuttling APP between the Golgi, early and late endosomes with help from cytosolic adaptors (GGA, PACS1, AP1) regulating APP cleavage in the amyloidogenic pathway by β-secretase (β) and γ-secretase (γ) in the late endosomes for Aβ production (B) (Willnow and Andersen, 2013).

The result of SorL1 retaining APP in the Golgi and shuttling the protein around the cell determines whether it is cleaved by α-secretase entering the non-amyloidogenic pathway or β-secretase for the amyloidogenic pathway (Schmidt *et al.,* 2007; Willnow and Andersen, 2013). Therefore, research states that SorL1 does not directly inhibit secretase cleavage, and only targets inhibiting these pathways through binding to APP directly (Schmidt *et al.,* 2012). Due to the role that SorL1 has in shuttling APP to enter the amyloidogenic pathway and therefore Aβ production, under expression of SorL1 is considered a risk factor for developing Alzheimer's disease; Section 1.2.3 (Schmidt *et al.,* 2017).

1.2.4.2 SorL1 and Alzheimer's Disease

Research suggests genetic variants of the *SORL1* gene are associated with a risk of Alzheimer's disease (Reitz *et al.,* 2011). Variants of the *SORL1* gene have been discovered following whole exome sequencing (WES) of a family covering 3 generations with familial Alzheimer's disease that do not have the known familial mutations of *APP, PSEN1* or *PSEN2* (Moreno *et al.,* 2022). WES identified rare *SORL1* variants, which along with structural changes, suggested reduced protein function and a contributing factor to the development of familial Alzheimer's disease (Moreno *et al.,* 2022). WES also identified rare *SORL1* mutations in EOAD and found a greater frequency of predicted missense *SORL1* variants in EOAD cases, which was enriched in those with a positive family history (Nicolas *et al.,* 2016). Furthermore, when a patient has one of these *SORL1* variants, it increases the risk of EOAD by approximately 5-fold (Alvarez-Mora *et al.,* 2022). As well as EOAD, WES has identified *SORL1* mutations in LOAD and found common *SORL1* mutations directly cause an increase in Aβ42 secretion, and in rare mutations of *SORL1* increased both Aβ40 and Aβ42 secretion (Vardarajan *et al.,* 2015). In addition, *SORL1* rare missense and loss of function variants have also been identified as risk factors for LOAD in sporadic Alzheimer's disease cases (Alvarez-Mora *et al.,* 2022; Barthelson *et al.,* 2020). Meta-analyses further confirm that multiple single nucleotide polymorphisms show a significant association with sporadic Alzheimer's disease, therefore concluding the *SORL1* gene may increase sporadic Alzheimer's disease risk (Jin *et al.,* 2013). It can be confirmed that all

mutations within the *SORL1* gene reduce the binding affinity between SorL1 and APP, which was also shown to increase the risk of Alzheimer's disease (Alvarez-Mora *et al.,* 2022; Cuccaro *et al.,* 2016).

Changes or loss of SorL1 protein expression and function has been shown to cause Alzheimer's disease, whether directly or indirectly, and therefore supports research showing a mutation in the *SORL1* gene results in a higher chance of Alzheimer's disease being a primary and pathogenic event (Rogaeva *et al.,* 2007; Raghavan *et al.,* 2018). A study showed SorL1 knockout mice led to an increase in Aβ secretion, similar to that seen in Alzheimer's disease, and so suggested that SorL1 is an important factor in the progression of Alzheimer's disease (Andersen *et al.,* 2005). Whilst another study used the CRISPR-Cas9 system to knockout SorL1 from human induced pluripotent stem cells (hiPSCs) which displayed neurones showing early endosome enlargement, characteristic to Alzheimer's disease cytopathology (Knupp *et al.,* 2020).

1.2.4.3 SorL1 and Cancer

Further to the role in Alzheimer's disease, SorL1 has also been implicated in various cancers. SorL1 is highly expressed in breast cancer cells of HER2 breast cancer (Pietilä *et al.,* 2019). HER2 breast cancer accounts for 15-20% of all breast cancers (Tapia *et al.,* 2023). SorL1 was found to increase 'oncogenic likeness' of HER2 in the breast cancer cell (Pietilä *et al.,* 2019). Increased SorL1 expression has been found in cancers of the pancreas and bile duct as patient's bile samples showed significant increase in SorL1 and SorL1 levels were especially elevated during the peak of proliferation (Terai *et al.,* 2016). Increased SorL1 was also found in serum of Non-Hodgkin's lymphoma and increased expression was found on the cell membrane of leukemic cells in acute leukaemia patients (Fujimura *et al.,* 2014; Sakai *et al.,* 2012).

The overarching relationship between SorL1, cancer and Alzheimer's disease is increased SorL1 expression is seen in cancer whilst in Alzheimer's disease, SorL1 levels are reduced. Even though SorL1 expression has been explored in

peripheral cancers and is known to have a key function within the CNS, SorL1 has never been explored in glioma brain tumours.

1.2.5 Amyloid Precursor Protein

The amyloid precursor protein (APP) is a single membrane protein with a long N-terminal, an Aβ domain and short cytoplasmic tail encoded by a single gene located on chromosome 21 and is 19 exons long (Wasco *et al.,* 1993; Gustaw-Rothenberg *et al.,* 2010; Chasseigneaux and Allinquant, 2012). APP is most commonly known as located in the brain within neural cells, astrocytes and neurones, however, is produced cellularly throughout the body, including epidermal cells of the skin and columnar epithelial cells of the intestines (Herzog *et al.,* 2004; Puig *et al.,* 2012; Puig and Combs, 2013). APP is also present at the early stages of CNS development, aiding with growth and maturation of cells (Dawkins and Small, 2014). There are also two APP-like proteins (ALP1 and ALP2) which are homologues to APP sharing a similar sequence except the Aβ domain, but are thought to aid in maturation and metabolism of APP (Wasco *et al.,* 1993; Zhang *et al.,* 2012). Similar to APP, ALP2 is found throughout the body, whereas ALP1 is only found in the brain (Zhang *et al.,* 2012).

Synthesised APP travels from the endoplasmic reticulum (ER) to the Golgi to the extracellular membrane, and in reaching the cell surface is known to assist with cell adhesion and aiding with cellular interactions within the CNS (Puig and Combs, 2013; Zheng and Koo, 2011). APP can also be cleaved at the cell membrane by α-secretase, or is internalised by the cell through clathrin-mediated endocytosis guided by clathrin adaptor protein 2 (AP2) (Willnow and Andersen, 2013). If internalised, APP is transported to early endosomes, where it can be shuttled to the late endosomes to be cleaved by β-secretase and γ-secretase or retrograded back to the Golgi (Andrew *et al.,* 2016) (Figure 1.3). Cleavage through β-secretase and γ-secretase produces amyloid beta (Aβ) (Brothers *et al.,* 2018).

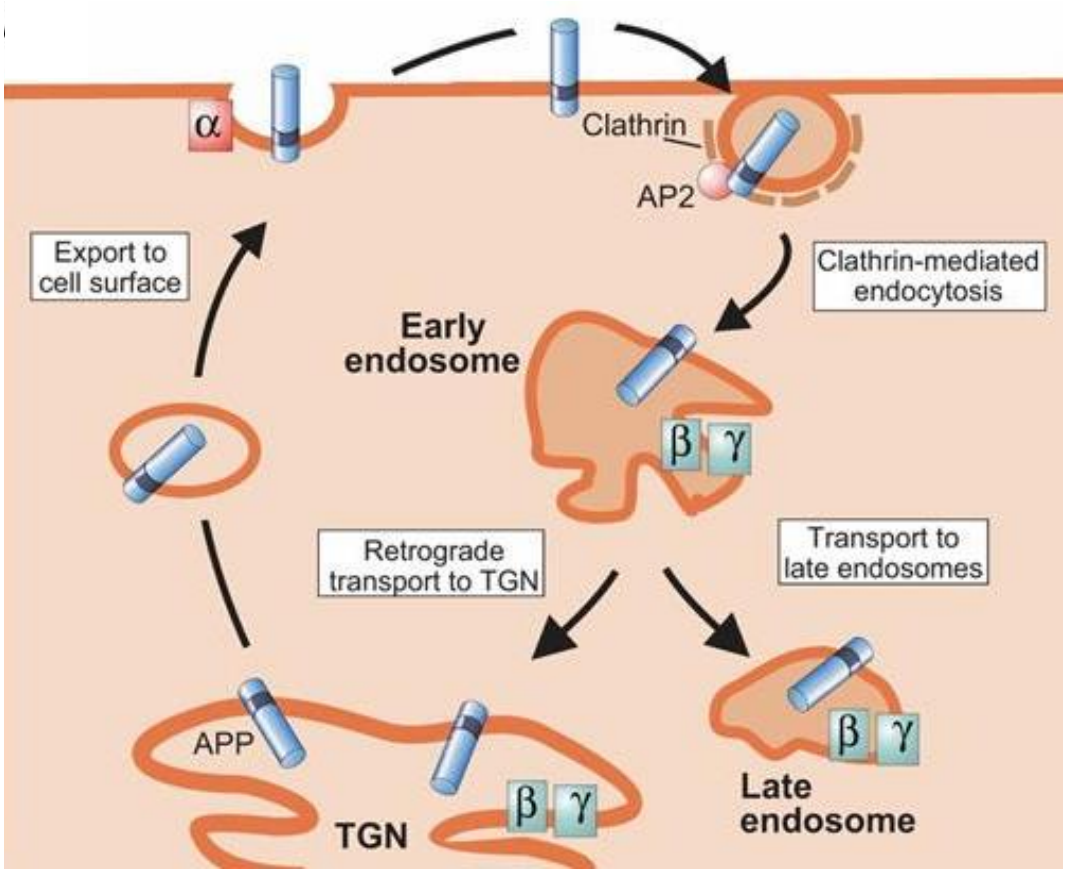

Figure 1.3 – Trafficking of APP around the cell.

APP trafficked from the Golgi (TGN) to the cell surface and is either cleaved by α-secretase (α) or enters the cell through clathrin-mediated endocytosis guided by the clathrin adaptor protein 2 (AP2) to early endosomes and are then either retrograded back to Golgi or moved to late endosomes and cleaved by β-secretase (β) and γ-secretase (γ) (Willnow and Andersen, 2013).

1.2.6 Amyloidogenic Pathway vs Non-amyloidogenic Pathway

Amyloid beta (Aβ) is cleaved from the amyloid precursor protein (APP) through the amyloidogenic pathway (Awasthi *et al.,* 2016). Initially APP is cleaved by β-site amyloid precursor protein cleaving enzyme 1 (BACE1), a β-secretase, releasing an extracellular soluble APPβ (sAPPβ) fragment and producing a membrane-bound C99 intermediate (Cameron *et al.,* 2012; Andrew *et al.,* 2016). There is very little literature on the function of sAPPβ, however, it has been found to decrease

cell adhesion and the protein contains domains required to promote neurite and axonal outgrowth (Chasseigneaux and Allinquant, 2012; Hesse *et al.,* 2018). However, sAPPβ fragment has very little neuroprotective characteristics and has also been linked to neurodegenerative processes (Copanaki *et al.,* 2010; Nikolaev *et al.,* 2009). A presenilin containing a multi-subunit complex encompassing γ-secretase then cleaves C99 within the transmembrane region extracellularly releasing Aβ and the APP intracellular domain (AIDC) (Cameron *et al.,* 2012; Andrew *et al.,* 2016) (Figure 1.4). Cleavage by γ-secretase of APP usually occurs at the ε-cleavage site producing Aβ with protein lengths between 39 and 43 amino acids, with the most abundant species being Aβ40 (Andrew *et al.,* 2016; Murphy and LeVine, 2010).

The alternative pathway, namely the non-amyloidogenic pathway, occurs when the initial cleavage point of APP is within the Aβ domain and thus an Aβ peptide is not produced (Chasseigneaux and Allinquant, 2012; Lichtenthaler, 2012; Vincent and Govitrapong, 2011). Instead of BACE1 initially cleaving APP, its cleaved by α-secretase through the metalloprotease A Disintegrin and Metalloprotease (ADAM10), releasing soluble APPα (sAPPα) and an alternative C-terminal APP fragment (CTFα) (Andrew *et al.,* 2016). Soluble APPα, in comparison to sAPPβ was found to be neuroprotective and contains domains crucial for promoting neuronal axon and dendrite growth (Chasseigneaux and Allinquant, 2012; Copanaki *et al.,* 2010). Due to the known neuroprotective effects against neurodegenerative disorders, it was considered as possible treatment and prevention of Alzheimer's disease, however, sAPPα was then found to increase proliferation of some cells leading to cancer of the colon and pancreas (Meng *et al.,* 2001; Hansel *et al.,* 2003). Cleavage by γ-secretase then occurs as it does with the amyloidogenic pathway releasing a truncated form of Aβ (P3) and AICD (Andrew *et al.,* 2016) (Figure 1.4). Depending upon whether α-secretase or β-secretase creates the initial cleavage, the function of AICD differs, even though the two pathways cleave the same peptide sequence (Andrew *et al.,* 2016). When AICD is produced through β-secretase cleavage, it is transported to the nucleus where its role is as a nuclear transcription factor and regulates the expression of

various genes including neprilysin, an Aβ degrading peptide. Whereas, when initial cleavage is α-secretase, AICD is rapidly degraded by the insulin-degrading enzyme, therefore has no function (Belyaev *et al.,* 2010; Andrew *et al.,* 2016).

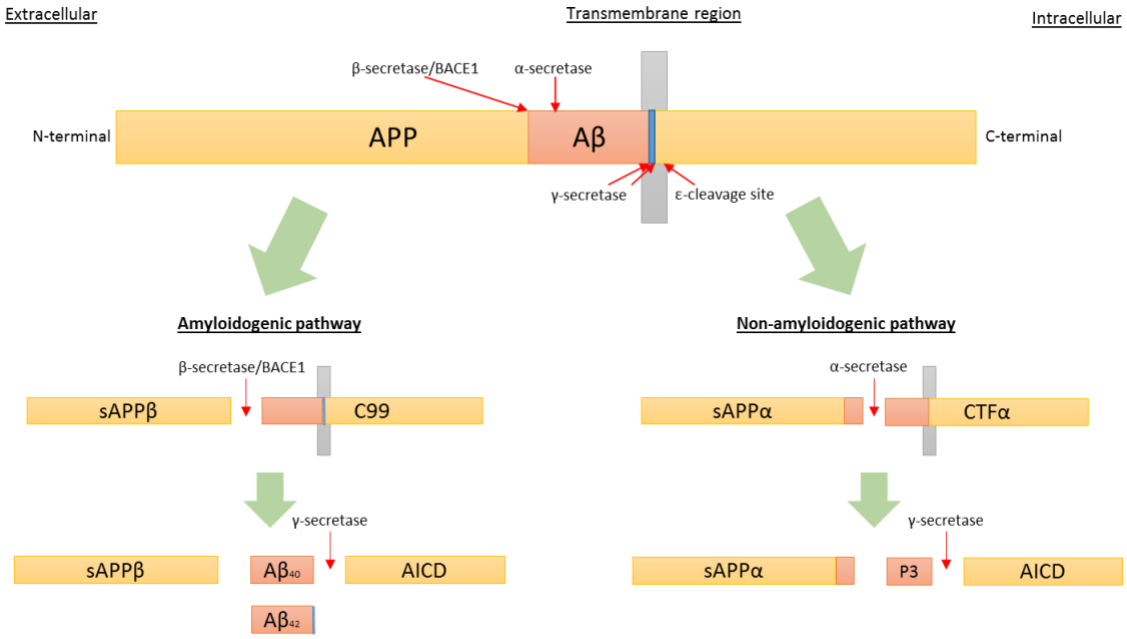

Figure 1.4 – Cleavage of APP through amyloidogenic and non-amyloidogenic pathways.

Amyloidogenic pathway cleaves APP initially with β-secretase and then γ-secretase producing sAPPβ, Aβ and AICD (Left). Non-amyloidogenic pathway cleaves APP initially with α-secretase followed by γ-secretase producing sAPPα, truncated form of Aβ (P3) and AICD (Right).

1.2.7 Amyloid Cascade Hypothesis

The amyloid cascade hypothesis was first hypothesised in 1992 whereby the accumulation of Aβ was the central event in the pathogenesis of Alzheimer's disease (Hardy and Higgins, 1992). The hypothesis suggests that extreme accumulation of Aβ, which deposits intracellularly and extracellularly, initiates a cascade causing the pathological occurrence of Alzheimer's disease (Awasthi *et al.,* 2016; Luo *et al.,* 2016). Aggregated Aβ deposits initiate a cascade triggering

process causing accumulation of hyperphosphorylated tau, which further leads to neurofibrillary tangles, causing synaptic degeneration, neuronal death and neurodegeneration (Jarosz-Griffiths *et al.,* 2016; Awasthi *et al.,* 2016). Supporting this hypothesis is the data surrounding familial Alzheimer's disease due to inheriting genetically mutated APP causing an overproduction of Aβ (Zhou and Wang, 2011; Musiek and Holtzman, 2015).

When looking at the genetic form, familial Alzheimer's disease, which displayed a strong correlation with inherited mutations in the *APP* gene causing an overproduction of Aβ42 (Zhou and Wang, 2011; Musiek and Holtzman, 2015). Further genetic association has been observed in sporadic Alzheimer's disease, as the apolipoprotein E (*APOE*) gene has a variant ε4 that significantly increases Aβ plaques and deposits (O'Brien and Wong, 2011).

Patients with Down's Syndrome also have a higher risk of developing Alzheimer's disease and do at a much earlier age between 30 and 50 (Gustaw-Rothenberg *et al.,* 2010; Sharma and Singh, 2016). This is due to the triplication of chromosome 21 where the *APP* gene is located. Therefore an overexpression of the gene causes an overproduction of APP and excess cleavage of Aβ, supporting the amyloid cascade hypothesis assuming Aβ is the causative agent for Alzheimer's disease (Gustaw-Rothenberg *et al.,* 2010; Sharma and Singh, 2016; Musiek and Holtzman, 2015).

The amyloid cascade hypothesis is debated however because of research into the unclear and highly complex sporadic Alzheimer's disease (Zhou and Wang, 2011; Musiek and Holtzman, 2015). Even though sporadic Alzheimer's disease cases present with Aβ plaques, it cannot be concluded that both familial and sporadic Alzheimer's disease share the same pathology trigger (Morris *et al.,* 2014; Ricciarelli and Fedele, 2017).

There is further controversy to the amyloid cascade hypothesis due to results of clinical trials. Clinical trials are investigating pharmaceutical treatments for early stage Alzheimer's disease assuming the amyloid cascade hypothesis, clearing Aβ

plaques using Aβ monoclonal antibodies, for example solanezumab and gantenerumab (Youn et al., 2015; Selkoe and Hardy, 2016; Ricciarelli and Fedele, 2017). Results of these clinical trials are however conflicting. There is suggestion the drugs slow cognitive decline therefore supporting Aβ as a possible causative agent for Alzheimer's disease, however, other clinical trials found that even though there was a reduction in Aβ levels in the brain, either cognitive function was not measured or patients did not show significant slowing in cognitive decline so consequentially these results do not support the hypothesis (Doody *et al.,* 2014; Selkoe and Hardy, 2016; Hampel *et al.,* 2021).

1.2.8 Amyloid Beta

Amyloid beta (Aβ) is a peptide derived from APP ranging in length from 39 to 43 amino acids (Figure 1.5A) (Brothers *et al.,* 2018; Cameron *et al.,* 2012). The most abundant species accounting for 80-90% of Aβ peptide is Aβ40, followed by Aβ42 accounting for 5-10% of Aβ, however is more aggregate prone and more commonly found in Alzheimer's disease (Murphy and LeVine, 2010).

Aβ40 is expressed by many cell types both within the CNS and the rest of the body and has a relatively benign role in normal cell metabolism (Awasthi *et al.,* 2016). Both Aβ40 and Aβ42 can be found within neurones of the brain as well as extracellularly. Even though Aβ40 can aggregate, it is known that Aβ42 has a much higher tendency to aggregate and oligomerise due to the protein being more hydrophobic, leading to neurotoxicity within the brain (Figure 1.5E) (Sandebring *et al.,* 2013). When oligomerisation occurs of Aβ42, plaques begin to form, which is the pathological characteristic of Alzheimer's disease (Awasthi *et al.,* 2016; Portelius *et al.,* 2011).

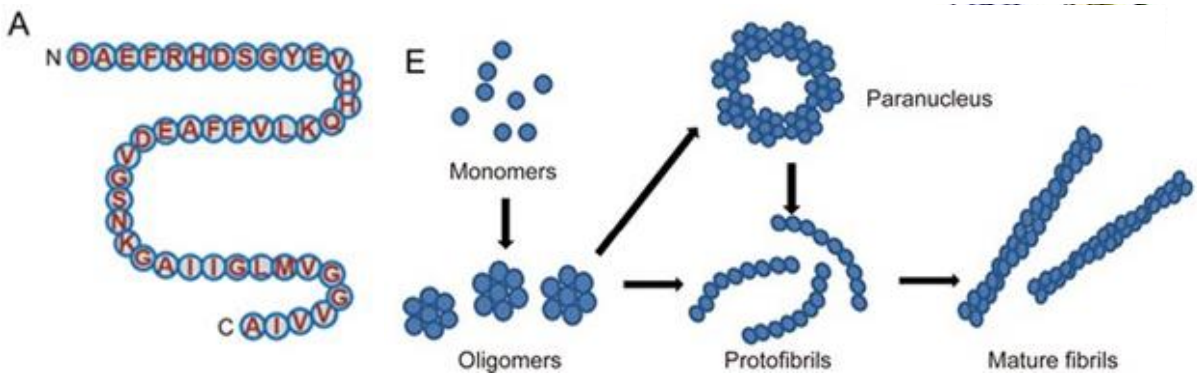

Figure 1.5 – General structures of Aβ monomer, fibril and oligomers.

Amino acid sequence of Aβ42 peptide (A). Proposed conversion pathway for Aβ from monomer to oligomers, including dimers through to dodecamers (creating a paranucleus), to protofibrils and fibrils (E) (Taken from Chen et al., 2017).

Even though the majority of research focuses on the accumulation of Aβ and its neurodegenerative effects characteristic to Alzheimer's disease, this protein has also been shown to have beneficial roles in the brain (Brothers *et al.,* 2018). As Aβ is a highly conserved protein between species, this too suggests it has an important and beneficial role (Guo *et al.,* 2012; Tharp and Sarkar, 2013). Some of these beneficial roles include sealing leaks in the blood brain barrier, regulating synaptic function and Aβ having antimicrobial properties (Gosztyla *et al.,* 2018; Puzzo and Arancio, 2013; Atwood *et al.,* 2003; Brothers *et al.,* 2018).

1.2.8.1 Amyloid Beta Sealing Leaks in the Blood Brain Barrier

Studies have suggested that when damage occurs to the blood brain barrier, soluble Aβ will bind to pro-inflammatory and neuroactive compounds from the blood essentially creating a 'scab' or insoluble mass plugging the leaky blood brain barrier and preventing the spread of toxic components that would cause damage to the brain (Bishop and Robinson, 2002; Atwood *et al.,* 2003; Brothers *et al.,* 2018). This supports a possible causal link suggested by one study between a leaky blood brain barrier and Aβ deposition (Stone, 2008). The blood brain barrier

within the hippocampal area of the brain has been shown to breakdown and become more permeable with age, therefore, suggesting accumulation of Aβ deposits due to leaky blood brain barrier contributes to early stages of Alzheimer's disease (Brothers *et al.,* 2018; Montagne *et al.,* 2015). Also supporting the hypothesis that one of the roles of soluble Aβ is to seal leaks in the blood brain barrier is clinical trials treating Alzheimer's disease. Studies evaluating clinical trials found the most common side effect to removal of soluble Aβ has been brain oedema and microhaemorrhages due to removing Aβ from plugging the permeable sites of the blood brain barrier (DiFrancesco *et al.,* 2015; Lannfelt *et al.,* 2014).

1.2.8.2 Amyloid Beta Regulating Synaptic Function

Aβ has another neurological role by regulating synaptic function in the hippocampus to aid with memory and plasticity of the brain (Brothers *et al.,* 2018; Puzzo and Arancio, 2013). Aβ is present in neurones from infancy and increases between the ages of 4 and 8 years old, and during this time in the brain's development there is an increase in brain plasticity, and approximately half of all neurones are 'Aβ-immunopositive' (Puzzo *et al.,* 2015). It can therefore be considered that Aβ is important in regulating synaptic function. Aβ has also been suggested as the trigger for a negative feedback loop to prevent synaptic hyperactivity. Neuronal activity stimulates an increase in Aβ secretion which then decreases excitatory synaptic activity preventing neuronal hyperactivity (Kamenetz *et al.,* 2003). Concentrations of Aβ in a healthy adult brain are in the picomolar range which in this range enhances synaptic memory and plasticity, however, when there is an accumulation of the protein, as is the case in Alzheimer's disease, it causes synaptic failure (Puzzo *et al.,* 2008, Puzzo *et al.,* 2012). *In vivo* experiments have also supported Aβ regulating synaptic function, as neurones in the hippocampus of mice showed enhanced plasticity and enhanced memory within minutes of addition of Aβ42, however, longer exposure resulted in reduced plasticity and impaired memory of the mice also consistent with Alzheimer's disease (Koppensteiner *et al.,* 2016).

1.2.8.3 Amyloid Beta Having Antimicrobial Properties

Antimicrobial activity was one of the first Aβ functions to be suggested, acting as a protective mechanism, known as the 'bioflocculant hypothesis' (Bishop and Robinson, 2002). The bioflocculant hypothesis is one such method of Aβ acting in an antimicrobial fashion, proceeding as a neuroprotective web intercepting and binding together pathogens, but also any toxic proteins or ions, which can then be later phagocytosed by glial cells (Bishop and Robinson, 2002). Studies have shown increased Aβ expression in presence of pathogens and following phagocytosis (Bitting *et al.,* 1996; Spitzer *et al.,* 2010; Gosztyla *et al.,* 2018). This hypothesis also has a theory to how Aβ plaques build up in the brain, characteristic of Alzheimer's disease, as the rate at which Aβ deposits bind to pathogens or toxins exceed the clearance rate by phagocytosis, these deposits will turn into plaques (Robinson and Bishop, 2002). Another method that has been suggested, is Aβ has microbicidal properties itself, and so can directly kill pathogens as an antimicrobial peptide (Brothers *et al.,* 2018). Antimicrobial activity has been shown by Aβ as a result to at least eleven known viruses, bacteria and fungus (Gosztyla *et al.,* 2018). Aβ has capacity to functionally form fibrils to directly disrupt cellular membranes of pathogens and therefore killing these microbes, or aggregate in order to immobilise them (Brothers *et al.,* 2018; Kagan *et al.,* 2012).

1.2.8.4 Amyloid Beta and Cancer

Aβ has also been suggested to supress tumour growth (Brothers *et al.,* 2018), supporting a possible protective mechanism involved in the inverse relationship between Alzheimer's disease and cancer; Section 1.1.2.

In vitro cancer cells were cultured with medium containing high levels of Aβ which significantly inhibited proliferation rates in glioblastoma cells, breast cancer cells, adenocarcinoma cells and melanoma cells (Zhao *et al.,* 2009). *In vivo*, Aβ was found to supress glioma tumours when directly injected into glioblastoma cells in xenograft mouse models in one study, and another implanted glioma cells in an Alzheimer's disease transgenic mouse model whereby Aβ is overexpressed

resulting in a slower proliferation and migration of the tumour compared to controls (Paris *et al.,* 2004; Paris *et al.,* 2010). Similar results were observed when acute promyelocytic leukaemia NB4 cells, lung cancer cell line A549 and breast cancer MCF-7 cells were all treated with amyloid, and cancer cell growth was inhibited (Pavliukeviciene *et al.,* 2019). Not only did the amyloid inhibit cell proliferation, it was observed that there was an accumulation of amyloid surrounding all cancer cell types, and over time, extracellular amyloid aggregated into the cell membrane and was even seen within the nucleus (Pavliukeviciene *et al.,* 2019).

Accumulation of amyloid has been observed in other cancers. In a mouse xenograft model of human inflammatory breast cancer, Aβ was observed within and surrounding the breast cancer cells, with a higher concentration present near blood vessels (Zayas-Santiago *et al.,* 2021). This may suggest systemic Aβ from the blood vessels forming aggregated amyloid with other amyloidogenic peptides already in and around the tumour (Zayas-Santiago *et al.,* 2021). Furthermore, an increase in Aβ levels in plasma has been reported in a multitude of cancers including oesophageal, colorectal, hepatic, lung, glioma, adenocarcinoma and melanoma (Jin *et al.,* 2017; Kleffman *et al.,* 2022; Munir *et al.,* 2021; Zayas-Santiago *et al.,* 2021). In addition to an increase in Aβ levels in melanoma, it has been reported that melanoma promotes brain metastasis and supresses neuroinflammation through secreting Aβ (Kleffman *et al.,* 2022). Melanoma has the highest rate of brain metastasis amongst all common cancer types, and possible reasoning for this is melanoma cells have been found to cleave APP to produce and secrete Aβ themselves which they require for survival and growth in the brain (Kleffman *et al.,* 2022). Secreted Aβ from melanoma cells enable the cancer to thrive within the brain as it triggers nearby astrocytes to become pro-metastatic and anti-inflammatory, as well as promoting anti-inflammatory microglial polarisation preventing phagocytosis of melanoma cells (Kleffman *et al.,* 2022).

1.3 Cancer

Originally proposed in the year 2000, there are six core hallmarks of cancer that cells acquire as they become a malignant tumour (Hanahan and Weinberg, 2011). They include evading growth suppressors, enabling replicative immortality, activating invasion and metastasis, inducing or accessing vasculature, resisting cell death, and sustaining proliferative signalling (Hanahan, 2022). A further two hallmarks were then suggested as emerging hallmarks, namely avoiding immune destruction, and deregulating cellular metabolism, however they are now considered core hallmarks (Hanahan and Weinberg, 2011; Hanahan, 2022). A further two enabling characteristics are also linked to the eight core hallmarks of cancer, namely tumour-promoting inflammation and genome instability and mutation (Hanahan, 2022) (Figure 1.6).

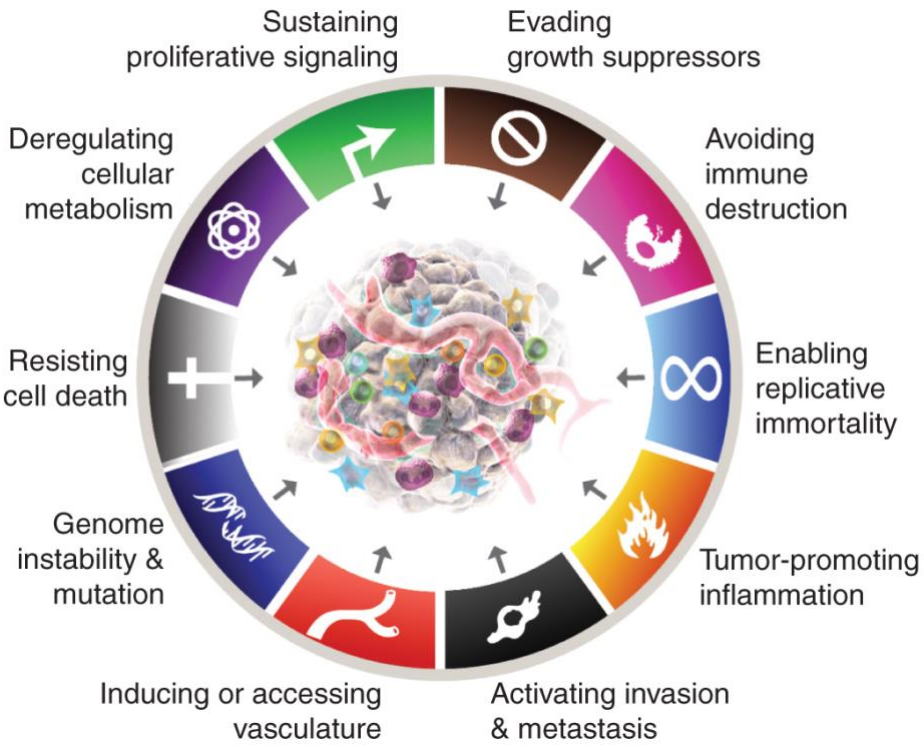

Figure 1.6 – Hallmarks of cancer.

Includes the original 6 core hallmarks, 2 emerging hallmarks and 2 enabling characteristics. They include evading growth suppressors, avoiding immune destruction, enabling replicative immortality, tumour-promoting inflammation, activating invasion and metastasis, inducing or accessing vasculature, genome and instability mutation, resisting cell death, deregulating cellular metabolism and sustaining proliferative signalling (Hanahan, 2022).

GLOBOCAN 2020 estimated 18.1 million new cancer cases globally and cancer was the cause of death for 9.9 million patients that year (Sung *et al.,* 2021). GLOBOCAN 2020 has also predicted the number of new cancer cases worldwide and projected incidence of new cancer cases are expected to increase by nearly 50% by 2040 (Sung *et al.,* 2021). Due to better sanitation, improvements in treatments and an aging and increasing worldwide population, there is a shift from communicable diseases to non-communicable diseases, and less premature mortality (GBD 2015 Mortality and Causes of Death Collaborators, 2016; Catalá-López *et al.,* 2014). Globally, cancer is the second leading cause of death and only beaten by cardiovascular diseases (Naghavi *et al.,* 2017).

1.3.1 Glioma Brain Tumours

Glioma brain tumours originate from non-neuronal glial cells and are the most common primary tumour accounting for 81% of all malignant brain tumours (Ostrom *et al.,* 2014). Approximately two thirds of primary gliomas develop in the brain, whilst the remainder occur within the rest of the CNS (Davis, 2016).

Glioma tumours were graded I-IV, using roman numerals, based upon their malignancy by the World Health Organisation (WHO) (Louis *et al.,* 2007). The WHO updated the classification of tumours in 2016 and then again in 2021 integrating histological and molecular properties of biopsies and constantly striving to aid the lives of patients (Louis *et al.,* 2016; Louis *et al.,* 2021). The new classification is moving more towards molecular diagnosis and genetic change as there has been a shift to 'within-tumour-type' grading (Louis *et al.,* 2021).

The new classification of glioma has involved dividing them into 6 groups. The first covers the majority of primary brain tumours in adults and is labelled 'Adult-type diffuse glioma'. The second group is 'Paediatric-type diffuse low-grade glioma' and third is 'Paediatric-type diffuse high-grade glioma'. The fourth group is 'Circumscribed astrocytic glioma' and so have more of a clear boundary between tumour and normal brain tissue. The fifth group is 'Glioneuronal and neuronal tumours' where the tumour has neuronal differentiation, and finally 'Ependymomas' which are their own separate tumour classification (Louis *et al.,* 2021).

The 2021 classification system has encountered a few general changes from the WHO 2016 classification system. For the first time, the 2021 classification separated adult and paediatric type gliomas and for all groups except ependymomas, uses molecular diagnostics and histological results to give an IDH status before the WHO grade (Park *et al.,* 2023). There has been an increase in complexity of molecular diagnostics of IDH-mutant and IDH-wildtype diffuse gliomas, which using the flowchart, reveals a tumour classification and grade (Figure 1.7).

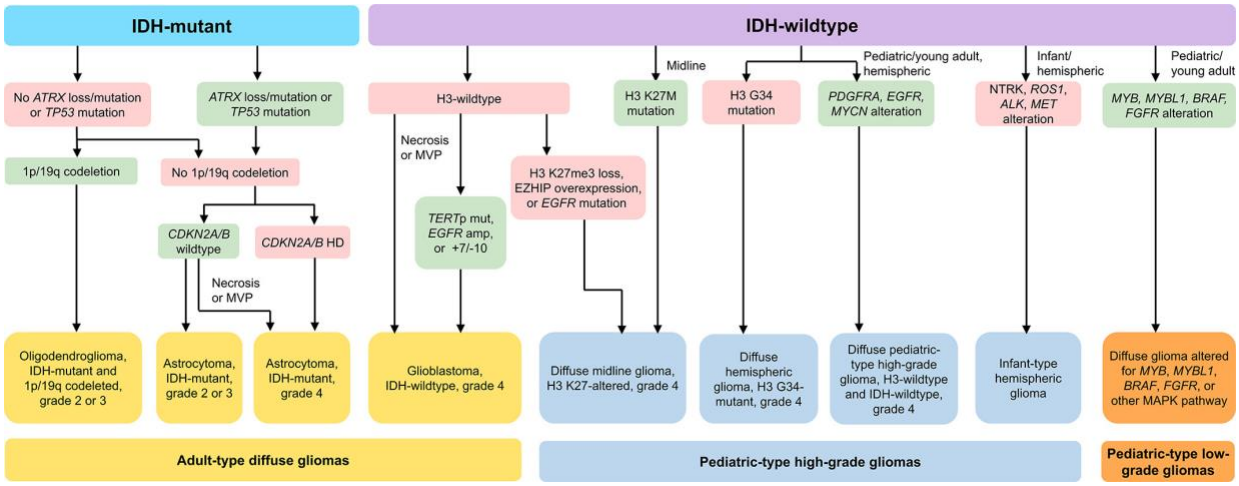

Figure 1.7 – Flowchart to classify glioma tumours on histological and molecular features.

Histology of biopsy is investigated first and then molecular testing determines IDH status and any other genetic features creating an integrated diagnosis (Park et al., 2023).

1.3.1.1 Glioblastoma Brain Tumours

Glioblastoma is a stage IV glioma tumour and is the most malignant primary brain tumour in adults accounting for 45% of glioma tumours (Thakkar *et al.,* 2014; Ostrom *et al.,* 2014). Furthermore, glioblastoma tumours are characteristically highly invasive and aggressive and have the worst prognosis out of all glioma tumours with survival following diagnosis rarely reaching 2 years (Culicchia *et al.,* 2008; Sánchez-Valle *et al.,* 2017; Woehrer *et al.,* 2014). Like Alzheimer's disease, glioblastoma tumours are predominantly found within the elderly population with an average occurrence between 75 and 84 years of age (Ostrom *et al.,* 2014).

1.3.1.1.1 Clinical Presentation of Glioblastomas

Depending on the location and size of the tumour, glioblastoma can present with a numerous set of symptoms (Kanderi and Gupta, 2023). Most often patients present with headaches, focal deficits and progressive neurological decline due to increased intracranial pressure (Alifieris and Trafalis, 2015). Seizures are also a

presenting symptom in roughly 25% of patients, which increases to 50% of patients in the later stages of glioblastoma diagnosis (Perry *et al.,* 2006; Schiff *et al.,* 2015).

Glioblastoma is typically diagnosed through imaging using computed tomography (CT) or magnetic resonance imaging (MRI) scans (Wirsching *et al.,* 2016). For glioblastoma to be diagnosed, presence of necrosis is required for the grade IV WHO classification, which is shown by a higher density centre within the mass of tumour cells on an MRI scan with contrast (Davis, 2016).

1.3.1.1.2 Risk Factors of Glioblastoma

There are known risk factors to increase likelihood of development of glioblastoma including exposure to ionising radiation (Alifieris and Trafalis, 2015), However, radiation induced glioblastoma is usually seen years later as a result of intense radiation treatment a patient received for another tumour or medical condition as associations with environmental exposures (Johnson *et al.,* 2015). Other environmental factors including smoking, pesticides and petroleum refining have been loosely connected as a risk factor to glioblastoma (Davis, 2016).

1.3.1.1.3 Current Treatments of Glioblastoma

The initial step in the current therapy approach to a glioblastoma is maximal safe surgical resection of the tumour (Johnson *et al.,* 2015). This is followed by radiotherapy and chemotherapy, most commonly temozolomide (Davis, 2016). There has not been any new pharmaceutical treatment for glioblastoma for 30 years because unlike treatments for other cancers, the drugs to treat glioblastoma have to cross the blood brain barrier (O'Reilly *et al.,* 1993; Arora and Somasundaram, 2019). Treatment varies for glioblastoma due to MGMT status of the tumour, as MGMT is responsible to promote DNA repair (Gerson, 2004; Annavarapu *et al.,* 2021; Szylberg *et al.,* 2022). If the tumour has a methylated MGMT status, the gene is silenced, impairing DNA repair of the cell and is more sensitive to temozolomide chemotherapy, whereas if the MGMT status is

unmethylated, temozolomide is not recommended and radiotherapy is given alone (Kanderi and Gupta, 2023).

Although a treatment called tumour treating fields (TTF) has been found to improve survival of patients (Toms *et al.,* 2019). TTF is a non-invasive approach to treating glioblastoma which involves electrodes attached to a cap that deliver electric fields through the brain at an optimal frequency of 200 kHz (Chaudhry *et al.,* 2015; Dorsey *et al.,* 2020; Kirson *et al.,* 2004). These electric signals target glioblastoma cells only, interrupting the metaphase of mitosis, causing abnormal spindle formation and resulting in cell death (Rominiyi *et al.,* 2021). However, due to the cost of the treatment, it is not currently provided on NHS, and can only be accessed privately or through clinical trial (McCabe *et al.,* 2008; Rominiyi *et al.,* 2021).

1.3.2 Comorbidity Between Glioma and Alzheimer's Disease

Glioma tumours, in particular glioblastoma, and Alzheimer's disease become more prevalent with age. However, it is rare that both diseases overlap within the same individual despite both diseases being negative hallmarks of aging, supporting the inverse relationship between Alzheimer's disease and cancer; Section 1.1.2 (Behrens *et al.,* 2009; Nelson, 2002). There is very limited data on the comorbidity between glioma as a specific cancer and Alzheimer's disease even though many epidemiological and longitudinal studies investigate the relationship between Alzheimer's disease and cancer in general; Section 1.1.2. Meta-analysis concluded a strong inverse comorbidity between Alzheimer's disease and cancer, however, unfortunately insufficient numbers in the meta-analysis precluded differentiation between protection from specific cancers, so it is unknown whether glioma was more or less protective than other cancers; Section 1.1.2 (Catalá-López *et al.,* 2014; Roe *et al.,* 2010; Driver *et al.,* 2012; Roe *et al.,* 2005). However, a study has compared the risk of Alzheimer's disease in patients with brain tumours, gliomas or glioblastomas and found a significantly lower prevalence of both glioblastomas and gliomas in patients who died from Alzheimer's disease compared to those who died from other causes (Xia *et al.,* 2023). The same was true in reverse as those with glioblastoma were found to have a significantly lower

risk of Alzheimer's disease compared to other tumours when controlled for 6 variables such as age at death, sex and radiation therapy (Xia *et al.,* 2023).

However, there have been reports of a direct link between Alzheimer's disease and glioblastoma based on a transcriptomic meta-analysis that identified expressed genes that were similarly deregulated in the same direction between Alzheimer's disease and glioblastoma (Sánchez-Valle *et al.,* 2017). Such claims of a direct link between Alzheimer's disease and glioma have been made previously due to a positive correlation between the incidence of the two diseases and questions were raised that there may be a possible common cause, however, a direct correlation between the two disease was hypothetical and not supported through evidence (Lehrer, 2010). A population based incidence study found that the observed number of Alzheimer's disease cases in patients with a nervous system cancer was higher than expected, however, in comparison, the risk of nervous system cancer occurrence for those with Alzheimer's disease was significantly reduced (Musicco *et al.,* 2013). One case of Alzheimer's disease was diagnosed, however, a further 2 cases that were initially flagged as cognitive decline were finally diagnosed as brain tumours (Musicco *et al.,* 2013). Due to glioblastoma being a rare cancer, this study did not investigate the differential risk of glioblastoma against Alzheimer's disease, only brain cancer as a whole, and so a conclusion on the comorbidity of glioblastoma and Alzheimer's disease cannot be made based on this study. The comorbidity status between glioma and Alzheimer's disease remains unclear. Preclinical experiments have investigated the pathological characteristic Aβ in Alzheimer's disease in glioma brain tumours as the next section discusses.

1.3.3 Interactions Between Glioma and Amyloid Beta

As there is limited data on the comorbidity between Alzheimer's disease and glioma specifically, certain studies have investigated a possible protective link between Aβ and glioma tumours. *In vivo* Alzheimer's transgenic mice that overexpress Aβ were implanted with GL261 glioma cells and tumour growth was found to be significantly inhibited (Paris *et al.,* 2010). The inhibition of tumour

growth was found not to be a direct result of toxicity but due to inhibition of angiogenesis (Paris *et al.,* 2010). A further *in vivo* study supported this as a xenograft mouse model was injected with Aβ directly into a U87MG glioblastoma tumour and found to inhibit growth, vascularisation and angiogenesis (Paris *et al.,* 2004).

Studies *in vitro* have also displayed similar inhibitory effects. Aβ was found to induce inhibition of angiogenesis without causing direct toxicity to the human brain microvascular endothelial cells they were co-cultured with, however, it was unknown whether inhibition occurred directly or indirectly (Paris *et al.,* 2010). Another study found high levels of exogenous Aβ inhibited proliferation rates of glioblastoma cells, breast cancer cells, adenocarcinoma cells and melanoma cells, when cultured with cell medium (Zhao *et al.,* 2009). These studies suggest that Aβ has anti-tumour properties that may contribute to the mechanisms supporting protective properties Alzheimer's disease has against cancer, corroborating the inverse correlation seen in literature; Section 1.2.2.

Further interaction between Aβ and glioma cells includes when Aβ is produced directly from the cells. Glioma cells cultured *in vitro* have been shown to generate the protein Aβ that co-migrates with synthetic Aβ and antibody (Morato and Mayor, 1993). Further studies have shown innate Aβ has been observed naturally accumulating in and around glioma tumours and blood vessels close to the tumour in xenograft mouse models (Kucheryavykh et al., 2019; Williams, 2019).

Even though interactions between Aβ and glioma tumours, including glioblastoma, have been investigated, individual species including Aβ40 and Aβ42, that is more commonly associated with Alzheimer's disease, have not. Expression or function of SorL1 has never been investigated in glioblastoma.

1.4 Aims and Objectives

The overarching aim of this thesis was to explore the role that SorL1 has in glioblastoma. The objectives to help determine the role of SorL1 are as follows:

1. Determine whether SorL1 is expressed in glioblastoma cells using immunofluorescence and western blotting. As Aβ40 and Aβ42 production is controlled by SorL1 protein, determine Aβ40 and Aβ42 expression levels in glioblastoma using immunofluorescence and ELISA.

2. Determine whether SorL1 is secreted into cell medium from glioblastoma cells and into serum from glioblastoma tumours in xenograft mouse model using western blotting.

3. Construct a knock down *in vitro* model of SorL1 in glioblastoma cells through transient transfection using siRNA encoding plasmids. Validation of this model through immunofluorescence and western blotting.

4. Investigate if knock down of SorL1 model alters Aβ40 and Aβ42 expression in glioblastoma cells using immunofluorescence and ELISA.

5. Investigate if knock down of SorL1 model effects glioblastoma cell function using MTS assay for proliferation and cell viability studies, and scratch assay for migration studies.

Chapter 2

Methods

2 Chapter 2 – Methods

2.1 Bioinformatics

The Cancer Genome Atlas (TCGA) PanCancer Atlas (Hoadley *et al.,* 2018) was explored in CBioPortal. CNS/brain was selected, and Reverse Phase Protein Array (RPPA) data was explored for SorL1 in glioblastoma and lower grade glioma.

2.2 Cell Culture

Commercially available immortalised cell lines U87MG and 1321N1 were obtained from ECACC, Porton Down, UK and SVGp12 from ATCC, Teddington, UK. Short term patient-derived (PD) cultures PD301 and PD304 cells were kindly donated by Professor Tracy Warr (University of Wolverhampton) and normal human astrocytes HA-SC1800 (NHA) were purchased from ScienCell Research Laboratories, California, US. The general maintenance of the patient derived cells were as stated in Brain Tumour North West (BTNW) guidelines.

Table 2.1 – Cell Lines.

Name of Cell Line	*Cancer / Cell Derived From*	*Immortal / Primary Cell*	*MGMT Status*	*IDH1*
U87MG	*Glioblastoma*	*Immortal*	-	-
1321N1	*Stage II Astrocytoma*	*Immortal*	-	-
SVGp12	*Foetal Astrocyte*	*Immortal*	-	-
PD301	*Glioblastoma*	*Primary*	*Methylated*	*Wildtype*
PD304	*Glioblastoma*	*Primary*	*Low Methylation*	*Wildtype*
NHA	*Human Astrocyte*	*Primary*	-	-

2.2.1 Media

All media and supplements were purchased from Lonza, UK unless otherwise stated. All other consumables used for cell culture, phosphate buffered saline (PBS), industrial methylated spirits (IMS), virkon, and all plastic-ware including tissue culture flasks, well plates, serological pipettes and centrifuge tubes were purchased from ThermoFisher, UK.

U87MG cells and SVGp12 cells were cultured in Eagle's Minimum Essential Medium (EMEM) supplemented with L-glutamine (2mM), 1% (w/v) non-essential amino acids, sodium pyruvate (1mM) and 10% (w/v) foetal bovine serum (FBS).

1321N1 cells were cultured using Dulbecco's Modified Eagle Medium (DMEM) supplemented with L-glutamine (2mM) and 10% (w/v) FBS.

PD301 and PD304 cells were cultured in Ham's F-10 Nutrient Mix (containing L-glutamine and HEPES) (Fisher Scientific, UK) supplemented with 10% (w/v) FBS.

Normal human astrocytes were grown in AGM™ Astrocyte Growth Medium BulletKit™ culture system containing ABM™ Basal medium and AGM™ SingleQuots™ Supplements supplemented with 3% (w/v) human serum male AB (Sigma, UK).

The immortalised cell lines and NHA cells were grown in standard T75 filtered cell culture flasks at 37°C in 5% CO_2, and the PD cells were grown in unfiltered T75 flasks at 37°C without CO_2.

2.2.2 Passaging

All cells were grown until 80% confluency before being passaged under aseptic conditions in a Class II microbiological safety cabinet.

Medium was removed before the flask was washed using PBS pH 7.3 to 7.5, detached from the surface using 2-3ml of Trypsin EDTA 0.025% (Lonza, UK) and incubated for 4-6 minutes depending on the cell type at 37°C either with or without 5% CO_2. The flask was then lightly tapped to detach the adhered cells from the flask which was confirmed by light microscopy. An equal or larger volume of medium was added to neutralise the trypsin and centrifuged at 200xg for 5 minutes at room temperature. The supernatant was removed, and the cell pellet was resuspended in medium before being split into an appropriate number of flasks. For the immortalised cell lines, 1 flask was split into between 4 and 8 flasks, whilst the human primary cells were split between 2 and 3 flasks.

2.2.3 Cryopreserving

For long term storage, cells were kept in liquid nitrogen dewars (-190°C). Freezing down cells occurred following the same protocol as passaging once cells were 80% confluent. Cells were trypsinised, neutralised and centrifuged at 200xg for 5 minutes; Section 2.2.2. For immortalised cell lines and PD cells, the pellet was resuspended in respective medium supplemented with 10% (w/v) DMSO. NHA cells were resuspended in human serum containing 10% (w/v) DMSO. Cell suspensions were aliquoted into cryovials and placed into a Nalgene Mr. Frosty freezing chamber filled with isopropanol and placed into a -80°C freezer for a minimum of 24 hours allowing the cells to freeze slowly. Cryovials were then transferred to liquid nitrogen dewars.

In contrast to the slow freezing process, cells were defrosted rapidly by placing cryovials in a water bath at 37°C until fully defrosted and the cell suspension was immediately added to media and mixed. This was then placed in the appropriate T75 flask and left to incubate for 24 hours at 37°C either with or without 5% CO_2. The following day, the cells had adhered to the flask and the medium replaced to remove the cryopreservatives.

2.2.4 Cell Counting

Cell counts were performed following trypsinisation and resuspension of the cell pellet following the passaging protocol; Section 2.2.2. A total of 200μl of cell suspension was collected. Equal volume of Trypan blue was added and the cells counted using a haemocytometer. A coverslip was placed over the haemocytometer chamber, ensuring Newton's rings were visible. Then 10μl of 1:1 suspension was added to the edge of the haemocytometer and through capillary action was sucked under the coverslip. Under the microscope a cell count was taken by counting the number of viable cells in the 4 outer corner quadrants of the grid (Figure 2.1).

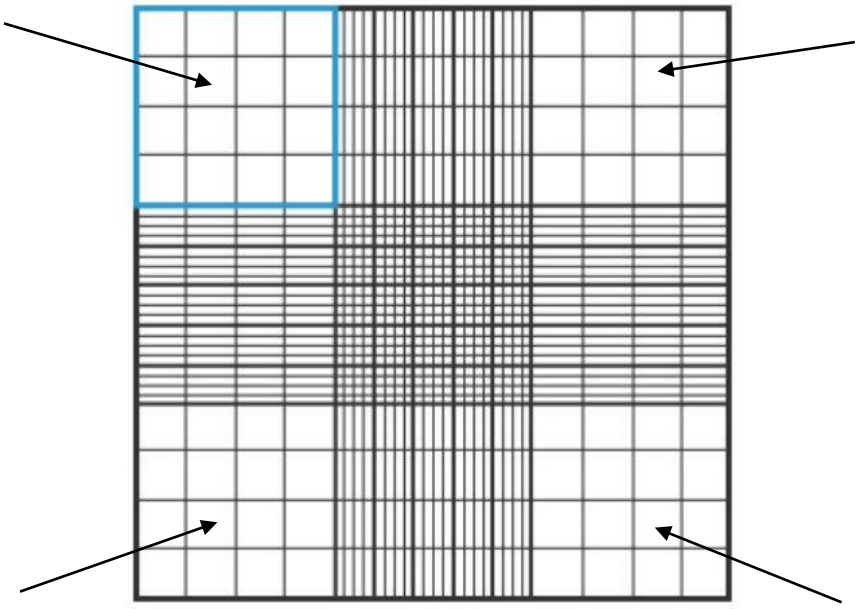

Figure 2.1 – Haemocytometer grid.

Displays Haemocytometer grid, arrows display the outer 4 quadrants that are counted. Haemocytometer from abcam (Cambridge, UK); https://www.abcam.com.

An average number of cells counted was calculated and corrected for Trypan blue dilution. The number of cells per ml was calculated by multiplying by 10^4.

2.2.5 Growth Curves

Growth curves for all cell types were to determine normal growth characteristics and how many cells to seed for future experiments. A total of 2000 cells were seeded into each well of a 24 well plate at a concentration of 2000 cells per ml. Wells were counted in triplicate daily to get biological replication over 10 days following seeding to determine division rates. This was also repeated in triplicate with 3 different passages. The mean was calculated, and growth curve produced.

2.3 Immunocytochemistry

2.3.1 Seeding Cells

Cells were seeded on sterilised 13mm diameter No. 1.5 coverslips (Scientific Laboratory Supplies Ltd) in 24 well plates. Due to the cells being different sizes, they were seeded at different cell densities in their respective media. PD301, PD304, SVGp12 and NHA cells were seeded at 20,000 cells per coverslip. The smaller 1321N1 cells were seeded at 40,000 cells per coverslip and U87MG cells were seeded at 50,000 cells as they did not adhere to the coverslips as well as the other cell lines and were liable to be washed off during fixation. Cells were seeded at this density to ensure after 24 hours they were not over 80% confluent. All cells were incubated at 37°C either with or without 5% CO_2 overnight.

2.3.2 Fixation

Cells were fixed 24 hours after being seeded on coverslips. The media was removed from the wells and the coverslips gently washed with PBS once to minimise cells being washed from the coverslips. The PBS was removed, and 4% (v/v) formaldehyde (ThermoFisher, UK) diluted in PBS was added for 8 minutes. This was removed and the cells were washed twice with PBS. The cells were then quenched of acetates with 0.1M glycine (ThermoFisher, UK) for 10 minutes. This was removed and cells washed twice more in PBS. Cells were permeabilised in

0.1% (v/v) Triton X-100 (ThermoFisher, UK) diluted in PBS, for no more than 4 minutes and washed three times in PBS.

2.3.3 Staining

All antibodies were obtained from Abcam, Cambridge, U.K. except SorL1, which was acquired from BD Biosciences, San Jose, California, U.S.

Table 2.2 – Primary antibodies used for immunocytochemistry.

Anti-	*Species*	*Isotype*	*Clone*	*Concentration/ dilution*	*Catalogue Number*
Aβ40	*Rabbit*	*IgG*	*Polyclonal*	*1:100*	*AB12265*
Aβ42	*Rabbit*	*IgG*	*Polyclonal*	*1:100*	*AB10148*
SorL1	*Mouse*	*IgG*	*Monoclonal*	*1:100*	*612633*
Aβ40	*Rabbit*	*IgG*	*Recombinant monoclonal*	*1:100*	*AB254345*
Aβ42	*Rabbit*	*IgG*	*Recombinant monoclonal*	*1:100*	*AB201061*

Table 2.3 – Secondary antibodies used for immunocytochemistry.

Anti-	*Species*	*Isotype*	*Conjugate*	*Concentration/ dilution*	*Catalogue Number*
Rabbit	*Goat*	*IgG*	*Alexa Fluor 488*	*1:500*	*AB150077*
Rabbit	*Goat*	*IgG*	*Alexa Fluor 555*	*1:500*	*A32732*
Mouse	*Goat*	*IgG*	*Alexa Fluor 555*	*1:500*	*A32727*
Rabbit	*Goat*	*IgG*	*Alexa Fluor 647*	*1:500*	*AB150083*
Mouse	*Goat*	*IgG*	*Alexa Fluor 647*	*1:500*	*AB150115*

Fixed cells were blocked with 1% bovine serum albumin (BSA) diluted in PBS for 1 hour at room temperature or overnight at 4°C to prevent non-specific staining. Primary antibodies (Table 2.2) were diluted in 1% BSA, added to the coverslips and incubated overnight at 4°C. Coverslips were washed 3 times with PBS before being incubated with a mixed solution of BSA, matched secondary antibody (Table 2.3) and 0.1µg/ml 4',6-diamidino-2-phenylindole (DAPI) in the dark for 30-60 minutes at room temperature. Coverslips were washed a further 3 times with PBS, mounted onto slides with Thermofisher ProLong diamond and left to cure for 24 hours before being sealed with nail varnish.

2.4 Fluorescent Microscopy

2.4.1 Deconvolution Microscopy

Initial validation of antibodies, determining expression of proteins in cells and transfection efficiency calculations were conducted using a Zeiss Cell Observer Axio Z1 system, equipped with a 25% intensity colibri LED light source and DAPI, GFP and dsRED filter sets (Zeiss, Cambridge). All images were taken using the

same exposure time (DAPI 120ms, GFP 400ms, dsRED 600ms). Expression of Aβ40, Aβ42 and SorL1 were visualised at x40 objective using ZEN pro software and AxioCam (Carl Zeiss, Cambridge, UK). At least 10 images were collected at the same time and under identical conditions and replicated in triplicate.

2.4.2 Confocal Microscopy

Images for validating antibodies and determining expression of SorL1, Aβ40 and Aβ42 were collected on a Leica TCS SP5 confocal microscope (Leica Biosystems, Newcastle, UK) using x20 objective. DAPI was detected using 405nm UV laser (15% power, gain 715), GFP was detected using 476nm and 488nm light lasers (15% power, gain 700) and Alexa Fluor 647 was detected using 633nm light laser (20% power, gain 700). Confocal settings for image acquisition remained identical whereby images were taken in 1024 x 1024 format and bidirectional scan for repeats in triplicate using Leica LAS AF software.

2.4.3 Image J Analysis

Primary cell images were quantified to compare Aβ40, Aβ42 and SorL1 protein expression between PD301, PD304 and NHA cells. Images were analysed using Image J Software. The free form tool was used to draw around each cell being analysed and the area, minimum and maximum grey values and mean grey value recorded, as well as background staining. The following formula was used to calculate the corrected total cell fluorescence (CTCF):

CTCF = Integrated Density – (Area of selected cell x Mean fluorescence of background).

2.4.4 Statistical Analysis

Statistical analysis on the immunocytochemistry images was performed using Prism (GraphPad Software, San Diago, USA). The data was deemed normally distributed and ANOVA (parametric data) was used to determine significance.

Comparisons of intensity of staining between the cell types was done by a Tukey's multiple comparisons test. A P-value of ≤ 0.05 was deemed significant.

2.5 Glioblastoma orthotopic xenograft in mice

All *in vivo* work was undertaken under Home Office Project Licence PPL70/7938 and authorised by University of Central Lancashire Animal Welfare and Ethical Review Board.

Mice (Balb/C, approximately 20-25g) were purchased from Charles River, UK and housed in groups with enrichment and *ad libitum* access to standard rodent food and water until use.

Mice were anaesthetised (1:1 isoflurane:nitrous oxide) and transferred to a stereotaxic frame where the skull was immobilised by ear bars and anaesthetic delivered via nose cone. The mouse was kept warm by heating lamp. The skull was shaved, sterilised (povidone iodine) and an incision made such that landmark bregma was clearly visible. The skull was thinned 1 mm lateral and 1 mm rostral to bregma with a dental drill such that a needle could easily pass through. A 10 µl microsyringe (Hamilton, USA) was held in a stereotaxic manipulator and the tip of the needle slowly advanced vertically through the skull 4 mm and retracted 1 mm to create a pocket. A total of 40,000 U87-MG cells in 2 µl PBS or 2 µl PBS were introduced over 5 minutes by a microinjection syringe pump (World Precision Instruments, UK). The needle was retracted slowly (1 mm / minute) to prevent the aspirant being drawn into the needle channel. The hole was closed with bone wax and the skin stapled. A bolus of warm saline (10 µl/g) and Metacam (20 µl) was given by subcutaneous injection and the animal allowed to recover in a warmed recovery chamber with wet mash. Once fully recovered, the animal was returned to home cage. Mice were culled by cervical dislocation at 30 days or if clinical scores deteriorated.

At weekly intervals, a tail vein blood sample was collected. Mice were briefly held in a Broome style restrainer such that the tail was accessible and could be warmed

in warm water. Skin was sterilised with an alcohol wipe and a 25G needle inserted into the lateral tail vein. Approximately 50-100 µl of blood was routinely collected and decanted into sterile centrifuge tubes, allowed to clot at room temperature for approximately 15 minutes. Tubes were spun at 10,000xg for 10 minutes in a refrigerated centrifuge to pellet the blood clot. Serum was removed and stored at -80°C until use.

On the day of culling, a terminal blood sample was taken by cardiac puncture immediately after euthanasia. Serum was prepared as for tail vein. Serum samples were used in western blotting experiments following the determination of protein concentration using a Pierce™ BCA Protein Assay Kit (ThermoFisher Scientific, UK).

2.6 Western Blotting

2.6.1 Cell Lysate Preparation

Confluent flasks of cells were washed with PBS, trypsinised, neutralised and centrifuged at 200xg for 5 minutes. The supernatant was removed, and the pellet was resuspended in 1ml of cold PBS and subsequently kept cold on crushed ice. The cell suspension was transferred to a 1.5ml Eppendorf tube and spun down again at 14,000xg for 5 minutes in a pre-cooled (4°C) centrifuge. PBS was removed and depending on the size of the cell pellet, it was resuspended in 150µl-200µl of cold RIPA buffer supplemented with Halt™ Protease and Phosphatase Inhibitor Cocktail EDTA-free. Alternatively a confluent flask of cells was washed with PBS and 150µl-200µl of cold RIPA buffer with supplements was added and cells were scraped and collected. The cell suspension was kept on crushed ice for 30 minutes whilst vortexing every 5 minutes. It was spun again for 20 minutes at 16,000xg at 4°C. Aliquots (50µl) of the lysed supernatant were stored at -20°C until use. Pierce™ BCA Protein Assay Kit (ThermoFisher Scientific, UK) was used as per manufacturer's instructions using the cell lysates to determine the protein concentration.

2.6.2 Cell Medium Collection

PD301, PD304 and NHA cells were seeded in a 24 well plate. Seeding 40,000 cells per well in 4 wells per cell type. Cells were left to adhere to the well plate, incubating for 24 hours at 37°C either with or without 5% CO_2 depending if the cells required it. Medium was then exchanged to serum free medium, without FBS for F10 or without human serum for ABM. Only 200µl of serum free medium was added to each well to ensure the cells were covered. Once again, the cells were left to incubate overnight at 37°C either with or without CO_2. This media was then collected and stored in an Eppendorf at -20°C until ready to use. Although the same number of cells were originally seeded, a BCA protein assay was carried out as per manufacturer's instructions to determine the protein content.

2.6.3 SDS-PAGE Gels

All western blot equipment was obtained from Biorad, Watford, UK. All buffers were made using distilled water (dH_2O) plus additional components.

Table 2.4 – Components to make up x2 gels.

Components	*Supplier*	*10% Gel*	*Stacking Gel*
Distilled Water (dH_2O)		*5.9ml*	*2.7ml*
30% Acrylamide Mix	*Sigma, UK*	*5ml*	*670µl*
1.5M Tris (pH 8.8)	*ThermoFisher, UK*	*3.8ml*	
1.0M Tris (pH6.8)	*ThermoFisher, UK*		*500µl*
10% sodium dodecyl sulphate (SDS)	*ThermoFisher, UK*	*150µl*	*40µl*
10% ammonium peroxodisulphate (APS)	*ThermoFisher, UK*	*150µl*	*40µl*
Tetramethylethylenediamine (TEMED)	*Biorad, UK*	*6µl*	*4µl*

Sodium dodecyl sulphate polyacrylamide gel electrophoresis (SDS-PAGE) gels were originally bought from Biorad, Watford, UK before being made. Two glass plates, one shorter than the other, were placed in a holder on a sponge and tested for leaks. The 10% gel was then made adding dH_2O, 30% acrylamide mix, 1.5M Tris (pH 8.8), 10% SDS, 10% APS and TEMED (Table 2.4). APS and TEMED were added to catalyse polymerisation of the gel and the mixture poured into the mould. Isopropanol was added on top to prevent drying out. Once the gel set, the isopropanol was removed and gel was washed with dH_2O. Stacking gel was prepared (Table 2.4), poured on top of resolving gel and a 10 well comb was inserted. This was then left to polymerise for 30 minutes at room temperature. The comb was gently removed, and the wells left behind were washed thoroughly with dH_2O.

2.6.4 Western Buffers

All buffers were made up using dH_2O and all laboratory reagents to make buffers were purchased from ThermoFisher Scientific, UK.

RIPA Buffer was used as the lysis buffer and composed 50mM Tris pH 8.0, 150mM sodium chloride (NaCl), 0.5% (w/v) sodium deoxycholate and 1% (v/v) Triton X100. Halt™ Protease and Phosphatase Inhibitor Cocktail EDTA-free was added before use.

Laemmli Buffer 2X was used as the loading buffer and composed 0.125M Tris-HCl, 4% (v/v) SDS, 20% (v/v) glycerol and 0.004% (w/v) bromophenol blue. The pH was adjusted to 6.8. Prior to use, 10% (v/v) beta-mercaptoethanol was added.

A 10X running buffer stock (pH 8.3) was made and stored at room temperature; 25mM Tris was added to 190mM glycine and 0.1% (v/v) SDS. A X1 working concentration was made on the day of experiment.

A 10X transfer buffer stock (pH 8.3) was also made and stored at room temperature. This was made the same way with 25mM Tris and 190mM glycine, however SDS was excluded. For the X1 working concentration, 20% (v/v) methanol was also added and made on the day of experiment.

A X10 TBS buffer was made through mixing 20mM Tris and 150mM NaCl and adjusting the pH to 7.6. A working wash buffer TBST was made using 10% (v/v) TBS X10 and 0.01% (v/v) Tween.

Blocking Solution was made using 7% (w/v) Marvel™ dried skimmed milk dissolved in TBST.

A mild stripping buffer to remove protein from the membrane was produced by adding 1.5% (w/v) glycine, 0.1% (v/v) SDS and 1% (v/v) Tween together and adjusting the pH to 2.2.

2.6.5 SDS-PAGE Gel Electrophoresis and Transfer

All western blot equipment was obtained from Biorad, Watford, UK.

A total of 10µg of protein from each cell lysate was mixed with equal volume of 2x Laemmli loading buffer (1:1, v/v). For medium, 10µg of protein was also collected, using BCA protein assay results, however, as no endogenous loading control was detectable in medium, 500ng recombinant human β-actin protein His-tag (AB240844) (Abcam, Cambridge, UK) was added before mixing with equal volume of Laemmli buffer. For mouse serum, 7.5µg of protein was mixed with equal volume of 2x Laemmli buffer. Lysates and medium were heated to 95°C for 5 minutes and centrifuged at 16,000xg for 5 minutes at room temperature prior to loading the gels, whilst mouse serum was only centrifuged prior to loading. Gels were placed in a tank with X1 running buffer before lysate, medium or serum were loaded into wells alongside PageRuler^{TM} plus prestained protein ladder (10 to 250 kDa (ThermoFisher Scientific). Gels were run at 50V for 10 minutes to allow the proteins to pass through the stacking gel before increasing voltage to run at 100V for approximately 90 minutes.

Following electrophoresis, gels were transferred onto Amersham Protran 0.45µm nitrocellulose blotting membrane (Sigma, UK). The tank was filled with X1 transfer buffer and an ice block was added to prevent overheating. Protein transfer from gel to nitrocellulose membrane was achieved by running the tank at 300mA for 80 minutes.

2.6.6 Staining

All antibodies were obtained from Abcam, Cambridge, U.K.

Table 2.5 – Primary antibodies used for western blotting.

Anti-	*Species*	*Isotype*	*Clone*	*Concentration/ dilution*	*Catalogue Number*
SorL1	*Rabbit*	*IgG*	*Recombinant monoclonal*	*1:1000*	*AB190684*
β-Actin	*Mouse*	*IgG1*	*Monoclonal*	*1:5000*	*AB6276*
6X His-tag	*Rabbit*	*IgG*	*Recombinant polyclonal*	*1:1000*	*AB9108*
Transferrin	*Rabbit*	*IgG*	*Monoclonal*	*1:1000*	*AB277635*

The SorL1 antibody (Table 2.5) was used for detecting SorL1 in lysates and secreted SorL1 in cell medium and mouse serum. It was able to be used for secreted SorL1 as the SorL1 antibody was an approximate 150kDa fragment antibody raised against the immunogen that corresponded with an internal portion of the SorL1 protein. As soluble SorL1 is known to be approximately 240 kDa in molecular weight losing 10kDa from its C-terminus (Motoi *et al.,* 1999), the antibody was still compatible with soluble SorL1.

Table 2.6 – Secondary HRP antibodies used for Western blotting.

Anti-	*Species*	*Isotype*	*Conjugate*	*Concentration/ dilution*	*Catalogue Number*
Mouse	*Rabbit*	*IgG*	*HRP*	*1:5000*	*AB6728*
Rabbit	*Goat*	*IgG*	*HRP*	*1:5000*	*AB6721*

Following the transfer onto nitrocellulose, membranes were cut to size and non-specific binding blocked in 7% milk in TBST on a rocker for 60 minutes at room temperature or 4°C overnight. Blocking solution was removed and the membrane washed 3 times with TBST before primary antibodies were added. Antibodies were

diluted in TBST (Table 2.5). Incubation for β-actin primary antibody was 60 minutes at room temperature, while the rest of the primary antibodies were incubated at 4°C overnight. Following incubation, the nitrocellulose membrane was washed three times for 15 minutes with TBST. The matched HRP (horseradish peroxidase) secondary antibodies diluted in TBST was then applied and incubated at room temperature for 60 minutes (Table 2.6). Following secondary antibody incubation, the nitrocellulose membrane was washed three times (twice for 10 minutes, and a further time for 60 minutes) with TBST.

2.6.7 Imaging

SuperSignal West Pico PLUS (Fisher, Loughborough, UK) was added to each cellulose membrane for 5 minutes before imaging. The membranes were imaged using Biorad ChemiDoc XRS+, equipped with Image Lab™ software. Final images were exported as TIFF for analysis.

Following imaging, membranes were washed again in TBST, and underwent the stripping protocol. A mild stripping buffer was added twice for 5-10 minutes. Membranes were then washed twice for 10 minutes in PBS and washed twice for 5 minutes in TBST. Membranes were blocked once again in 7% milk and re-probed for β-actin.

2.6.8 Image Analysis

Images were compared and quantified using Image J. The thickest band on the western blot image was selected as a region of interest and this same frame was used over all bands of interest so standardised. The same sized frame of region of interest was also taken below each band to account for the background. The same was done for the loading control western blot images and a note of all grey mean values were noted down. Once all protein of interest data and backgrounds with loading control data and backgrounds was collected, a calculation was conducted. All grey mean values recorded by Image J were subtracted from 255. The inverted background value was deducted from the inverted protein of interest

value to determine the net value. A ratio was then calculated of the net protein of interest value over the net loading control to determine the final relative quantification value and a bar chart was constructed to compare.

2.6.9 Statistical Analysis

Statistical analysis on the western blot images was performed using Prism (GraphPad Software, San Diago, USA). The data was deemed normally distributed and ANOVA (parametric data) was used to determine significance. Comparisons of intensity of the bands between the cell types was done by a Tukey's multiple comparisons test. A P-value of ≤ 0.05 was deemed significant.

2.7 ELISA

Enzyme-linked immunosorbent assays (ELISA) were used to determine levels of Aβ40 and Aβ42 protein in PD301, PD304 and NHA cell lysates. Cells began with the lysing process; Section 2.6.1. Three passages of each cell type were lysed and each lysate was assayed in triplicate. A total of 45μg of protein was assayed per well in both Aβ40 and Aβ42 ELISA kits. Amyloid beta 42 Human ELISA Kit Ultrasensitive and Amyloid beta 40 Human ELISA Kit were used as per manufacturer's instructions (ThermoFisher Scientific, UK). Data was quantified against standard curves that ranged from 7.81 to 5,000 pg/ml for Aβ40 and 1.56 to 1,000 pg/ml for Aβ42. Data was expressed as picograms of protein (either Aβ40 or Aβ42) per mg of total protein.

2.8 Transient Transfections

To determine influence of SorL1 on cell function, PD301 and PD304 cells were transiently transfected with siRNA to knock down SorL1 protein prior to functional studies.

2.8.1 Plasmids

Short interfering ribonucleic acid (siRNA's) were purchased from Applied Biological Materials Inc (abm) (Richmond, BC. Canada). SORL1-set siRNA/shRNA/RNAi Lentivector (Human) with 4 individual targets were purchased to knock down SorL1 (siRNA target A, siRNA target B, siRNA target C and siRNA target D) rather than pooled to determine if any were better than others, along with a Scrambled siRNA GFP Lentivector as a control (Table 2.7).

Table 2.7 – Plasmids

Vector Name	*Vector Type*	*Bacterial Selection*	*Mammalian Selection*	*Gene*	*Function*
piLenti-siRNA-GFP	*Lentiviral siRNA vector*	*Kanamycin*	*Puromycin*	*SorL1*	*Knock down of SorL1 protein*
piLenti-siRNA-GFP-Scrambled	*Lentiviral siRNA vector*	*Kanamycin*	*Puromycin*	*Scrambled*	*Knock down control*

Both piLenti-siRNA-GFP for SorL1 and piLenti-siRNA-GFP-Scrambled for knock down control had the same sequencing primers in the U6 promoter region:

5'--TACGTCCAAGGTCGGGCAGGAAGA--3'

The vector maps are shown for both piLenti-siRNA-GFP for SorL1 knock down and piLenti-siRNA-GFP-Scrambled for knock down control (Figure 2.2).

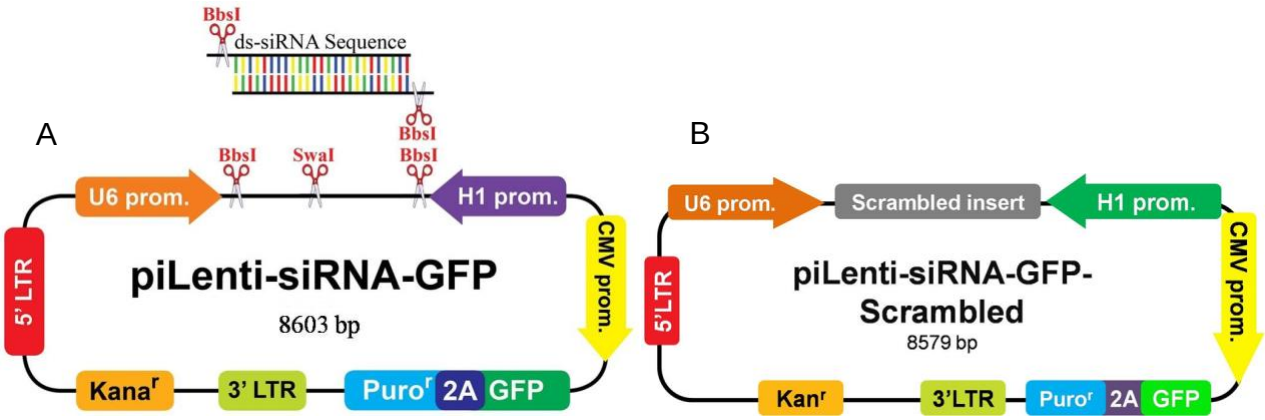

Figure 2.2 – pLenti-siRNA-GFP vector maps.

piLenti-siRNA-GFP vector map (A) and piLenti-siRNA-GFP-Scrambled vector map (B). Vector maps from Applied Biological Materials Inc (abm) (Richmond, BC. Canada); https://www.abmgood.com.

2.8.2 Bacterial Reagents

When making bacterial reagents, aseptic technique was adhered to.

LB Broth was made through dissolving Miller LB Broth powder (ThermoFisher Scientific, UK) in dH_2O. The concentration was 20g/L and was autoclaved to sterilise. This was stored until use and if antibiotics were needed, they were added on the day of use.

LB Agar was produced at a concentration of 32g/L by adding LB agar powder (ThermoFisher Scientific, UK) to dH_2O. This was autoclaved to sterilise. When ready to use, agar was melted by microwaving and once hand-hot, antibiotics were added. Approximately 25ml of agar was poured into 10cm petri dishes and left to set.

Kanamycin sulphate powder (ThermoFisher Scientific, UK) was dissolved in sterile dH_2O to make 100x stock solution (10mg/ml). This was further filter sterilised. Kanamycin was added to LB broth and LB agar at a working concentration of 100μg/ml to make a x1 solution.

2.8.3 Bacterial Transformation

When conducting bacterial work, aseptic technique was abided by at all times either around a flame or in a Class II microbiological safety cabinet.

Five vials of competent dH5α *E.coli* cells were taken from -80°C freezer due to having one scrambled siRNA and four siRNA targets to knock down SorL1. Each bacteria vial was split in half and 1μl of an siRNA and 1μl of sterile water was added into each half, so each vial of bacteria had its own control. The 10 Eppendorf's were placed on crushed ice for 1 hour, before being heat shocked for 2 minutes at 42°C. They were then placed back on crushed ice for 2 minutes and approximately 800μl of LB broth was added to each Eppendorf. Tubes were placed into the Thermo Scientific MaxQ™ 8000 shaking incubator at 180rpm for 1 hour at 30°C.

Following incubation, tubes were centrifuged at 13,000rpm for 30 seconds in the Eppendorf centrifuge 5424 (Eppendorf, UK). The majority of the supernatant was removed leaving enough to resuspend the pellet of bacteria. Ten agar plates were made up containing 1x kanamycin for each siRNA and control, as the siRNA all contain bacterial selection for kanamycin. Each Eppendorf of bacteria either containing one of the siRNA's or its control was added to an agar plate with sterile balls to spread the bacteria evenly over the agar surface. Agar plates were then incubated overnight at 37°C.

The following day, small colonies of *E.coli* bacteria were present on the siRNA targets for SorL1 knock down and scrambled siRNA, whereas the control plates were clean suggesting no contamination. One or two colonies were collected from each agar plate containing one of the siRNAs and they were placed in 100ml of LB broth containing 1x kanamycin. Each conical flask was placed in the Thermo Scientific MaxQ™ 8000 shaking incubator at 180rpm at 30°C overnight.

2.8.4 Plasmid Purification

A Maxi prep kit (Qiagen, Crawley, UK) was carried out the following day to purify the siRNA plasmids. The bacterial cultures were harvested by centrifuging at 6000xg for 15 minutes in a precooled centrifuge at 4°C. Pellets of each siRNA were collected after following manufacturer's instructions of Maxi Prep and dissolved in 50μl of TE buffer (pH 8.0). Vials of the purified plasmids of siRNA targets A, B, C and D to knock down SorL1 and scrambled siRNA were stored at -20°C until they were needed.

2.8.5 NanoDrop

Concentrations of these siRNAs needed to be determined. This was done using the NanoDrop™ 2000/2000c Spectrophotometer (Thermo Scientific, UK). A blank was measured first using TE buffer (pH 8.0) as this was used to dissolve the purified siRNA, followed by the individual siRNAs. A note was made of the individual siRNA concentrations, typically between 1,000-3,000ng/μl and their 260/280 ratios as a ratio of approximately 1.8 is considered to be pure for DNA and RNA.

2.8.6 Transfections

PD301 and PD304 cells were seeded on 13mm diameter No. 1.5 sterile coverslips (Scientific Laboratory supplies Ltd) in 24 well plates. Cells were seeded at a density of 20,000 cells per coverslip and were incubated for 24 hours at 37°C without CO_2. The following day, the medium was exchanged prior to transfection to serum free medium. Transfection was achieved using Invitrogen™ Lipofectamine™ 3000 Transfection Reagent (Invitrogen, UK) and OptiMEM Reduced Serum Medium (ThermoFisher Scientific, UK). Optimal transfection conditions were found through adding different ratios and concentrations of Lipofectamine 3000, P3000 (both from the Lipofectamine Transfection kit) and the siRNAs. As well as the transfection conditions (knock down SorL1 and scrambled),

Lipofectamine only and non-transfected conditions were used as controls. Cells were incubated for 72 hours at 37°C without CO_2. Following incubation, medium was exchanged. Medium for non-transfected and Lipofectamine only cells was exchanged with fresh medium containing serum, whilst medium for the transfected cells was exchanged with fresh medium containing serum supplemented with 5μg/ml puromycin following results from the puromycin kill curve.

2.8.7 Puromycin Kill Curve

PD301 and PD304 cells were trypsinised, neutralised and centrifuged at 200xg for 5 minutes. A cell count was performed to seed 1000 cells per well in a 96 well plate. The 96 well plate was left to incubate for 24 hours at 37°C without CO_2. The following day, puromycin was added in different concentrations 0μg/ml, 1μg/ml, 2μg/ml, 3μg/ml, 4μg/ml and 5μg/ml in triplicate. Medium was also added to wells containing no cells to use later as a control. The plate was then left to incubate for 72 hours at 37°C without CO_2.

Following the incubation for 3 days, a viability assay was performed using resazurin (ThermoFisher, UK). There was 200μl of medium per well, and so 20μl of resazurin was added to each well as per manufacturer's instructions. The plate was then incubated again for 4 hours at 37°C. Fluorescence was then read at 535nm on Tecan Genios Pro plate reader (Tecan, UK). This experiment was carried out in triplicate.

The mean values were calculated and corrected using the media only average. Percentage viability was then calculated and the puromycin kill curve was produced.

2.9 Knock Down of SorL1

2.9.1 Staining

Cells seeded on coverslips were fixed (Section 2.3.2) following the transfection protocol; Section 2.8.6. Cells were stained using DAPI. The transfected cells contained Green Fluorescent Protein (GFP) and so DAPI staining the nuclei allowed a comparison to determine transfection success during the optimisation process. Comparisons were made through randomly taking 10 images of each condition.

Staining all conditions with SorL1 and using fluorescent microscopy allowed comparison and proved knock down.

2.9.2 Western blotting

Further to using staining as proof of knock down, the western blotting technique was also used. All PD301 and PD304 cells were trypsinised and transferred to T25 flasks. Once at 80% confluency, cells were lysed and a western blot was carried out to prove knock down; Section 2.6.

2.10 Functional Studies

In the functional studies, non-transfected cells, Lipofectamine only cells, SorL1 siRNA transfected cells, and scrambled siRNA transfected cells were all compared. This was done for both PD301 and PD304 cells.

2.10.1 MTS Assay

A total of 100µl of cell suspension was seeded at an optimal cell density of 5000 cells per well in a 96 well plate. This was enough to have a substantial seeding density whilst not wanting them to be overconfluent by the end of the 72 hour experiment. All cells were seeded in biological triplicate on three 96 well plates,

one for each time point: 24, 48 and 72 hours, as well as having wells containing just F10 medium. Well plates were incubated at 37°C until each time point needed for experiment.

CellTiter 96® AQueous One Solution Cell Proliferation Assay (MTS) (Promega, UK) was used and taken out the freezer the morning of each time point of the experiment. Due to the MTS solution being light sensitive, the defrosting of the MTS bottle and the experiment was carried out in dark conditions, as much as possible. At the selected time point, at 24, 48 and 72 hours, the well plate was taken out of the incubator and 20µl of the MTS solution was added to each well containing cells as well as the medium only wells as per manufacturer's instructions. This was completed 2 hours prior to measurement which aligned with 0hr at the point the cells were seeded. Manufacturer's instructions suggested reading the plate anytime from 1 to 4 hours after addition of MTS solution. When the MTS solution was added to the wells, the plate was placed back in the incubator in the dark at 37ºC for 2 hours. The plate was then carried to the Tecan Genios Pro (Tecan, U.K.) and the plate was read at 485nm. This experiment was carried out over four replicates.

2.10.2 Statistical Analysis

The absorbances were collected at each time point and the mean values were calculated and corrected using the media only average. A graph was produced to display rate of proliferation. The mean values were also used to determine cell viability of PD301 and PD304 cell conditions, against the non-transfected cells as they did not have any differentiating factors and regarded as having a cell viability of 100%.

Statistical analysis on proliferation and cell viability data was performed using Prism (GraphPad Software, San Diago, USA). The data was deemed normally distributed and ANOVA (parametric data) was used to determine significance. Comparisons between the cell types was done by a Tukey's multiple comparisons test. A P-value of ≤ 0.05 was deemed significant.

2.10.3 Scratch Assay

Following optimisation of PD301 and PD304 cells, the optimal seeding density for this protocol was 30,000 cells per well in a 12 well plate. All cells were seeded in biological triplicate on a 12 well plate for all conditions within PD301 cells and PD304 cells. Cells were seeded and incubated for 24 hours for cells to adhere and cover the base of the well at an 80% confluency. Following 24 hours the medium was removed and the wells were washed with PBS. New PBS was added and a scratch was performed through the centre of each well using a sterilised pipette tip. The PBS was then removed which also removed any dead or detached cells. Serum free medium was added to each well so migration was being measured as opposed to proliferation. Scratches were visualised with x4 objective on a Motic AE2000 light microscope (Motic, Barcelona, Spain) and images were taken straight away at 0 hours, and then further images were taken at 12 hour intervals until 72 hours with MShot Image Analysis System. Migration of cells were compared between each condition.

2.10.4 Statistical Analysis

Images taken on the microscope were analysed using Image J Software with Wound Healing Assay plug-in. The plug-in determined the area and widths of scratches which were then used to determine percentage wound closure over time and rate of cell migration. The percentage wound closure was calculated by the area of a scratch at different time points subtracted from the area of the original scratch (0 hr) divided by the area of the original scratch (0 hr) and multiplied by 100. The calculation for percentage wound closure was as follows:

$$\frac{\text{(Initial wound area – Wound area after 'n' hours of initial scratch)}}{\text{Initial wound area}} \times 100$$

The rate of cell migration used the widths of the scratches and was calculated by the width of a scratch at any time point subtracted from the original scratch (0 hr)

divided by the number of hours between the two scratches. The calculation for the rate of cell migration was as follows:

$$\frac{\text{Average of initial wound width} - \text{Average wound width after 'n' hours}}{\text{Time span between scratches ('n' hours)}}$$

Statistical analysis on the percentage wound closure and rate of cell migration images was performed using Prism (GraphPad Software, San Diago, USA). The data was deemed normally distributed and ANOVA (parametric data) was used to determine significance. Comparisons between the cell types was done by a Tukey's multiple comparisons test. A P-value of ≤ 0.05 was deemed significant.

Chapter 3

Expression of SorL1, Aβ40 and Aβ42 in Glioblastoma Cells

3 Chapter 3 – Expression of SorL1, Aβ40 and Aβ42 in Glioblastoma Cells

3.1 Background

A reduction of SorL1 protein expression has been found to cause increased risk of Alzheimer's disease (Andersen *et al.,* 2005). One function of SorL1 involves returning APP to the Golgi from the endosomes, thus preventing Aβ production (Willnow and Andersen, 2013; Schmidt *et al.,* 2017). When a reduction of SorL1 occurs, such as in Alzheimer's disease, shuttling of APP is decreased, allowing more cleavage of Aβ40 and Aβ42 to occur (Schmidt *et al.,* 2017).

In this chapter, a range of methods including immunocytochemistry, western blotting, and ELISA were used to determine expression of SorL1, Aβ40 and Aβ42 in both immortalised cell lines and primary patient derived cells.

3.1.1 Aβ Expression

Given the role of APP in familial Alzheimer's disease and the increase of Aβ plaques in the brains of individuals with Alzheimer's disease, a great deal of research has been performed on the dynamics of Aβ expression. Aβ40 is the most abundant form, approximately making up 80-90% of Aβ, followed by Aβ42 accounting for between 5 and 10% of Aβ, which is the more aggregate prone species of Aβ that increases in production within the Alzheimer's disease brain (Murphy and LeVine, 2010). These two species of Aβ are being investigated in this chapter, Aβ40 and Aβ42.

Even though Aβ is most commonly associated with Alzheimer's disease, Aβ expression has been investigated in various forms of cancer. The precursor to Aβ peptide, APP, has been shown to accumulate and have increased expression in pancreatic and breast cancer tumours (Hansel *et al.,* 2003; Tsang *et al.,* 2018).

An increase in Aβ levels have also been shown in certain cancers as plasma Aβ40 and Aβ42 peptide levels were increased in oesophageal cancer, colorectal cancer, hepatic cancer and lung cancer when compared to matched controls (Jin *et al.,* 2016). In addition to increased plasma Aβ levels in numerous cancers, expression of Aβ in and around cancerous tumours has been shown in glioma (Zayas-Santiago *et al.,* 2020). Aβ expression has been explored in xenograft mouse models implanted with glioma cells. Immunostaining of brain slices showed that Aβ peptide was present in glioma tumours and blood vessels supplying the tumour, and also large amounts of Aβ peptide was also found surrounding nearby ruptured blood vessels (Kucheryavykh *et al.,* 2019; Williams, 2019). A later study showed increased expression of Aβ in adult glioma, and specifically in cells around blood vessels and in perivascular spaces. However, they could not determine whether the Aβ expression was due to a protective mechanism against the tumour or whether the Aβ peptide was produced by the glioma cells themselves (Zayas-Santiago *et al.,* 2020). The isoform of Aβ expressed was also not determined.

3.1.2 SorL1 Expression

SorL1 expression was originally investigated in Alzheimer's disease where it controls how APP is processed and the relative levels of Aβ isoforms; Section 1.2.6.1 (Andersen *et al.,* 2005). Multiple studies have demonstrated a direct link between SorL1 and Alzheimer's disease with reduced SorL1 expression in mouse models initiating the characteristic pathology of increased brain Aβ, to levels similarly seen in Alzheimer's disease patients (Andersen *et al.,* 2005; Dodson *et al.,* 2008; Rohe *et al.,* 2008). Moreover, SorL1 overexpression resulted in decreased Aβ concentration within the brain (Caglayan *et al.,* 2014).

In addition to Alzheimer's disease, SorL1 has also been implicated in various cancers. Whilst in Alzheimer's disease, SorL1 expression is reduced, in cancer, the opposite is seen. An increase of SorL1 expression was found in HER2 breast cancer, with SorL1 aiding in regulating expression of HER2, giving the protein an oncogenic likeness (Pietilä *et al.,* 2019). Following the trend of an increase in SorL1, expression was found in cancers of the pancreas and bile duct as patients'

bile samples showed a significant increase in SorL1, and SorL1 levels were especially elevated during the peak of proliferation (Terai *et al.,* 2016). An increase of expression of SorL1 was also found in the cell membrane of leukemic cells in acute leukaemia patients, and an increase of SorL1 was found in the serum of non-Hodgkin's lymphoma (Fujimura *et al.,* 2014; Sakai *et al.,* 2012). Even though SorL1 expression has been explored in peripheral cancers and is even known to have a key function within the CNS, SorL1 expression has not yet been explored in glioma brain tumours.

To address whether Aβ and SorL1 expression is altered in glioma, the work in this chapter will determine expression of Aβ40, Aβ42 and SorL1 in glioma cell lines and PD cells through immunocytochemistry, western blotting and ELISA.

3.2 Results – Expression

3.2.1 Characterising Glioblastoma Cell Growth

Cells were seeded on a 24 well plate with an initial cell seeding density of 2000 cells per well and counted daily to determine growth characteristics and inform optimal cell seeding density; Section 2.2.5. U87MG cells, the glioblastoma stage IV cell line, entered exponential phase on day 4 until day 9 when the cell growth started to plateau (Figure 3.1A). Stage II astrocytoma cell line 1321N1 entered the exponential stage at day 3, however, after 10 days, there was not any sign of growth plateauing (Figure 3.1B). In comparison the control foetal astrocytes SVGp12 cell line showed exponential growth between day 6 and day 9, and plateau began at day 10 (Figure 3.1C). The 1321N1 cell line showed very robust growth and proliferation compared to U87MG and SVGp12 cells (Figure 3.1D). The doubling time for 1321N1, U87MG and SVGp12 cells was determined to be 28.0, 30.9 and 39.4 hours respectively.

Characterising cell growth also allowed optimal seeding densities to be determined. It was noted that for that for U87MG and SVGp12 cells between 10,000 and 25,000 cells needed to be seeded while 1321N1 cells required

between 25,000 and 75,000 cells be seeded. These densities resulted in 70-80% confluency 24 hours after seeding.

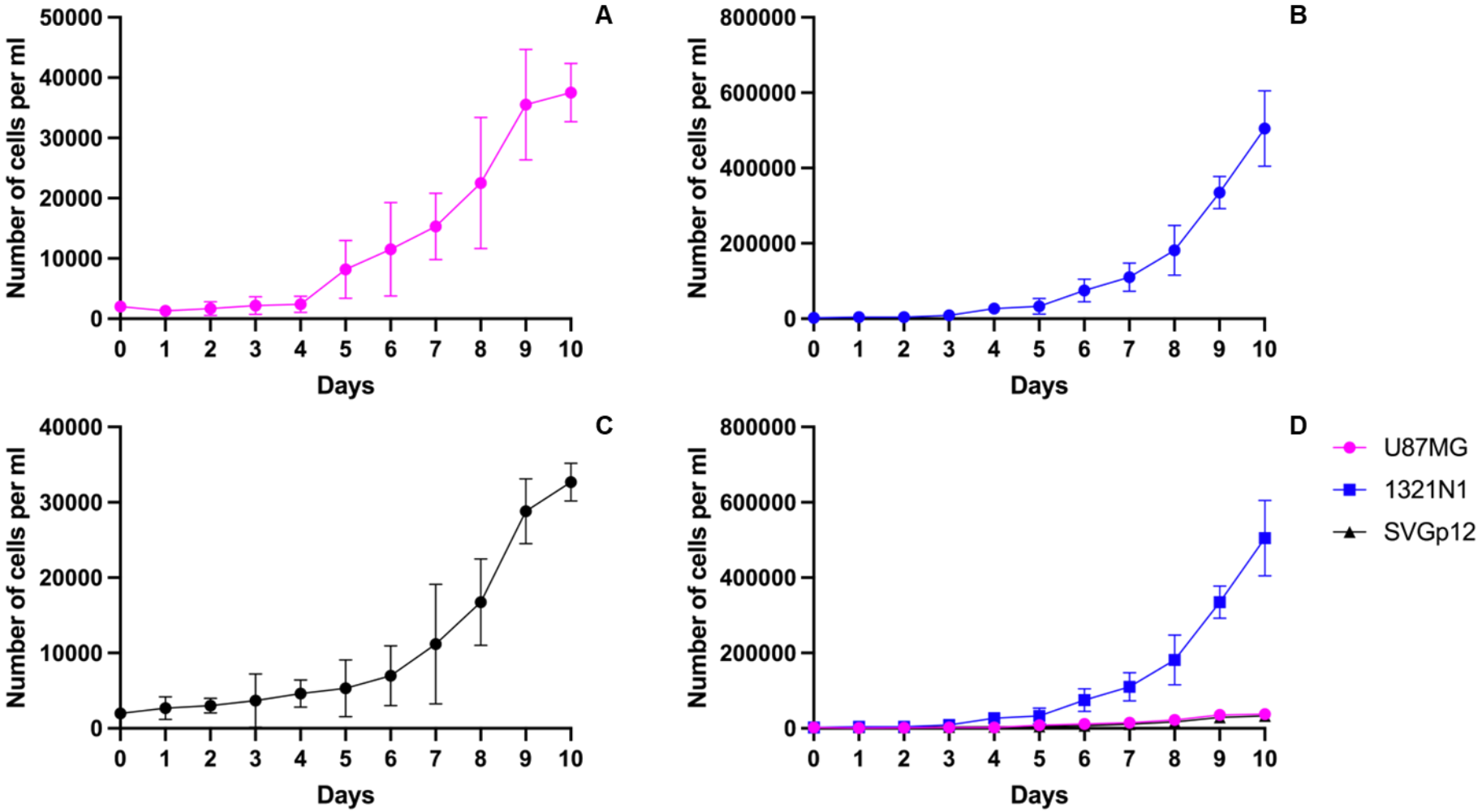

Figure 3.1 – Growth analysis for human cell lines.

10 day growth curves for U87MG cells (A), 1321N1 cells (B), SVGp12 cells (C) and overlaid U87MG, 1321N1 and SVGp12 cells (D).

Understanding the growth characteristics of cells allowed later experiments to be timed so that cells reached confluency together or understand how many cells to seed for immunocytochemistry studies.

Growth curves were also determined for the primary PD301 cells, PD304 cells and NHA cells; Section 2.2.5. PD301 cells began the exponential growth at day 4 and a plateau phase was not observed (Figure 3.2A). The same growth pattern was observed in PD304 cells, entering the exponential stage at day 5 with subsequent continuous growth without plateauing (Figure 3.2B). In contrast, NHA cells took longer to reach exponential stage (day 6) and started to plateau around day 9 and day 10 (Figure 3.2C). NHA cell growth was less robust at day 10 with lower cell densities reached.

The growth of PD301 cells and PD304 cells were similar with doubling times of 42.1 hours and 40.9 hours respectively. In contrast, NHA cells had the slowest doubling time at exponential growth of 53.8 hours, and the lowest cell number at day 10 (Figure 3.2).

For PD301 and PD304 cells, the optimal seeding density was determined to be between 15,000 and 30,000 cells, whilst for NHA cells, it was between 10,000 and 20,000 cells. These seeding densities allowed for 70-80% confluency 24 hours after seeding.

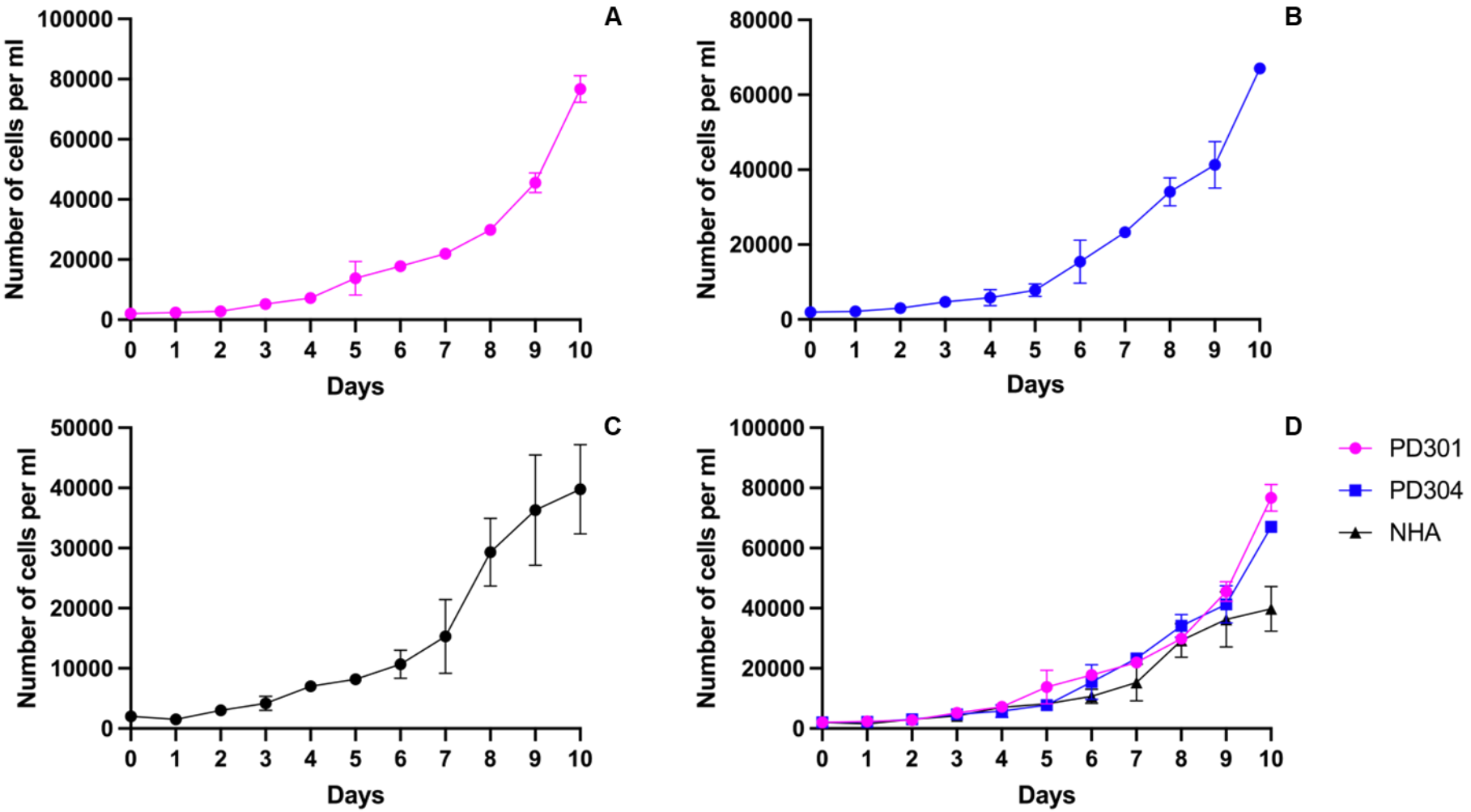

Figure 3.2 – Growth analysis for primary cells.

10 day growth curves for PD301 cells (A), PD304 cells (B), NHA cells (C) and overlaid PD301, PD304 and NHA cells (D).

3.2.2 Expression of Aβ40, Aβ42 and SorL1 in Immortalised Cell Lines

The initial experiment was to characterise and validate Aβ40, Aβ42 and SorL1 antibodies and confirm expression by immunocytochemical staining of fixed immortalised human cell lines U87MG, 1321N1 cells and SVGp12 cells. Cells were incubated with primary antibodies for Aβ40, Aβ42 or SorL1, and secondary antibody conjugated to AlexaFluor 555 or 488 after being fixed; Section 2.3.

3.2.2.1 Immunocytochemical Expression of Aβ40 in Cell Lines

Immunolabelling of Aβ40 was seen in all immortalised cell lines. Fluorescent signal in U87MG cells was distributed uniformly throughout the cytoplasm and nucleus, while 1321N1 cells showed almost exclusively nuclear fluorescence. SVGp12 cells had both cytoplasmic labelling with a stronger signal seen in the nucleus. See Figures 3.3, 3.4 and 3.5 for representative images. When primary antibody for Aβ40 was omitted, no fluorescence was seen (e.g. Figure 3.3).

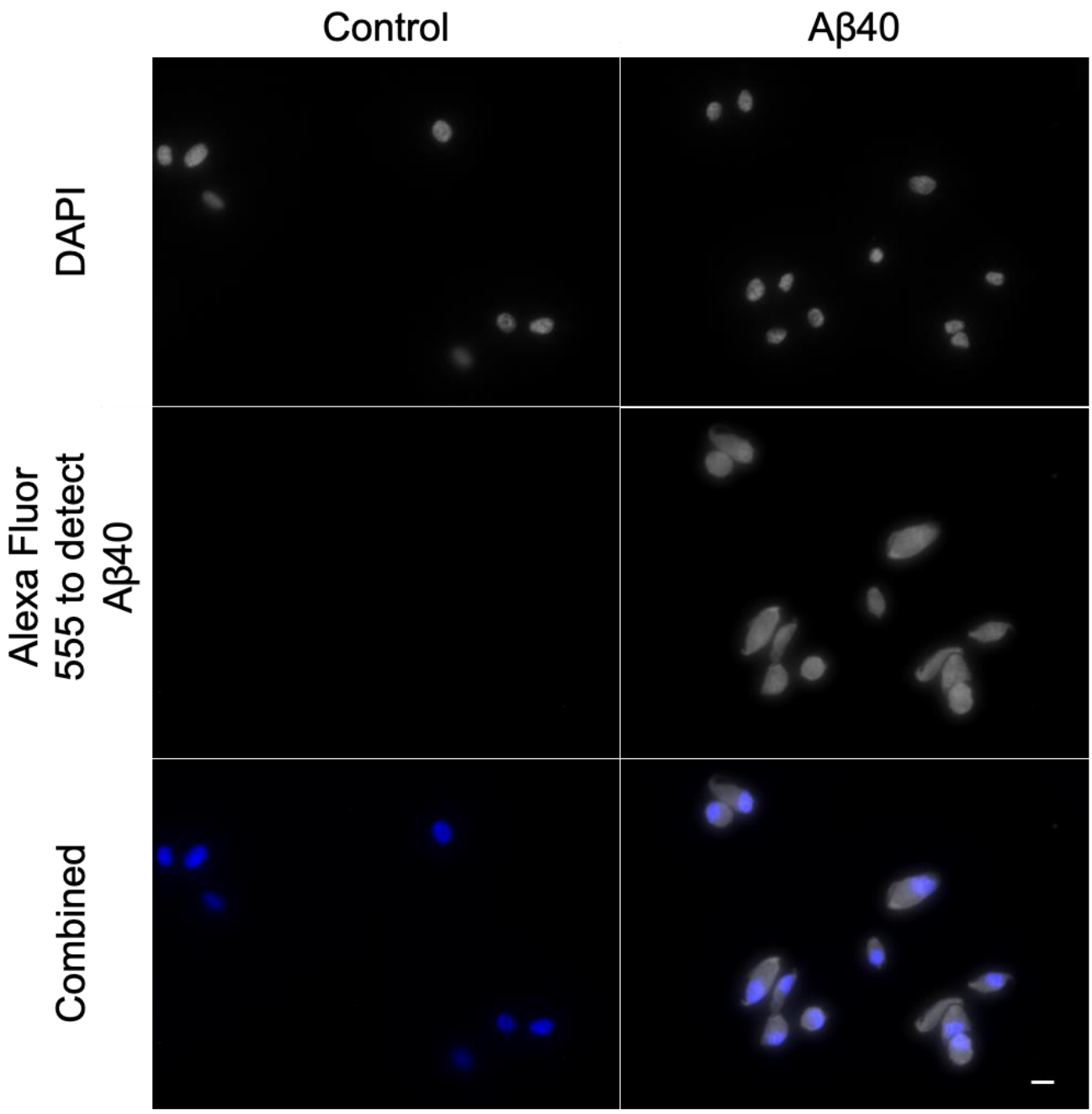

Figure 3.3 – Aβ40 expression in U87MG cells.

Cells stained with Aβ40 antibody and subsequently Alexa Fluor 555 secondary antibody and DAPI (right). Alexa Fluor 555 secondary antibody and DAPI used as a control (Left). N=2. Magnification = x40. Scale bar = 20µm.

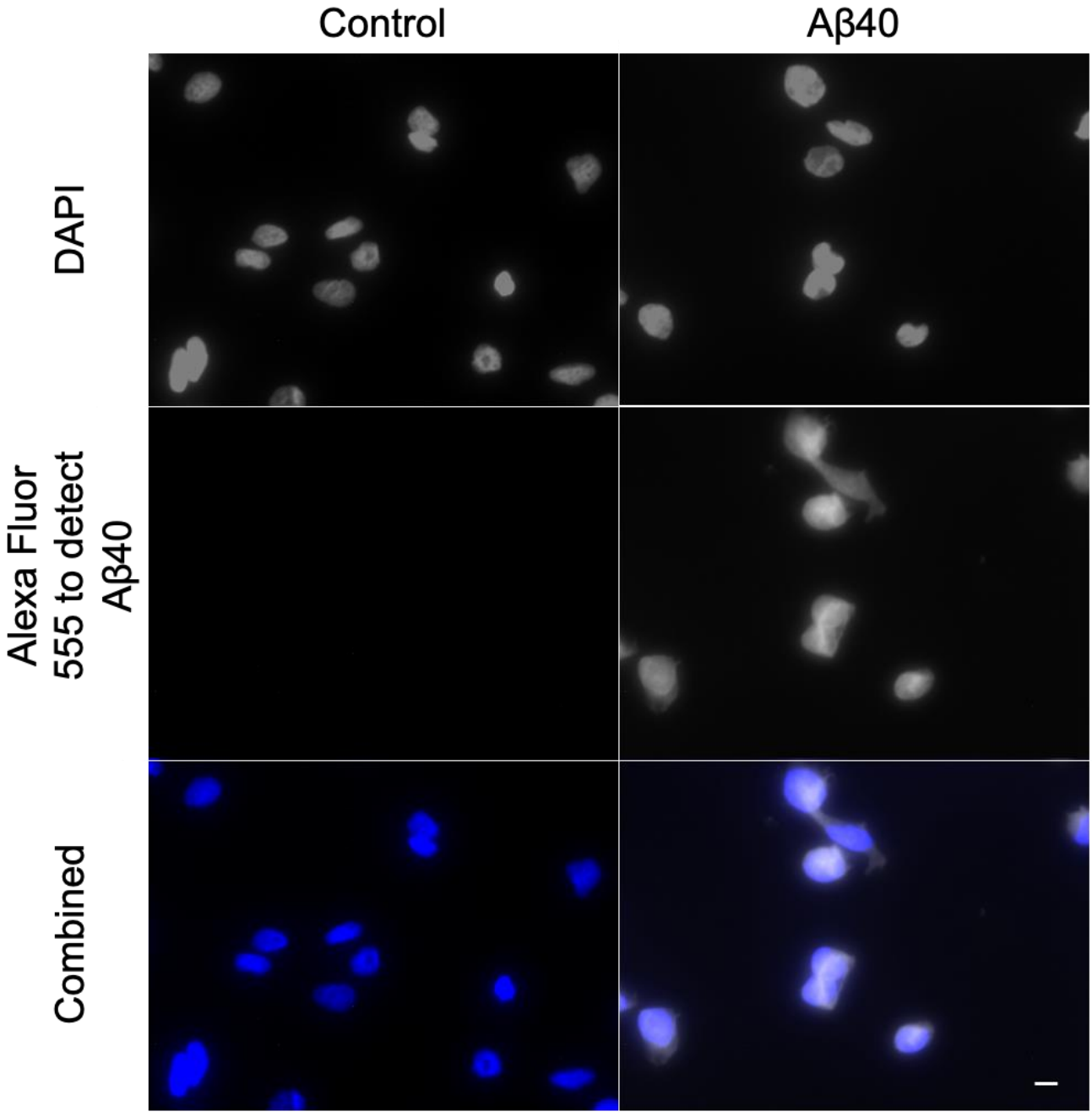

Figure 3.4 – Aβ40 expression in 1321N1 cells.

Cells stained with Aβ40 antibody and subsequently Alexa Fluor 555 secondary antibody and DAPI (right). Alexa Fluor 555 secondary antibody and DAPI used as a control (Left). N=2. Magnification = x40. Scale bar = 20µm.

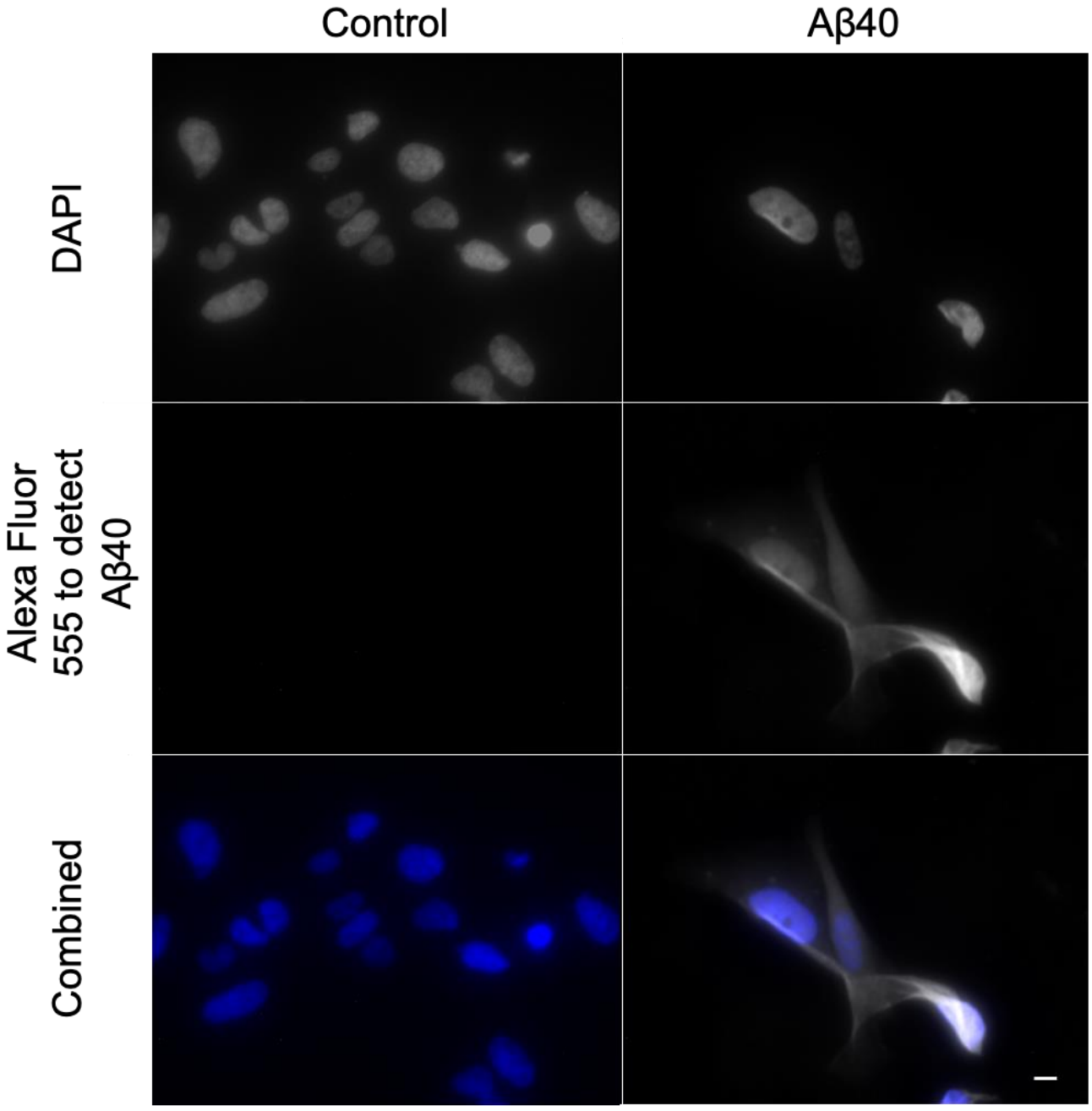

Figure 3.5 – Aβ40 expression in SVGp12 cells.

Cells stained with Aβ40 antibody and subsequently Alexa Fluor 555 secondary antibody and DAPI (right). Alexa Fluor 555 secondary antibody and DAPI used as a control (Left). N=2. Magnification = x40. Scale bar = 20µm.

3.2.2.2 Immunocytochemical Expression of Aβ42 in Cell Lines

Fluorescent immunolabelling of Aβ42 was seen in all immortalised cell lines. Fluorescent signal in U87MG cells was distributed throughout the cytoplasm with greatest intensity at the nucleus. This is in direct contrast to Aβ40 staining in U87MG cells that was not as evident in the nucleus. Similar to the distribution of Aβ40 in 1321N1 cells, Aβ42 fluorescence was almost exclusively seen in the nucleus. SVGp12 cells had both cytoplasmic labelling with a clearly demarcated stronger signal seen in the nucleus. See Figures 3.6, 3.7 and 3.8 for representative images. When primary antibody for Aβ42 was omitted, no fluorescence was seen (e.g. Figure 3.6).

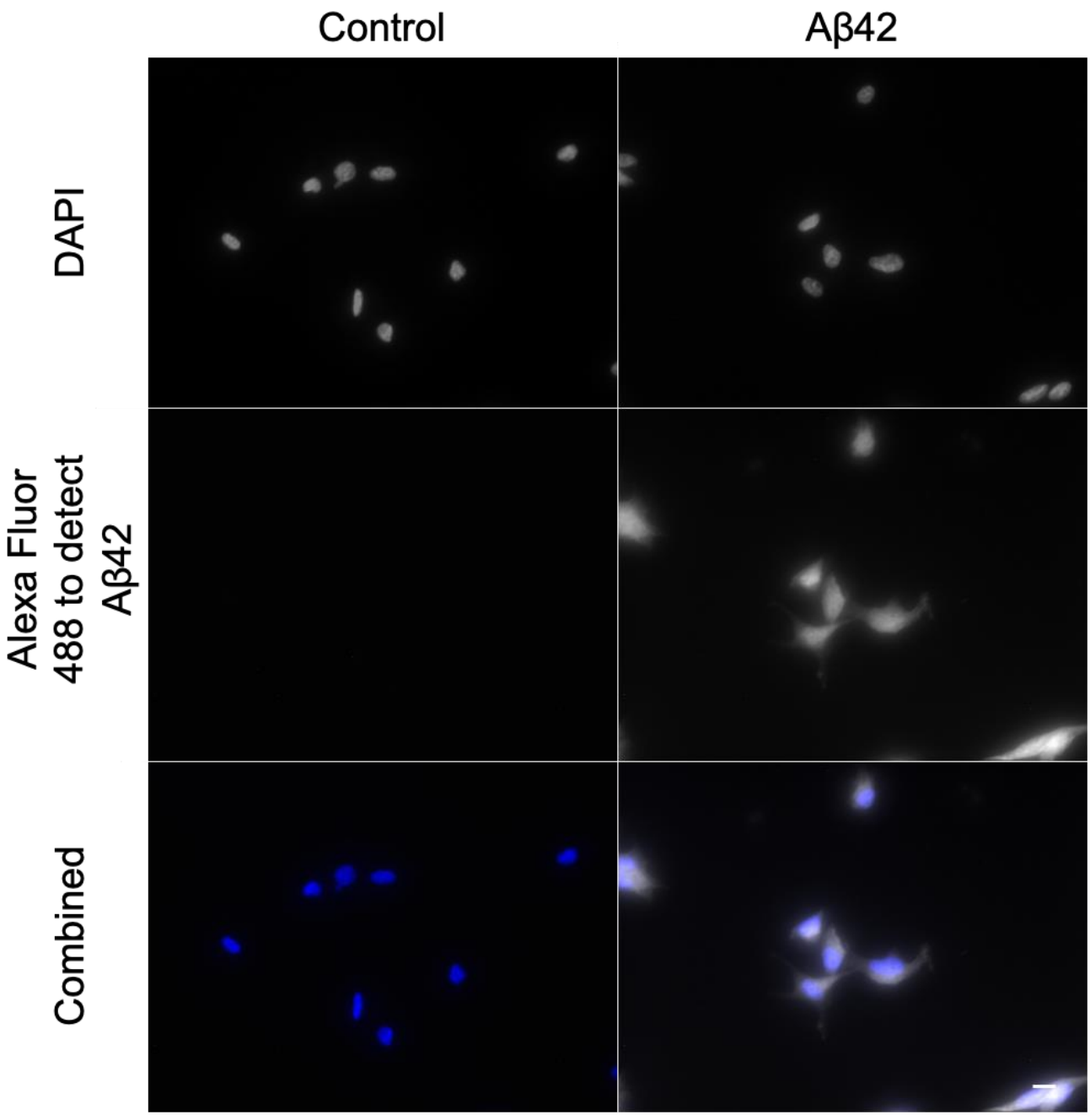

Figure 3.6 – Aβ42 expression in U87MG cells.

Cells stained with Aβ42 antibody and subsequently Alexa Fluor 488 secondary antibody and DAPI (right). Alexa Fluor 488 secondary antibody and DAPI used as a control (Left). N=2. Magnification = x40. Scale bar = 20µm.

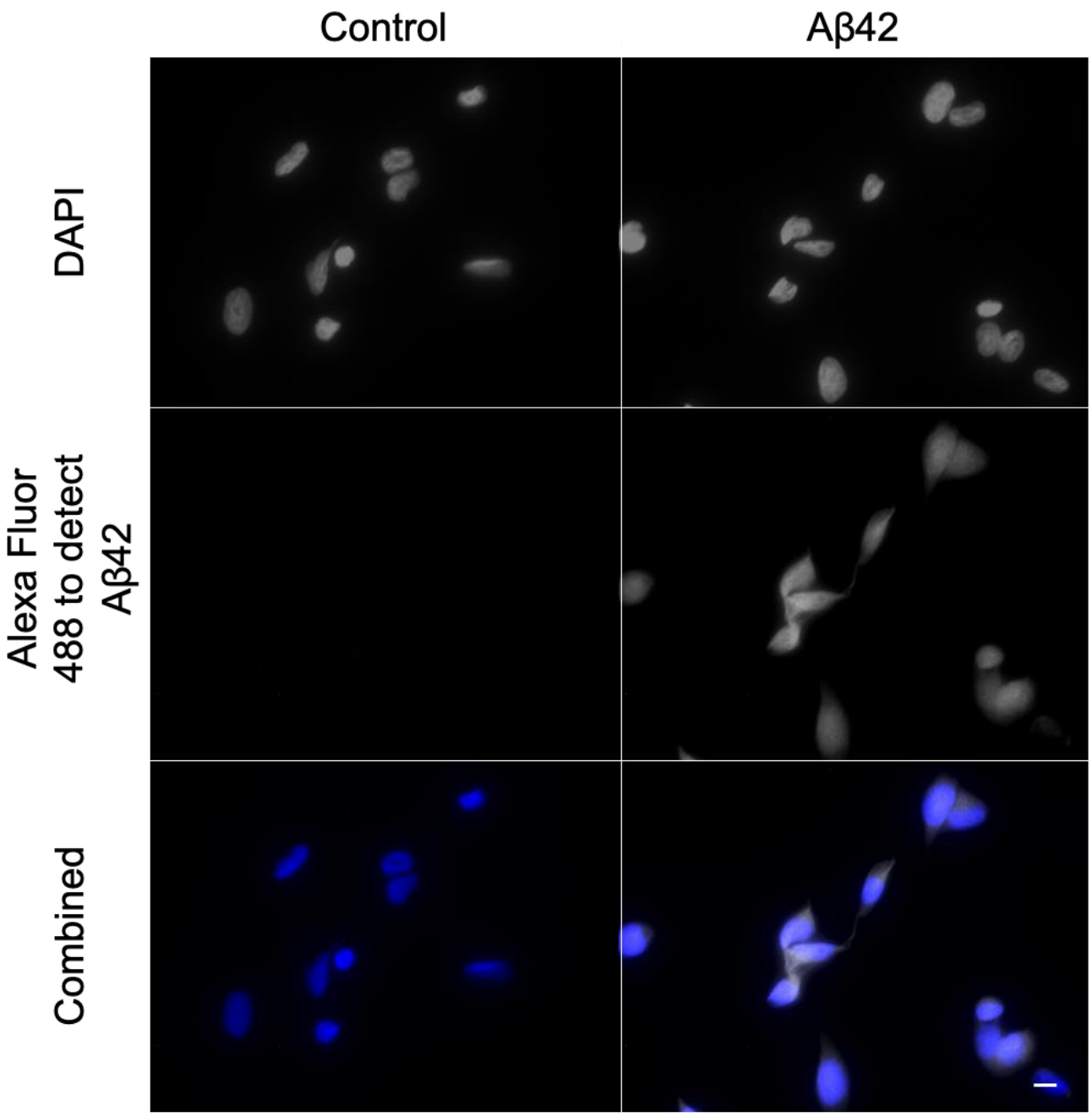

Figure 3.7 – Aβ42 expression in 1321N1 cells.

Cells stained with Aβ42 antibody and subsequently Alexa Fluor 488 secondary antibody and DAPI (right). Alexa Fluor 488 secondary antibody and DAPI used as a control (Left). N=2. Magnification = x40. Scale bar = 20µm.

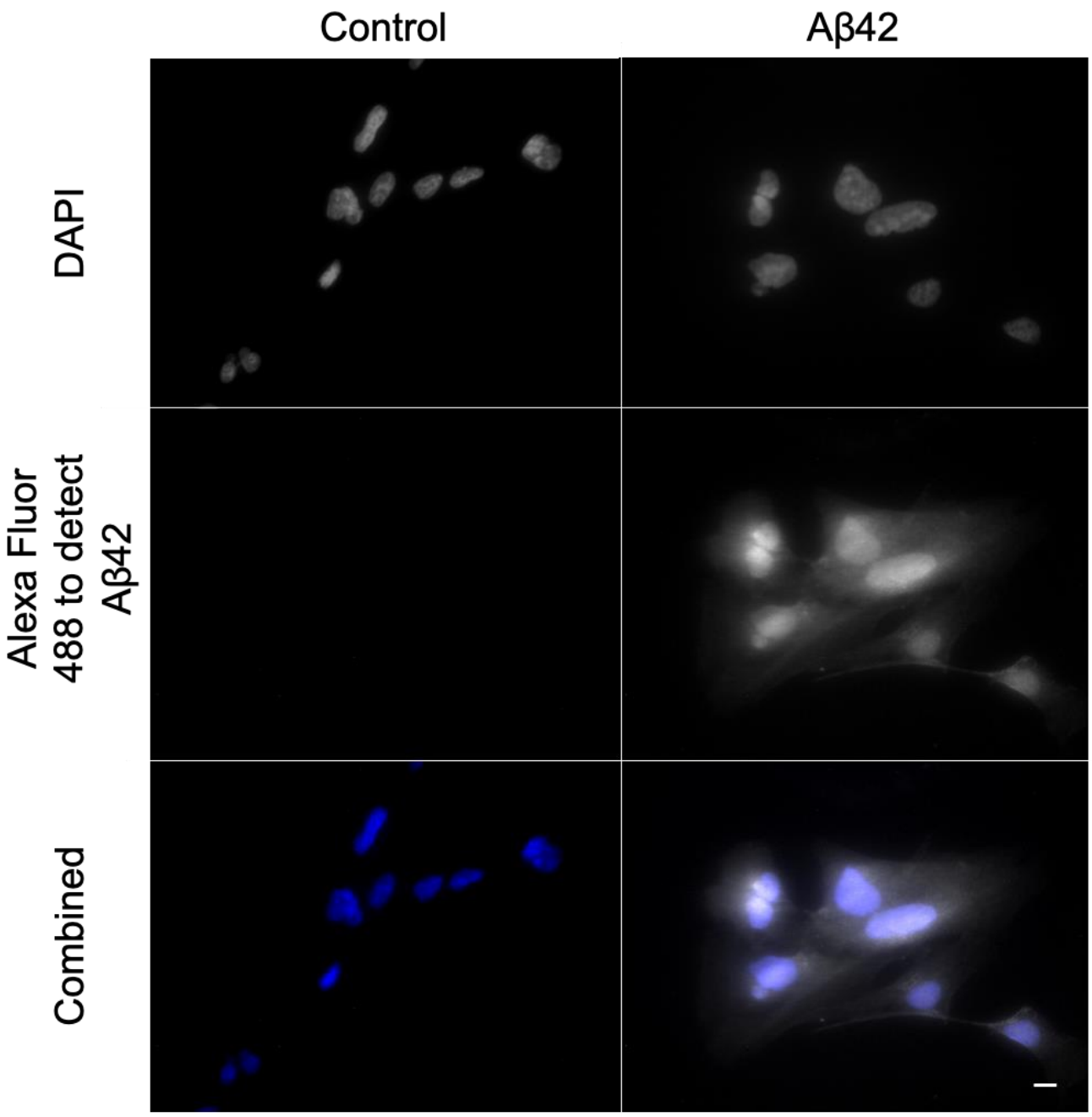

Figure 3.8 – Aβ42 expression in SVGp12 cells.

Cells stained with Aβ42 antibody and subsequently Alexa Fluor 488 secondary antibody and DAPI (right). Alexa Fluor 488 secondary antibody and DAPI used as a control (Left). N=2. Magnification = x40. Scale bar = 20µm.

3.2.2.3 Immunocytochemical Expression of SorL1 in Cell Lines

A markedly similar distribution of fluorescent signal for SorL1 was seen in the three immortalised cell lines U87MG, 1321N1 and SVGp12. Fluorescence was seen throughout the cytoplasm with prominent strong signal over the nucleus. There was noticeable variation in the level of signal in the U87MG and 1321N1 cells, with some cells having intensely labelled nuclei (Figures 3.9 and 3.10). The level of SorL1 fluorescence in the SVGp12 cells was noticeably less than in U87MG or 1321N1 cells, but the cytoplasmic distribution with nuclear enrichment was still evident (Figure 3.11). When primary antibody for SorL1 was omitted, no fluorescence was seen (e.g. Figure 3.9).

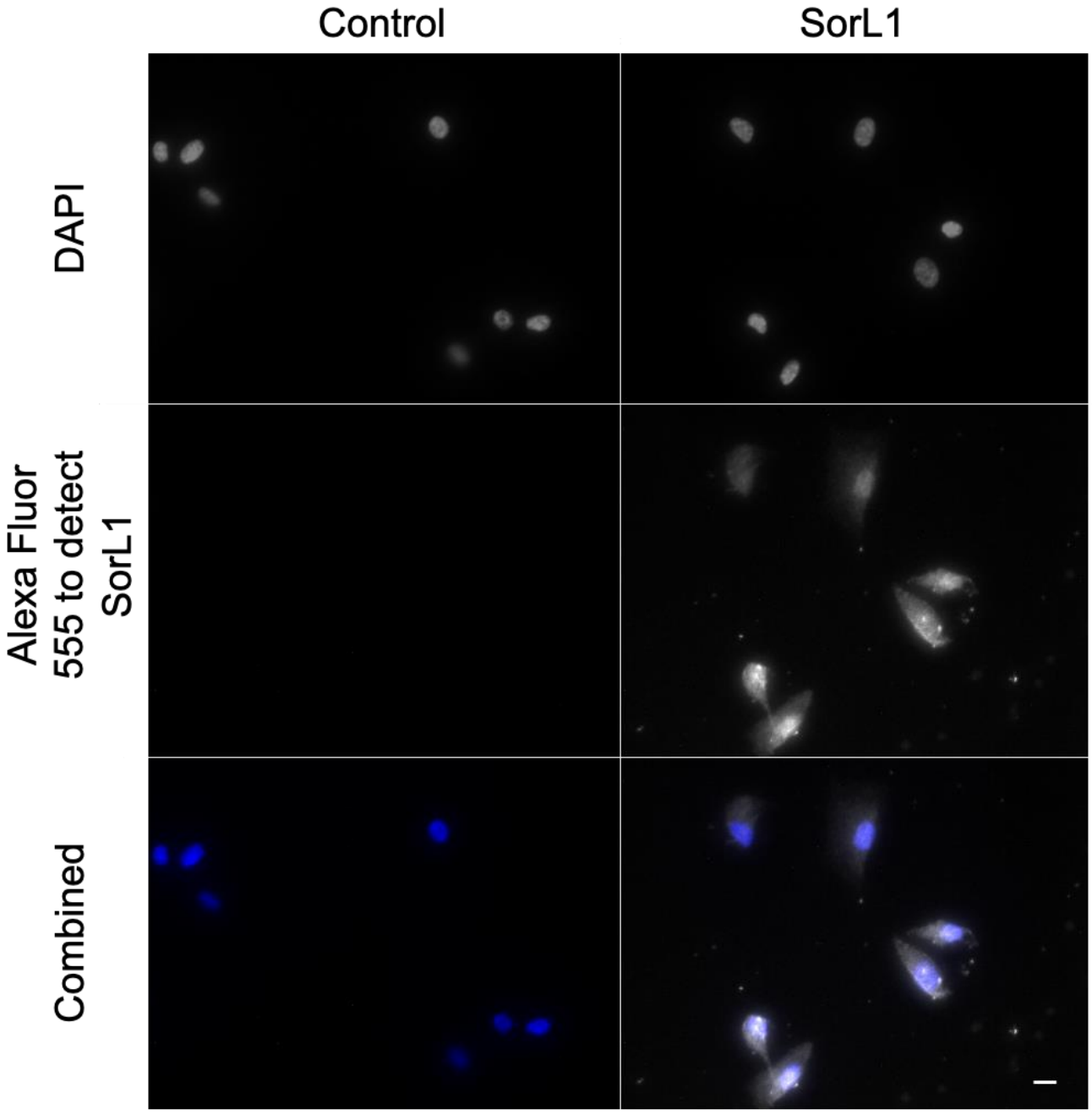

Figure 3.9 – SorL1 expression in U87MG cells.

Cells stained with SorL1 antibody and subsequently Alexa Fluor 555 secondary antibody and DAPI (right). Alexa Fluor 555 secondary antibody and DAPI used as a control (Left). N=2. Magnification = x40. Scale bar = 20µm.

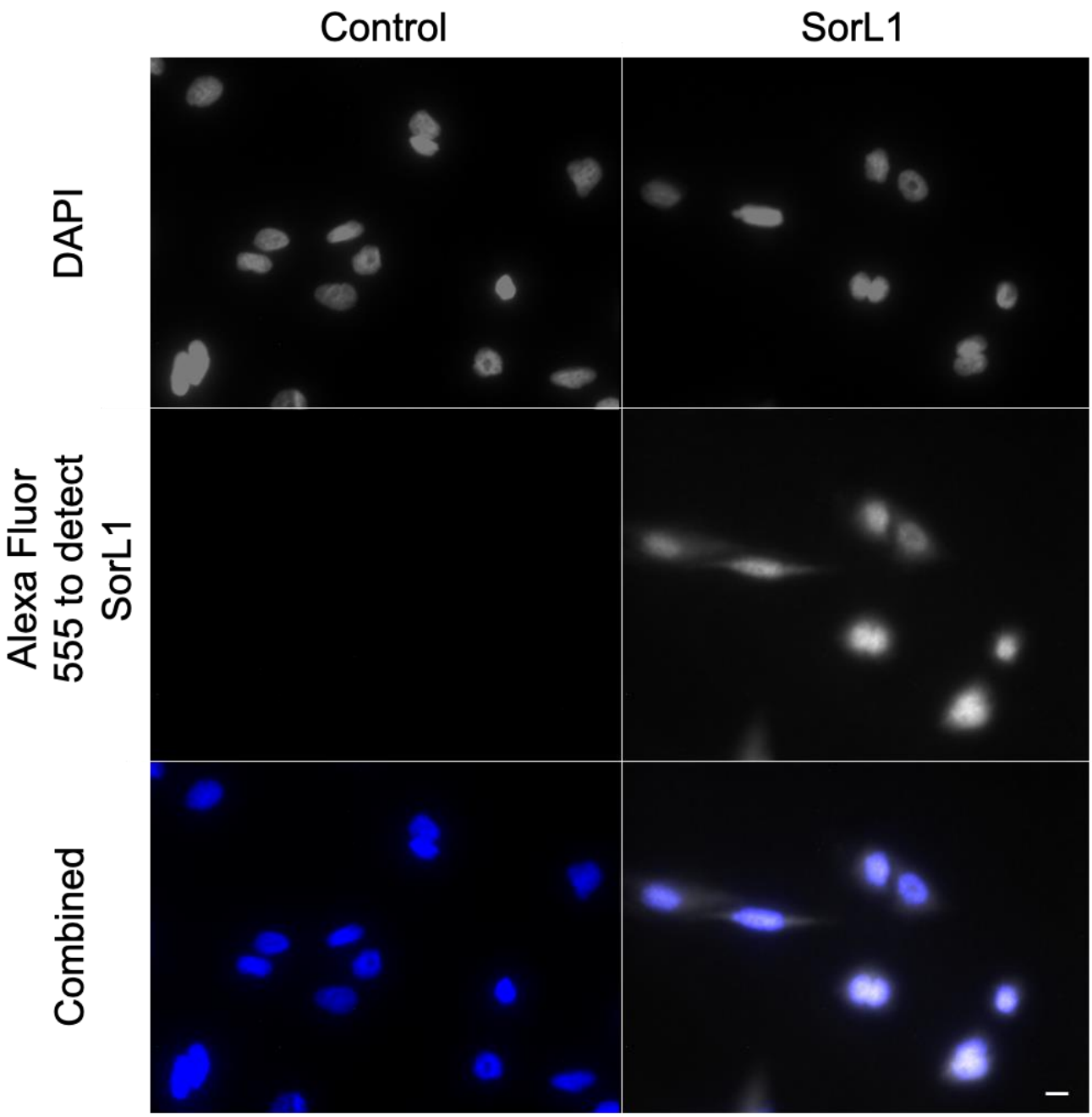

Figure 3.10 – SorL1 expression in 1321N1 cells.

Cells stained with SorL1 antibody and subsequently Alexa Fluor 555 secondary antibody and DAPI (right). Alexa Fluor 555 secondary antibody and DAPI used as a control (Left). N=2. Magnification = x40. Scale bar = 20µm.

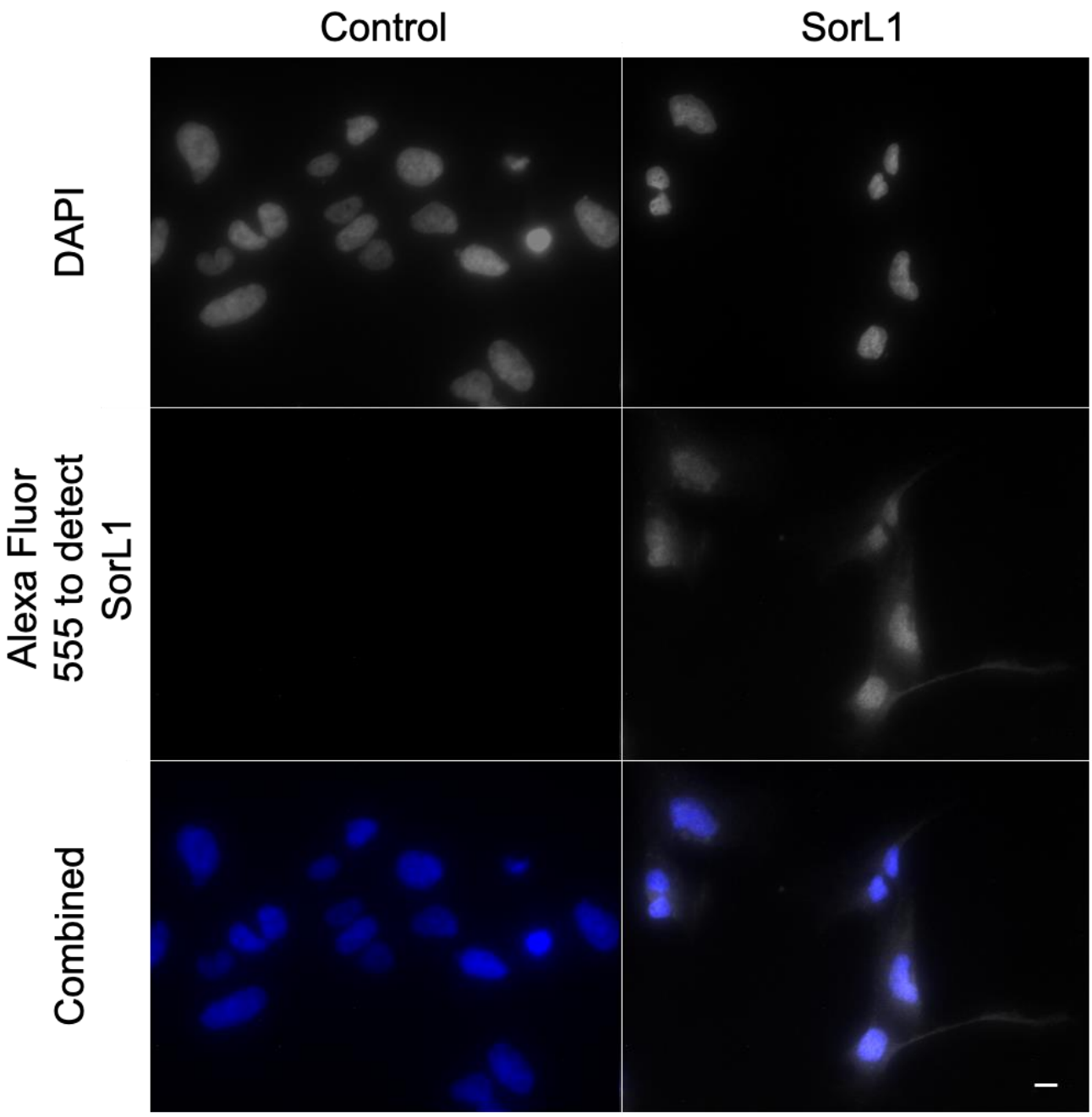

Figure 3.11 – SorL1 expression in SVGp12 cells.

Cells stained with SorL1 antibody and subsequently Alexa Fluor 555 secondary antibody and DAPI (right). Alexa Fluor 555 secondary antibody and DAPI used as a control (Left). N=2. Magnification = x40. Scale bar = 20µm.

3.2.2.4 Quantification of SorL1 Protein in Cell Lines

Western blotting was used to quantify SorL1 expression in lysates from U87MG, 1321N1 and SVGp12 cell lines. Three passages of each cell type underwent the western blotting protocol and probed for SorL1 and β-actin as loading control; Section 2.5. A band corresponding to SorL1 was seen around 250 kDa, consistent with the known molecular weight of SorL1 (Motoi *et al.,* 1999) (Figure 3.12).

Lysates from U87MG cells produced an intense SorL1 band, with less present in 1321N1 cell lysates and almost absent in SVGp12 cell lysates. Western blotting for human immortalised cell line lysates was repeated three times with similar relative levels between the same cell type at each repeat. Full blot for western blot is appended; Appendix 1, Figure A1.1.

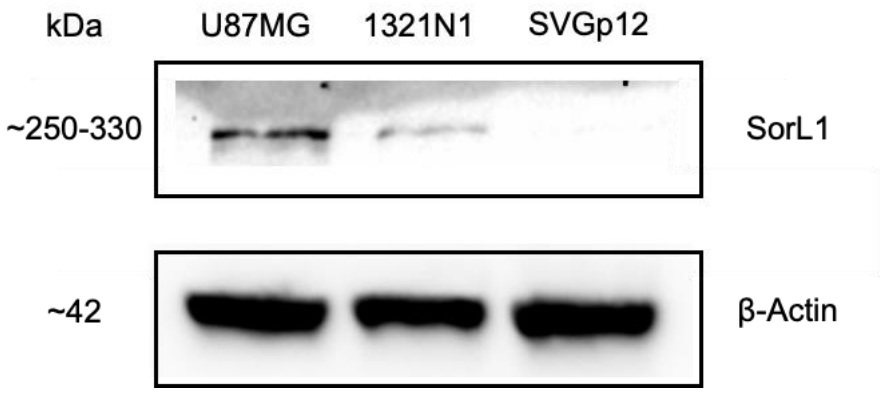

Figure 3.12 – SorL1 expression in U87MG, 1321N1 and SVGp12 lysates.

Western blot of SorL1 at 250 kDa (top) and β-actin at 42 kDa (bottom) in U87MG, 1321N1 and SVGp12 lysates. 10µg of protein was loaded. (N=3).

Quantification took place to determine significance. Densitometric analysis confirmed SorL1 expression relative to β-actin expression was approximately five-fold higher in U87MG cells than 1321N1 cells and approximately hundred-fold higher than SVGp12 cell ($p<0.01$ Tukey's test, N=3, Figure 3.13). There was no significant difference in SorL1 expression between 1321N1 cells and SVGp12

cells, although a trend towards more SorL1 present in 1321N1 than SVGp12 cells could be observed. This shows SorL1 expression occurs in a grade dependent manner in immortalised cell lines with greatest expression in U87MG (stage IV glioblastoma), followed by 1321N1 (stage II astrocytoma) and least expression in SVGp12 (foetal astrocytes).

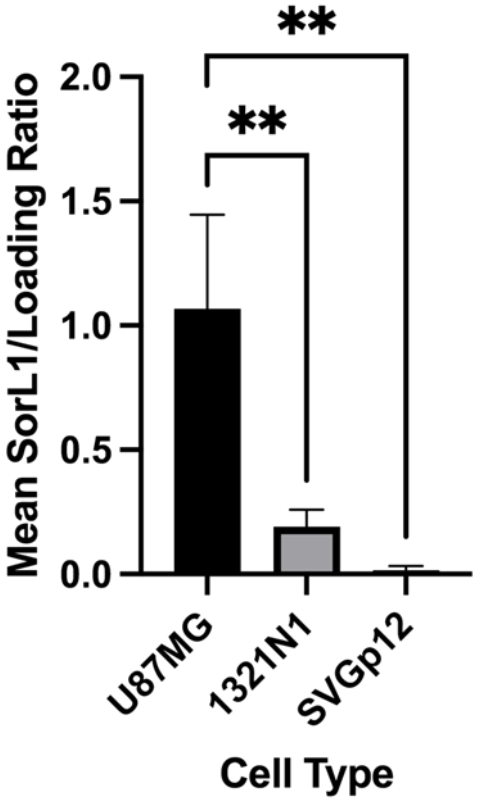

Figure 3.13 – Significantly higher SorL1 expression in U87MG cells than 1321N1 and SVGp12 cells.

SorL1 expression relative to β-actin expression is significantly higher in U87MG cells than SVGp12 cells. P<0.01, Tukey's test. N=3. SorL1 expression relative to β-actin expression is significantly higher in U87MG cells than 1321N1 cells. P<0.01, Tukey's test. N=3.

3.2.2.5 Expression of SorL1 using Bioinformatics

Amplification of SorL1 protein was observed in some studies of lower grade glioma and some studies of glioblastoma. The heat map shows 2% of all studies have an amplification of SorL1 protein (Figure 3.14).

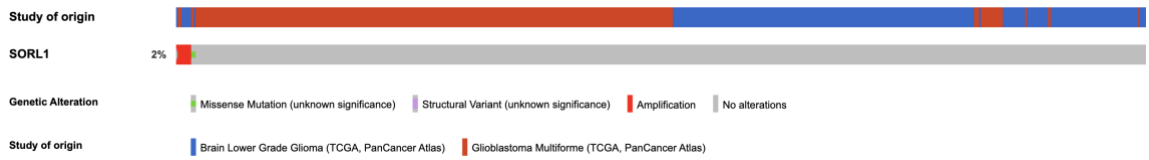

Figure 3.14 – Heat map of SorL1 protein in glioblastoma and lower-grade glioma.

SorL1 protein expression shows amplification in glioblastoma and lower grade glioma. Heat map taken from https://www.cbioportal.org.

Within the TCGA PanCancer Atlas, there were alterations within SorL1 expression observed as amplification, mutation or multiple alterations. There was amplification found in SorL1 protein expression in lower grade glioma with an alteration frequency in over 2% of studies (Figure 3.15). Glioblastoma also showed amplification of SorL1 protein expression with an alteration frequency in approximately 0.75% of studies (Figure 3.15). Mutations of *SORL1* were also found in approximately 0.5% of studies of both lower grade glioma and glioblastoma, whilst multiple alterations of the protein were only observed in lower grade glioma studies (Figure 3.15).

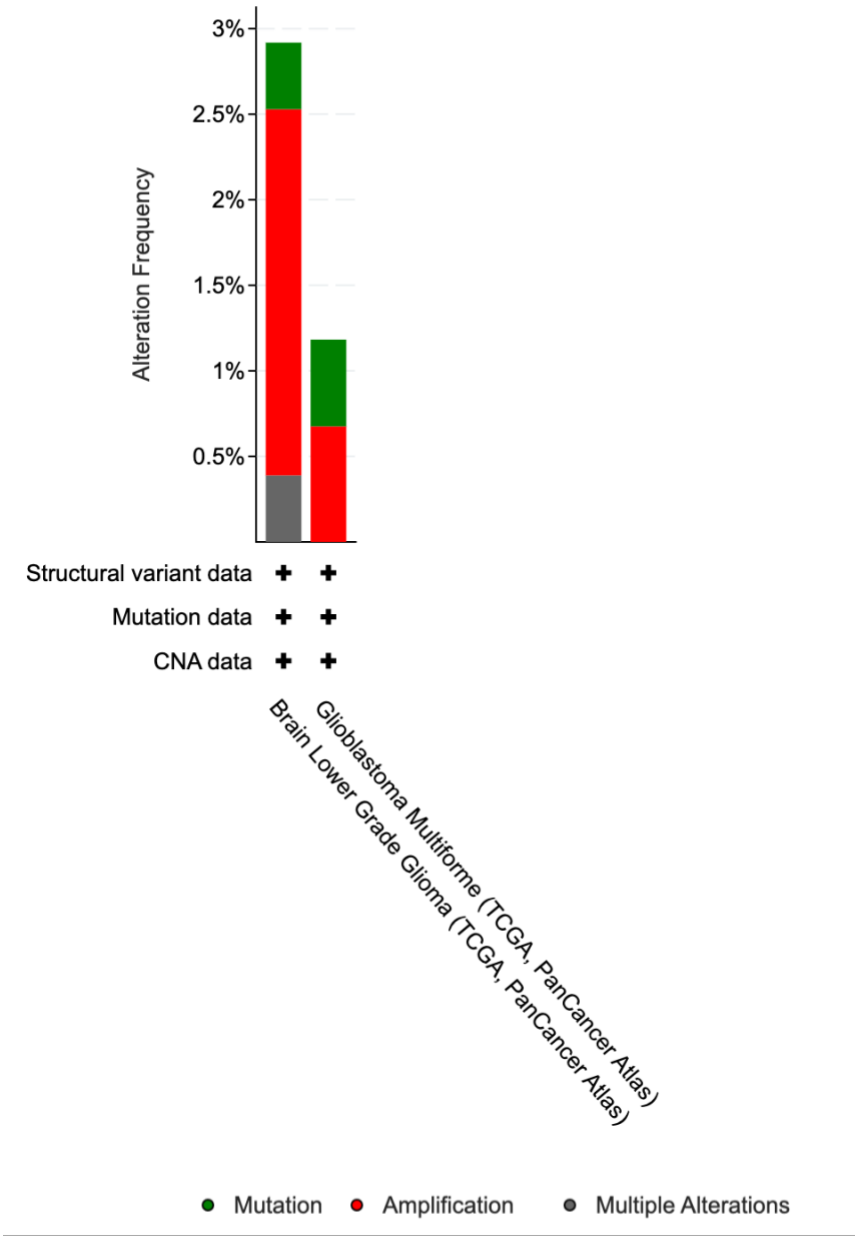

Figure 3.15 – Alteration frequency of SorL1 in lower grade glioma and glioblastoma.

Data shows lower grade glioma and glioblastoma studies showing mutations, amplification and multiple alterations of SorL1. Graph taken from https://www.cbioportal.org.

A survival curve combining glioblastoma and lower grade glioma studies showed a significant increase in probability of overall survival if the glioblastoma or lower grade glioma tumours had an altered SorL1 expression ($P<0.05$) (Figure 3.16).

However, the sample numbers need to be taken into account as the unaltered group had a total of 1,072 patients, compared to the altered group only having 22.

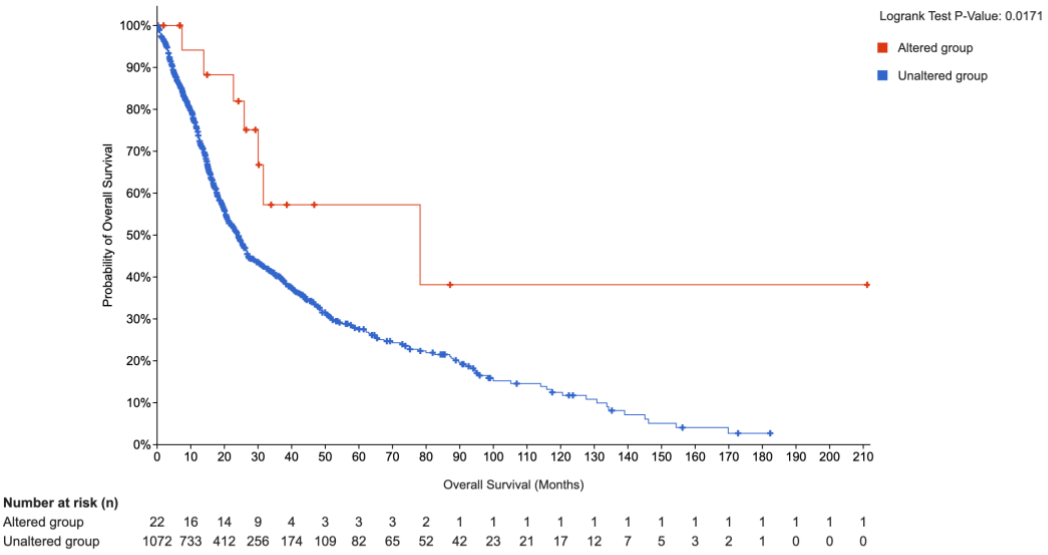

Figure 3.16 – Survival Curve of glioblastoma and lower grade glioma studies with altered SorL1 expression compared to unaltered group.

A probability of overall survival was significantly increased when the patient with glioblastoma or lower grade glioma also had an altered SorL1 expression (P<0.05). Graph taken from https://www.cbioportal.org.

3.2.3 Expression of Aβ40, Aβ42 and SorL1 in Patient Derived Primary Cells

Following observation of amplification of SorL1 protein observed in lower grade glioma and glioblastoma studies, and significantly higher expression of SorL1 protein in the immortalised glioblastoma cell line, a similar experiment was executed with PD cells that originated from stage IV glioblastoma tumours. PD301, PD304 and NHA cells were grown and either seeded onto coverslips in 24 well plates for subsequent immunocytochemistry, or cells were lysed to quantify protein by western blot or ELISA; Sections 2.3, 2.6 and 2.7. Immunocytochemistry experiments were timed to allow direct comparison between primary cell types.

3.2.3.1 Expression of SorL1 in Primary Cells

On reaching confluency, lawns of PD301, PD304 and NHA cells were lysed and the level of SorL1 protein determined by western blot. A band consistent with the molecular weight of SorL1 was seen at approximately 250 kDa (Motoi *et al.,* 1999) (Figure 3.17). Lysates from the PD cells produced a more densely stained band than the normal human astrocytes (Figure 3.17). Full blot for western blot is appended; Appendix 1, Figure A1.2.

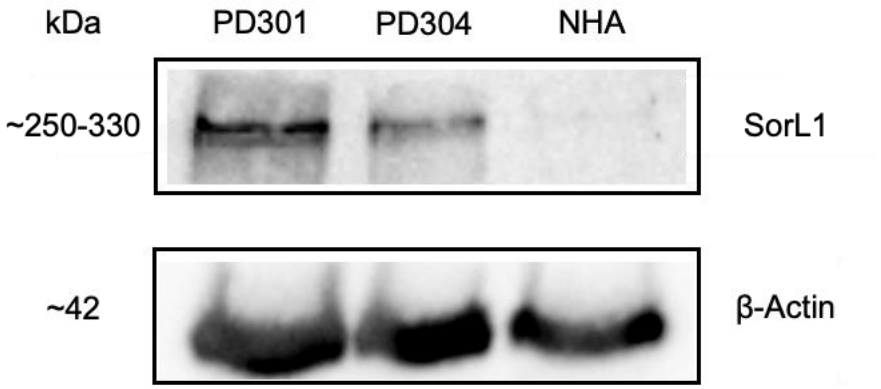

Figure 3.17 – SorL1 expression in PD301, PD304 and NHA cell lysates.

Western blot confirming expression of SorL1 at 250 kDa (top) and β-actin at 42 kDa (bottom) in PD301, PD304 and NHA lysates. 10µg of protein was loaded. (N=3).

Densitometric analysis confirmed that the amount of SorL1 present was approximately 6-fold and 5-fold greater than NHA for PD301 and PD304 respectively ($P<0.01$, Tukey's test N=3, Figure 3.18). Western blotting for human primary cell lysates was repeated in triplicate in lysates from three different passages of cells and similar relative levels were seen between the same cell type at each repeat.

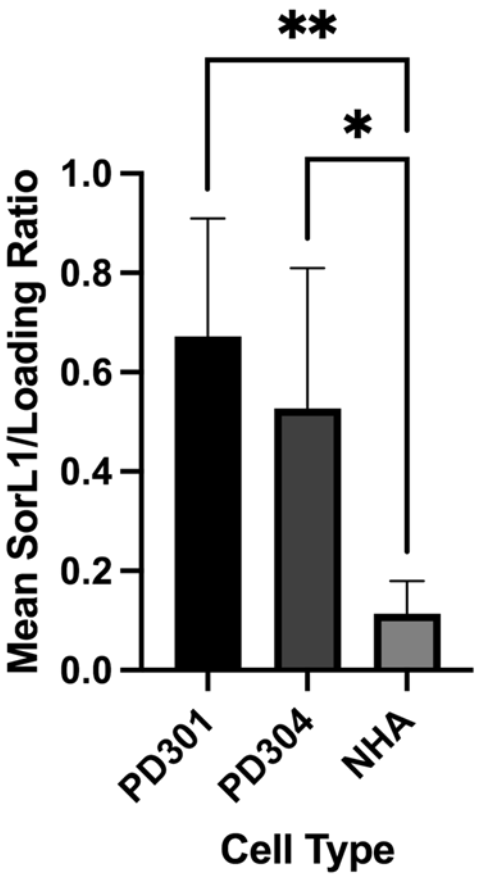

Figure 3.18 – Significantly higher SorL1 expression in PD301 and PD304 cells than NHA cells.

*SorL1 expression relative to β-actin expression is significantly higher in PD301 cells and PD304 cells than NHA cells. *P<0.05, **P<0.01, Tukey's Test. N=3.*

Expression of SorL1 was also quantified by immunocytochemistry in fixed PD301, PD304 and NHA cells. Immunocytochemical fluorescence staining visually supported the western blot result using the SorL1 primary antibody and Alexa Fluor 555 secondary antibody (Figure 3.19). Fluorescence was observed throughout the cytoplasm with higher fluorescence over the nucleus (Figure 3.19) and was consistent with the localisation of SorL1 seen previously in immortalised cell lines. In contrast to the U87MG cells, PD301 and PD304 cells also showed nuclear bright punctate spots of fluorescence.

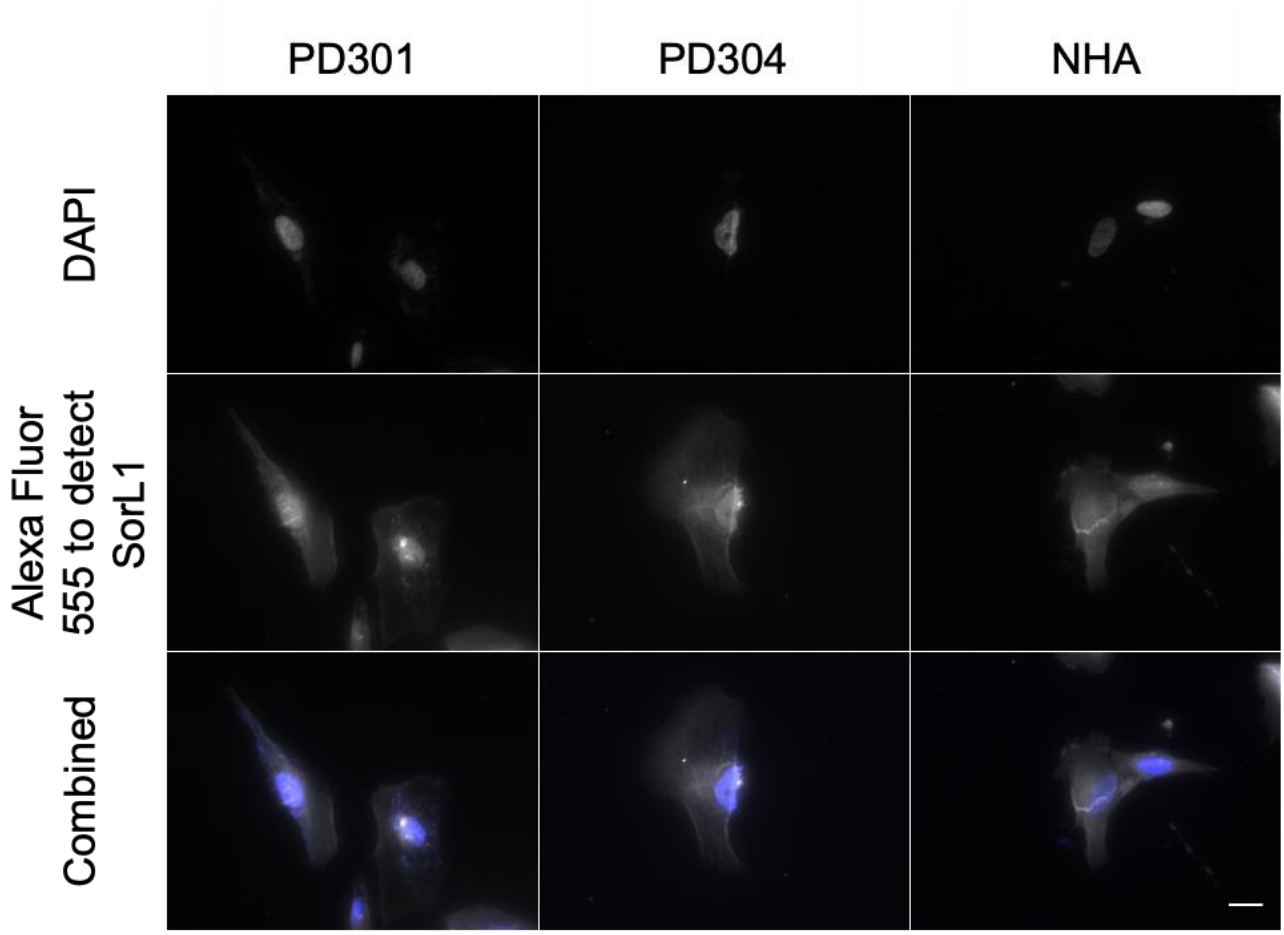

Figure 3.19 – Immunofluorescence confirms SorL1 expression in PD301, PD304 and NHA cells.

SorL1 expression in PD301 (left), PD304 (middle) and NHA (right) cells. Cells stained with DAPI (top), SorL1 antibody and Alexa Fluor 555 secondary antibody (middle) revealing a combined image (bottom). N=3. Magnification = x40. Scale bar = 20µm.

As over 10 images were taken in each of the three replicates of three separate passages of each cell type, quantification of total cell fluorescence was undertaken to compare cell expression. SorL1 expression corrected for the background staining was increased two-fold in both PD301 and PD304 cells compared to NHA cells ($p<0.01$ Tukey's test, N=3) (Figure 3.20).

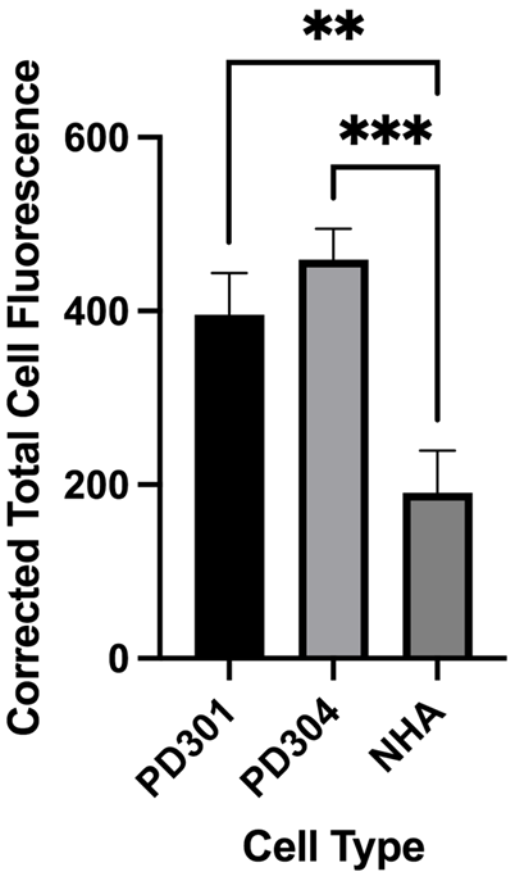

Figure 3.20 – Corrected total cell fluorescence of SorL1 expression is increased in PD301 and PD304 cells.

*Mean SorL1 expression relative to background PD301, PD304 and NHA cells. N>10 images per cell type per replicate. SorL1 expression is significantly higher in PD301 and PD304 cells than NHA cells. **P<0.01, ***P<0.001, Tukey's Test. N=3.*

3.2.3.2 Expression of Aβ40 in Primary Cells

Expression of Aβ40 was quantified by immunocytochemistry in fixed PD301, PD304 and NHA cells. Primary cells were stained with the same Aβ40 antibody and Alexa Fluor 555 secondary antibody as was used for the immortalised cell lines; Section 3.2.2.1. Fluorescence was observed in all cells throughout the cytoplasm with clearly demarcated higher intensity fluorescence in the nucleus. Intense punctate spots were seen around the nucleus in all cell types. No visible discernible differences were noted between cell types (Figure 3.21).

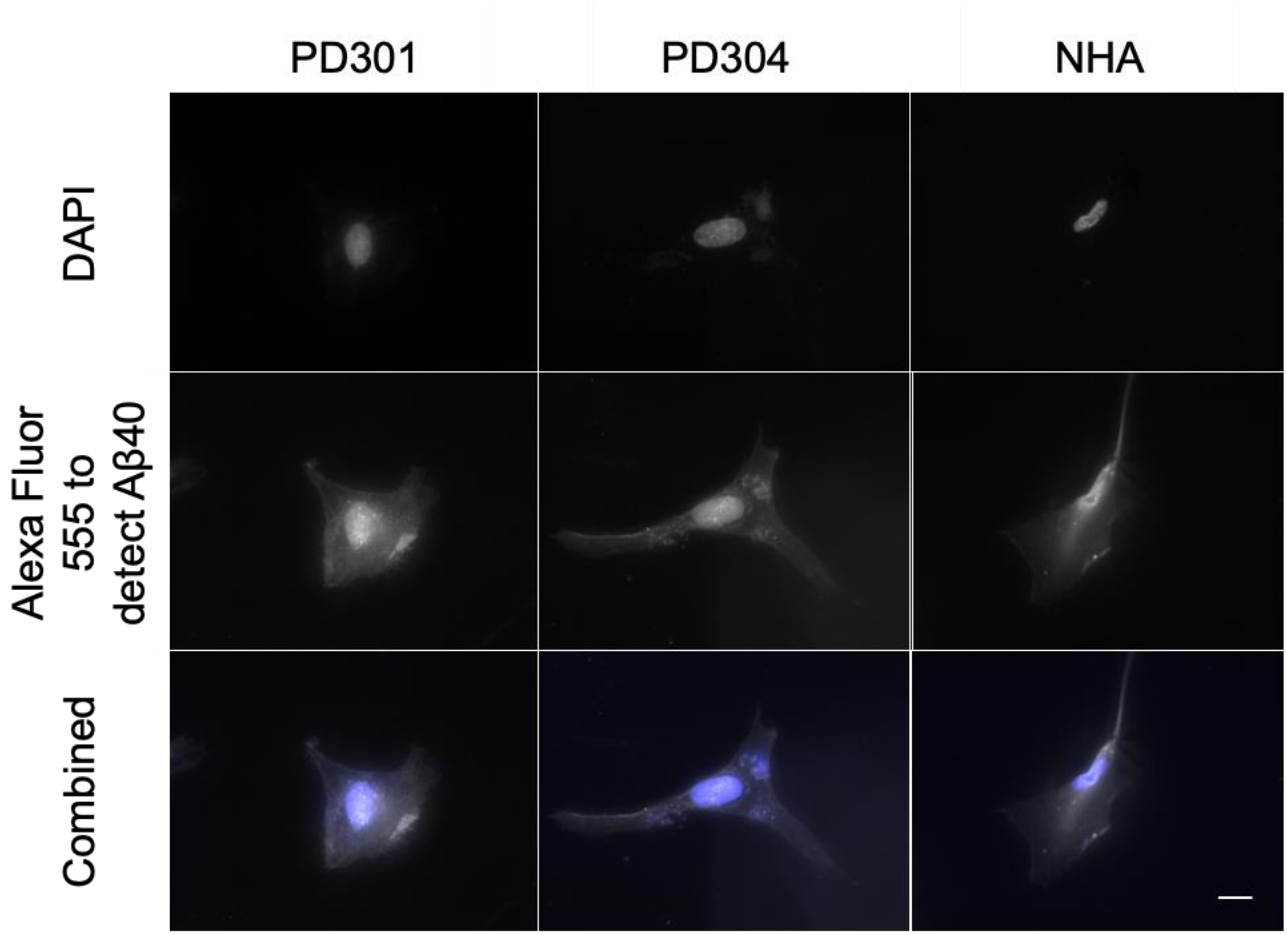

Figure 3.21 – Immunofluorescence confirms Aβ40 expression in PD301, PD304 and NHA cells.

Aβ40 expression in PD301 (left), PD304 (middle) and NHA (right) cells. Cells stained with DAPI (top), Aβ40 antibody and Alexa Fluor 555 secondary antibody (middle) revealing a combined image (bottom). N=3. Magnification = x40. Scale bar = 20µm.

Quantification of fluorescence confirmed there was no significant difference between the three cell types (P>0.05 Tukey's test N=3, Figure 3.22).

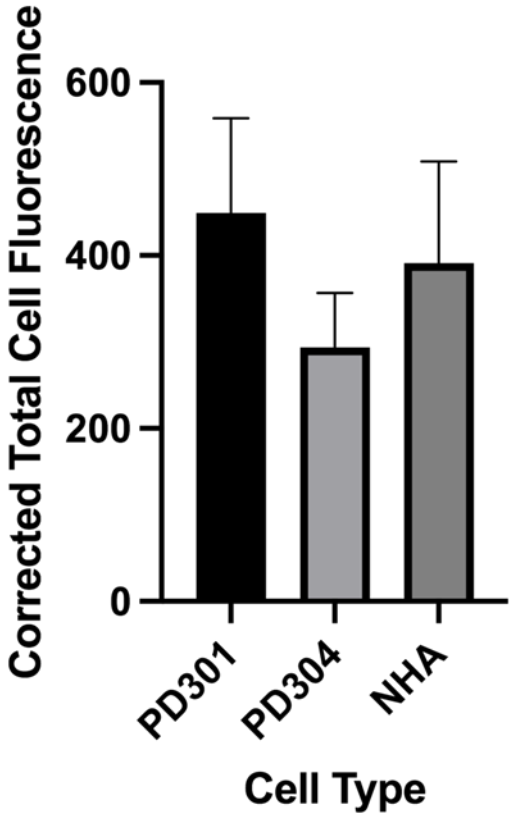

Figure 3.22 – Corrected total cell fluorescence of Aβ40 expression in PD301, PD304 and NHA cells

Mean Aβ40 expression relative to background in PD301, PD304 and NHA cells. N>10 images per cell type per replicate. Aβ40 expression did not differ between PD301, PD304 or NHA cells (P>0.05 Tukey's test N=3).

To confirm Aβ40 expression in the different primary cells, Aβ40 was also quantified by ELISA using a commercially available kit. Cell lysates from three passages of PD301, PD304 and NHA cells were assayed in triplicate and data was expressed as picograms of Aβ40 per mg of total protein; Section 2.7. Comparable amounts of Aβ40 was detected in cell lysates from the different cell types with no significant differences detected between PD and NHA cells (P>0.05 Tukey's test, N=3) (Figure 3.23).

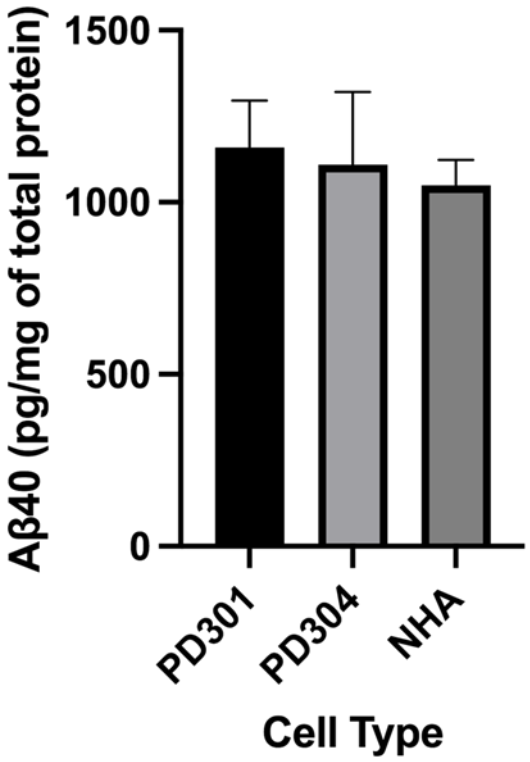

Figure 3.23 - Aβ40 expression in PD301, PD304 and NHA cells

Aβ40 protein in picograms per milligram of total protein of PD301, PD304 and NHA cells. Data collected in triplicate, N=3. Aβ40 expression had no significant difference between PD301 cells and NHA cells and no significant difference between PD304 cells and NHA cells (P>0.05 Tukey's test N=3).

3.2.3.3 Expression of Aβ42 in Primary Cells

Expression of Aβ42 was quantified by immunocytochemistry in fixed PD301, PD304 and NHA cells. Primary cells were stained for Aβ42 antibody and Alexa Fluor 555 secondary antibody that was used for the immortalised cell lines; Section 3.2.2.2. Fluorescence was observed in NHA cells throughout the cytoplasm with clearly demarcated higher intensity fluorescence in the nucleus (Figure 3.24). Cytoplasmic fluorescence for Aβ42 was noticeably less evident in both PD301 and PD304 cells. Nuclear labelling was evident in all cell types.

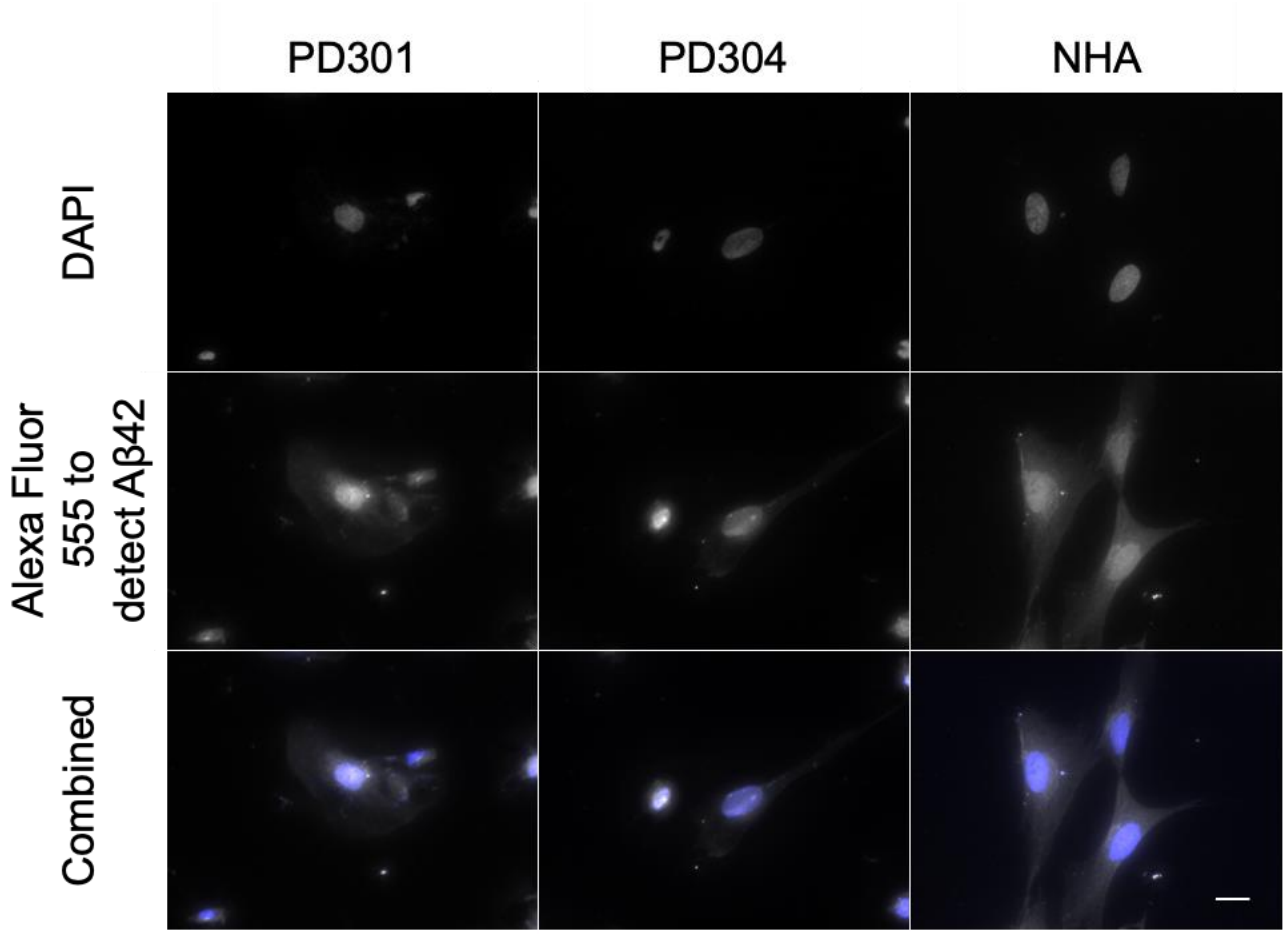

Figure 3.24 – Immunofluorescence confirms Aβ42 expression in PD301, PD304 and NHA cells.

Aβ42 expression in PD301 (left), PD304 (middle) and NHA (right) cells. Cells stained with DAPI (top), Aβ42 antibody and Alexa Fluor 555 secondary antibody (middle) revealing a combined image (bottom). N=3. Magnification = x40. Scale bar = 20µm.

As over 10 images were taken in each of the three replicates of each cell type, quantification of total cell fluorescence was undertaken. This confirmed the corrected total cell fluorescence in both PD301 and PD304 cells was approximately half that seen in NHA ($P<0.01$ Tukey's test N=3, Figure 3.25).

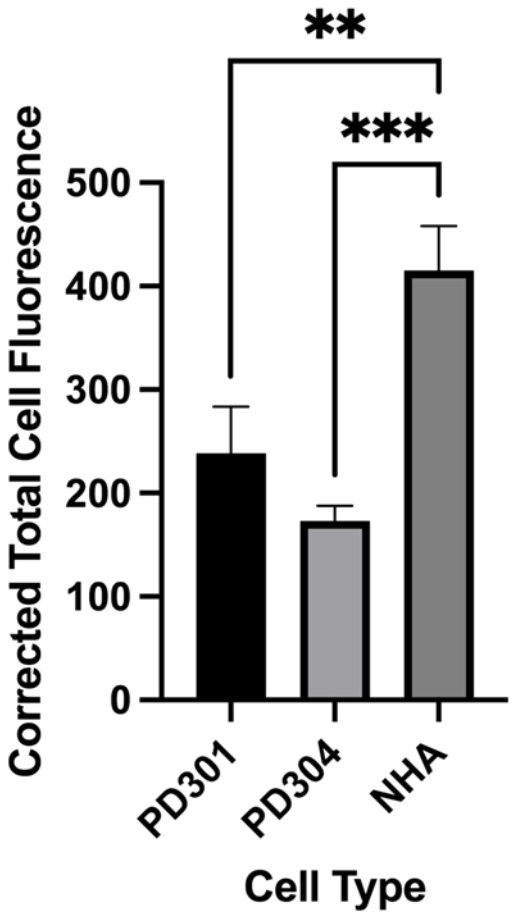

Figure 3.25 – Corrected total cell fluorescence of Aβ42 expression is decreased in PD301 and PD304 cells.

*Aβ42 expression relative to background noise in PD301, PD304 and NHA cells. N>10 images per cell type per replicate. Aβ42 expression is significantly lower in PD301 and PD304 cells than NHA cells. **P<0.01, ***P<0.001, Tukey's Test. N=3.*

To confirm differential Aβ42 expression in the different primary cells, Aβ42 was also quantified by ELISA using a commercially available kit. Cell lysates from three passages of PD301, PD304 and NHA cells were assayed in triplicate and data was expressed as picograms of Aβ42 per mg of total protein; Section 2.7. Lysates from cells derived from both patients contained less than half the amount of Aβ42 seen in NHA lysates (P<0.05, Tukey's test N=3, Figure 3.26). Comparable amounts of Aβ42 was seen in lysates between PD301 and PD304 cells.

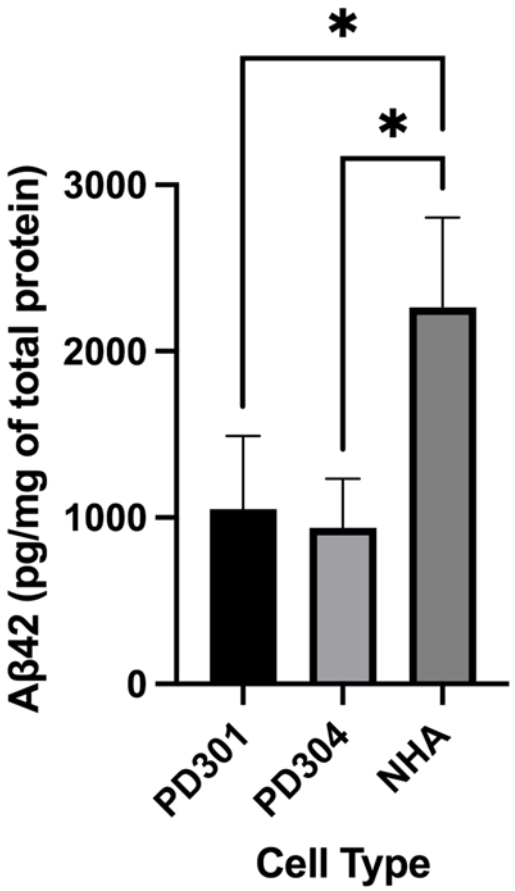

Figure 3.26 - Aβ42 expression in decreased in PD301 and PD304 cells.

Aβ42 protein in picograms per milligram of total protein of PD301, PD304 and NHA cells. Data collected in triplicate, N=3. Aβ42 expression is significantly lower in PD301 and PD304 cells than NHA cells. P<0.05, Tukey's Test. N=3.

3.3 Discussion

3.3.1 Cell Line vs Patient Derived

Antibodies were initially optimised and validated on immortalised human cell lines to confirm protein expression and determine working antibody concentrations. The use of immortalised cell lines have been criticised as they have been manipulated to divide indefinitely (Carter *et al.,* 2022), In particular U87MG cells have become notorious within the glioma research community as subsequent genotyping revealed they are not the original cells described, however, despite this, U87MG

were still confirmed to be glioblastoma in origin (Allen *et al.,* 2016). Recognising the cell line limitations, they do remain a cheap and readily available resource to optimise experiments with few ethical issues. They grow quickly and reliably, important for early experiments of this project. The project then utilised PD cells and primary human astrocytes once the protocols were optimised.

The change to PD cells was a better model than the human immortalised cell lines as it allowed for a more representative overview of glioblastoma due to the cells originating from biopsies of patient's glioblastoma tumours. Also using primary human astrocytes allows for a more accurate control within the experiments. Data collected from PD cells compared to the primary human astrocytes are also more clinically relevant than those obtained from the human immortalised cell lines. Limitations came with the primary cells however, as the quiescent cells are deselected with every passage and therefore the higher the passage number, the less patient like they became.

3.3.2 Growth Curve Troubleshooting

Initial characterisation monitored cell growth over 10 days and produced growth curves for each cell type. A normal pattern of cell growth was seen for all cell types with a lag phase lasting 2-4 days and an exponential phase lasting at least 7 days. As some cells (U87MG, SVGp12, NHA) were starting to enter stationary phase at day 10, all subsequent experiments were timed to take this into account. The growth curves display a natural growth of each cell type in their own mediums. The exponential phase determined the cell densities to seed on to coverslips to be approximately 80% confluent 24 hours later. The cell seeding density was determined from the exponential phase of the growth curves for all primary cells and 1321N1 and SVGp12 cell lines. For U87MG cells however, while the exponential phase suggested an ideal seeding density between 10,000 and 25,000 cells, in practice cells were prone to detach during immunostaining and so the cell density seeded was doubled to 50,000 cells per coverslip.

The growth curves revealed that 1321N1 cells had a much higher rate of growth than U87MG or SVGp12 cells. The reason for this remains unclear as other studies have shown similar growth, particularly between the two cancer cell lines (Liappas *et al.,* 2011). This study showed that U87MG and 1321N1 cells displayed similar proliferation rates reaching approximately 400,000 cells after 4 days (Liappas *et al.,* 2011). This therefore indicates there is an issue with U87MG cells proliferation being slow, as 1321N1 cells proliferation rates are similar to that of the study.

3.3.3 Relative Expression of SorL1 to the Stage of Cancer

This chapter demonstrates SorL1 is expressed in glioma cells. Bioinformatics data shows SorL1 amplification in both lower grade glioma and glioblastoma, and then further demonstrated through immunostaining and western blotting of glioma cells. Additionally, a greater expression of SorL1 was seen in glioma cells compared to the astrocyte controls with SorL1 present in all immortalised cell lines and primary cell types. The human immortalised cell lines demonstrated the cells express SorL1 in a grade dependent manner as SorL1 expression is greater in U87MG cells than 1321N1 cells and even less SorL1 expression is present in SVGp12 cells. Therefore, suggesting the higher the grade of glioma tumour, the more SorL1 is present and expressed within the cell. This was supported through the replicates using different passages of each cell type, and further supported through the quantitative data collected from the primary cells. Data collected from the PD cells compared against the NHAs mirrored the immortalised cell line data showing a greater expression of SorL1 in PD301 and PD304 cells than NHA cells and significantly so. Again, the multiple replicates of the western blots and the immunocytochemistry experiments conveyed the same result. Primary cells supporting the immortalised cell data is important as expression profiles can often differ between cell lines and primary cells (Pan *et al.,* 2009).

Even though cancer genomic software revealed that SorL1 protein was amplified in some patients with lower grade glioma or glioblastoma, it was important to determine expression of SorL1 in glioma cells and quantify it as the protein has not

been fully investigated in glioma tumours. However, SorL1 has been linked to various cancers previously. In particular, SorL1 has been demonstrated to contribute to HER2 expression in HER2 breast cancer (Pietilä *et al.,* 2019). The report of SorL1 shepherding HER2 around in breast cancer cells has obvious similarities with the known role of SorL1 shuttling APP around neurones in the brain (Willnow and Andersen, 2013). The effect that SorL1 has within HER2 breast cancer raises the interesting possibility that SorL1 may play a similar role in glioma, either with Aβ or a further unknown substrate.

As SorL1 has not been investigated in glioma tumours, it was logical to hypothesise that there was a link due to the association that SorL1 has with Alzheimer's disease and as they are both neuro related diseases. The results show an increase of expression of SorL1 in all glioma tumours, whereas the reverse is true for Alzheimer's disease, whereby, SorL1 is found to be reduced, therefore increasing the chance for Aβ42 production.

3.3.4 Relative Expression of Aβ40 and Aβ42 in Glioma

The experiments in this chapter demonstrate that both Aβ40 and Aβ42 are expressed in glioma cells. Previous studies demonstrating amyloid accumulation in glioma either looked for non-specific amyloid or only Aβ40 (Zayas-Santiago *et al.,* 2020, Kucheryavykh *et al.,* 2019). Data presented therefore extends this to now include Aβ42 which could have different implications on glioma cell biology. Early studies were able to utilise higher and lower grade immortalised cell lines, however, no low grade glioma like 1321N1 (a stage II astrocytoma) was available as a primary cell type, so the only comparison within primary cells was between stage IV glioblastoma cells and NHAs.

Statistically, the PD cells and the primary astrocyte control show no significant difference and a similar expression of Aβ40 protein. In comparison, there was a significant difference in Aβ42 expression between the PD cells and the NHAs. This was supported through the quantitative data produced from ELISA and immunocytochemistry experiments occurring in triplicate using different passages

of each cell type, and always conveyed the same result. As in Alzheimer's disease SorL1 is decreased and Aβ42 is elevated, the opposite would be expected in cancer, specifically glioma, and evidently, it appears to be.

This chapter showed that:

i. Expression of SorL1, Aβ40 and Aβ42 is present in U87MG, 1321N1 and SVGp12 cell lines.
ii. Levels of expression of SorL1 are U87MG > 1321N1 > SVGp12.
iii. Expression of SorL1, Aβ40 and Aβ42 is present in PD301, PD304 and NHA primary cells.
iv. Levels of expression of SorL1 are higher in PD301 and PD304 cells than NHA cells.
v. Levels of expression of Aβ42 are lower in PD301 and PD304 cells that NHA cells.

Chapter 4
Secretion of SorL1

4 Chapter 4 – Secretion of SorL1

4.1 Background

4.1.1 Synthesis of SorL1

SorL1 is a 250kDa transmembrane protein that is synthesised from the *SORL1* gene (also known as *LR11* or *SorLA*). SorL1 is a multifunctional sorting receptor, expressed throughout the body, with especially high levels in the CNS (Motoi *et al.,* 1999).

4.1.2 Secretion of Soluble SorL1

To understand how SorL1 is secreted as its soluble form, the structure must be considered; Section 1.2.6. It is important to note the pro-peptide and trans-membrane domain regions (TMD) of the protein as cleavage at these points allow for soluble SorL1 (sSorL1) to be secreted (Figure 4.1) (Barthelson *et al.,* 2020; Ma *et al.,* 2009). The point cleavage occurs in the TMD is shown by the black arrow (Figure 4.1).

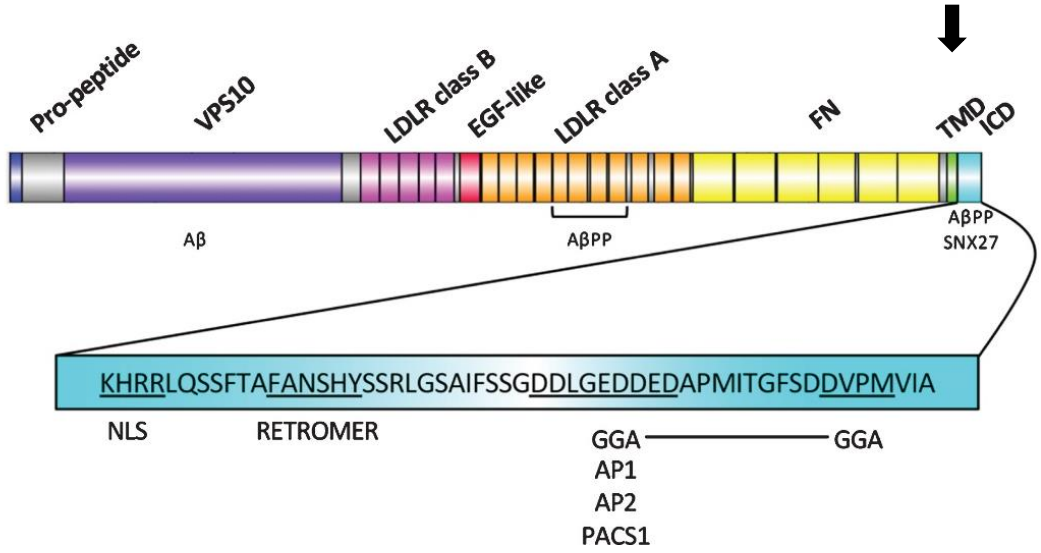

Figure 4.1 – Structure of SorL1.

Structure displaying domains in SorL1 protein. Important for secretion of SorL1 is pro-peptide that is cleaved to form active SorL1. Arrow over transmembrane region (TMD) where cleavage occurs to release soluble SorL1 (Barthelson et al., 2020).

From synthesis of SorL1, the protein follows the secretory pathway, generated in the endoplasmic reticulum (ER) and moves into the Golgi (Rovelet-Lecrux *et al.,* 2021). Within the Golgi, the pro-peptide is cleaved and removed from SorL1 by the enriched enzyme furin, resulting in the transport of the active SorL1 receptor to the cell surface membrane (Barthelson *et al.,* 2020; Schmidt *et al.,* 2017). At the cell surface, there is a constant proteolytic shedding of SorL1, known as soluble SorL1 (sSorL1) (Hermey *et al.,* 2006; Shimizu *et al.,* 2011).

Ectodomain proteolytic shedding of SorL1 into sSorL1 is cleaved by Tumour necrosis factor-A Converting Enzyme (TACE) also known as A Disintegrin And Metalloprotease 17 (ADAM17) (Black, 2002). The ADAM family of proteinases, including TACE have been linked to biological processes involved with pathogenesis of cancer, Alzheimer's disease and inflammatory responses (Wong *et al.,* 2016). Furthermore, the upregulation of the ADAM family has been found to have a positive correlation to cancer malignancy (Yang *et al.,* 2023). In particular ADAM17/TACE has been found to be overexpressed in glioblastoma supporting the positive correlation as glioblastoma is the most malignant primary brain tumour

(Thakkar *et al.,* 2014; Yang *et al.,* 2023). The exact point on the SorL1 protein where TACE cleaves to release sSorL1 is unclear, however it is known cleavage is close to the TMD and the molecular mass of sSorL1 is only approximately 10kDa less than that of the membrane bound full-length 250kDa form (Barthelson *et al.,* 2020; Böhm *et al.,* 2006; Ma *et al.,* 2009).

As well as the secretory pathway that SorL1 can take, the alternative is the trafficking pathway, where SorL1 is internalised via clathrin-mediated endocytosis, which then functions by shuttling between the Golgi and endosomes (Schmidt *et al.,* 2017; Barthelson *et al.,* 2020).

4.1.3 Diagnostic Properties

As sSorL1 can be detected in both cerebrospinal fluid (CSF) and blood plasma, sSorL1 has been considered a potential diagnostic tool (Andersen *et al.,* 2016). Even though investigation into using SorL1 as a diagnostic tool for Alzheimer's disease is undetermined, it has been suggested that the circulating sSorL1 levels can estimate the levels of SorL1 or its activity in brain tissue (Andersen *et al.,* 2016). However, the limited peripheral biomarker studies of SorL1 in Alzheimer's disease are inconclusive (Yin *et al.,* 2014). An early study found sSorL1 levels were significantly reduced in the CSF of patients with mild to moderate Alzheimer's disease and from CSF taken from autopsy confirmed cases, which supports the reduction of SorL1 found in Alzheimer's disease brain (Ma *et al.,* 2009). Whilst another found an increase in sSorL1 levels in CSF in Alzheimer's disease patients (Ikeuchi *et al.,* 2010). There is limited research studying sSorL1 in CSF or blood plasma as the majority of studies investigating Alzheimer's disease biomarkers have investigated Aβ levels such as Andersen *et al.,* 2022; Chou *et al.,* 2016; Rovelet-Lecrux *et al.,* 2021; Simoes *et al.,* 2020.

In addition to Alzheimer's disease, sSorL1 has been investigated in some cancers too. Soluble SorL1 was highly elevated in serum of patients with Non-Hodgkin's lymphoma and acute leukaemia (both acute myeloid leukaemia and acute lymphoblastic leukaemia). Importantly biomarkers of sSorL1 reduced to normal

levels as the patient went into remission (Fujimura *et al.,* 2014; Sakai *et al.,* 2012). An increase in SorL1 expression was also found in bile samples in patients with cancers of the pancreas and bile duct, and SorL1 levels were especially elevated during the peak of proliferation (Terai *et al.,* 2016). This therefore suggests sSorL1 could also be used as a diagnostic tool in cancer. To date sSorL1 levels have not been investigated in glioblastoma. The work in this chapter will determine if sSorL1 secretion is different in glioblastoma cell medium and can be detected in the serum of mice implanted with glioblastoma cells.

4.2 Results – Secretion

As sSorL1 can be seen increased in serum from patients with various cancers (Sakai *et al.,* 2012; Fujimura *et al.,* 2014) it was determined whether sSorL1 was detected in medium taken from glioblastoma cells or NHAs, and serum from mice implanted with U87MG glioblastoma cells.

4.2.1 SorL1 Secretion in Medium

As shown in Chapter 3, human primary glioblastoma cells had significantly higher expression of SorL1 protein than human primary astrocytes. Therefore, SorL1 levels in cell medium was investigated to see if the increased expression was due to retention of SorL1 and therefore not being secreted, or if the cell was producing SorL1 protein at a faster rate.

Cells were weaned off medium containing serum and maintained for 24 hours in minimal volume of medium to cover the cells. Levels of sSorL1 in cell medium were determined by western blot using the same primary antibody as was used previously to determine expression; Section 2.6. The SorL1 antibody was an approximate 150kDa fragment antibody that was raised against the immunogen that corresponded with an internal portion of the SorL1 protein. The bands produced when SorL1 was probed displayed a band at 240 kDa, consistent with the known molecular weight of sSorL1 (Motoi *et al.,* 1999).

As cells don't secrete the β-actin and β-tubulin proteins routinely used as lysate loading controls, lysates were spiked with a fixed amount of exogenous 6X His-tag human β-actin peptide to correct for loading variation. Consistent bands were shown over all three cell media when probed with antibody against the 6X His-Tag β-actin peptide. Medium containing no serum and had not been in contact with any cells was also run to confirm any SorL1 present was due to secretion from cells and not previously contained within the medium. No SorL1 was detected in virgin medium (data not shown).

SorL1 was only present in NHA medium, with no visible bands present in the PD301 or PD304 medium (Figure 4.2). Western blotting for primary cell medium was repeated in triplicate from three different passages. Full blot for western blot is appended; Appendix 1, Figure A1.3.

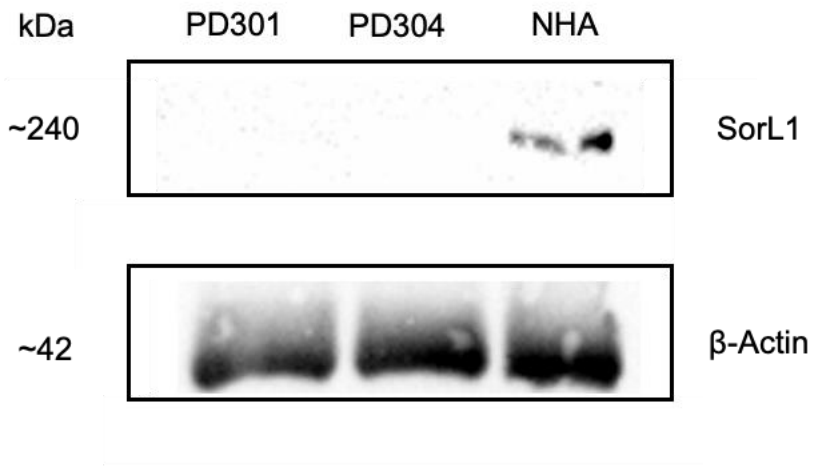

Figure 4.2 – Western blot of PD301, PD304 and NHA cell medium using SorL1 antibody.

Western blot confirming presence of SorL1 at 240 kDa (top) and β-actin at 42 kDa (bottom) in PD301, PD304 and NHA medium. 10µg of protein was loaded. (N=3).

Densitometric analysis on sSorL1 bands relative to spiked actin confirmed significantly higher levels of sSorL1 in medium from NHA cells than in medium from both PD301 and PD304 cells ($p<0.01$ Tukey test, N=3) (Figure 4.3).

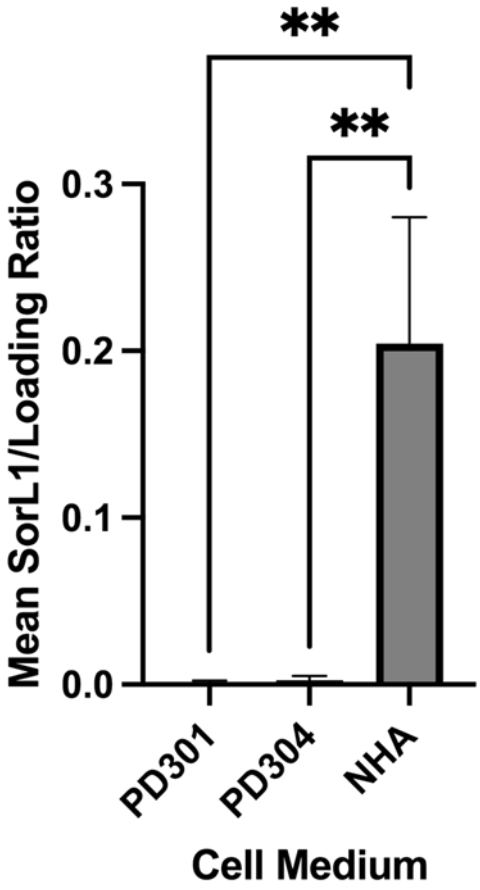

Figure 4.3 – Soluble SorL1 secretion in PD301, PD304 and NHA cell medium.

SorL1 secretion relative to β-actin is significantly lower in PD301 medium and PD304 medium than NHA medium. P<0.01, Tukey's Test. N=3.

4.2.2 SorL1 Secretion in Mouse Serum

As cell culture medium from PD glioblastoma cells showed an absence of sSorL1, the next step was to see if that was replicated in serum *in vivo*. SorL1 was subsequently assayed in surplus serum from mice with intracranial glioblastoma; Section 2.5.

As serum was surplus to a previous unrelated study, volume of serum was very limited and therefore methodology had to be optimised to maximise what could be run. Consequently, technical replicates were forfeited and only limited

independent replicates were possible. Some samples had undergone a lot of haemolysis and were subsequently discarded.

Secretion of SorL1 in mouse serum was confirmed using the same SorL1 primary antibody as was used previously to demonstrate secretion of sSorL1 into cell medium. In mouse serum, sSorL1 bands shown were seen at 240 kDa, consistent with the known molecular weight of sSorL1 (Motoi *et al.,* 1999) (Figure 4.4).

Western blots revealed sSorL1 present in all serum taken from pre-bleed through to week 3, in both glioblastoma mice and sham mice. Due to the limited amount of serum from initial weeks where blood was taken from the tail vein, a western blot could only be achieved once per mouse, therefore Figure 4.4 shows a representative image of sSorL1 western blot of serum taken weekly from a mouse implanted with glioblastoma cells alongside serum taken weekly from a sham mouse. While sSorL1 bands appear less intense on the serum taken from the glioblastoma mouse, this was less evident when the loading control was taken into account. That variability possibly reflects the varying degree of haemolysis and blood contamination in the serum that may skew Bradford assay and protein loading. Full blot for western blot is appended; Appendix 1, Figure A1.4.

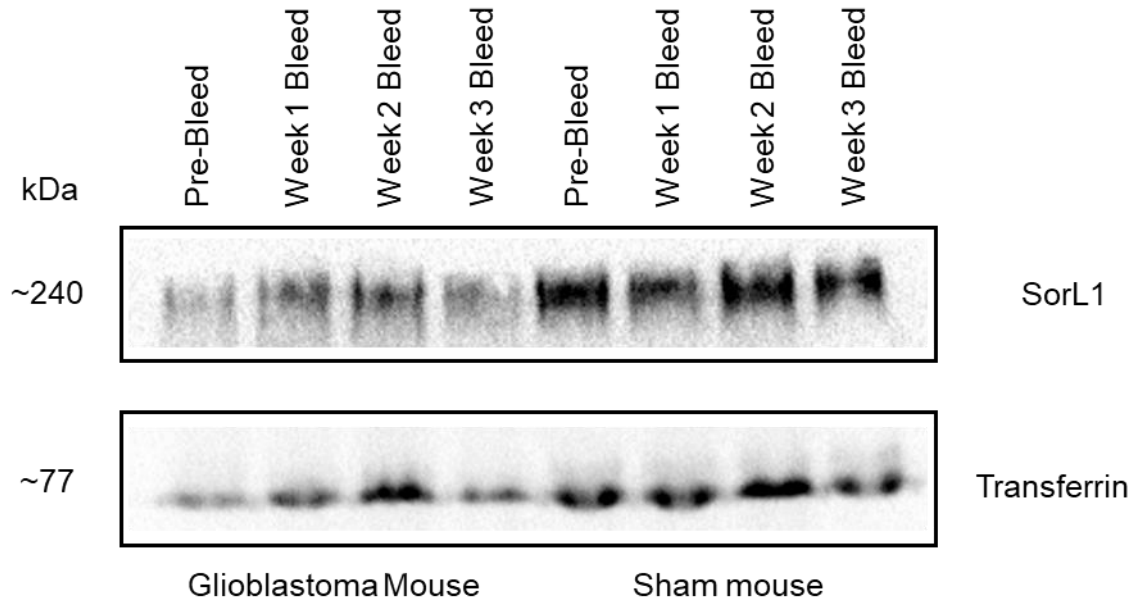

Figure 4.4 – Western blot of serum from weekly bleeds from mice implanted with U87MG cells and sham mice with SorL1 antibody.

Representative western blot of sSorL1 at 240 kDa (top) and transferrin at 77 kDa (bottom) in weekly serum samples from a mouse implanted with U87MG glioblastoma cells or following sham surgery. Serum samples taken from each mouse pre-surgery, week 1, week 2 and terminal bleed at week 3. 7.5µg of protein was loaded. (N=1).

Marked variability was also evident when considering samples at the different time points from the individual glioblastoma (Figure 4.5) or sham (Figure 4.6) mice. While sSorL1 was detected in most serum samples from both glioblastoma or sham mice, the SorL1 levels corrected for loading had almost five-fold variation within a group at single time point (e.g. week 1 in glioblastoma group or week 3 in sham group, Figures 4.5 and 4.6). Indeed, there was almost an eight-fold range in sSorL1 levels before glioblastoma cells had even been implanted (Figure 4.5).

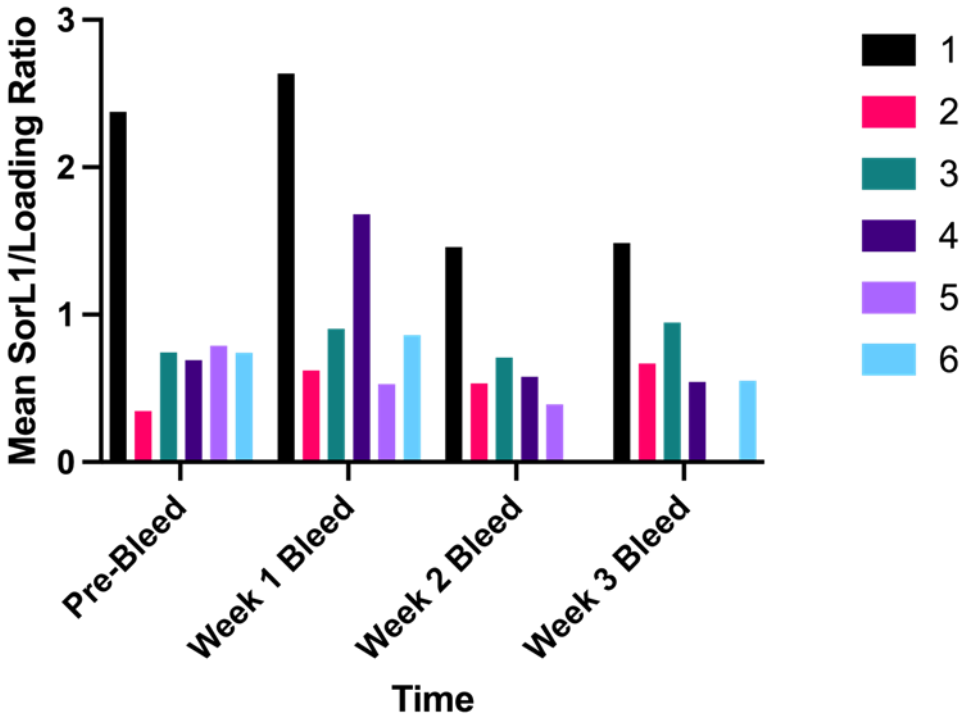

Figure 4.5 – Soluble SorL1 secretion in serum from weekly bleeds of mice implanted with U87MG cells.

SorL1 relative to transferrin in serum taken weekly from individual mice implanted with glioblastoma cells into striatum. The numbers 1, 2, 3, 4, 5 and 6 on the right represent the individual mice. N=1.

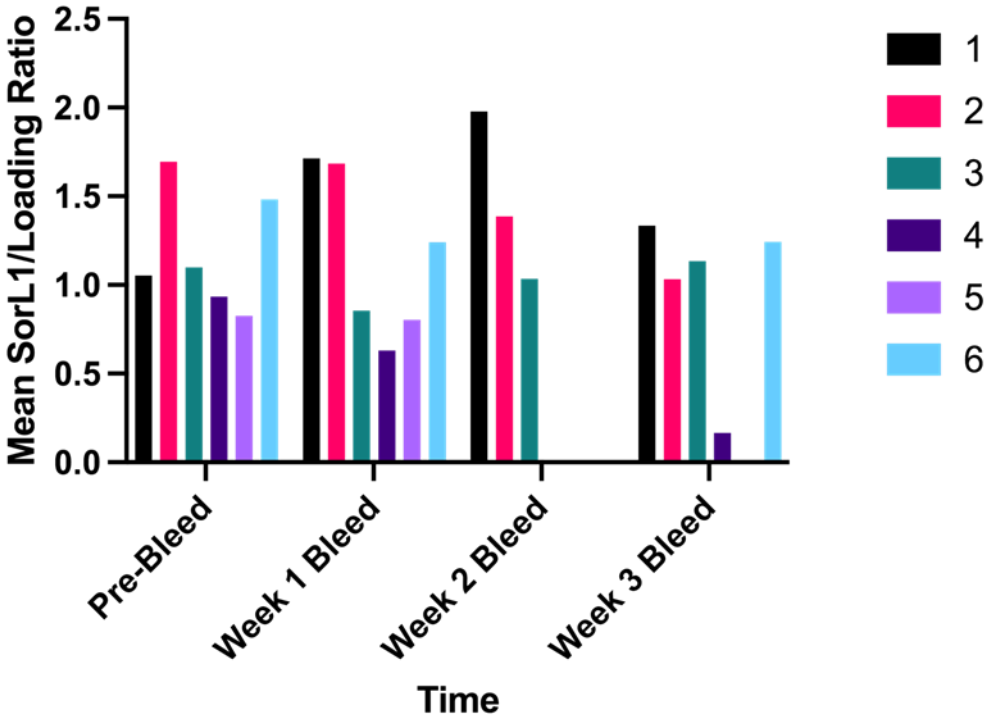

Figure 4.6 – Soluble SorL1 secretion in serum from weekly bleeds of sham mice.

SorL1 relative to transferrin in serum taken weekly from individual mice following vehicle injection into striatum. The numbers 1, 2, 3, 4, 5 and 6 on the right represent the individual mice. N=1.

A possible trend was noted towards mean sSorL1 levels being lower in serum from mice following implantation with glioblastoma cells (Figure 4.7) but no statistical significance was detected between the two groups at any weekly timepoint (P>0.05, N=3-6).

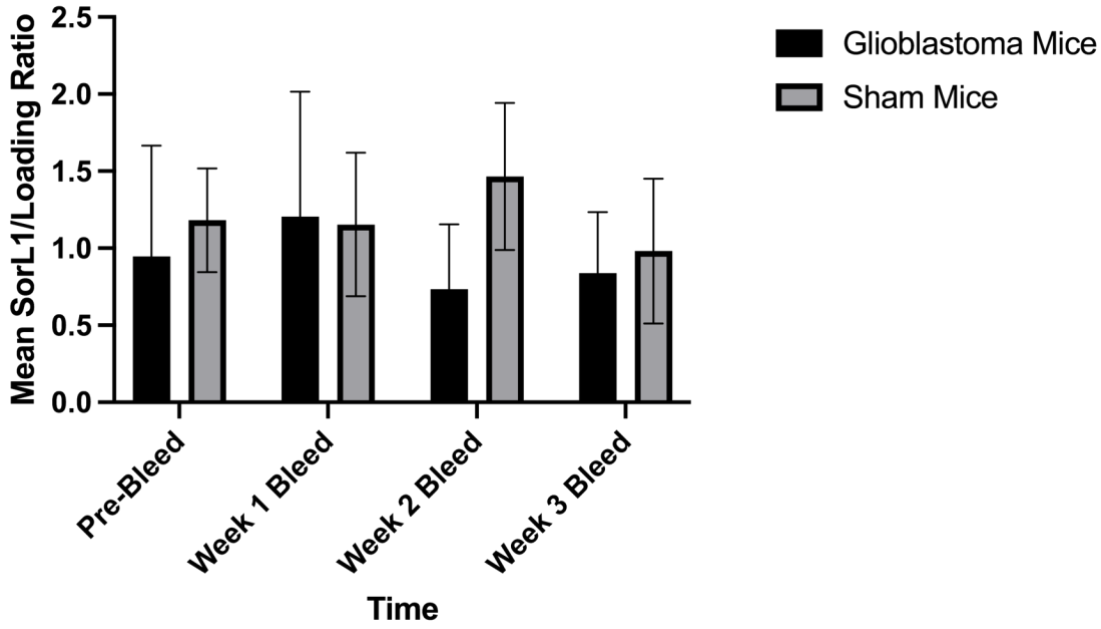

Figure 4.7 – Mean sSorL1 secretion comparing serum from glioblastoma and sham mice over weekly bleeds.

Mean sSorL1 relative to transferrin from serum samples taken from glioblastoma mice and sham mice. Samples taken pre-surgery and at weekly intervals. SorL1 secretion was no different between mice implanted with glioblastoma cells and those following sham surgery at any time point. P>0.05, Tukey's Test. N=3.

As alluded to, serum samples obtained through tail vein were frequently subject to haemolysis and contaminated with erythrocyte contents. In contrast, blood obtained at the point of euthanasia via cardiac puncture was more likely to be clear. SorL1 was quantified in serum from terminal bleeds in triplicate with a representative western blot (Figure 4.8). Full blot for western blot is appended; Appendix 1, Figure A1.5.

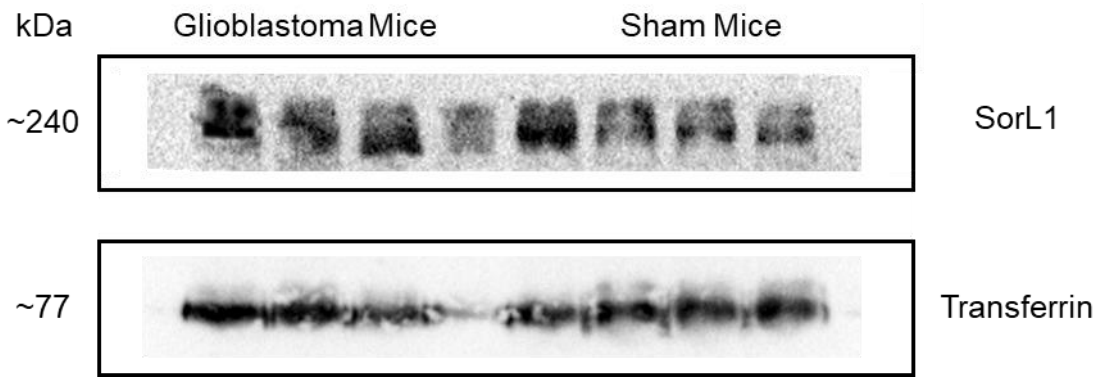

Figure 4.8 – Western blot of serum from terminal bleeds from mice implanted with U87MG cells and sham mice with SorL1 antibody.

Western blot confirming secretion of SorL1 at 240 kDa (top) and transferrin at 77 kDa (bottom) in serum taken from a mouse implanted with U87MG glioblastoma cells and taken from a sham mouse. Displays 4 serum samples from separate mice implanted with U87MG glioblastoma cells (left) and 4 serum samples taken from sham mice (right). 7.5µg of protein was loaded. (N=3).

Soluble SorL1 levels in serum from glioblastoma or sham mice were comparable with means corrected against loading controls and showed no significant difference in sSorL1 levels between glioblastoma or sham mice at point of euthanasia ($P>0.05$ two-tailed T test, Figure 4.9).

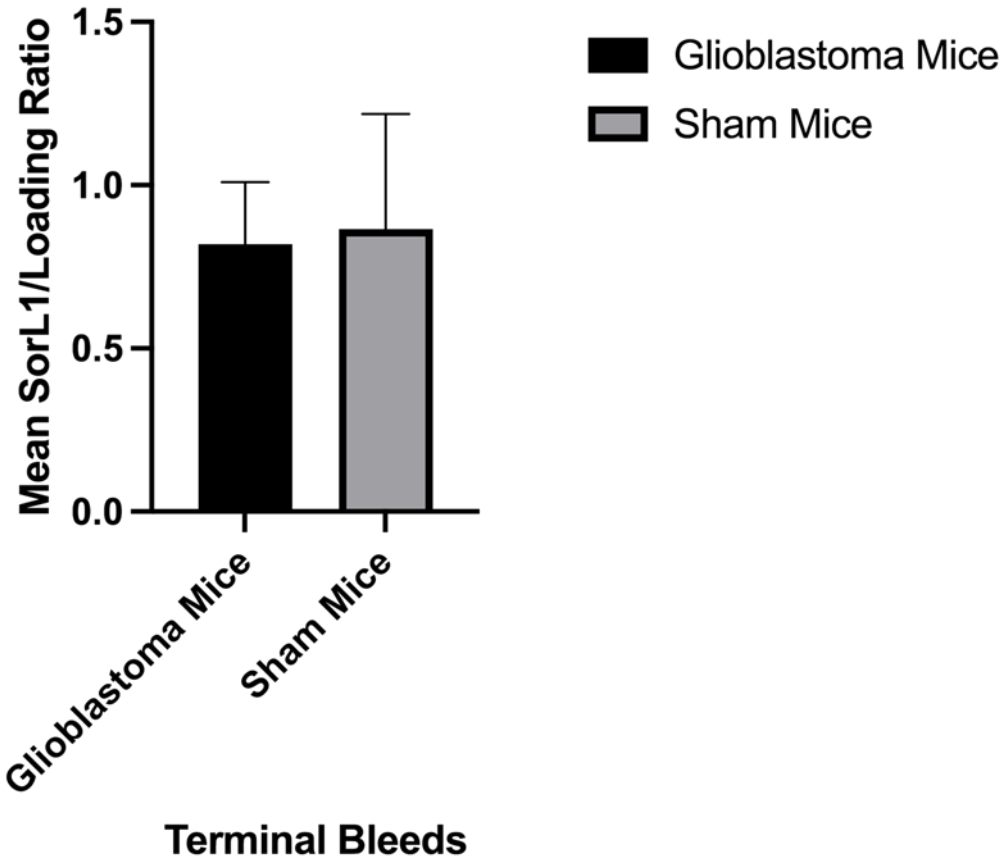

Figure 4.9 – Soluble SorL1 secretion comparing serum from terminal bleeds from glioblastoma and sham mice.

SorL1 secretion relative to transferrin in sera following terminal bleed from mice implanted with U87MG glioblastoma cells or PBS. SorL1 secretion was not different mice receiving GBM cells or those injected with PBS. P>0.05, two sided T test. N=3.

4.3 Discussion

4.3.1 Decreased Secretion of Soluble SorL1 in Glioblastoma Medium

This chapter shows little if any sSorL1 was present in glioblastoma cell medium when compared to normal astrocyte medium. Despite the results showing such a significant difference, literature investigating sSorL1 levels in certain cancers of the blood found opposite results. Soluble SorL1 was found to be elevated in acute

leukaemia and Non-Hodgkin's lymphoma compared to controls (Sakai *et al.,* 2012; Fujimura *et al.,* 2014). Glioblastoma and acute leukaemia, specifically acute myeloid leukaemia, have been studied together. Both types of cancer have similarities as they have many mutations in common, for example isocitrate dehydrogenase (IDH), however, the main difference is glioblastoma is a solid tumour, whilst acute leukaemia is a hematologic malignancy (Dang *et al.,* 2010; Goethe *et al.,* 2018). Also, there might be more of an effect as shown in the bloodborne cancers due to constant proteolytic shedding of SorL1 from the cancerous bone marrow into the blood, and therefore readily present within serum.

It was expected that trace amount of sSorL1 would be visible in glioblastoma cell medium due to understanding that proteolytic cleavage occurs by TACE/ADAM17. The active cell surface form of TACE or ADAM17 that cleaves SorL1 extracellularly releasing the soluble form, has been found to be dysregulated in autoimmune and cardiovascular diseases, infection, neurodegeneration, inflammation and cancer (Wong *et al.,* 2016). More specifically, in cancer, ADAM17 was found to have an increased protein expression in hypoxic conditions of 9L glioma cells (Zheng *et al.,* 2007). A study further found ADAM17 to be overexpressed in glioblastoma and the upregulation of the ADAM family to have a positive correlation to cancer malignancy (Yang *et al.,* 2023). However, as shown in this chapter when looking at secretion in medium, little if any sSorL1 was present in the patient cell medium compared to the normal astrocyte medium. The difference seen when compared to literature could be due to the well-known different expression profiles between primary cells and cell lines (Pan *et al.,* 2009). Furthermore, SorL1 is a protein that also functions intracellularly and therefore it is reasonable to assume that the cell may move SorL1 into the trafficking pathway as opposed to the signalling secretory pathway (Barthelson *et al.,* 2020). The shuttling of APP around the cell is one such function SorL1 has within the trafficking pathway, controlling the amount of Aβ production (Andersen *et al.,* 2005).

Unlike lysates and serum, there is no known good housekeeping gene that can be used as a loading control for secretory proteins in cell medium. Literature that tested cell medium for sSorL1 protein have not executed a loading control, only

the membrane probed for sSorL1 was shown (Monti *et al.,* 2021; Hermey *et al.,* 2006). The loading for medium was based on the protein assay to load the same amount of protein in each well and a ponceau red stain to confirm protein levels were consistent. However, to quantify SorL1 ratio to protein loaded, human β-actin peptide was added and stained for to determine significance.

4.3.2 Serum from Mice Implanted with Glioblastoma has no Difference in Soluble SorL1

Whilst a significant reduction in sSorL1 was seen in cell culture medium, this was not supported by the serum of mice implanted with glioblastoma cells. The results showing a significant increase in SorL1 expression in PD301 and PD304 cell lysates compared to NHA lysates was further supported by U87MG cell lysates compared to SVGp12 cell lysates conveying glioblastoma cells have an increase in SorL1 expression (Chapter 3). It therefore stands to reason that as the mice were implanted with U87MG cells the serum should show the same reduction in sSorL1 as the cell medium.

There are however various reasons that could explain this difference. The serum sample quality was substandard with many samples contaminated with blood, and so interfered with the protein assay affecting the absorbance at 535nm and therefore affected the protein loading amounts. The terminal bleeds were of better quality, and also had a larger volume as collection was via a cardiac puncture. This therefore meant that the serum could be separated out of the whole blood easier. There was a lack of volume for the weeks where blood was taken from the tail vein to separate the serum from the whole blood, therefore justifying the poor quality. However, the procedure for collecting the sample was more intricate and volumes collected could not be as large.

Due to the serum loading control, transferrin, sSorL1 levels could be corrected, and significance determined. No significant difference was found between the mice implanted with glioblastoma cells and the sham mice. In comparison, certain cancers of the blood, acute leukaemia and Non-Hodgkin's lymphoma, found a

significant increase in serum SorL1 levels, compared to the controls (Sakai *et al.,* 2012; Fujimura *et al.,* 2014). Due to the blood-borne nature of cancers of the blood, it may be expected that sSorL1 is more readily present in serum. Therefore, when investigating levels of sSorL1 from glioblastoma, looking in CSF may show more of a difference due to SorL1 production in the CNS, including in the brain, and one function being to remove waste (Guthrie, 2012). Also as previously mentioned SorL1 expression is highest within the CNS (Motoi *et al.,* 1999). CSF has already been investigated and shown preference over blood serum investigating levels of SorL1 to diagnose Alzheimer's disease, however this too had conflicting results (Andersen *et al.,* 2016).

Despite this chapter having varying results, overall, these results show:

i. SorL1 is not being secreted by PD301 and PD304 cells to the levels that is secreted by NHA cells.
ii. SorL1 is being retained in PD301 and PD304 cells.
iii. Secretory levels of SorL1 are similar in serum levels of mice with a glioblastoma and those without.

Chapter 5
Knock Down Model of SorL1 in PD301 and PD304 Cells

5 Chapter 5 – Knock Down Model of SorL1 in PD301 and PD304 Cells

5.1 Background

5.1.1 Gene Silencing Systems – RNAi vs CRISPR

Two methods for gene silencing are RNA interference (RNAi) and clustered regularly interspaced short palindromic repeats (CRISPR). Both methods result in a silenced gene expression, however, the mechanisms to reach the same goal are different as RNAi silences genes through degradation of messenger RNA (mRNA) whilst CRISPR silences genes at the DNA level (Xu *et al.,* 2019).

RNAi was accidently first discovered in 1990 in botany when an introduced gene, intending to be overexpressed, unexpectedly blocked expression resulting in a 50-fold reduction of mRNA expression of the gene. However, at the time it was unclear what the underlying mechanism of the gene silencing was only later discovered that double-stranded RNA was more efficient at gene interference than single-stranded RNA resulting in gene silencing (Napoli *et al.,* 1990; Fire *et al.,* 1998).

Early studies employing RNAi added double-stranded RNA, however, it was also found that RNAi occurred through endogenous small interfering RNAs (siRNA), microRNAs (miRNA) and short hairpin RNAs (shRNA) (Lam *et al.,* 2015). All are short RNA forms that bind to mRNA to prevent translation and result in gene silencing. Differences can be found between the three RNAi methods. When comparing siRNA and miRNA, siRNA are highly specific to only one mRNA target due to binding sites being fully complimentary to the target mRNA, whereas miRNA have multiple targets as miRNA only needs to be partially complementary to target mRNA and therefore one miRNA stand can recognise multiple mRNAs (Lam *et al.,* 2015). Similar to siRNA being highly specific to one mRNA target, so are shRNAs,

however unlike the linear sequence of siRNA of two complementary RNA strands, shRNA encodes a single-stranded RNA molecule that loops around due to complementary pairings that allows the RNA to fold back on itself creating a hairpin loop (Farrell, 2010; Rao *et al.,* 2009).

Alternatively, CRISPR results in a silenced gene expression. Identification of palindromic segments of DNA in *E. Coli* bacteria in 1987 was the first step to eventually developing CRISPR (Ishino *et al.,* 1987). Over the years, more components were discovered which eventually led to the CRISPR-Cas9 system being first used in eukaryotic cells in 2013 (Cong *et al.,* 2013).

CRISPR results in permanent gene editing. Within the CRISPR-Cas9 system, there is a guide RNA to help locate the specific DNA sequence and CRISPR-associated endonuclease protein (Cas) which cuts the DNA at that site, therefore resulting in protein disruption and causing a knockout of the gene of interest (Asmamaw and Zawdie, 2021).

To explore SorL1 functions further, either RNAi or CRISPR could be employed to use to specifically knock down or knock out gene expression respectively.

5.1.2 SorL1 Mutations in Alzheimer's Disease

A disease already known to have a reduction in SorL1 when compared to normal pathology is Alzheimer's disease. The reduction of SorL1 protein is due to mutations occurring within the *SORL1* gene, a change at the genomic level that leads to an increase in Aβ40 and Aβ42 production (Cuccaro *et al.,* 2016). Meta analyses have conducted sequencing on Alzheimer's related genes and found variants of *SORL1* to be protein-truncating and contain missense mutations (Campion *et al.,* 2019). Furthermore, strong evidence is presented for rare and loss of function variants in the *SORL1* gene to be considered as important genetic risk factors for Alzheimer's disease (Raghavan *et al.,* 2018). Mutations of *SORL1* gene resulted in a reduction of capacity for SorL1 protein to bind to APP (Alvarez-Mora *et al.,* 2022; Cuccaro *et al.,* 2016). Due to mutations reducing binding

capacity of SorL1 to APP, the common variant resulted in an increase in Aβ42 secretion whereas, rare mutations resulted in increased Aβ40 and Aβ42 secretion (Vardarajan *et al.,* 2015). Furthermore, supporting SorL1 having a role in increasing the risk of Alzheimer's disease, one study used the CRISPR-Cas9 system to knockout SorL1 from human induced pluripotent stem cells (hiPSCs) which displayed neurones showing early endosome enlargement, characteristic to Alzheimer's disease cytopathology (Knupp *et al.,* 2020).

Due to the knockout nature of the *SORL1* gene in Alzheimer's disease, in terms of glioma cells and the increase of SorL1 expression already shown in previous chapters, using CRISPR to knockout *SORL1* at the DNA level may possibly induce Alzheimer's disease pathology. Therefore, to use RNAi technology to knock down SorL1 protein within glioblastoma cells would give a better indication to how the cells would be affected as a drug induced inhibition, as other studies have done (Pietilä *et al.,* 2019).

5.1.3 Knock Down Model of SorL1 in Cancer

Previous studies have used vectors to transiently transfect SorL1 siRNA to knock down SorL1 protein using Lipofectamine 3000 with P3000 enhancer reagent and four individual SorL1 targeting siRNA (Pietilä *et al.,* 2019). Successful transfection occurred in breast cancer cells and silencing SorL1 induced an accumulation of HER2, however, knock down of SorL1 has not been undertaken in brain tumours. The same Lipofectamine reagents were used in this chapter.

5.1.4 Gene Silencing siRNAs Chosen

A set of 4 SorL1 targeting siRNAs were chosen to knock down the gene using the RNAi method rather than using CRISPR to knock out the SorL1 gene. This therefore will aid in giving a loss of function to SorL1, mimicking what a drug would do to reduce SorL1 expression in PD301 and PD304 cells.

The transfection method used was a siRNA/shRNA/RNAi Lentivector. The siRNA or shRNA were used to silence a SorL1 gene expression by cleaving mRNA. The combining of siRNA and shRNA creates a better transfection method to knock down SorL1 expression. A limitation of siRNA is it is relatively short lived once introduced to cells, compared to shRNA which is cloned into a vector allowing a much longer expression within the cell. However, the hairpin loop in shRNA makes it difficult to construct. Therefore, an alternative system was used which employed a dual convergent promoter system (ABM) with sense and antisense strands of siRNA expressed by two promoters, therefore removing the hairpin loop. This therefore means the cloned siRNA will be less likely to form secondary structures allowing the plasmid to replicate easier. This combination allows the siRNA vector to have the same longevity in the cell as shRNA.

Gene knock down used a lentivector encoding the siRNA to transfect PD301 and PD304 cells. Lentiviruses are stable plasmids and are therefore an ideal candidate for stable gene transfer (Elsner and Bohne, 2017). A lentivirus also has a high transduction efficiency in integrating into the genome of a cell and therefore a better model than other viruses if the cells have low transfection efficiency, which when working with primary cells, it is known they are difficult to transfect (Fus-Kujawa *et al.,* 2021; Gresch and Altrogge, 2012). To reduce the risk of using live lentivirus, a 3rd generation self-inactivating lentiviral vector was used with enhanced biosafety as it lacks any virulence factors and is incompetent in replication due to the viral genome being split (Milone and O'Doherty, 2018).

5.2 Results – Developing a Knock Down Model of SorL1

SorL1 expression was significantly upregulated in PD glioblastoma cells which accompanied reduced extracellular secretion of SorL1; Chapter 3 and Chapter 4. Therefore, the next step was to determine functional effects on the cell following knock down of SorL1 protein in the PD glioblastoma cells. To achieve this, PD cells were transiently transfected with a vector to express siRNA against SorL1. Small interfering RNA vectors also encoded GFP to allow visualisation of cells and determine successful transfection.

5.2.1 Optimising Transient Transfection of PD301 and PD304 Cells

Initial optimisation treated PD301 and PD304 cells with different amounts of siRNA and Lipofectamine 3000 kit components: Lipofectamine and P3000. SorL1 siRNA came as 4 individual targets to allow one to be omitted if required or ineffective. Scrambled siRNA was also used as a negative control. Both SorL1 and scrambled siRNA had a GFP tag to ensure cells that took on the siRNA could be seen under fluorescence. Additionally, some cells were only treated with Lipofectamine and some were not treated or transfected to act as a further control group.

PD301 and PD304 cells were treated with either 0.75µl or 1.5µl Lipofectamine as per the manufacturer's instructions. Either 1µl or 2µl of P3000 was used coupled with either 0.5µg or 1µg of scrambled siRNA or the individual SorL1 siRNA respectively. Different variations of the above reagents were used, and an optimal transfection efficacy was found for each siRNA (Appendix 2).

Following initial optimisation success of individual SorL1 siRNAs, transfection was further optimised to transfect PD301 and PD304 cells, however the Lipofectamine was kept constant using 1.5µl due to previous results displaying this volume in the optimal transfection conditions. Furthermore, investigation into whether pooling the SorL1 siRNA would increase the rate of transfection success also occurred, as it was logical to assume the individual targets would bind to different regions of the mRNA encoding the SorL1 protein.

PD301 cells were transfected with either 0.5µg or 1µg of individual SorL1 siRNA, pooled SorL1 siRNA or scrambled siRNA. Within each siRNA condition, some cells were incubated with P3000 and some without to determine whether it impacted PD301 transfection success. It transpired that the optimal conditions when PD301 cells had the highest rate of transfection was when 1µg of SorL1 siRNA were pooled in addition to 2µl of P3000 resulting in 66.62% transfection efficacy (Table 5.1). Scrambled siRNA achieved an optimal transfection success of 34.32% using 1µg and 2µl of P3000.

***Table 5.1* – Optimal ratio of transfection reagents for PD301 cells.**

Final optimal conditions of SorL1 siRNA and scrambled siRNA with percentage of transfection efficacy for transient transfection of PD301 cells.

siRNA	***siRNA (µg)***	***P3000 (µl)***	***Lipofectamine (µl)***	***Transfection Efficacy (%)***
SorL1 siRNA A, B, C, D	*1µg*	*2µl*	*1.5µl*	*66.62%*
Scrambled siRNA	*1µg*	*2µl*	*1.5µl*	*34.32%*

Immunofluorescence was used to determine transfection efficacy of PD301 cells using the DAPI channel to determine the number of cells present and the GFP channel to determine how many cells had been transfected by either SorL1 siRNA or scrambled siRNA (Figure 5.1).

Following transfection, no GFP fluorescence was seen in non-transfected and Lipofectamine only PD301 cells indicating no siRNA had been transfected. GFP fluorescence was evident in PD301 cells transfected with both SorL1 siRNA and scrambled siRNA (Figure 5.1).

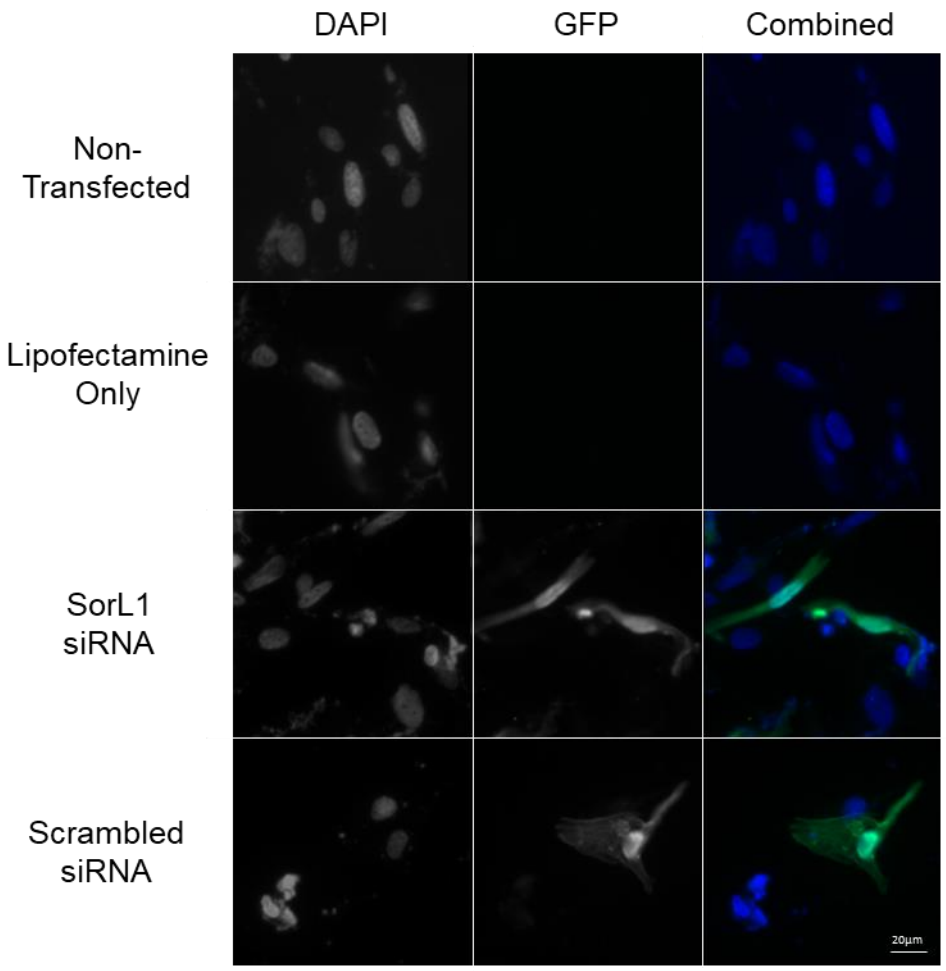

Figure 5.1 – Transfection success in PD301 cells.

Non-transfected PD301 cells, Lipofectamine only PD301 cells, SorL1 siRNA transfected PD301 cells and scrambled siRNA transfected PD301 cells (top to bottom) stained with DAPI and imaged under the DAPI channel (left), imaged under the GFP channel (middle) and combined image (right). N=3. Magnification = x40. Scale bar = 20µm.

Transfection conditions for PD304 cells were also further optimised, keeping Lipofectamine volume constant using 1.5µl due to previous transfection success. PD304 cells were transfected with either 0.5µg or 1µg of individual SorL1 siRNA, pooled SorL1 siRNA or scrambled siRNA. Within each siRNA condition, some cells were incubated with P3000 and some without to determine whether it impacted PD304 transfection success. Optimisation revealed PD304 cells had the highest rate of transfection when 1µg of SorL1 siRNA were pooled in addition to 2µl of P3000 resulting in a transfection efficacy of 74.5% (Table 5.2). Scrambled

siRNA achieved an optimal transfection success of 33.00% using 1µg and 2µl of P3000.

Table 5.2 – *Optimal ratio of transfection reagents for PD304 cells.*

Final optimal conditions of SorL1 siRNA and scrambled siRNA with percentage of transfection efficacy for transient transfection of PD304 cells.

siRNA	***siRNA (µg)***	***P3000 (µl)***	***Lipofectamine (µl)***	***Transfection Efficacy (%)***
SorL1 siRNA A, B, C, D	*1µg*	*2µl*	*1.5µl*	*74.5%*
Scrambled siRNA	*1µg*	*2µl*	*1.5µl*	*33.00%*

Similar to transfected PD301 cells, no GFP fluorescence was seen in non-transfected and Lipofectamine only PD304 cells indicating no siRNA had been incorporated. GFP fluorescence was evident in PD304 cells transfected with both SorL1 siRNA and scrambled siRNA (Figure 5.2).

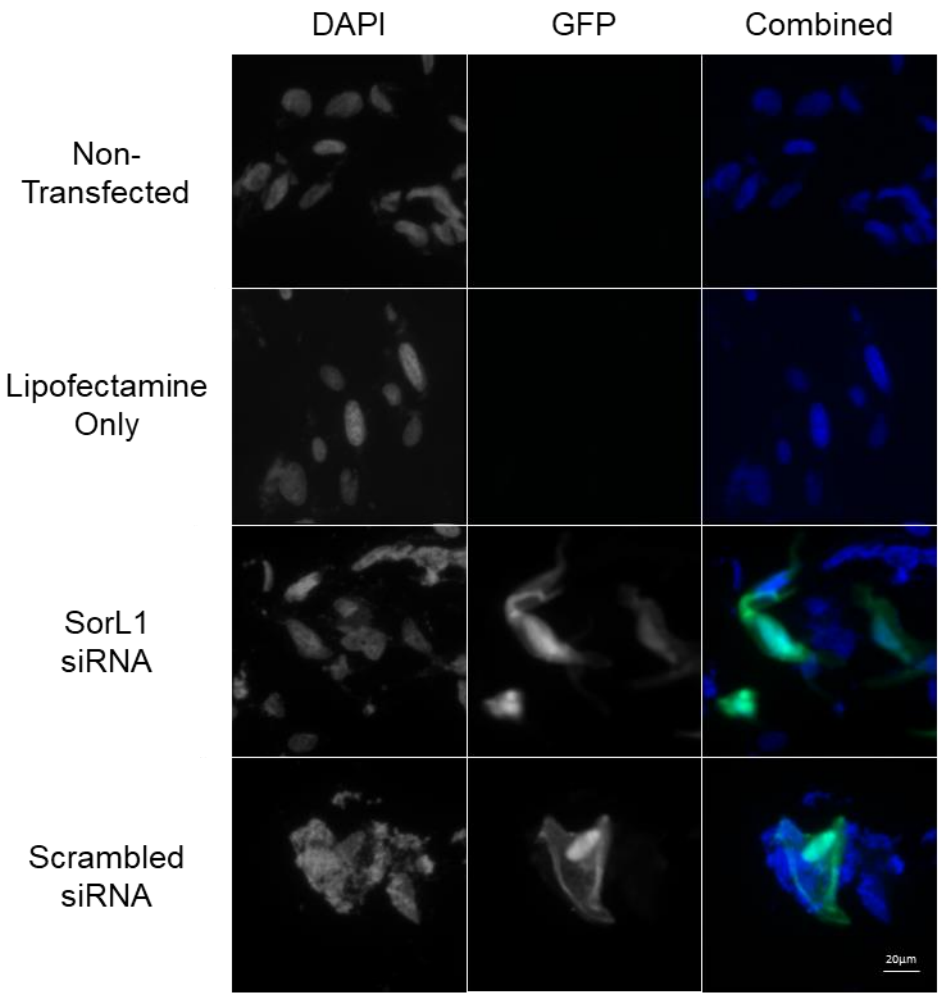

Figure 5.2 – Transfection success in PD304 cells.

Non-transfected PD304 cells, Lipofectamine only PD304 cells, SorL1 siRNA transfected PD304 cells and scrambled siRNA transfected PD304 cells (top to bottom) stained with DAPI and imaged under the DAPI channel (left), imaged under the GFP channel (middle) and combined image (right). N=3. Magnification = x40. Scale bar = 20µm.

As siRNA vectors also encoded for puromycin selection, to further enhance PD301 or PD304 cells transfected with either SorL1 siRNA or scrambled siRNA, medium was supplemented with puromycin. PD301 and PD304 cells were exposed to medium containing varying concentrations of puromycin and viability of cells determined after 72 hours; Section 2.8.7. A dose response curve (puromycin kill curve) was created to determine the optimal concentration of puromycin to select for transfected PD301 and PD304 cells (Figure 5.3).

PD301 and PD304 cells treated with 0µg/ml concentration of puromycin did not have any other differentiating factors, so considered the control group and was regarded as 100% cell viability. Viability of cells treated with puromycin were calculated from the cell viability of the 0µg/ml concentration. All concentrations (1-5µg/ml) of puromycin in medium reduced PD301 and PD304 cell viability. The concentration of puromycin chosen was 5µg/ml as it only left 2% of viable cells and had the greatest effect enriching the PD301 and PD304 siRNA transfected cells (Figure 5.3).

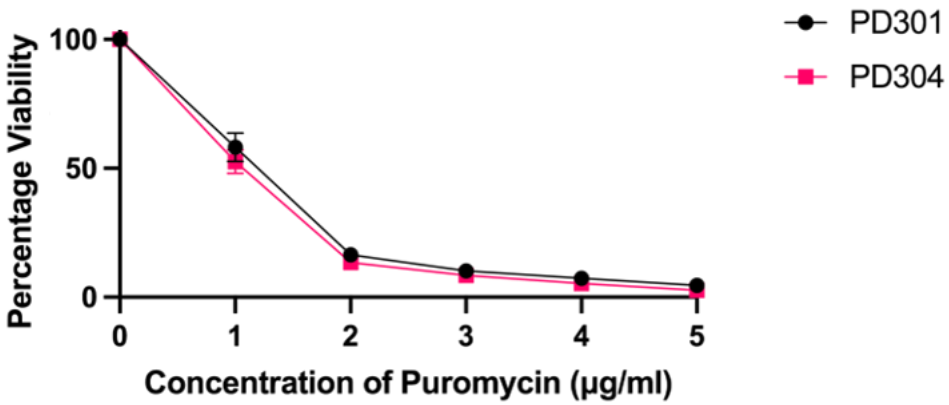

Figure 5.3 – Puromycin kill curve.

Percentage viability of PD301 and PD304 cells after 72 hours in the presence of increasing concentrations of puromycin (0-5µg/ml) added to cell medium. Resazurin was used to determine cell viability after 72 hours. Percentage viability was calculated for PD301 and PD304 cells against 0µg/ml concentration as control and regarded as 100%. N=3.

5.2.2 Transfection with SorL1 siRNA Knocks Down SorL1

Expression of SorL1 in enriched transfected PD301 cells was determined using immunofluorescence as used in optimisation stages. Transfected cells were formalin fixed and labelled with SorL1 antibody and Alexa Fluor 647 secondary antibody; Section 2.4. All four PD301 cell conditions were stained simultaneously to determine whether the difference in SorL1 expression was solely due to SorL1 siRNA. Three separate passages were stained independently.

Confirming previous successful transfection, GFP was absent in non-transfected cells and cells treated with Lipofectamine. GFP signal was seen in almost every cell transfected with either SorL1 siRNA or scrambled siRNA suggesting near 100% efficiency. Fluorescence corresponding to SorL1 was seen in all cell conditions and was visibly less prominent in cells transfected with SorL1 siRNA (Figure 5.4).

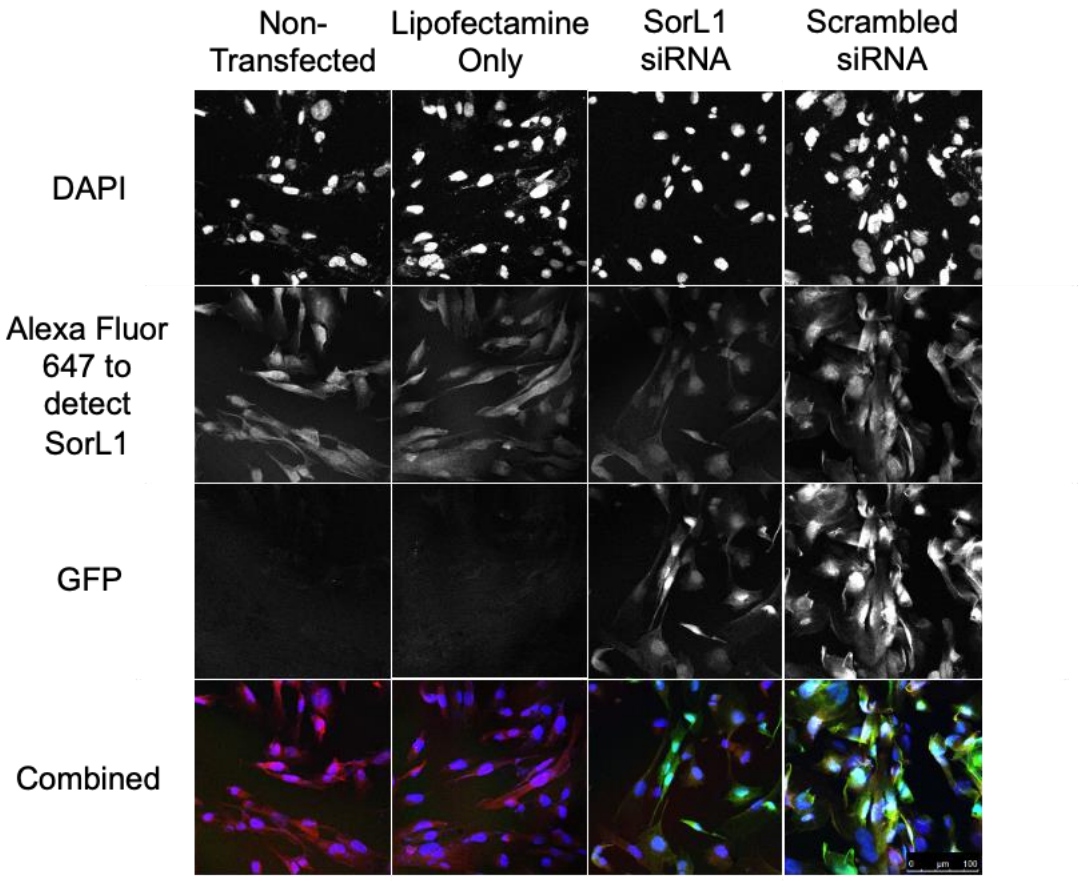

Figure 5.4 – Fluorescence of SorL1 is reduced in PD301 cells transfected with SorL1 siRNA vector.

SorL1 expression in non-transfected PD301 cells, PD301 cells treated with Lipofectamine 3000 only, PD301 cells transfected with SorL1 siRNA and PD301 cells transfected with scrambled siRNA (left to right). Cells stained with DAPI (top) and SorL1 antibody and subsequently Alexa Fluor 647 secondary antibody (upper middle). GFP channel to determine which PD301 cells were transfected with either siRNA (lower middle) and a combined image with all channels (bottom). N=3. Magnification = x20. Scale bar = 100µm.

At least 10 images were taken over random fields of view in each of the three replicates of each PD301 cell condition to allow quantification of fluorescence corrected against the background. Corrected total cell fluorescence of cells expressed with SorL1 siRNA was less than 50% of non-transfected cells, Lipofectamine treated and scrambled siRNA transfected cells ($P<0.01$ Tukey's test, $N=3$) (Figure 5.5). As no significant difference was found between any of the control PD301 cell conditions, adding either Lipofectamine only or scrambled siRNA had no effect on SorL1 expression.

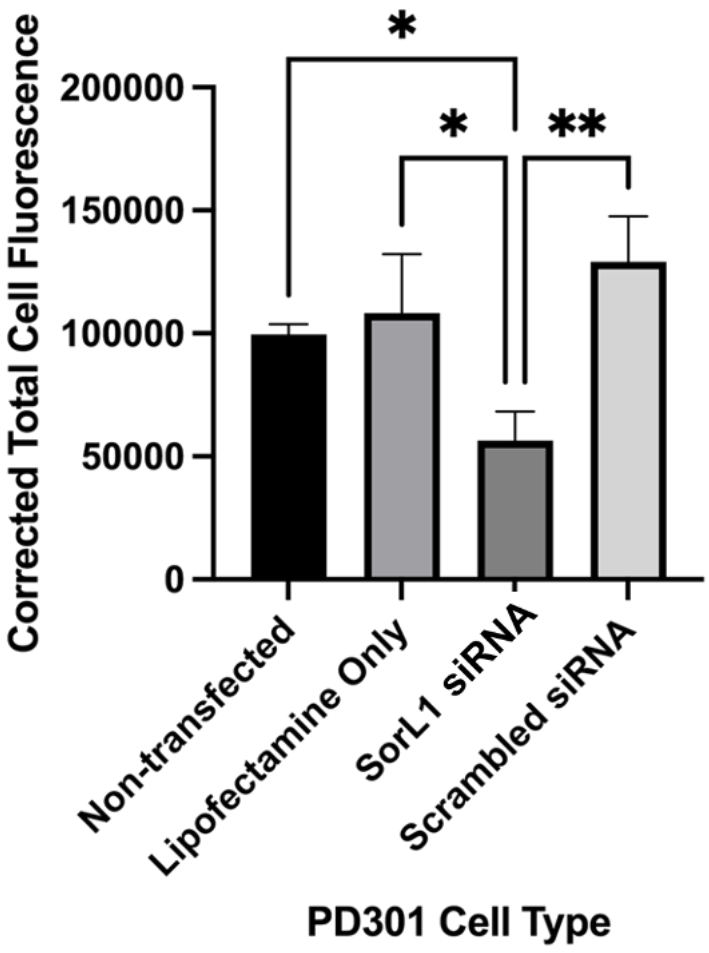

Figure 5.5 – Corrected total cell fluorescence of SorL1 expression is reduced in PD301 cells transfected with SorL1 siRNA vector.

*Semi-quantification of SorL1 fluorescence relative to background in non-transfected PD301 cells, Lipofectamine only PD301 cells, PD301 cells transfected with SorL1 siRNA and PD301 cells transfected with scrambled siRNA. N=10 images per cell type per replicate. SorL1 expression in PD301 cells transfected with SorL1 siRNA was significantly less than non-transfected cells, Lipofectamine treated cells and cells expressing scrambled siRNA. *P<0.05, **P<0.01 Tukey's Test. N=3.*

To confirm knock down of SorL1 seen in the immunocytochemistry data, western blots were undertaken in triplicate on three passages of cell lysates. A comparison of SorL1 expression between non-transfected PD301 cells, Lipofectamine only PD301 cells and PD301 cells transfected with SorL1 siRNA and scrambled siRNA once transfected cells were enriched due to puromycin selection.

When the membrane was probed for SorL1, PD301 cells transfected with SorL1 siRNA had a fainter band than the other three cell conditions. Bands were seen around 250kDa for all PD301 cell conditions, however, there appears to be a second fainter smaller band under all PD301 cell conditions when probed for SorL1 (Figure 5.6). The second thinner band underneath is likely an immature form of SorL1 that undergoes post-translational modifications to become the mature form seen as the thicker band above (Monti *et al.,* 2021; Rovelet-Lecrux *et al.,* 2021). Full blot for western blot is appended; Appendix 1, Figure A1.6. Also shown is consistent bands between all PD301 cell conditions when probed for β-actin as a loading control.

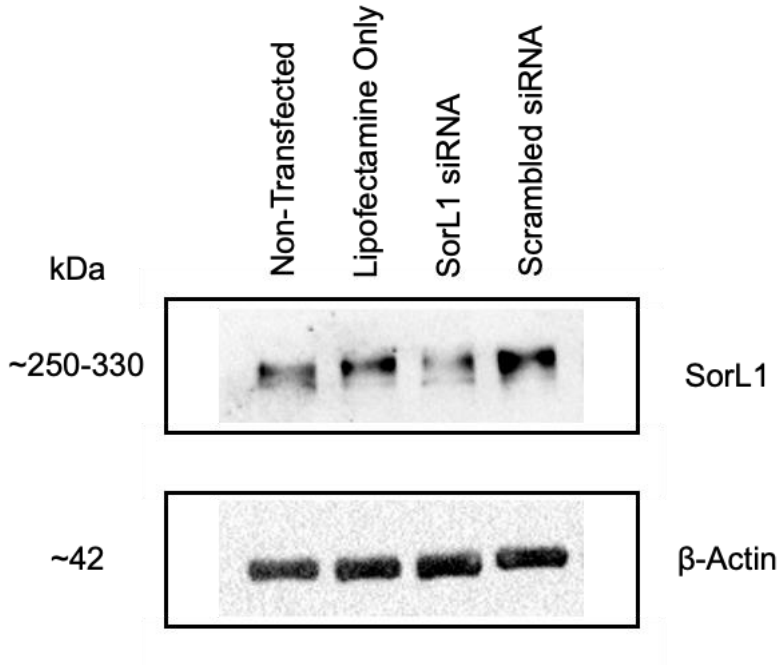

Figure 5.6 – SorL1 expression is reduced in PD301 cells transfected with SorL1 siRNA vector.

Representative western blot of SorL1 in PD301 cell lysates of non-transfected cells, Lipofectamine only cells and cells transfected with either SorL1 or scrambled siRNAs. Western blot showed less expression of SorL1 at 250 kDa (top) in PD301 cells transfected with SorL1 siRNA than the other three PD301 cell conditions. β-actin at 42 kDa (bottom). 10µg of protein was loaded. (N=3).

Densitometric analysis revealed SorL1 expression relative to β-actin expression in PD301 cells transfected with SorL1 siRNA was reduced by approximately 60% when compared to non-transfected PD301 cells, Lipofectamine treated cells and cells transfected with scrambled siRNA ($p<0.01$ Tukey's test, N=3) (Figure 5.7).

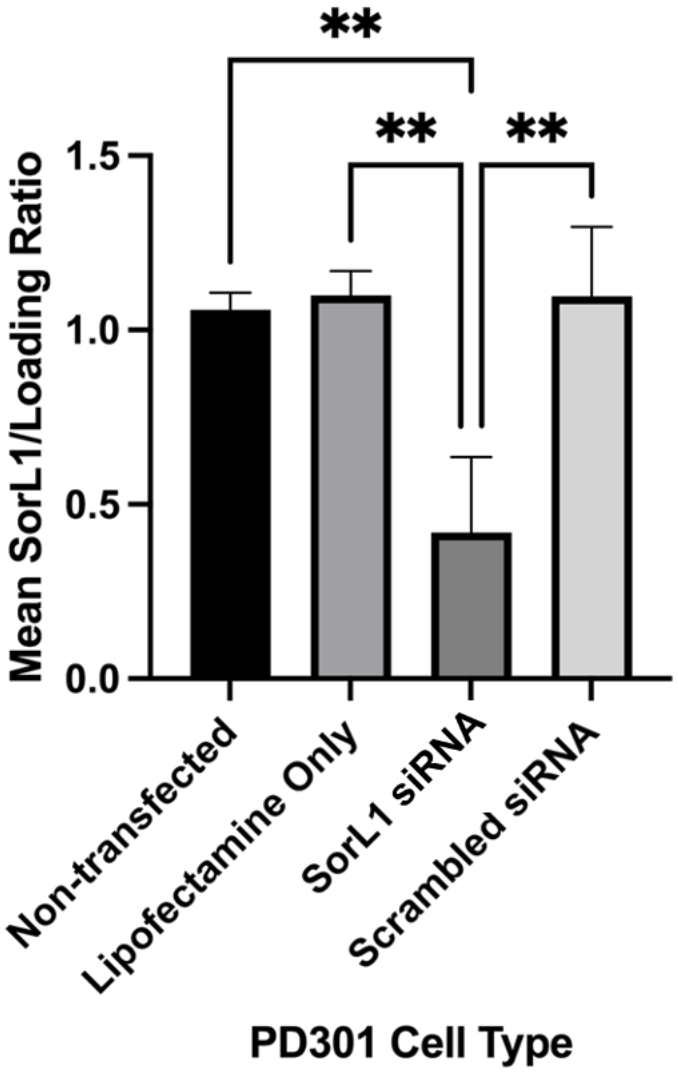

Figure 5.7 – Reduction of SorL1 expression in PD301 cells transfected with SorL1 siRNA vector.

*Densitometry of SorL1 expression relative to β-actin expression in non-transfected PD301 cells, Lipofectamine only PD304 cells, PD304 cells transfected with SorL1 siRNA and PD304 cells transfected with scrambled siRNA. SorL1 expression in PD304 cells transfected with SorL1 siRNA was significantly less than non-transfected PD304 cells, Lipofectamine only PD304 cells and PD304 cells transfected with scrambled siRNA. **P<0.001, Tukey's test. N=3.*

Enriched PD304 cells transfected with either siRNA encoded with SorL1 vector or scrambled vector due to puromycin selection were also imaged similar to PD301 cells. Confirming previous successful transfection, GFP was absent in non-transfected cells and cells treated with Lipofectamine. GFP signal was seen in almost every cell transfected with either SorL1 siRNA or scrambled siRNA suggesting near 100% efficiency. Fluorescence corresponding to SorL1 was seen in all cell conditions and was visibly less prominent in cells transfected with SorL1 siRNA (Figure 5.8).

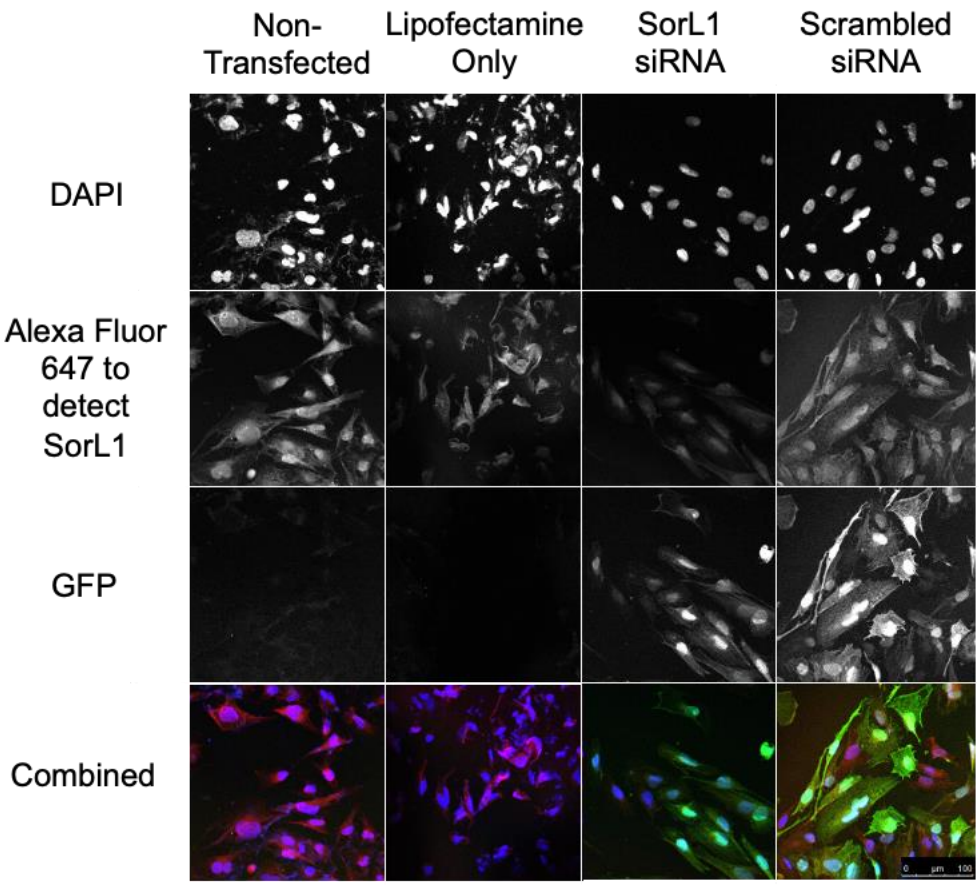

Figure 5.8 – Fluorescence of SorL1 is reduced in PD304 cells transfected with SorL1 siRNA vector.

SorL1 expression in non-transfected PD304 cells, PD304 cells treated with Lipofectamine 3000 only, PD304 cells transfected with SorL1 siRNA and PD304 cells transfected with scrambled siRNA (left to right). Cells stained with DAPI (top) and SorL1 antibody and subsequently Alexa Fluor 647 secondary antibody (upper middle). GFP channel to determine which PD304 cells were transfected with either siRNA (Lower Middle) and a combined image with all channels (bottom). N = 3. Magnification = x20. Scale bar = 100µm.

At least 10 images were taken over random fields of view in each of the three replicates of each PD304 cell condition to allow quantification of fluorescence corrected against the background. Corrected total cell fluorescence of cells expressed with SorL1 siRNA was less than 50% of non-transfected cells, Lipofectamine treated and scrambled siRNA transfected cells ($P<0.01$ Tukey's test, N=3) (Figure 5.9). As no significant difference was found between any of the

control PD304 cell conditions, adding either Lipofectamine only or scrambled siRNA had no effect on SorL1 expression.

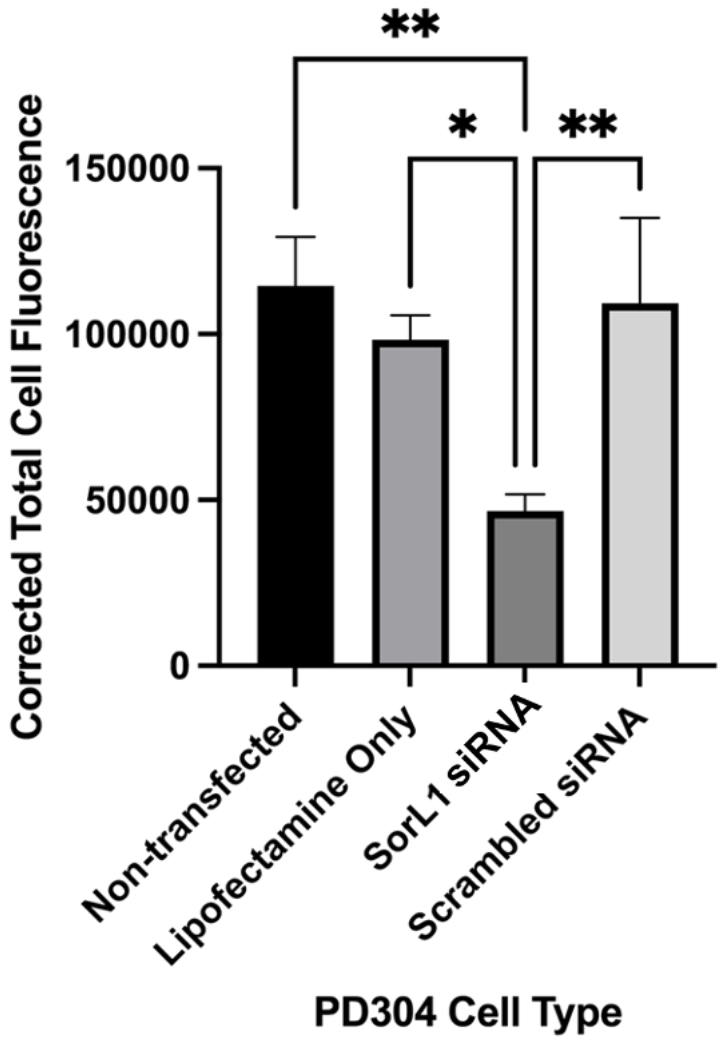

Figure 5.9 – Corrected total cell fluorescence of SorL1 expression is reduced in PD304 cells transfected with SorL1 siRNA vector.

*Semi-quantification of SorL1 fluorescence relative to background in non-transfected PD304 cells, Lipofectamine only PD304 cells, PD304 cells transfected with SorL1 siRNA and PD304 cells transfected with scrambled siRNA. N=10 images per cell type per replicate. SorL1 expression in PD304 cells transfected with SorL1 siRNA was significantly less than non-transfected cells. Lipofectamine treated cells and cells expressing scrambled siRNA *P<0.05, **P<0.01, Tukey's Test. N=3.*

To confirm knock down of SorL1 seen in the immunocytochemistry data, western blots were undertaken in triplicate on three passages of cell lysates. A comparison of SorL1 expression occurred between non-transfected PD304 cells, Lipofectamine only PD304 cells and PD304 cells transfected with SorL1 siRNA and scrambled siRNA once transfected cells were enriched due to puromycin selection.

When the membrane was probed for SorL1, PD304 cells transfected with SorL1 siRNA had a fainter band compared to the other 3 cell conditions. Bands were seen around 250kDa for all PD304 cell conditions, however there appears to be a second fainter smaller band under non-transfected PD304 cell lysates when probed for SorL1 (Figure 5.6). The second thinner band underneath is likely an immature form of SorL1 that undergoes post-translational modifications to become the mature form seen as the thicker band above (Monti *et al.,* 2021; Rovelet-Lecrux *et al.,* 2021). Full blot for western blot is appended; Appendix 1, Figure A1.7. Also shown is consistent bands between all PD304 cell conditions when probed for β-actin as a loading control.

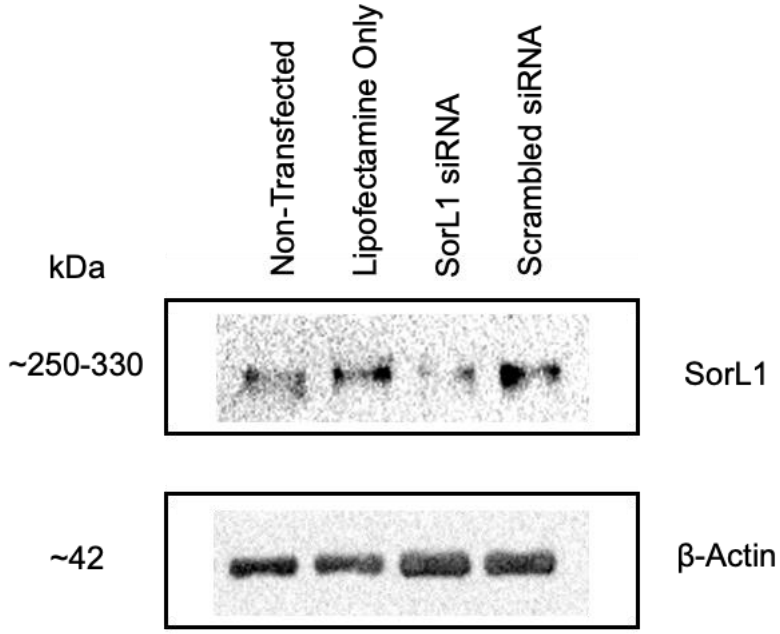

Figure 5.10 – SorL1 expression is reduced in PD301 cells transfected with SorL1 siRNA vector.

Representative western blot of SorL1 in PD304 cell lysates of non-transfected cells, Lipofectamine only cells and cells transfected with either SorL1 or scrambled siRNAs. Western blot showed less expression of SorL1 at 250 kDa (top) in PD301 cells transfected with SorL1 siRNA than the other three PD304 cell conditions. β-actin at 42 kDa (bottom). 10µg of protein was loaded. (N=3).

Densitometric analysis revealed SorL1 expression relative to β-actin expression in PD301 cells transfected with SorL1 siRNA was reduced by approximately 60% when compared to non-transfected PD301 cells, Lipofectamine treated cells and cells transfected with scrambled siRNA ($p<0.0001$ Tukey's test, N=3) (Figure 5.11).

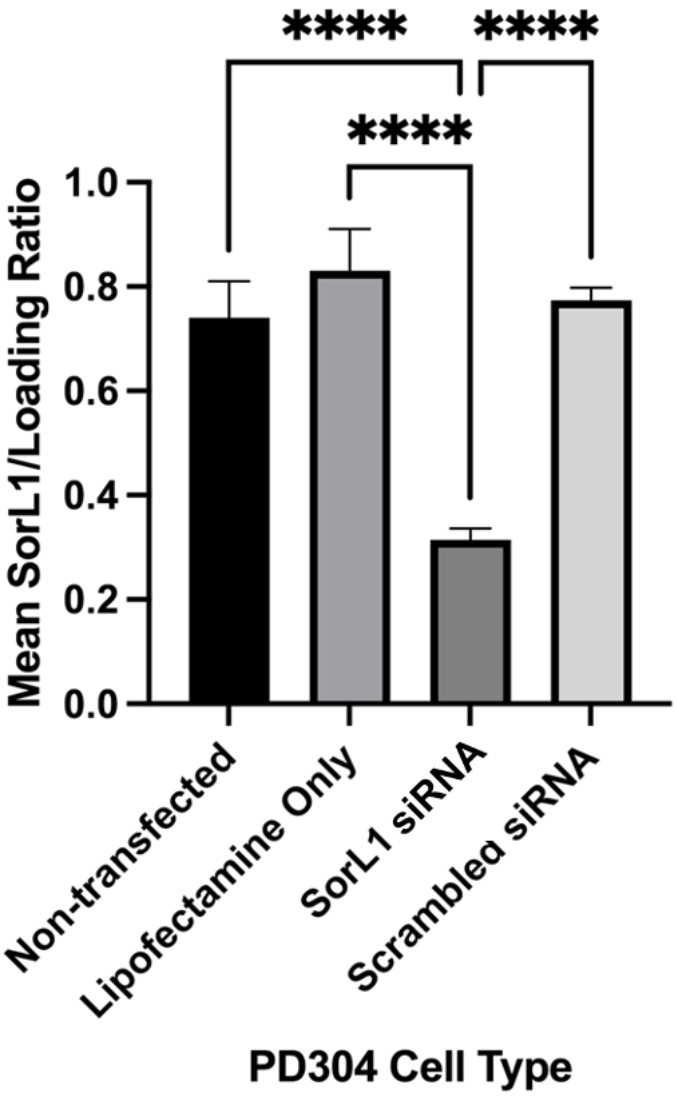

Figure 5.11 – Reduction of SorL1 expression in PD304 cells transfected with SorL1 siRNA vector.

*Densitometry of SorL1 expression relative to β-actin expression in non-transfected PD304 cells, Lipofectamine only PD304 cells, PD304 cells transfected with SorL1 siRNA and PD304 cells transfected with scrambled siRNA. SorL1 expression in PD304 cells transfected with SorL1 siRNA was significantly less than non-transfected PD304 cells, Lipofectamine only PD304 cells and PD304 cells transfected with scrambled siRNA. ****P<0.0001, Tukey's test. N=3.*

5.3 Discussion

The overarching aim was to explore the role of SorL1 in glioblastoma cells, which required a method to knock down the protein within cells to understand how the cells react. One way in achieving this outcome was by transiently transfecting a vector encoding SorL1 siRNA to create a knock-down model in PD301 and PD304 glioblastoma cells. As it was seen that an approximate 50% reduction in SorL1 protein and there was approximately 70% transfection efficiency, it can confidently be said that a successful SorL1 knock-down model in PD301 and PD304 cells was created. Successful transfection efficiency was validated through immunocytochemistry due to siRNA vectors encoding GFP. This allowed for visualisation of cells for analysis to determine transfection rate. Due to both immunocytochemistry and western blotting being semi-quantitative in nature, both techniques were needed to validate and confirm reduced protein levels once puromycin selection had enriched the cells transfected with siRNA.

It is widely recognised that transfecting immortalised cell lines is easier than transfecting primary patient cells (Gresch and Altrogge, 2012). Therefore, a greater effect may have been seen if immortalised cells had been used, instead of the primary patient cells. Immortalised cell lines are more amenable to transfection and more readily available, however, their biological system is considered to be more artificial (Pan *et al.,* 2009; Gresch and Altrogge, 2012). Transfection to knock down SorL1 protein was successful in the breast cancer cell line MDA-MB-361, however, even though transfection was a success, it was not conducted within a primary cell line (Pietilä *et al.,* 2019). In this chapter, managing to get successful transfection of primary patient cells allows for a more representative overview of glioblastoma cells due to the cells originating from patient glioblastoma tumours.

Vector-based siRNAs can be used for transient and stable knock down by plasmid transfection due to the efficient and stable expression of siRNA in both dividing and non-dividing cells, including difficult to transfect primary cells (Fus-Kujawa *et al.,* 2021). Puromycin selection enriched the proportion of transfected cells there were, so when cells were monitored, they were observed becoming small colonies

and eventually expanded the cell population containing either the SorL1 siRNA or scrambled siRNA. The siRNA used in this case being longer designs of 27-29 nucleotides, are more potent and efficient when compared to the standard 21-mer siRNAs when creating a stable transfection to knock down the gene, however, do not effect cellular response *(*Kim *et al.,* 2005; Igoucheva *et al.,* 2006).

Treating cells with RNAi gene silencing method allowed for a drug-induced response for reducing SorL1 expression in PD301 and PD304 cells. This is through interrupting SorL1 production at the mRNA level and effectively acting as a therapeutic if SorL1 becomes an interesting target for glioblastoma in the future, such like other siRNAs currently being investigated as therapeutics against undruggable targets for the treatment of B-cell lymphoma and cardiovascular diseases (Lu *et al.,* 2008; Dana *et al.,* 2017). In comparison to knocking down SorL1 at mRNA level, using CRISPR to knock out the *SORL1* gene at the DNA level may have induced Alzheimer's disease pathology characteristics, as such was shown knocking out *SORL1* from hiPSCs using the CRISPR-Cas9 system (Knupp *et al.,* 2020).

This chapter successfully shows:

i. Knock down of SorL1 was achieved by transient transfection of PD301 and PD304 cells with a set of four siRNA lentiviral vectors.
ii. Transient transfection of PD301 and PD304 cells with scrambled siRNA lentiviral vector.
iii. Creation of stable and transiently transfected PD301 and PD304 cells using SorL1 siRNA and scrambled siRNA to be used as a model to investigate functional effects.

Chapter 6

Functional Effects due to SorL1 Knock Down

6 Chapter 6 – Functional Effects due to SorL1 Knock Down

6.1 Background

6.1.1 Function of SorL1

Early studies of SorL1 revealed an association with cytoplasmic structure and hinted to a role of SorL1 in intracellular trafficking and lipoprotein metabolism in neurones (Motoi *et al.,* 1999). Following synthesis of SorL1, the protein can move through the secretory pathway through the Golgi to the cell surface releasing sSorL1, however, there is also the trafficking pathway of SorL1; Section 1.2.6.1. SorL1 is internalised via clathrin-dependent endocytosis guided by the clathrin adaptor protein 2 that binds to SorL1 in the cytoplasmic domain and transported to early endosomes (Barthelson *et al.,* 2020; Nielsen *et al.,* 2007; Schmidt *et al.,* 2017) (Figure 6.1). SorL1 binds directly to APP shuttling between the Golgi and endosomes sorting into endocytic or recycling pathways, and further alternative routes involve SorL1 shuttling from endosomes to the cell surface or to lysosomes (Schmidt *et al.,* 2017; Rovelet-Lecrux *et al.,* 2021; Lee *et al.,* 2008) (Figure 6.1). With SorL1 present within endosomes and at the cell surface, studies have suggested SorL1 may have additional roles in mediating APP endosome to cell surface trafficking (Andersen *et al.,* 2005; Herskowitz *et al.,* 2012).

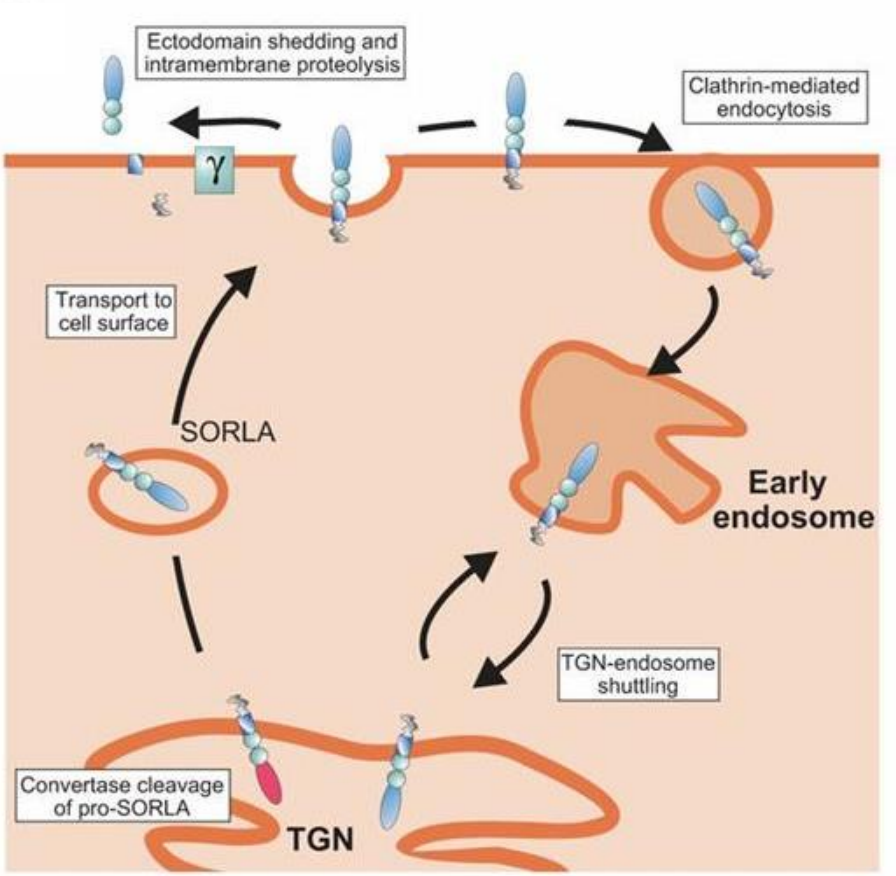

Figure 6.1 – SorL1 trafficking around the cell.

Active form of SorL1 is trafficked to the cell surface through the secretory pathway from the Golgi (TGN). At the cell surface, SorL1 is secreted through ectodomain shedding or enters the trafficking pathway entering the cell through clathrin-mediated endocytosis and is shuttled between endosomes and Golgi (Willnow and Andersen, 2013).

SorL1 is a multifunctioning sorting receptor (Offe *et al.,* 2006). It binds to APP and slows down its cellular transport out of the Golgi, as well as retrograding APP back to the Golgi from the endosomes. Therefore, the release of APP to amyloid pathways is controlled and the amount of amyloidogenic (Aβ) and nonamyloidogenic products is reduced (Mehmedbasic *et al.,* 2015; Andersen *et al.,* 2005; Offe *et al.,* 2006; Schmidt *et al.,* 2007). In absence of SorL1, there is no retrograde of APP back to the Golgi and therefore is released to the late endosomes, leading to excess Aβ production as seen in Alzheimer's disease (Lee *et al.,* 2008). Therefore, in Alzheimer's disease patients, it has been suggested

that restoring the SorL1 function may reduce the effect of Aβ neuro toxicity associated with age onset (Huang *et al.,* 2016).

6.1.2 Functional Implications when SorL1 Protein is Knocked Down or Reduced

Under expression of SorL1 increases the risk of developing Alzheimer's disease (Schmidt *et al.,* 2017). SorL1 was implicated as an important factor in Alzheimer's disease as SorL1 knockout mice led to an increase in Aβ secretion, similar to that seen in Alzheimer's disease (Andersen *et al.,* 2005). As well as an increase in amyloid proteins leading to an increased risk of Alzheimer's disease, mutations in the *SORL1* gene also reduced the binding affinity between SorL1 and APP (Alvarez-Mora *et al.,* 2022; Cuccaro *et al.,* 2016). As a direct result of common mutated forms of *SORL1*, Aβ42 secretion is increased, and in rare *SORL1* mutations, increased secretion is found in both Aβ40 and Aβ42 (Vardarajan *et al.,* 2015). Changes in SorL1 expression or loss of function due to acquired or inherited reasons mechanistically increases the risk of Alzheimer's disease and a reduction in the *SORL1* gene has been considered to be a primary and pathogenic event (Raghavan *et al.,* 2018; Rogaeva *et al.,* 2007).

SorL1 has also been experimentally silenced in cancer. SorL1 was knocked down in breast cancer cells to determine its effect on the HER2 protein and on cell (Pietilä *et al.,* 2019). However, the role SorL1 has on brain tumour cells has never been explored. This chapter aims to confirm the biochemical link between SorL1 and amyloid production by determining Aβ40 and Aβ42 levels following knock down. Furthermore, as a higher expression of SorL1 in glioblastoma cells may indicate a pathological role, it was then sought to determine the functional effects silencing SorL1 will have on cell proliferation, viability and migration.

6.2 Results – Functional Effects

Transfecting PD301 and PD304 cells with SorL1 siRNA reduced SorL1 expression; Chapter 5. This chapter investigates the functional significance of SorL1 by determining the effect SorL1 knock down had on expression of Aβ40 and Aβ42, cell proliferation, viability, and migration.

The following sections all have the same experimental groups: PD301 or PD304 cells transfected with SorL1 siRNA, cells transfected with scrambled siRNA, cells treated with Lipofectamine 3000 (ThermoFisher, UK) or naïve cells that were untreated and un-transfected. Unfortunately, the antibodies previously used to label Aβ40 and Aβ42 were unavailable. Two alternatives were characterised in both PD301 and PD304 cells and revealed comparable labelling to that seen previously; Chapter 3. Images characterising new antibodies are appended; Appendix 3.

6.2.1 Functional Effect of SorL1 Knock Down in PD301 and PD304 Cells: Aβ40 Expression

To determine Aβ40 expression in PD cells following transfection of SorL1 siRNA, cells were fixed and stained; Section 2.3.

For all PD301 cell conditions, GFP was imaged to confirm transfection success and Aβ40 expression with Alexa Fluor 647 secondary antibody was imaged. The experiment was repeated in triplicate in three different passages. At least 10 images were taken from each of the three replicates to allow for quantification of fluorescence intensity; Section 2.4.

Low intensity fluorescence corresponding to Aβ40 was seen in all PD301 cell conditions and predominantly in a punctate pattern throughout the cytoplasm (Figure 6.2). GFP signal was seen in almost all cells transfected with SorL1 siRNA or scrambled siRNA and never in naïve or Lipofectamine treated cells confirming high transfection success. Cells transfected with SorL1 siRNA occasionally

showed individual cells with an intense Aβ40 signal. These were not seen in cells transfected with scrambled siRNA.

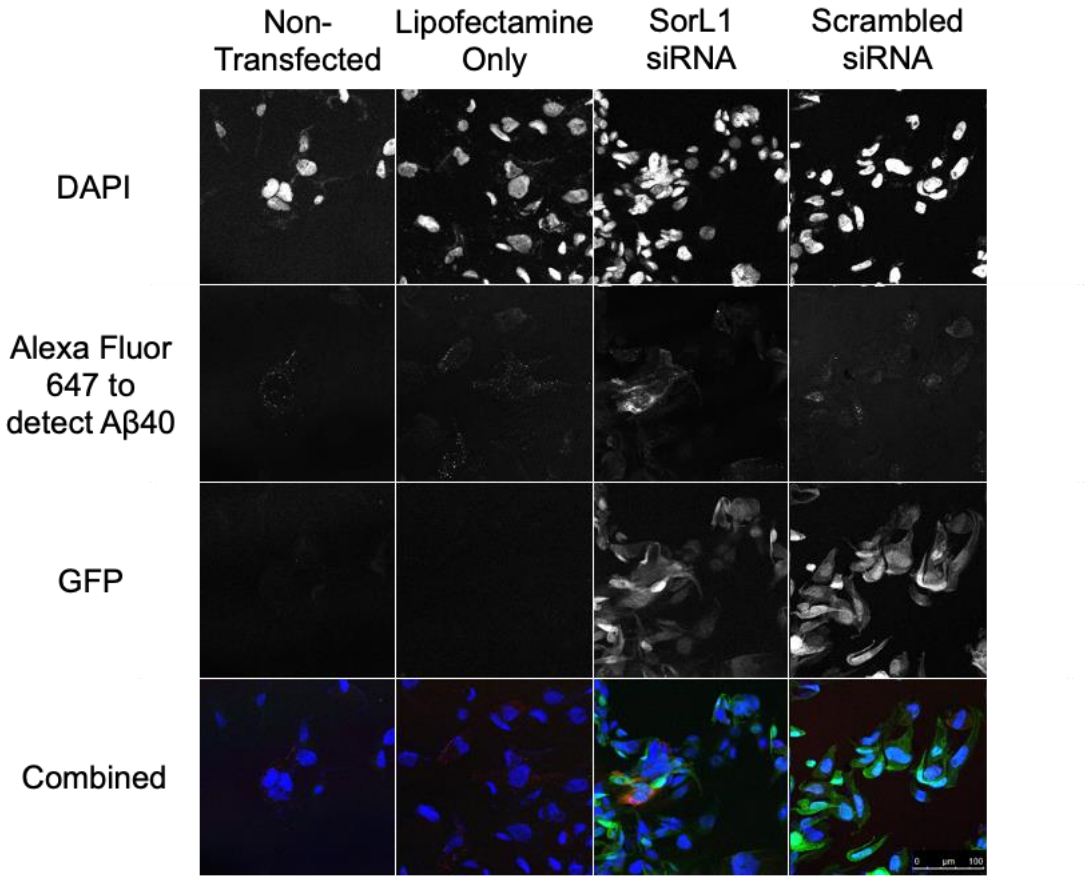

Figure 6.2 – Immunofluorescence of Aβ40 in SorL1 siRNA transfected PD301 cells.

Aβ40 expression in non-transfected PD301 cells, PD301 cells treated with Lipofectamine 3000 only, PD301 cells transfected with SorL1 siRNA and PD301 cells transfected with scrambled siRNA (Left to Right). Cells stained with DAPI (Top) and Aβ40 antibody and subsequently Alexa Fluor 647 secondary antibody (Upper Middle). GFP channel to determine which PD301 cells were transfected with either siRNA (Lower Middle) and a combined image with all channels (Bottom). N = 3. Magnification = x20. Scale bar = 100µm.

Mean fluorescence intensity of SorL1 siRNA transfected PD301 cells was approximately two-fold higher than non-transfected cells ($P<0.05$ Tukey's test, N=3, Figure 6.3). The mean fluorescence intensity of cells transfected with

scrambled siRNA was not significantly different to non-transfected cells or Lipofectamine only cells, but similarly not significantly different to cells transfected with SorL1 siRNA (P>0.05 Tukey's test, N=3, Figure 6.3).

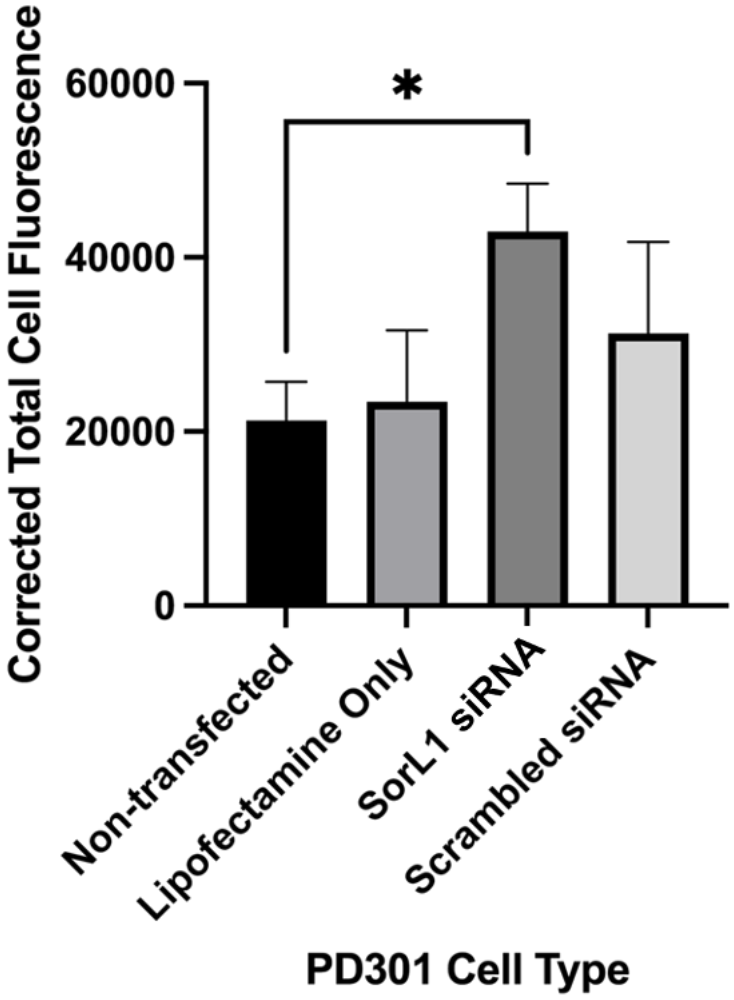

Figure 6.3– Corrected total cell fluorescence of Aβ40 expression is increased in SorL1 knock down PD301 cells.

Aβ40 expression relative to background in non-transfected PD301 cells, Lipofectamine only PD301 cells, PD301 cells transfected with SorL1 siRNA and PD301 cells transfected with scrambled siRNA. N=10 images per cell type per replicate. Aβ40 expression was significantly higher in PD301 cells transfected with SorL1 siRNA than non-transfected PD301 cells. P<0.05, Tukey's Test. N=3.

Similar to PD301 cells, low intensity fluorescence corresponding to Aβ40 was seen in all PD304 cell conditions and predominantly in a punctate pattern throughout the cytoplasm. Some high intensity fluorescent areas were observed in all cell

conditions but were most prominent in PD304 cells transfected with SorL1 siRNA (Figure 6.4). GFP signal was seen in almost all cells transfected with SorL1 siRNA or scrambled siRNA and never in naïve or Lipofectamine treated cells confirming high transfection success.

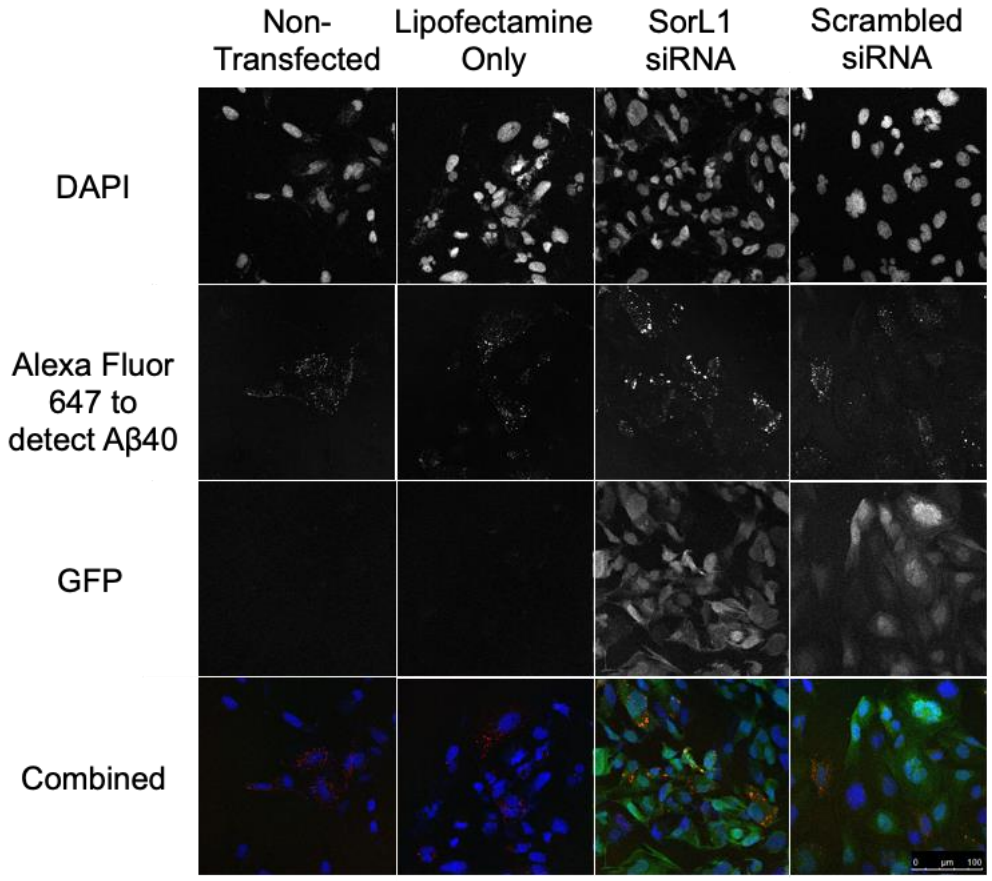

Figure 6.4 – Immunofluorescence of Aβ40 in SorL1 siRNA transfected PD304 cells.

Aβ40 expression in non-transfected PD304 cells, PD304 cells treated with Lipofectamine 3000 only, PD304 cells transfected with SorL1 siRNA and PD304 cells transfected with scrambled siRNA (Left to Right). Cells stained with DAPI (Top) and Aβ40 antibody and subsequently Alexa Fluor 647 secondary antibody (Upper Middle). GFP channel to determine which PD304 cells were transfected with either siRNA (Lower Middle) and a combined image with all channels (Bottom). N = 3. Magnification = x20. Scale bar = 100µm.

Mean fluorescent intensity of SorL1 siRNA transfected PD304 cells was between two-fold and 2.5-fold higher than non-transfected and Lipofectamine treated cells

respectively ($P<0.01$ Tukey's test, N=3, Figure 6.5). The mean fluorescence intensity of PD304 cells transfected with scrambled siRNA was also significantly increased compared to PD304 cells treated with Lipofectamine only ($P<0.05$ Tukey's test, N=3), however, there were not significantly different to non-transfected cells or cells transfected with SorL1 siRNA.

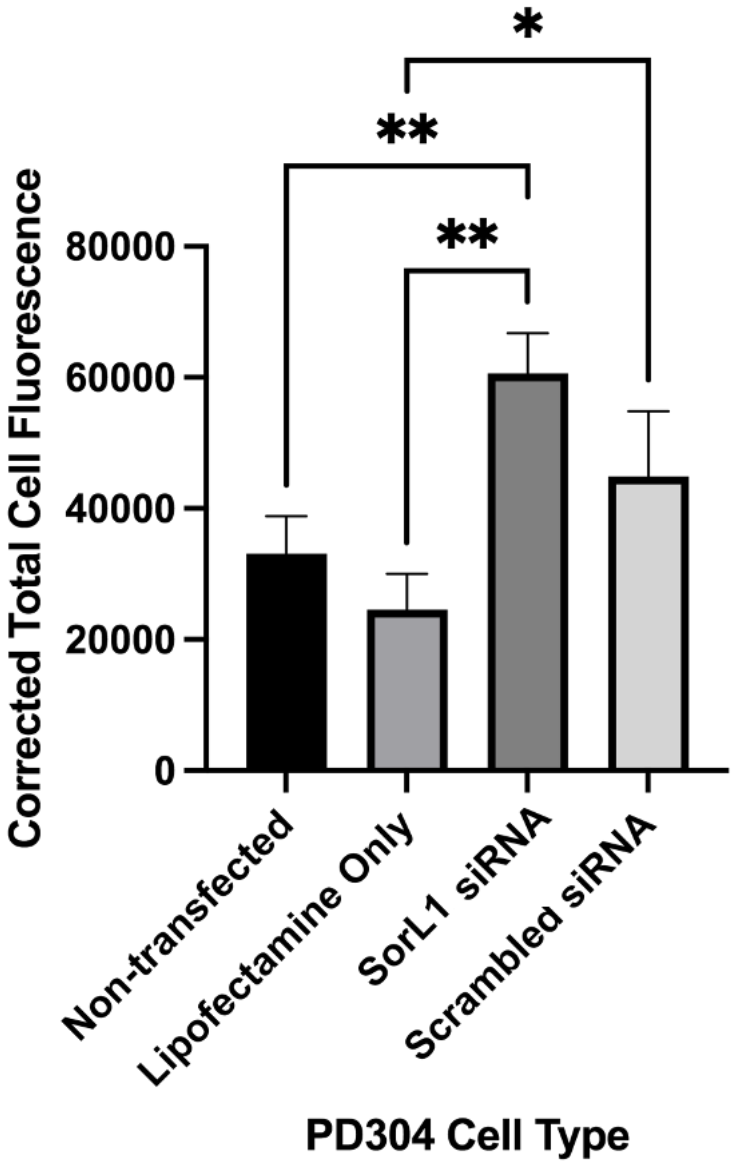

Figure 6.5 – Corrected total cell fluorescence of Aβ40 expression is increased in SorL1 knock down PD304 cells.

*Aβ40 expression relative to background noise in non-transfected PD304 cells, Lipofectamine only PD304 cells, PD304 cells transfected with SorL1 siRNA and PD304 cells transfected with scrambled siRNA. N=10 images per cell type per replicate. Aβ40 expression was significantly higher in PD304 cells transfected with SorL1 siRNA than non-transfected PD304 cells and Lipofectamine only PD304 cells. **P<0.01, Tukey's Test. N=3. Aβ40 expression was significantly higher in PD304 cells transfected with scrambled siRNA than Lipofectamine only PD304 cells. *P<0.05, Tukey's Test. N=3.*

To support the semi-quantitative observation of increased Aβ40 expression in PD301 cells and PD304 cells transfected with SorL1 siRNA, an Aβ40 ELISA was performed on cell lysates from 3 passages to quantify Aβ40 expression in duplicate. Protein concentration was quantified against a standard curve ranging from 7.81-500pg/ml. Standard curve is appended; Appendix 4. Data are expressed as picograms of Aβ40 per milligram of total protein, Section 2.7.

A consistent level of Aβ40 was detected in lysates from all PD301 cell conditions with no variation detected between any transfected or treated cells ($P>0.05$ Tukey's test, N=3, Figure 6.6).

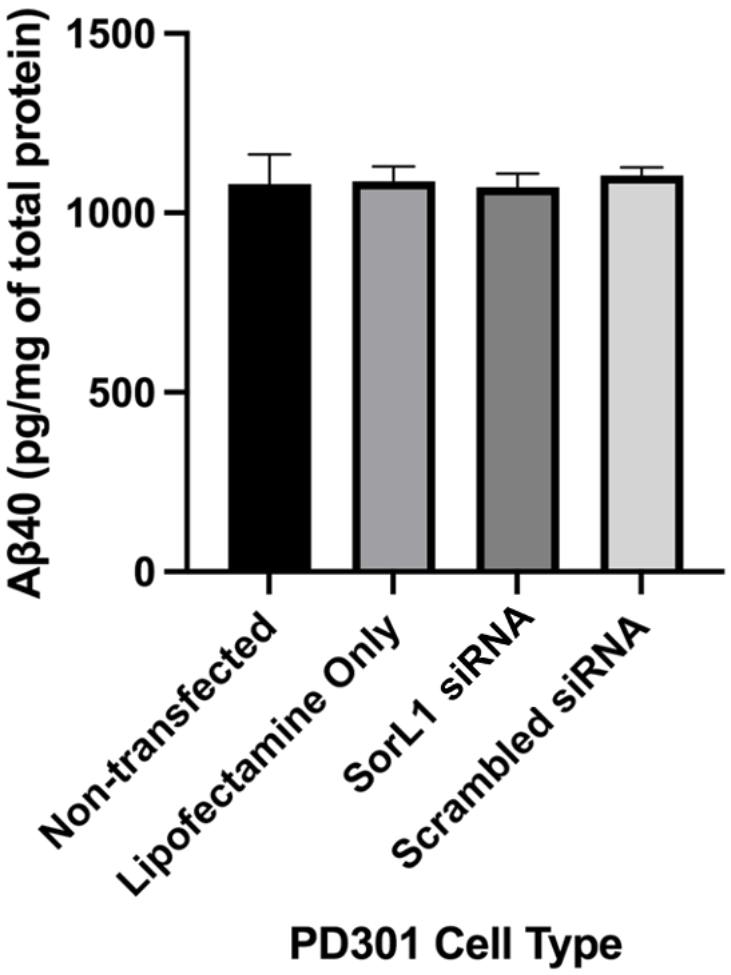

Figure 6.6 – Aβ40 expression in SorL1 knock down PD301 cells.

Aβ40 protein in picograms per milligram of total protein of non-transfected PD301 cells, PD301 cells treated with Lipofectamine only, PD301 cells transfected with SorL1 siRNA and PD301 cells transfected with scrambled siRNA. Aβ40 expression had no significant difference between any of the PD301 cell conditions. Data collected in duplicate, N=3.

Similarly, no variation was seen between any PD304 cell condition with all lysates having a mean Aβ40 content of approximately 1000 pg/mg of total protein (P>0.05 Tukey's test, N=3, Figure 6.7).

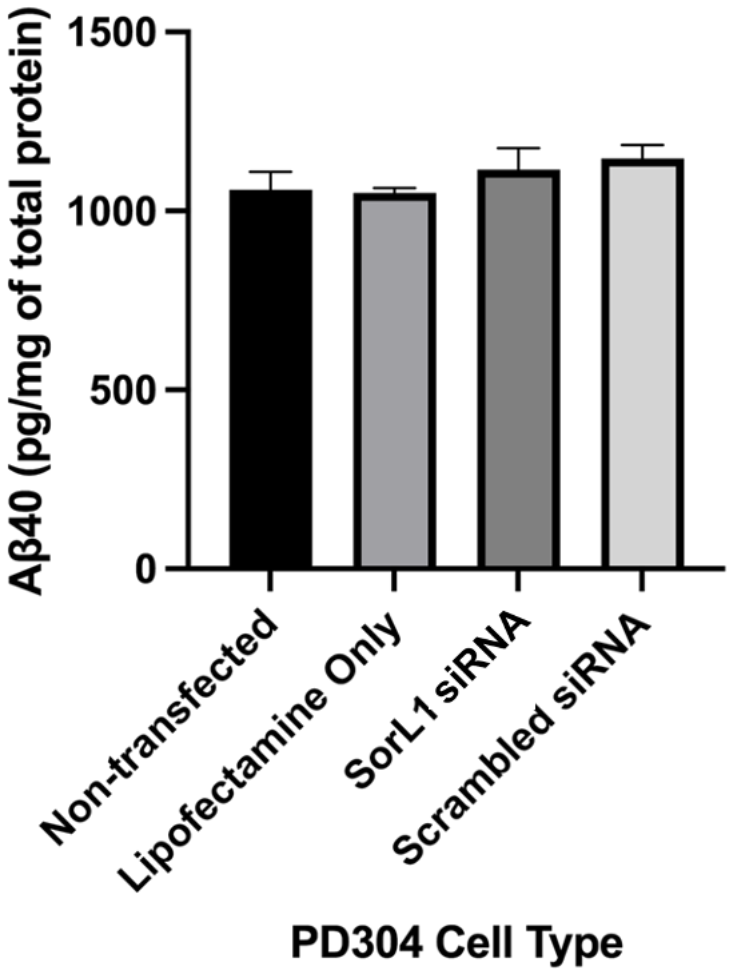

Figure 6.7 – Aβ40 expression in SorL1 knock down PD304 cells.

Aβ40 protein in picograms per milligram of total protein of non-transfected PD304 cells, PD304 cells treated with Lipofectamine only, PD304 cells transfected with SorL1 siRNA and PD304 cells transfected with scrambled siRNA. Aβ40 expression had no significant difference between any of the PD304 cell conditions. Data collected in duplicate, N=3.

6.2.2 Functional Effect of SorL1 Knock Down in PD301 and PD304 Cells: Aβ42 Expression

To determine Aβ42 expression in PD cells following transfection of SorL1 siRNA, cells were fixed and stained; Section 2.3.

For all PD301 cell conditions, GFP was imaged to confirm transfection success and Aβ42 expression with Alexa Fluor 647 secondary antibody was imaged. The experiment was repeated in triplicate in three different passages. At least 10 images were taken from each of the three replicates to allow for quantification of fluorescence intensity; Section 2.4.

Low to moderate intensity fluorescence corresponding to Aβ42 was seen in all PD301 cell conditions and distributed evenly across the cytoplasm. Higher fluorescence was seen in the nuclei (Figure 6.8). A GFP signal was seen in almost all cells transfected with SorL1 siRNA or scrambled siRNA and never in naïve or Lipofectamine treated cells to confirm high transfection success. Cells transfected with SorL1 siRNA had predominantly a uniform label throughout the cytoplasm similar to non-transfected cells, however some cells showed noticeably more variable fluorescence. In these cells, the occasional regions of high intensity surrounded the nuclei and did not overlay the DAPI nuclei signal (Figure 6.8). This change in localisation was not seen in cells transfected with scrambled siRNA.

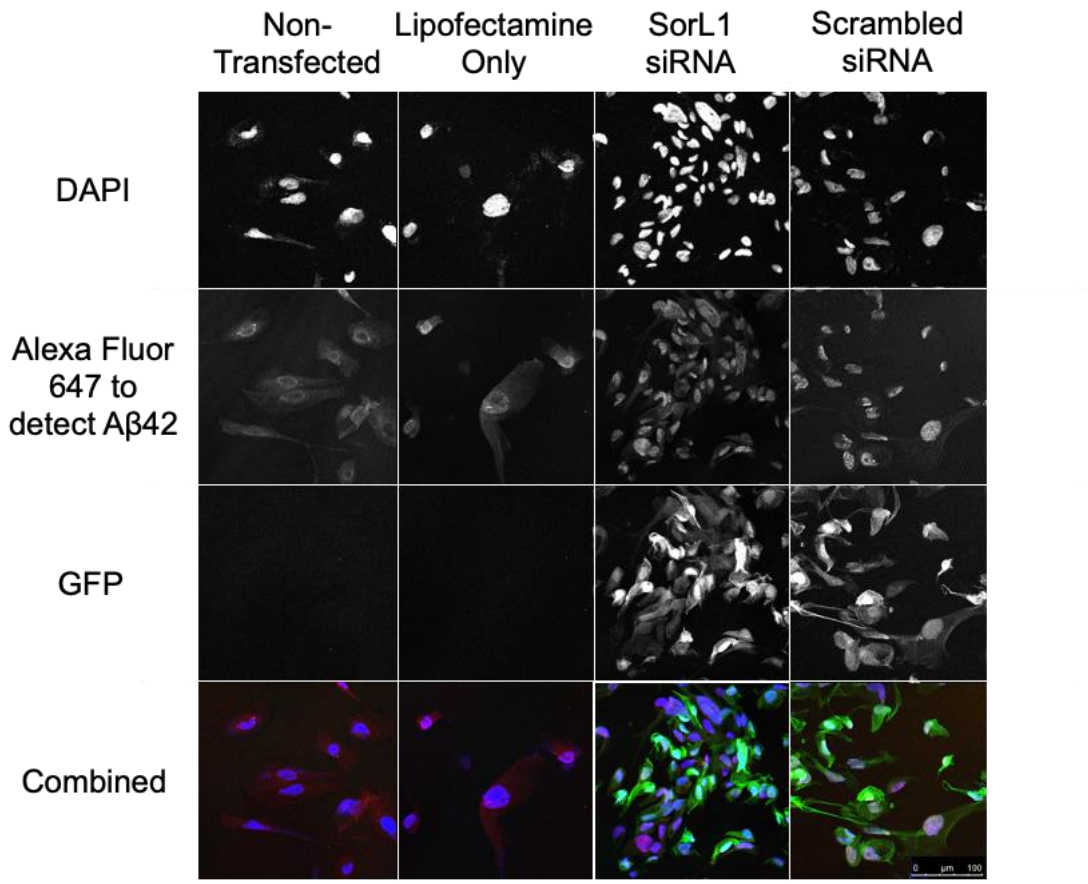

Figure 6.8 – Immunofluorescence of Aβ42 in SorL1 siRNA transfected PD301 cells.

Aβ42 expression in non-transfected PD301 cells, PD301 cells treated with Lipofectamine 3000 only, PD301 cells transfected with SorL1 siRNA and PD301 cells transfected with scrambled siRNA (Left to Right). Cells stained with DAPI (Top) and Aβ42 antibody and subsequently Alexa Fluor 647 secondary antibody (Upper Middle). GFP channel to determine which PD301 cells were transfected with either siRNA (Lower Middle) and a combined image with all channels (Bottom). N = 3. Magnification = x20. Scale bar = 100µm.

The mean fluorescence intensity corresponding to Aβ42 was more variable than the mean fluorescence intensity corresponding to Aβ40 in PD301 cells. The mean fluorescence of SorL1 siRNA transfected PD301 cells was approximately two-fold higher than naïve cells, however, no significant differences were seen in mean fluorescence intensities for Aβ42 in any of the PD301 cell groups ($P>0.05$ Tukey's test, N=3, Figure 6.9).

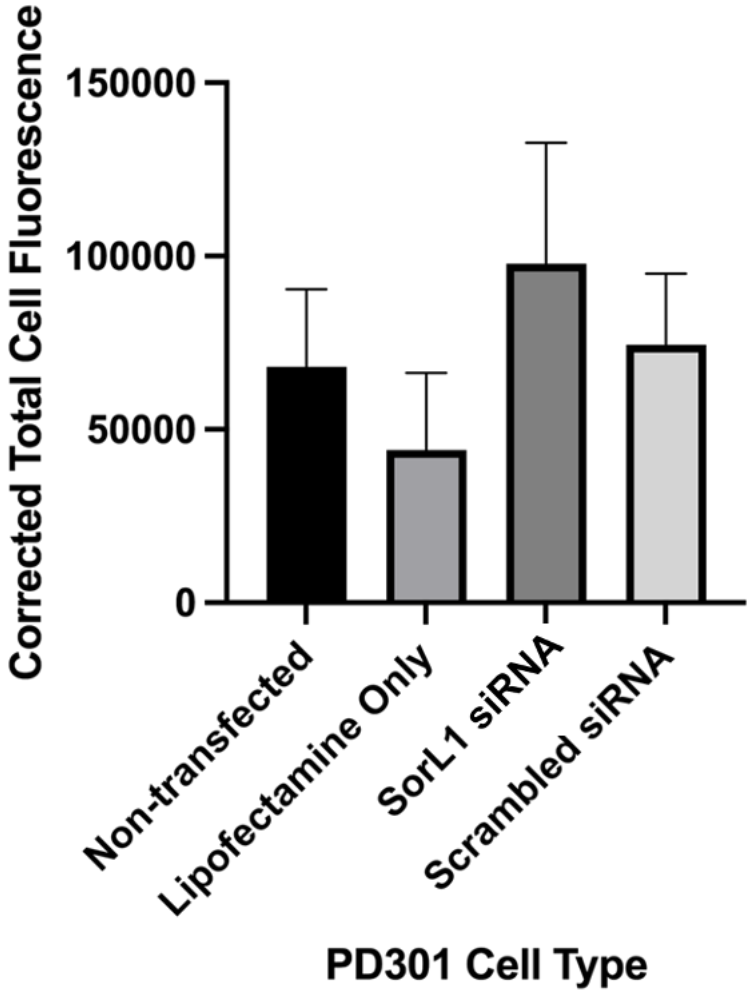

Figure 6.9 – Corrected total cell fluorescence of Aβ42 expression is increased in SorL1 knock down PD301 cells.

Aβ42 expression relative to background noise in non-transfected PD301 cells, Lipofectamine only PD301 cells, PD301 cells transfected with SorL1 siRNA and PD301 cells transfected with scrambled siRNA. N=10 images per cell type per replicate. Aβ42 expression had no significant difference between any PD301 cell conditions. N=3.

Moderate to high fluorescence corresponding to Aβ42 was seen in PD304 cells. Fluorescence was seen throughout the cytoplasm in some cells but was sparsely distributed in the cytoplasm of most cells and most predominant in the nuclei (Figure 6.10). A GFP signal was seen in almost all cells transfected with SorL1 siRNA or scrambled siRNA and not in naïve or Lipofectamine treated cells to confirm high transfection success. PD304 cells transfected with SorL1 siRNA had

high intensity label in almost all nuclei with limited fluorescence in the cytoplasm. PD304 cells transfected with scrambled siRNA did not show the same pattern of fluorescence as SorL1 siRNA transfected cells with only occasional cells having showing high intensity in the nucleus. However, most nuclei of PD304 cells transfected with scrambled siRNA did not label strongly, with highest signal seen surrounding the nuclei (Figure 6.10).

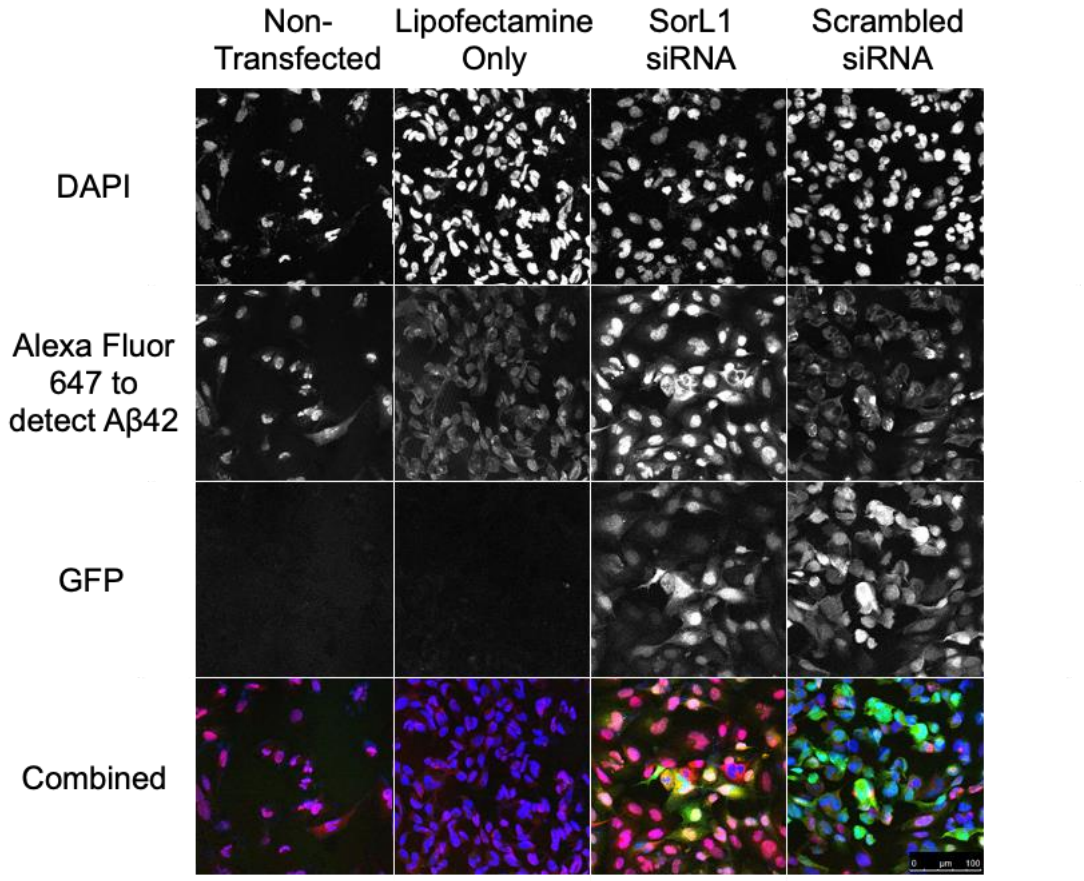

Figure 6.10 – Immunofluorescence of Aβ42 in SorL1 siRNA transfected PD304 cells.

Aβ42 expression in non-transfected PD304 cells, PD304 cells treated with Lipofectamine 3000 only, PD304 cells transfected with SorL1 siRNA and PD304 cells transfected with scrambled siRNA (Left to Right). Cells stained with DAPI (Top) and Aβ42 antibody and subsequently Alexa Fluor 647 secondary antibody (Upper Middle). GFP channel to determine which PD304 cells were transfected with either siRNA (Lower Middle) and a combined image with all channels (Bottom). N = 3. Magnification = x20. Scale bar = 100µm.

Mean fluorescence intensity of SorL1 siRNA transfected PD304 cells was over two-fold higher than Lipofectamine treated cells ($P<0.01$ Tukey's test, N=3, Figure 6.11). The fluorescence intensity of scrambled siRNA transfected PD304 cells was not significantly different to non-transfected or Lipofectamine treated, but was also not significantly different to the SorL1 siRNA group.

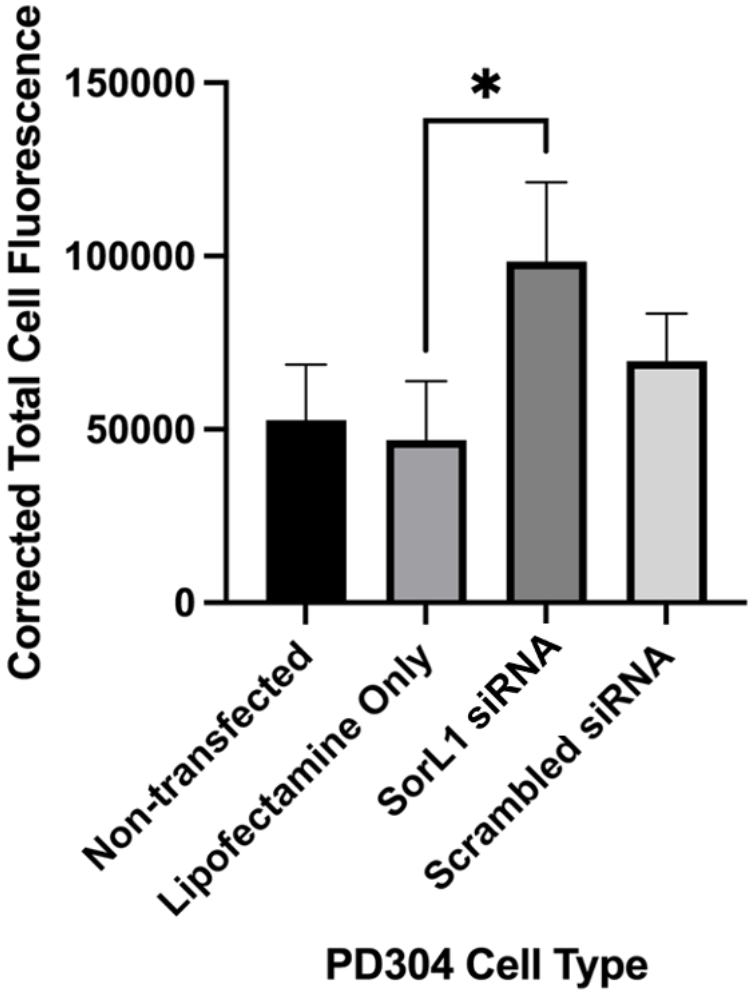

Figure 6.11 – Corrected total cell fluorescence of Aβ42 expression is increased in SorL1 knock down PD304 cells.

Aβ42 expression relative to background noise in non-transfected PD304 cells, Lipofectamine only PD304 cells, PD304 cells transfected with SorL1 siRNA and PD304 cells transfected with scrambled siRNA. N=10 images per cell type per replicate. No significant differences in Aβ42 expression between PD304 cells transfected with SorL1 siRNA and non-transfected cells or cells transfected with scrambled siRNA. Aβ42 expression is significantly higher in PD304 cells transfected with SorL1 siRNA than Lipofectamine only PD304 cells. P<0.05, Tukey's Test. N=3.

To validate the semi-quantitative observation from immunofluorescence data showing increased Aβ42 expression in PD301 cells and PD304 cells transfected with SorL1 siRNA, an ultrasensitive Aβ42 ELISA was performed on cell lysates from 3 passages to quantify Aβ42 expression in duplicate. Protein concentration was quantified against a standard curve ranged between 1.56-100pg/ml. Standard

curve is appended; Appendix 4. Data are expressed as picograms of Aβ42 per milligram of total protein, Section 2.7.

The data were quite variable and no statistically significant differences in Aβ42 expression were detected between any cell condition in either PD301 or PD304 lysates (P>0.05 Tukey's test, Figures 6.12 and 6.13).

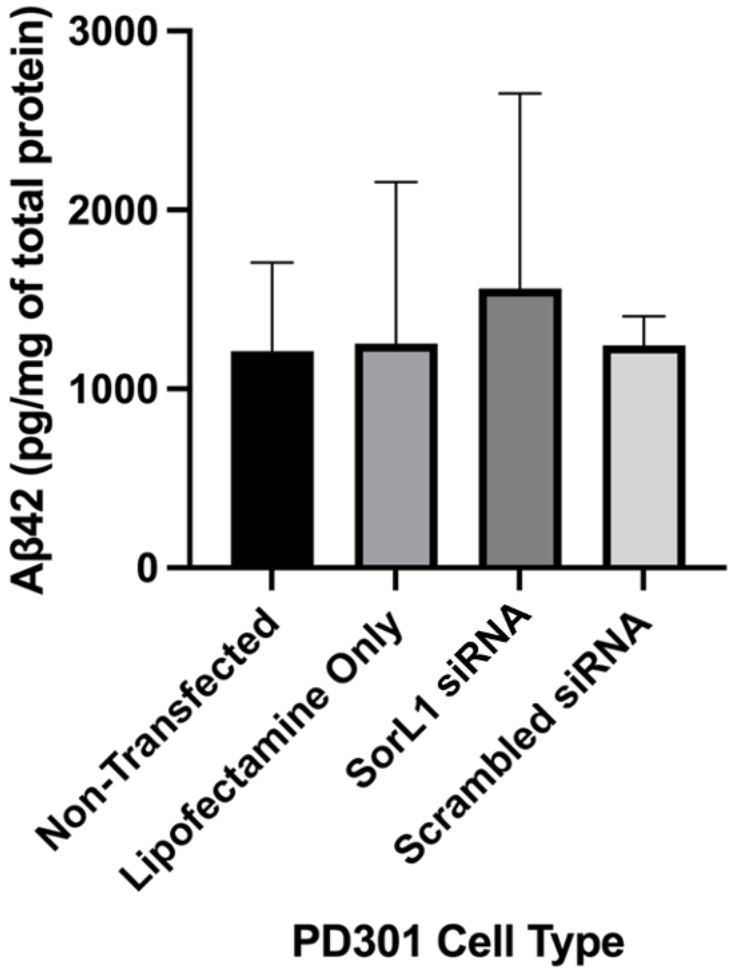

Figure 6.12 – Aβ42 expression SorL1 knock down PD301 cells.

Aβ42 protein in picograms per milligram of total protein of non-transfected PD301 cells, PD301 cells treated with Lipofectamine only, PD301 cells transfected with SorL1 siRNA and PD301 cells transfected with scrambled siRNA. Aβ42 expression had no significant difference between any of the PD301 cell conditions. Data collected in duplicate, N=3.

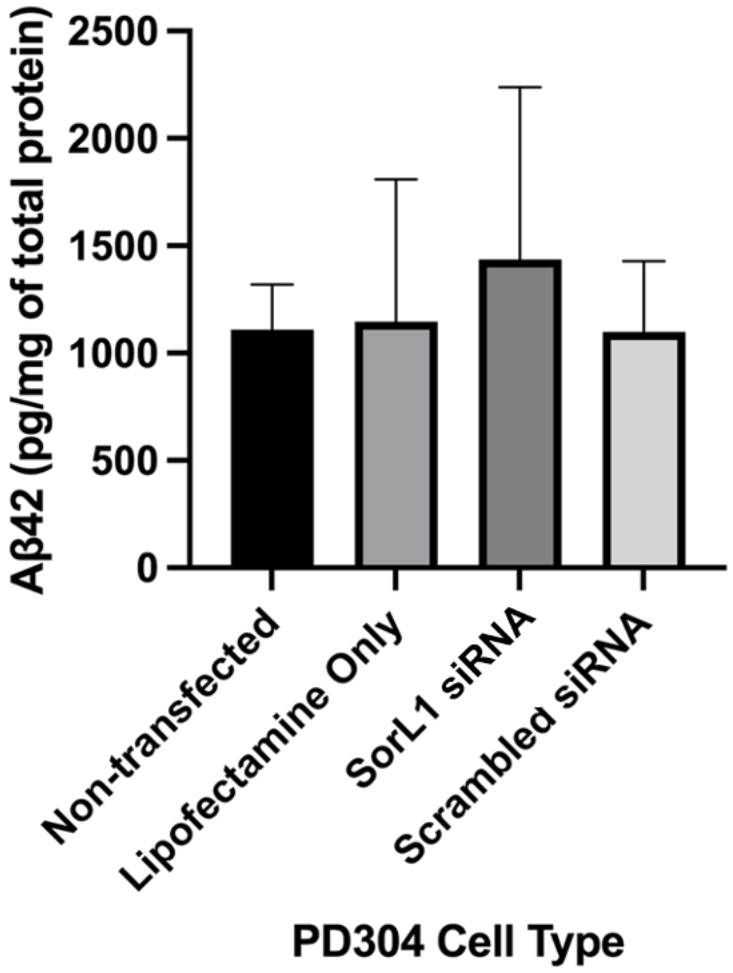

Figure 6.13 – Aβ42 expression SorL1 knock down PD304 cells.

Aβ42 protein in picograms per milligram of total protein of non-transfected PD304 cells, PD304 cells treated with Lipofectamine only, PD304 cells transfected with SorL1 siRNA and PD304 cells transfected with scrambled siRNA. Aβ42 expression had no significant difference between any of the PD304 cell conditions. Data collected in duplicate, N=3.

6.2.3 Functional Effect of SorL1 Knock Down in PD301 and PD304 Cells: Proliferation and Viability

To determine whether knock down of SorL1 protein influenced proliferation and cell viability in PD301 and PD304 glioblastoma cells, a 3-(4,5-dimethylthiazol-2-yl)-5-(3-carboxymethoxphenyl)-2-(4-sulfophenyl)-2H-tertazolium (MTS) assay was performed over 72 hours; Section 2.10.1. Cell proliferation was expressed as

mean absorbance from four independent experiments performed in triplicate. Percentage viability was calculated for each cell condition against the non-transfected cells regarded as 100%.

Proliferation was seen in all 4 cell conditions for both PD301 and PD304 cells with proliferation starting to plateau at 24 hours (Figure 6.14 and Figure 6.16). PD301 cells transfected with SorL1 siRNA had lower absorbance values than the other three cell types (Figure 6.14). At 24 hours, PD301 cells transfected with SorL1 siRNA had significantly lower absorbance than naïve cells and Lipofectamine only treated cells ($P<0.05$ Tukey's test N=3, Figure 6.14). Absorbance of PD301 cells transfected with scrambled siRNA was not significantly different to absorbance of naïve cells or Lipofectamine treated cells, but were also not significantly different to the siRNA transfected cells at 24 hours. No significant differences were seen between any of the PD301 cell conditions at any other time point.

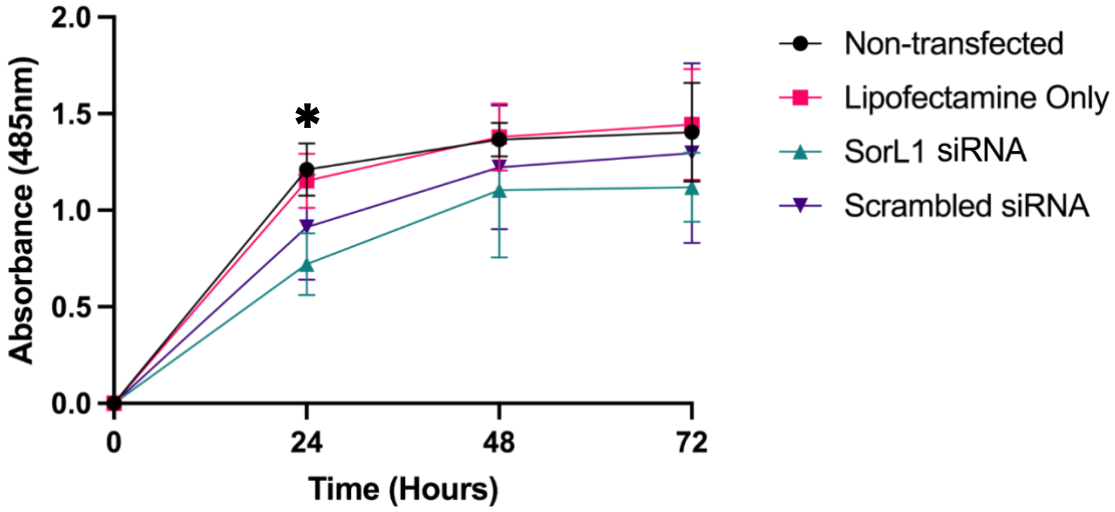

Figure 6.14 – Proliferation rate of PD301 cells transfected with SorL1 siRNA vector.

*Proliferation of PD301 cells transfected with SorL1 siRNA or scrambled siRNA, PD301 cells treated with Lipofectamine alone or non-treated, non-transfected cells. Absorbance was read at 485nm 2 hours after MTS assay. Proliferation of SorL1 siRNA transfected cells were significantly lower than naïve and Lipofectamine treated cells after 24 hours (*P<0.05, Tukey's test. N=4).*

PD301 cells transfected with SorL1 siRNA had the lowest cell viability at 24 hours and was significantly different to viability of naïve cells and cells treated with Lipofectamine ($P<0.05$ Tukey's test, N=4, Figure 6.15). Viability of cells transfected with scrambled siRNA was not significantly different to naïve and Lipofectamine treated cells at 24 hours. No cell condition was significantly different to any other group at either 48 or 72 hours. While not significant, it was noted that the SorL1 siRNA condition appeared to have lowest percentage viability at the later time points (Figure 6.15).

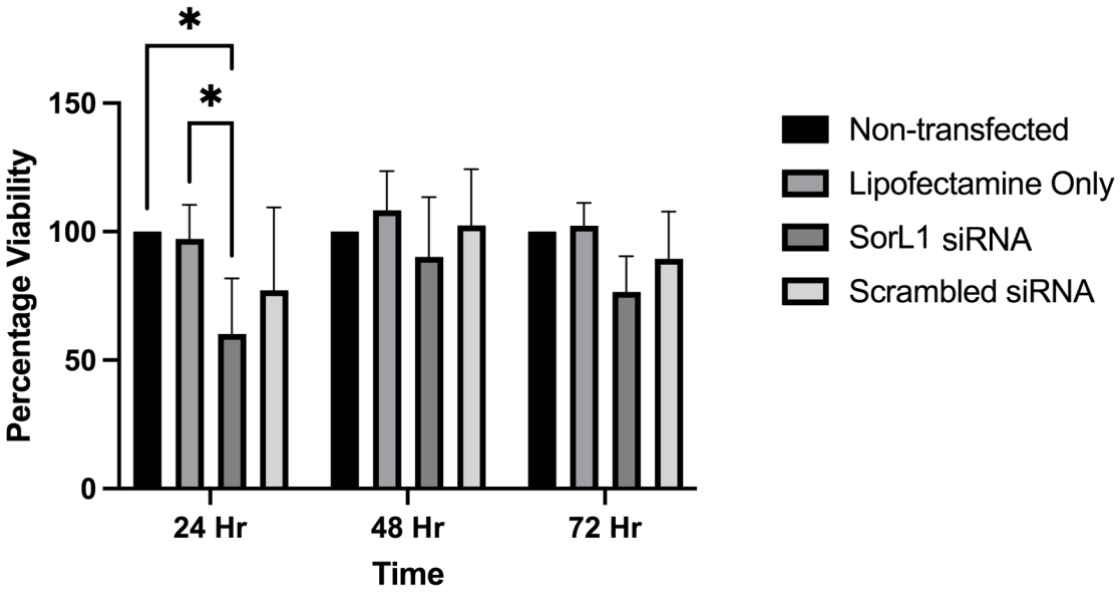

Figure 6.15 – Percentage cell viability of PD301 cells transfected with SorL1 siRNA vector.

Percentage viability of PD301 cells transfected with SorL1 siRNA or scrambled siRNA, PD301 cells treated with Lipofectamine alone or non-treated, non-transfected cells. Percentage viability of SorL1 siRNA transfected cells was significantly lower than non-transfected and Lipofectamine treated PD301 cells at 24 hours ($P<0.05$, Tukey's test. N=4).

Similar to PD301 cells, PD304 cells transfected with SorL1 siRNA had lower absorbance values than naïve cells and Lipofectamine only treated cells at 24 hours ($P<0.05$ Tukey's test N=3, Figure 6.16). Absorbance of PD304 cells transfected with scrambled siRNA was also significantly lower than absorbance of

naïve cells or Lipofectamine treated cells at 24 hours. No significant differences were seen between the PD304 cell conditions at the later time points.

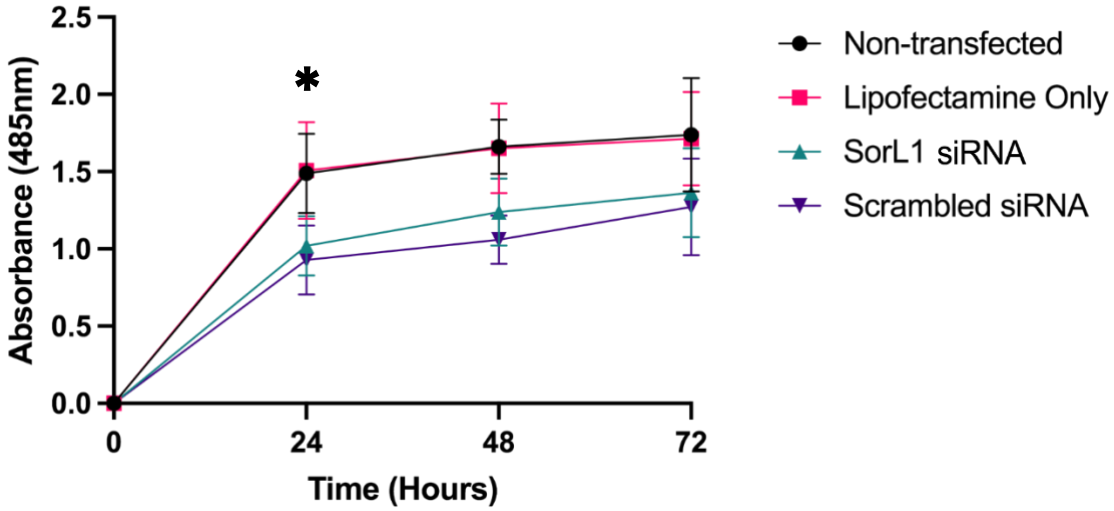

Figure 6.16 – Proliferation rate of PD304 cells transfected with SorL1 siRNA vector.

*Proliferation of PD304 cells transfected with SorL1 siRNA or scrambled siRNA, PD301 cells treated with Lipofectamine alone or non-treated, non-transfected cells. Absorbance was read at 485nm 2 hours after MTS assay. Proliferation of SorL1 siRNA transfected cells and scrambled siRNA treated cells were significantly lower than naïve and Lipofectamine treated cells after 24 hours (*P<0.05, Tukey's test. N=4).*

Percentage viability of PD304 cells transfected with both SorL1 siRNA and scrambled siRNA were lower than the viability of naïve and Lipofectamine treated cells at all three time points (P<0.0001 Tukey's test, N=4, Figure 6.17). The greatest reduction of approximately 40% was seen in SorL1 siRNA transfected cells at 24 hours. The reduced viability of transfected cells was maintained for 3 days and was still reduced by 20% at 72 hours. There was no significant difference between PD304 cells transfected with SorL1 siRNA and those transfected with scrambled siRNA at any time point.

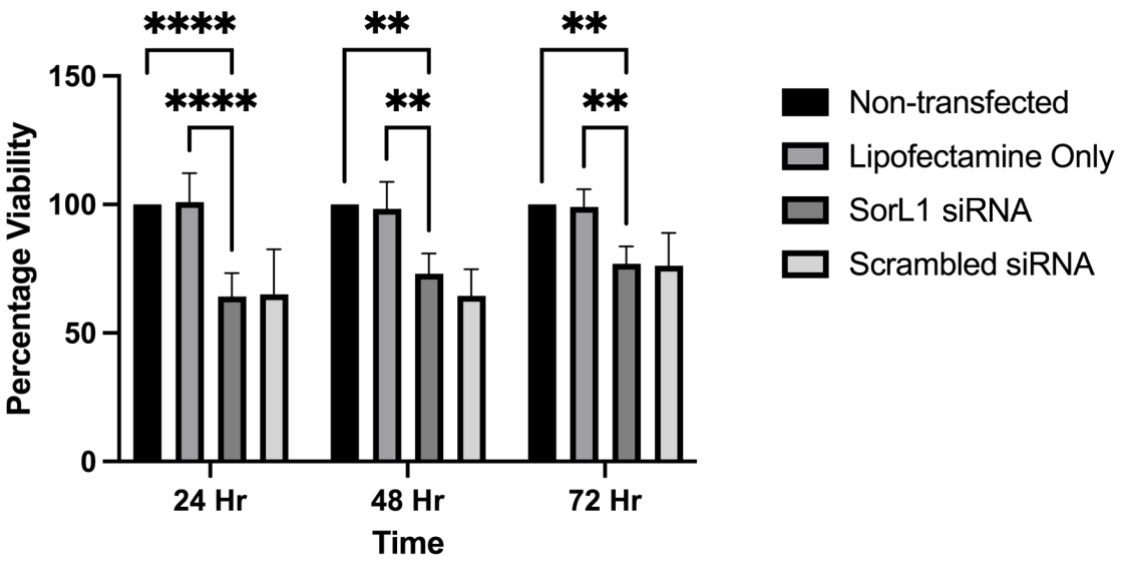

Figure 6.17 – Percentage cell viability of PD304 cells transfected with SorL1 siRNA vector.

*Percentage viability of PD304 cells transfected with SorL1 siRNA or scrambled siRNA, PD301 cells treated with Lipofectamine alone or non-treated, non-transfected cells. Percentage viability of SorL1 siRNA transfected cells were significantly lower than non-transfected or Lipofectamine treated cells (****P<0.0001 Tukey's test, N=4). Viability of PD304 cells transfected with scrambled siRNA was significantly lower than viability of non-transfected or Lipofectamine treated cells at each time point (**P<0.01 Tukey's test, significance not shown for clarity).*

6.2.4 Functional Effect of SorL1 Knock Down in PD301 and PD304 Cells: Migration

To determine whether knock down of SorL1 protein influenced migration of PD301 and PD304 glioblastoma cells, a scratch assay was performed with images taken every 12 hours for a 72 hour period; Section 2.10.3. Images were taken in the same place along the scratch to determine the percentage of wound closure and the rate of cell migration. Representative images of the assay for PD301 and PD304 cells are shown (Figures 6.18 and 6.19).

The Wound Healing Assay plug-in for Image J was used to determine percentage wound closure from images of transfected and treated cells. Percentage wound closure from the original scratch was used as opposed to area of scratch to account for any differences in scratch sizes.

All four cell conditions of PD301 cells showed some degree of wound closure but none fully closed the wound. The non-transfected cells, PD301 cells treated with Lipofectamine 3000 or cells transfected with scrambled siRNA achieved wound closure approaching 80% (Figure 6.18).

All four cell conditions of PD304 cells also showed a gradual wound closure but none fully closed the wound (Figure 6.19).

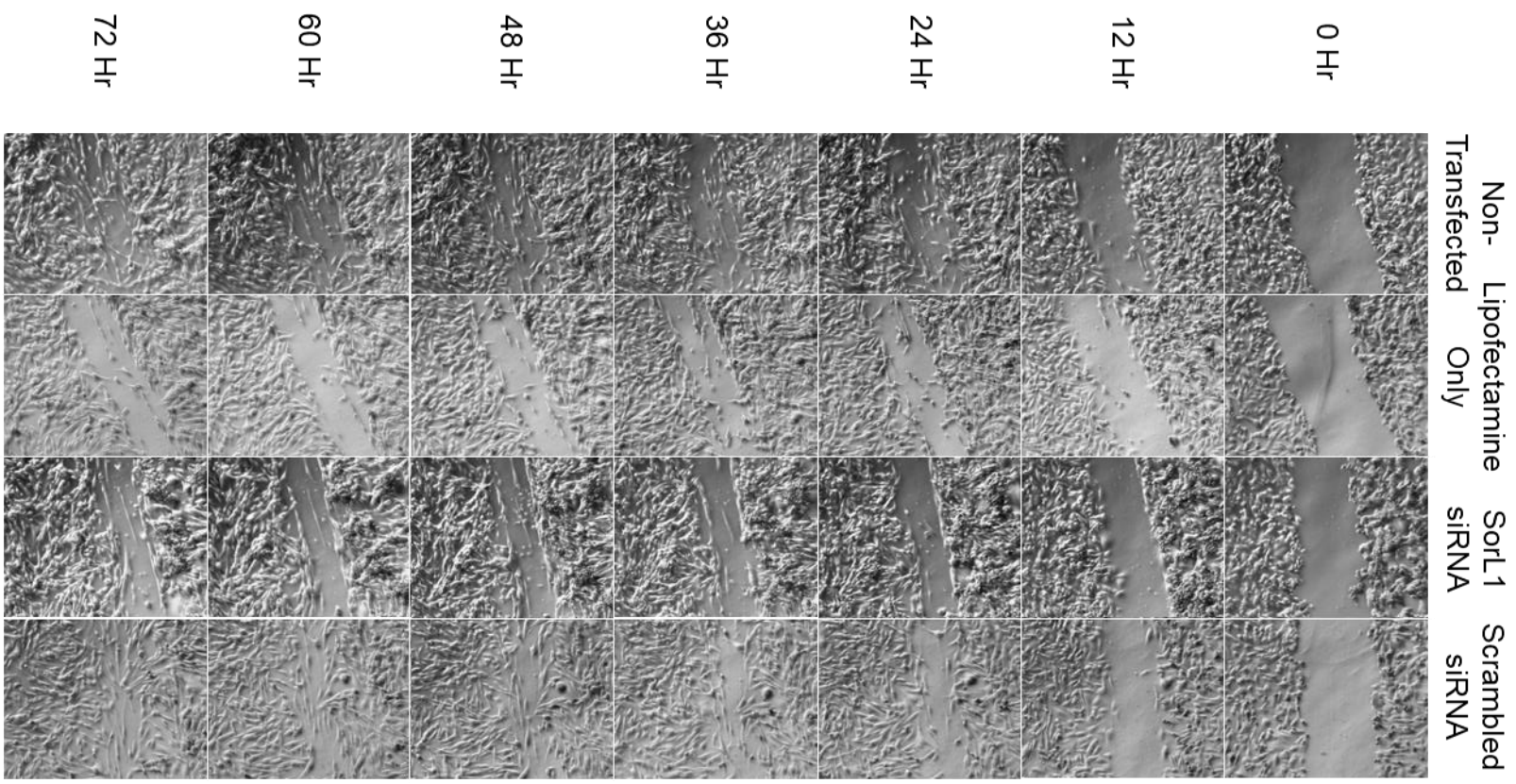

Figure 6.18 – Representative images of scratch assay on PD301 cells.

Scratch Assay in non-transfected PD301 cells, PD301 cells treated with Lipofectamine, PD301 cells transfected with SorL1 siRNA and PD301 cells transfected with scrambled siRNA (left to right). Scratch assay performed at 0 hours and images taken every 12 hours for 72 hours.

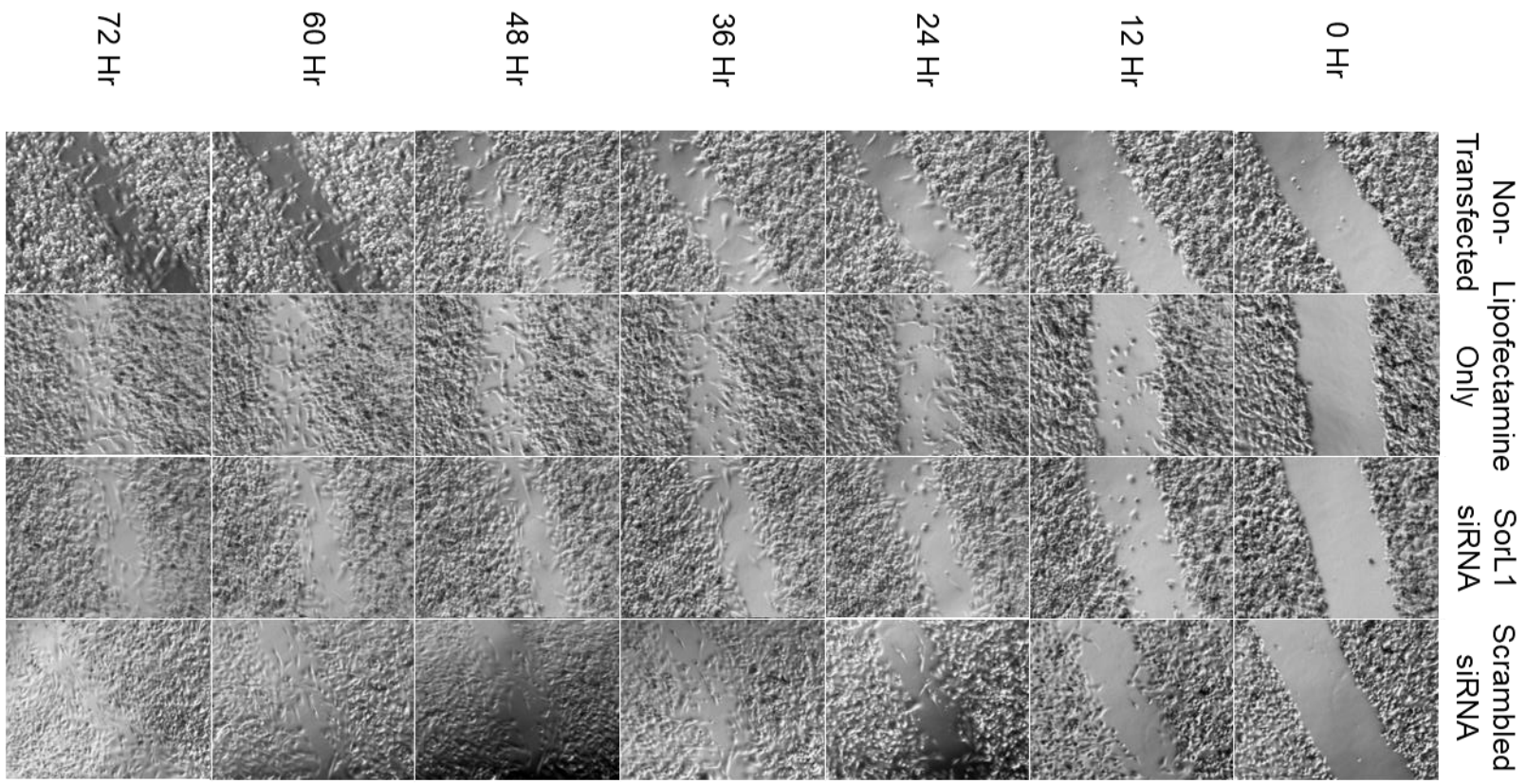

Figure 6.19 – Representative images of scratch assay on PD304 cells.

Scratch Assay in non-transfected PD304 cells, PD304 cells treated with Lipofectamine, PD304 cells transfected with SorL1 siRNA and PD304 cells transfected with scrambled siRNA (left to right). Scratch assay performed at 0 hours and images taken every 12 hours for 72 hours.

Wound closure was significantly less in PD301 cells transfected with SorL1 siRNA at 48 hours ($p<0.05$, Tukey's test, $n = 3$, Figure 6.20). However, the wound closure was overcome so there was no significant difference between the groups at 72 hours. However, wound closure of approximately 75% was achieved. There was no significant difference in percentage wound closure between the PD301 cell conditions at any other time point.

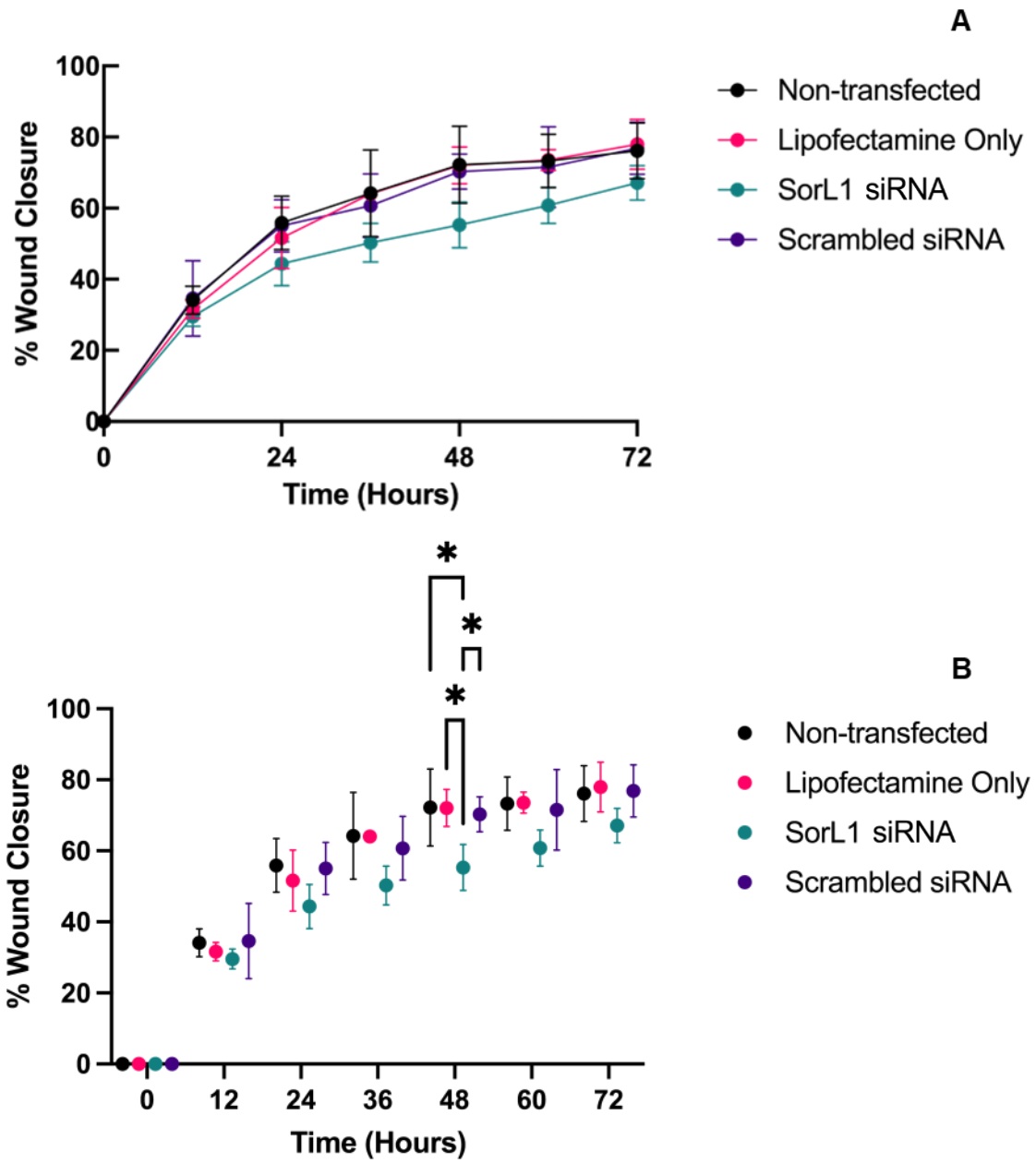

Figure 6.20 – Percentage wound closure of PD301 cells transfected with SorL1 siRNA vector.

Percentage wound closure over 72 hours of PD301 cells transfected with SorL1 siRNA or scrambled siRNA, PD301 cells treated with Lipofectamine alone or non-treated, non-transfected cells. (A) Percentage wound closure was calculated against the initial scratch at 0 hours. (B) Percentage wound closure was reduced at 48 hours in PD301 cells transfected with SorL1 compared to non-transfected cells, Lipofectamine only cells and PD301 cells transfected with scrambled siRNA (P<0.05, Tukey's test. N=3).*

Scratch images were also used to determine the rate of cell migration. The rate of cell migration was highest at 24 hours for all cell conditions and slowed as time progressed. The rate of cell migration of PD301 cells transfected with SorL1 siRNA was significantly slower than Lipofectamine treated cells at 24 hours and slower than all cell conditions at 36 hours ($P<0.05$ Tukey's test, N=3, Figure 6.21). Rate cell of migration in SorL1 siRNA cells was less than 50% compared to all other cell conditions at 36 hours. There were no significant differences between any of the PD301 cell conditions at any other time point in rate of cell migration.

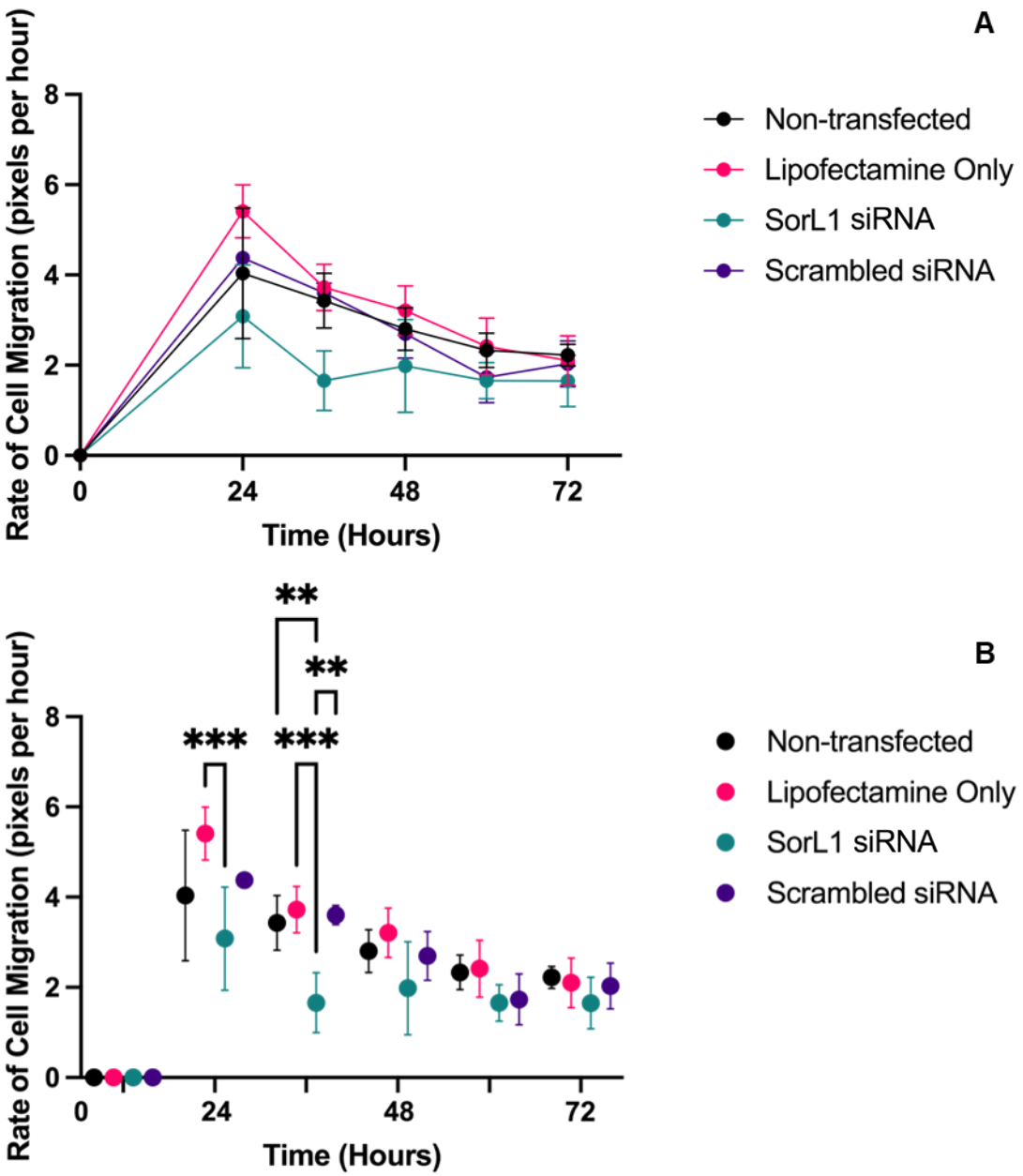

Figure 6.21 – Rate of cell migration of PD301 cells transfected with SorL1 siRNA vector.

*Rate of migration over 72 hours of PD301 cells transfected with SorL1 siRNA or scrambled siRNA, PD301 cells treated with Lipofectamine alone or non-treated, non-transfected cells. (A) Rate of cell migration was calculated from the widths of scratches and against the initial scratch at 0 hours. (B) Rate of migration was lower in SorL1 siRNA transfected cells at 24 and 36 hours (***P<0.001, **P<0.01, Tukey's test, N=3)*

All four cell conditions of PD304 cells showed some degree of wound closure but none fully closed the wound. All cell conditions achieved approximately 70% closure after 72 hours. There was no difference in percentage wound closure between the cell conditions at any time point (P>0.05 Tukey's test N=3, Figure 6.22).

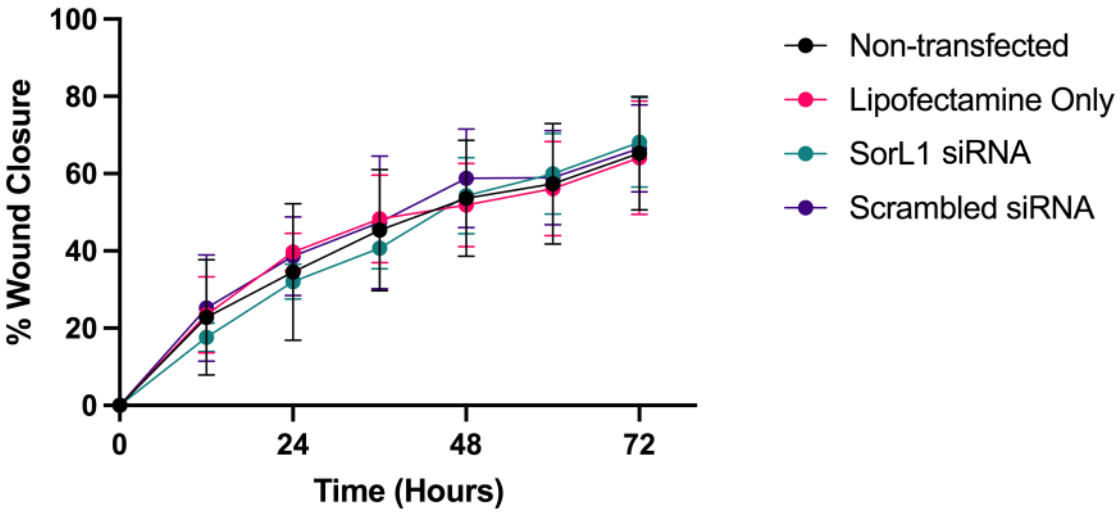

Figure 6.22 – Percentage wound closure of PD304 cells transfected with SorL1 siRNA vector.

Percentage wound closure of PD304 cells transfected with SorL1 siRNA or scrambled siRNA, PD304 cells treated with Lipofectamine alone or non-treated, non-transfected cells. Percentage wound closure was not significantly different between any PD304 cell conditions at any time point (P>0.05, Tukey's test, N=3).

Similar to PD301 cells, the rate of cell migration for PD304 cells was highest at 24 hours for all cell conditions and slowed as time progressed. The rate of cell migration of PD304 cells was not significantly different between any of the cell conditions at any of the timepoints (P>0.05 Tukey's test, N=3, Figure 6.23).

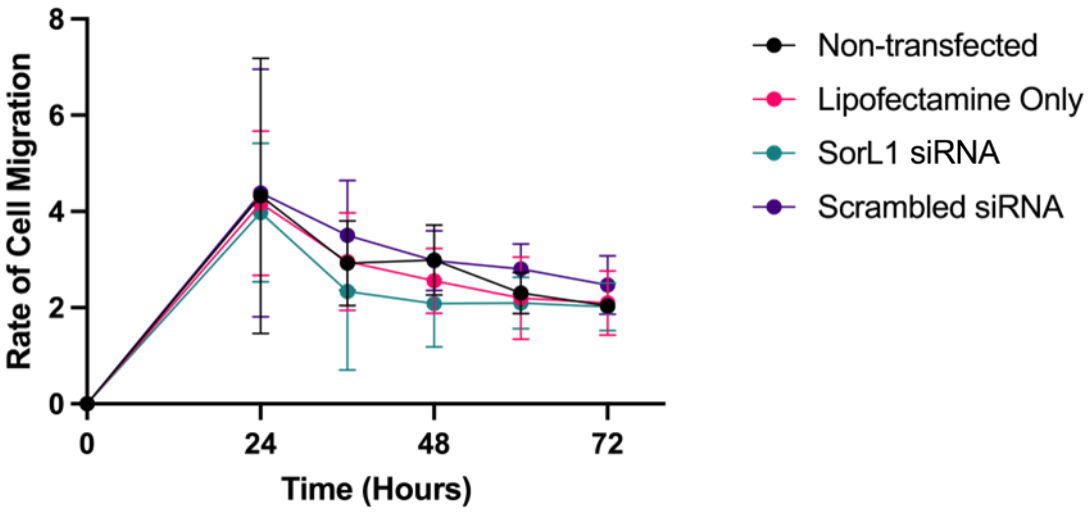

Figure 6.23 – Rate of cell migration of PD304 cells transfected with SorL1 siRNA vector.

Rate of cell migration of PD304 cells transfected with SorL1 siRNA or scrambled siRNA, PD304 cells treated with Lipofectamine alone or non-treated, non-transfected cells. Rate of cell migration was not significantly different between any PD304 cell conditions at any time point (P>0.05, Tukey's test N=3).

6.3 Discussion

6.3.1 SorL1 Knock Down Likely Increases Expression of Amyloid Beta

An increase in Aβ40 and Aβ42 protein assessed by immunocytochemistry was seen in both PD301 and PD304 cells transfected with SorL1 siRNA when compared to Lipofectamine treated and naïve cells. This supports the well reported role of SorL1 regulating Aβ production by controlling the release of APP to amyloid pathways and the known risk factor of reduced SorL1 expression being a known risk factor for Alzheimer's disease (Mehmedbasic *et al.,* 2015; Andersen *et al.,* 2005; Offe *et al.,* 2006; Schmidt *et al.,* 2007). While the presence of amyloid has been shown in glioma cells previously (Kucheryavykh *et al.,* 2019, Zayas-Santiago *et al.,* 2020) the direct biochemical link with SorL1 had not been established in glioma cells. Indeed, it was suggested that the amyloid seen within the tumours was vascular in origin (Kucheryavykh *et al.,* 2019). Data from this

chapter shows amyloid is present in cells without exogenous sources which refutes that study and suggests glioblastoma cells are capable of synthesising amyloid independently similar to the way melanoma cells have been shown to produce and secrete Aβ (Kleffman *et al.,* 2022). SorL1 knock down increasing amyloid expression further supports there being biochemical pathways within glioblastoma that remain unstudied.

The knock down of SorL1 did not have universal effects to increase amyloid levels however. Transfected cells with scrambled siRNA were not statistically different to cells transfected with SorL1 siRNA, suggesting that there might be a non-specific effect of transfection on general cell biology and function. Nevertheless, there were no significant differences between cells transfected with scrambled siRNA and the Lipofectamine and naïve, suggesting the effects seen on Aβ40 and Aβ42 when SorL1 was knocked down may be viable.

To quantify the levels of Aβ, an ELISA was undertaken on cell lysates following transfection. Unfortunately, some disparity was evident between the immunocytochemical and ELISA data with ELISA data not replicating the relative pattern in expression seen in either amyloid isoform in cell lysates following transfection. Both methods have been used frequently elsewhere, with more literature using tissue rather than cells (Christensen and Pike, 2020; Pedrero-Prieto *et al.,* 2019; Schmidt *et al.,* 2012). ELISA was used as an alternative method to western blotting which has been successful in previous studies, however, when western blot was attempted for both Aβ40 and Aβ42 quantification, it was unsuccessful (Haytural *et al.,* 2019; Pedrero-Prieto *et al.,* 2019). The proteins being approximately 4kDa in size proved tricky to separate by electrophoresis and so ELISA was used instead (LeBlanc and Gambetti, 1994). This too had its own limitations: the PD cells grew slowly so gathering sufficient volume of concentrated lysate from three different passages in duplicate was prone to loss through contamination. It may also be possible that despite Aβ40 and Aβ42 protein levels being within the published level of detection, the levels were pushing the limit of detection and near the extreme lower end of the standard curve (Appendix 4).

6.3.2 SorL1 Knock Down has Detrimental Effect on Glioma Cell Function

Functional studies conducted suggest that SorL1 knock down inhibits proliferation and migration of PD301 and PD304 glioblastoma cells. Although not always significant, SorL1 knock down in PD cells had varying reduced rates of migration, proliferation, cell viability and percentage wound closure when compared to naïve and Lipofectamine treated PD301 and PD304 cells.

After 24 hours PD301 cells transfected with SorL1 siRNA had a significant reduction in proliferation and percentage cell viability compared to naïve and Lipofectamine only cells. In addition, PD304 cells transfected with SorL1 siRNA also had a significantly reduced proliferation after 24 hours, and reduced cell viability over the 72 hour experiment. However, in both cell types, cells transfected with SorL1 siRNA was not significantly different to cells transfected with scrambled siRNA. Migration assays using PD301 cells were the only experiments that showed a significant reduction in percentage wound closure and rate of cell migration in cells transfected with SorL1 siRNA compared to all control cell conditions, including scrambled siRNA.

No significant differences between cells transfected with SorL1 siRNA and cells transfected with scrambled siRNA in the proliferation and cell viability studies could be due to effects of the cell being transfected with siRNA. It has been shown that transfecting siRNA as a negative control can have off-target effects in mammalian cells. This may be due to triggering the interferon response within the cell when siRNA is added (Tschuch *et al.,* 2008). The interferon response occurs as a defence mechanism when cells are infected with viruses or viral products, which could have occurred when the cells were transfected with siRNA plasmids (McNab *et al.,* 2015; Murira and Lamarre, 2016). Therefore, due to the little difference seen between SorL1 knock down cells and scrambled siRNA cells, it cannot be determined that a reduction of SorL1 protein leads to the reduction in proliferation and cell viability studies, it may be an interferon response. Decreasing the

scrambled siRNA concentration when transfecting PD cells is a possible resolution for this issue in the future.

Nevertheless, PD301 cells showed a significant reduction in percentage wound closure and rate of cell migration in cells transfected with SorL1 siRNA compared to all control cell conditions, including scrambled siRNA. The role of SorL1 within the cell is to shuttle APP around the cell controlling Aβ production, and when SorL1 protein is reduced, higher levels of Aβ40 and Aβ42 are produced (Andersen *et al.,* 2005; Offe *et al.,* 2006; Schmidt *et al.,* 2007). Therefore, one possible explanation causing the decrease in proliferation and migration in the glioblastoma cells is higher production of Aβ40 and Aβ42. Several studies have demonstrated Aβ has a role in supressing cancer cells. *In vitro* proliferation of glioblastoma cells, breast cancer cells, adenocarcinoma cells and melanoma cells was significantly inhibited when cultured with medium containing high levels of Aβ (Zhao *et al.,* 2009). While *in vivo*, Aβ was found to supress glioma tumours when directly injected into glioblastoma cells in xenograft mouse models, whilst another study implanted glioma cells in an Alzheimer's disease transgenic mouse model whereby Aβ is overexpressed and resulted in a slower proliferation and migration of the tumour compared to controls (Paris *et al.,* 2004, Paris *et al.,* 2010a). The mechanism of how amyloid inhibits cancer cells has recently been studied in more detail and suggests that two routes exist depending on whether the amyloid is in monomeric or oligomeric forms (Tang *et al.,* 2023). When amyloid was a monomer it inhibited pancreatic cancer cells by forming reactive oxygen species while oligomers directly disrupted membranes (Tang *et al.,* 2023).

Alternatively, Alzheimer's disease clinical trial data suggest this is not a direct role (Brothers *et al.,* 2018). Analysis specifically in clinical trials into γ-secretase inhibitors, found patients having an increased rate of skin cancers, in particular squamous and basal cell carcinomas, as well as a meta-analysis concluding γ-secretase inhibitors are associated with more than a 4-fold increased risk of skin cancer (Coric *et al.,* 2015; Doody *et al.,* 2013; Penninkilampi *et al.,* 2016). However, as clinical trials targeting Aβ have not reported an increased rate of

cancer, it can be concluded that another function of γ-secretase must be the link, not its role in cleavage to form Aβ peptide (Huang *et al.,* 2020; Andrew *et al.,* 2016).

6.3.3 Functional Effects on the Different Patient Derived Cells

It was noted that there were differences in the proliferation and migration between PD301 cells and PD304 cells. Reduction of proliferation and migration appeared to be more obvious when SorL1 was knocked down in PD301 cells than PD304 cells, even significantly different from all cellular controls at certain time points in migration studies. This could be due to differences within the source cells. The PD cells (kindly donated from Prof Tracy Warr, University of Wolverhampton) come from patients with different glioblastoma characteristics: specifically the O^6-methylguanine-DNA methyltransferase (MGMT) status; Section 2.2. The role of MGMT is to promote DNA repair, however when the promoter is methylated, the gene is silenced and impairs DNA repair of the cell. When tumour cells have methylation of the MGMT promoter, it impairs the cells' DNA repair (Gerson, 2004; Annavarapu *et al.,* 2021; Szylberg *et al.,* 2022). Therefore, it has been found treatment of temozolomide chemotherapy improves survival of methylated MGMT status tumours compared to patients with unmethylated MGMT glioblastoma tumours due to cells lacking the DNA repair (Binabaj *et al.,* 2018; Mansouri *et al.,* 2019; Yuan *et al.,* 2017). MGMT status of PD301 cells was methylated, whereas PD304 cells had low methylation. A suggestion as to why SorL1 knock down PD301 cells had a greater reduction of proliferation and migration compared to SorL1 knock down PD304 cells could be due to this methylation status of MGMT. The PD301 cells that had methylated MGMT status may have been more susceptible to the effects the reduction of SorL1 had upon the cell. Therefore, PD301 cells that lack DNA repair due to methylated MGMT status may have been more susceptible to the increase in Aβ, which has been shown to have anti-prolific effects (Zhao *et al.,* 2009).

The data presented in this chapter suggests:

i. Expression of Aβ40 was higher in PD301 and PD304 cells transfected with SorL1 siRNA according to immunofluorescence data only.
ii. Expression of Aβ42 was higher in PD301 and PD304 cells transfected with SorL1 siRNA according to immunofluorescence data only.
iii. PD301 cells with SorL1 knock down had a reduced proliferation rate and reduction in cell viability.
iv. PD304 cells with SorL1 knock down had a reduced proliferation rate and reduction in cell viability.
v. However, PD301 cells and PD304 cells had a reduced proliferation rate and reduction in cell viability when transfected with scrambled siRNA.
vi. PD301 cells with SorL1 knock down had a reduced percentage wound closure and reduced rate of cell migration.
vii. PD304 cells with SorL1 knock down had a reduced percentage wound closure and rate of cell migration.
viii. However, PD304 cells had a reduced percentage wound closure and rate of cell migration when transfected with scrambled siRNA

Chapter 7
General Discussion

7 Chapter 7 – General Discussion

The aim of this thesis was to investigate the role of SorL1 in glioblastoma, a protein never previously considered in this type of cancer. This thesis has shown SorL1 to be more highly expressed in glioblastoma cells than NHAs, and when successful knock down occurred in the PD glioblastoma cells, proliferation and migration were reduced. As SorL1 is overexpressed in glioblastoma cells and a reduced cell function was seen when cells knocked down, it would suggest SorL1 could contribute to oncogenic properties and may make a viable therapeutic target.

7.1 SorL1 as a Therapeutic Target

Silencing of SorL1 reduced proliferation and migration of PD cells, and significantly so in PD301 cells against all controls at certain time points. These functional effects due to SorL1 knock down suggest a possible therapeutic to inhibit SorL1 in glioblastoma cells. There are currently no pharmacological agents that inhibit SorL1 protein, however, similar therapeutic potential has been shown in breast cancer (Al-Akhrass *et al.,* 2022) suggesting SorL1 to be a viable druggable target. Here, SorL1 expression was successfully knocked down by approximately 50% in PD301 and PD304 cells, which reduced proliferation and migration but only modestly, possibly as the siRNA was not stably transfected. It is possible a greater degree of inhibition could occur through inhibiting SorL1 pharmacologically.

As was seen during knock down of SorL1 in PD301 and PD304 cells, Aβ40 and Aβ42 expression increased. This was expected due to the known relationship between SorL1 and Aβ as shown in Alzheimer's disease models, when SorL1 expression is reduced, Aβ secretion increases (Andersen *et al.,* 2005; Offe *et al.,*2006; Schmidt *et al.,* 2007). Therefore, reducing the expression of SorL1 in glioblastoma and observing an increase in Aβ40 and Aβ42 expression may be mimicking Alzheimer's pathology. However, in initial experiments of this thesis, expression of Aβ42 was significantly reduced in PD301 and PD304 cells compared to NHA cells; Chapter 3. Therefore, the increase of Aβ42 expression observed in

SorL1 knock down PD301 and PD304 cells compared to the non-transfected cells may increase to normal baseline levels seen in NHA cells. This therefore suggests inhibiting SorL1 with drug therapy will not only reduce proliferation and migration of glioblastoma cancer cells, but also levels of Aβ40 and Aβ42 will not rise to that consistent with Alzheimer's disease.

Furthermore, inhibiting SorL1 as a therapeutic target in glioblastoma cells may result in quick acute accumulation of Aβ prompting anti-tumour effects as opposed to the chronic build-up seen in Alzheimer's disease pathology. Studies have shown Aβ to have a role in inhibiting glioma cancer cells with growth significantly inhibited when treated with cell medium containing high levels of Aβ (Zhao *et al.,* 2009). Further *in vivo* studies support anti-tumour effects of Aβ as the glioma tumours were supressed when Aβ was directly injected into glioblastoma cells in xenograft mouse models, whilst another showed slower proliferation of glioma tumour that was implanted in an Alzheimer's disease transgenic mouse model where Aβ was overexpressed (Paris *et al.,* 2004, Paris *et al.,* 2010a). Therefore, therapeutically inhibiting SorL1 in glioblastoma may mechanistically within the cell allow build-up of Aβ to act with anti-tumour properties. Knock down of SorL1 expression resulting in an increase in Aβ anti-tumour properties may contribute to the mechanisms supporting Alzheimer's disease has protective properties against cancer corroborating the inverse correlation seen in literature.

However, if a SorL1 therapeutic does inhibit SorL1 to the extent that chronic accumulation of Aβ occurs, the drug can also be removed, taking away the effects caused from SorL1 reduction.

7.1.1 SorL1 as a Therapeutic Adjunct

An alternative to the strategy to inhibit SorL1 as a direct anti-cancer treatment comes from the report that SorL1 inhibition can change drug sensitivity to other treatments, opening up potential to use it as adjunct treatment. Pietilla and colleagues showed knock down of SorL1 opened up sensitivity to a drug called

ebastine in various models of breast cancer (Pietilä *et al.,* 2019). Low doses of ebastine caused cells with SorL1 knock down to undergo apoptosis.

Ebastine is a histamine H1 receptor antagonist (Wiseman and Faulds, 1996). Typically antihistamines are used to alleviate allergic symptoms, however a subset of antihistamines have cationic amphiphilic drug (CAD) characteristics which have previously been shown to induce cell death in certain cancerous cells (Church and Church, 2013; Verdoodt *et al.,* 2020). The repurposing of these drugs are gaining popularity in cancer therapy (Ellegaard *et al.,* 2016). Properties of CADs include hydrophobic and hydrophilic domains (amphiphilic) and due to this property accumulate in acidic lysosomes, causing damage and inducing cell death (Halliwell, 1997; Petersen *et al.,* 2013). In particular, CADs have been found to target cancer cells over normal cells due to tumour acidity caused by one hallmark of cancer which is inducing or accessing vasculature (Bogdanov *et al.,* 2022). An altered cellular vasculature in tumour cells leads to a change in perfusion of nutrients and oxygen and leads to an increase of acidic metabolites (McDonald *et al.,* 2016). CADs have been shown effective in reducing cell viability against many cancers cells, including lung, colon, pancreatic, liver, prostate, bladder and brain, and in particular glioblastoma cell lines (Berg *et al.,* 2022; Ellegaard *et al.,* 2016; van der Horst *et al.,* 2020; Le Joncour *et al.,* 2019; Kwak *et al.,* 2021).

Therefore, this all supports the results seen when breast cancer cells with SorL1 knock down were treated with ebastine. The cells were treated with 15μM of ebastine, and found significant apoptosis of cells knocked down with SorL1 when compared to scrambled siRNA control cells, which also did not have significant apoptotic effects caused by ebastine when compared to no treatment (Pietilä *et al.,* 2019). In comparison, 40μM of a different CAD, (HMA) caused cytotoxic effects, reducing cell viability to glioblastoma cells, whilst had no significant effect to cells dissociated from normal mouse brain tissue used as their control (Berg *et al.,* 2022). The obvious difference here is the different concentrations of CAD used on cancer cells, and if a larger dose was used in the Pietilä paper, an effect may have been seen in the control scrambled siRNA breast cancer cells. Due to the cytotoxic effect being so great in glioblastoma cells, when taking the logic from

Pietilä results, knocking down SorL1 in glioblastoma cells as shown in this thesis, may only intensify the apoptotic effects of the drug to the cancer cells (Pietilä *et al.,* 2019). It has been theorised that due to SorL1 downregulation compromising lysosomal integrity, this increases the sensitivity of the cancerous cell to CADs to accumulate in lysosomes and cause apoptosis (Pietilä *et al.,* 2019).

A further study also showed that inhibiting SorL1 with a monoclonal SorL1 antibody and trastuzumab inhibited breast cancer tumour growth (Al-Akhrass *et al.,* 2022). The monoclonal antibody targeted the low-density lipoprotein receptor (LDLR) class A section of SorL1 as it is known for ligand binding to HER2 (Schmidt *et al.,* 2017). The study used a monoclonal antibody to inhibit the SorL1 protein as opposed to reducing SorL1 through siRNA as was the chosen method in this thesis. Trastuzumab is a known HER2 breast cancer drug, however, the breast cancer cells used were known to be resistant, and therefore, treatment with the drug alone did not inhibit the cells (Greenblatt and Khaddour, 2023; Al-Akhrass *et al.,* 2022). Only treating the cells with SorL1 monoclonal antibody also did not significantly reduce the cell viability of breast cancer cells either. SorL1 inhibition with monoclonal antibody was found to reduce resistance of the cancer cells to trastuzumab and also combination treatment inhibited tumour cell proliferation and tumour cell density (Al-Akhrass *et al.,* 2022). Therefore, in terms of glioblastoma, inhibiting SorL1 through monoclonal antibody or silencing SorL1 protein through siRNA may reduce resistance of glioblastoma cells to temozolomide, as development of resistance is a common limiting factor to effective treatment (Singh *et al.,* 2021).

7.2 Mechanisms of SorL1

All glioblastoma cell types (U87MG, PD301 and PD304) had a significantly higher expression of SorL1 in comparison to their ‘normal’ counterparts (SVGp12 and NHA); Chapter 3. Immortalised glioma cells demonstrated expression of SorL1 in a grade dependent manner with the highest expression levels in U87MG cells, followed by 1321N1 cells and finally the SVGp12 cells. As already discussed, the U87MG cell line is a grade IV glioblastoma cell line, whilst 1321N1 is a stage II

astrocytoma cell line and SVGp12 are foetal astrocytes used as the control. As U87MG cells are glioblastoma from origin, glioblastoma is the most aggressive and highly malignant glioma tumour (Wirsching *et al.,* 2016). In comparison, although astrocytomas are infiltrative and have an increased cellular proliferation, it is not as great as the highly infiltrative and proliferative nature of glioblastomas (Pan and Prados, 2003). This therefore may suggest that the difference in SorL1 expression may be linked to the proliferative nature of the glioma cell whether directly or indirectly as the more SorL1 expressed the higher the rate of proliferation of the cell. This theory also fits with results that showed knocking down SorL1 from PD301 and PD304 cells resulted in a reduction of proliferation suggesting a direct or indirect cause and effect due to SorL1 expression; Chapter 6. This is further re-iterated as silenced SorL1 breast cancer cells reduced proliferation compared to scrambled control, and the same study found silencing SorL1 also induces HER2 accumulation in dysfunctional lysosomes suggesting a mechanistic role in the maintenance of lysosomal function (Pietilä *et al.,* 2019). The same group of researchers further found SorL1 was necessary for HER2-HER3 driven oncogenic proliferation of breast cancer cells as the SorL1 bound directly to HER3 creating a SORL1-HER2-HER3 complex compromising cell proliferation, and further found reduction of SorL1 to sensitise resistant anti-HER2 breast cancer cells to the drug neratinib (Al-Akhrass *et al.,* 2021). Other research has however found opposing results that knock down SorL1 in pancreatic cells βTC3 that were inoculated into the pancreas of immunocompromised mice increased tumour growth by approximately 2-fold compared to control tumour (Michael *et al.,* 2019). Nevertheless, the majority of research carried out this far reiterate results found in this thesis, with another study investigating SorL1 expression in cutaneous melanoma through bioinformatics and found SorL1 expression levels to be increase in tumour samples (Wang *et al.,* 2023). Despite the known mechanisms of SorL1 in Alzheimer's disease functioning through the shuttling of APP around the cell, the potential function in cancer progression and proliferation has not been fully established and remains unknown (Willnow and Andersen, 2013; Michael *et al.,* 2019).

Another mechanism observed in SorL1 knock down of glioblastoma cells was a reduction in cell migration; Chapter 6. It is believed that SorL1 stimulates cell migration through the N-terminus section of the protein, in particular the fibronectin domain (Ling *et al.,* 2021; Moreno *et al.,* 2022). As already discussed, SorL1 is regarded a member of the LDLR family and previous studies have suggested the LDLR family of receptors are necessary regulators for the migration of neurones, fibroblasts and smooth muscle (Lane-Donovan *et al.,* 2014; Weaver *et al.,* 1997; Zhu *et al.,* 2002). The same group of researchers then investigated SorL1 involvement in migration of smooth muscle cells (Zhu *et al.,* 2004). It was suggested that SorL1 induces upregulation of urokinase-type plasminogen activator receptor (uPAR) to enhance migration of smooth muscle cells (Zhu *et al.,* 2004). Known mechanisms of uPAR include regulating cell adhesion, migration and proliferation and has further been discovered that uPAR is expressed at higher levels in cancerous cells compared to healthy cells (Montuori *et al.,* 2016; Zhai *et al.,* 2022). Therefore, as mechanisms of SorL1 include upregulating uPAR this will therefore increase rate of migration. Therefore, this may explain the reduction of rate of migration observed in SorL1 knocked down glioblastoma cells.

Other roles of SorL1 may exist and contribute to other pathophysiology of diseases. As seen in literature, there is an inverse comorbidity between cancer and neurodegenerative diseases, however the greatest risk reduction of co-occurrence was Alzheimer's disease at 68% (Catalá-López *et al.,* 2014). Therefore, Alzheimer's disease associated proteins (SorL1 and Aβ) were investigated in glioblastoma cells. As SorL1 is reduced in Alzheimer's disease, as seen in literature, and an increase of SorL1 expression was seen in glioblastoma cells in this thesis and also in breast cancer cells, it may be plausible that SorL1 could be the protective mechanism (Rogaeva *et al.,* 2007; Pietilä *et al.,* 2019).

Furthermore, the same study of meta-analyses investigating the inverse comorbidity between neurodegenerative diseases also found a risk reduction rate of 47% between cancer and Huntington's disease and 17% reduction risk between cancer and Parkinson's disease (Catalá-López *et al.,* 2014). Due to the well established association between SorL1 and Alzheimer's disease, studies have

investigated SorL1 in both Huntington's disease and Parkinson's disease (Rohe *et al.,* 2009; Xiromerisiou *et al.,* 2021; Maple-Grødem *et al.,* 2018). A study found an impaired SorL1 expression in transgenic mouse models with loss of brain-derived neurotrophic factor (BDNF), mimicked Huntington's disease (Rohe *et al.,* 2009). BDNF is a neurotrophic factor that is responsible for survival of neurones in the CNS which is found to be decreased in neurodegenerative diseases, such as Huntington's disease (Huang and Reichardt, 2001; Zuccato *et al.,* 2008). Further identification of a SorL1 A528T variant, originally associated with Alzheimer's disease, has been found to be a risk factor for Parkinson's disease, and a further mutation in SorL1 was found in sporadic Parkinson's disease when conducting whole exome sequencing on a Greek family (Maple-Grødem *et al.,* 2018; Xiromerisiou *et al.,* 2021). Therefore, other roles of SorL1 may exist and contribute to the pathophysiology of both neurodegenerative disorders and cancer as SorL1 appears to be a common biological link whereby the protein is expressed in opposite directions and supporting the inverse comorbidity seen in epidemiological studies.

7.3 Using SorL1 as a Diagnostic Tool

Due to extracellular proteolytic shedding of SorL1 into sSorL1, it has been considered to treat sSorL1 as a diagnostic biomarker. Although investigating secretion of sSorL1 in this thesis resulted in ambiguous results, further investigation is warranted. It was shown that medium taken from glioblastoma cells had a significantly reduced sSorL1 expression in comparison to medium from NHAs, therefore suggesting a reduction of sSorL1 as a diagnostic tool could be indicative of glioblastoma. However, serum from mice implanted with glioblastoma cells did not support the results seen in the cell medium and no significant difference in sSorL1 levels were observed between serum taken from mice implanted with U87MG cells and those injected with vehicle. However, there are various reasons that could explain the difference. The serum samples historic and therefore protein degradation may have occurred, therefore reducing protein quality. Furthermore, the serum samples were contaminated with blood due to the small quantities taken from the bleeds of the mice and therefore separation of

serum from whole blood was difficult. The erythrocyte contamination of serum interfered with the absorbance in protein assay quantification and therefore affected loading volumes, however, this was corrected against the loading control transferrin. However, as it is understood that SorL1 expression is highest within the CNS, a greater difference in sSorL1 levels may be seen in CSF due to one of its roles being removing waste in the CNS and will be in the vicinity of glioma brain tumours (Motoi *et al.,* 1999; Guthrie, 2012). CSF has been previously investigated as preferential over serum for investigating levels of sSorL1 secretion in other diseases of the brain, to diagnose Alzheimer's disease (Andersen *et al.,* 2016). Furthermore, biomarkers for Alzheimer's disease have been investigated in CSF at the stages of mild cognitive impairment to diagnosis of Alzheimer's disease dementia (Lewczuk *et al.,* 2018). A decrease in Aβ42 concentration in CSF is one such biomarker for diagnosis in Alzheimer's disease as well as the concentration ratio between Aβ40 and Aβ42 (Hampel *et al.,* 2021). CSF biomarkers for Alzheimer's disease have been found to have a greater diagnostic accuracy than biomarkers in blood, plasma or serum (Hampel *et al.,* 2008). Aβ is the most studied biomarker in serum, however different studies found contradicting results (Hampel *et al.,* 2008). Some studies found high Aβ42 plasma levels in Alzheimer's disease patients and no difference between Aβ40 levels in control cases, whilst others found high Aβ40 and low Aβ42 protein levels in plasma as a risk for Alzheimer's disease dementia (Irizarry, 2004; Mayeux *et al.,* 2003; Graff-Radford *et al.,* 2007; Pomara *et al.,* 2005; van Oijen *et al.,* 2006). Biomarkers in plasma are not reliable for diagnosing Alzheimer's disease, and CSF biomarkers are considered much more accurate. Therefore, investigating levels of sSorL1 in CSF, rather than plasma as was done in this thesis may prove to have more definitive answers.

Previous studies have shown an increase in sSorL1 in the bodily fluids surrounding the cancerous cells or tumour. An increase of sSorL1 was observed to be in patient's bile samples with cancers of the pancreas and bile duct, and especially elevated during the peak of proliferation of the cancers (Terai *et al.,* 2016). Further studies investigating cancers of the blood, acute leukaemia and Non-Hodgkin's lymphoma found an increase of sSorL1 secretion in presence of cancer compared to controls, but also showed a decrease in sSorL1 secretion when acute myeloid

leukaemia and acute lymphoblastic leukaemia cancer patients went into remission and so found that sSorL1 was produced directly from leukemic cells (Sakai *et al.,* 2012; Fujimura *et al.,* 2014). There are remaining questions surrounding the mechanism that causes an increase in circulating sSorL1 in leukemic cells, however, one theory is due to the dysregulation of TACE/ADAM17 shown in cancerous cells, the proteinase known to cleave SorL1 (Wong *et al.,* 2016; Black, 2002).

7.4 Future Work

The initial results chapter showed an increase in expression of SorL1 in glioblastoma cells (U87MG, PD301 and PD304) compared to 'normal' controls (SVGp12 and NHA), with expression of stage II astrocytoma cells (1321N1) somewhere in the middle. Biopsies of glioma brain tumours where patients have had their tumours resected would be useful to determine expression of SorL1 in human glioma tissue and compare to the margins around the tumour including normal brain tissue.

To fully assess utility of SorL1 as diagnostic biomarker, the obvious next step would be to determine sSorL1 levels in serum from patients with glioblastoma compared to matched controls. As serum sSorL1 has been considered a biomarker for Alzheimer's disease previously with limited success, it may be beneficial to consider other biological sources, namely CSF. The relationship between sSorL1 levels in CSF and serum have not been fully characterised, a greater understanding of which would potentially aid both Alzheimer's field and cancer.

As SorL1 knock down of PD301 and PD304 reduced proliferation and migration of the cells, using a drug to pharmacologically inhibit the SorL1 protein would be advantageous. Various drug repurposing and repositing databases exist and a cursory look suggests there are no notable drug candidates as SorL1 ligands. Consequently, *in silico* modelling would therefore be the next step. Furthermore, it would be interesting to know whether adding an antihistamine that has CAD

characteristics to the SorL1 knock down PD301 and PD304 cells would increase sensitivity to apoptosis as has been shown in SorL1 silenced breast cancer cells.

Overall, there are multiple experiments that can be conducted based on the findings of this thesis to help determine further pathophysiological roles of SorL1 in cancer and more specifically glioblastoma. This is the first time SorL1 has been investigated in glioma tumours and results from this thesis and other literature suggest SorL1 may be considered a therapeutic target for cancer in the future.

Appendices

8 Appendices

8.1 Appendix 1 – Full Blots from Westerns

Following western blotting, images were taken of the full blots, before snips were taken for Figures throughout the thesis (e.g. Figure 3.12).

Full western blots show specific binding to SorL1 in immortalised cell lines (Figure A1.1) with double bands present and primary cell lines (Figure A1.2) from Chapter 3. The second thinner band underneath is likely an immature form of SorL1 that undergoes post-translational modifications to become the mature form seen as the thicker band above (Monti *et al.,* 2021; Rovelet-Lecrux *et al.,* 2021).

Figure A1.1 – SorL1 expression in U87MG, 1321N1 and SVGp12 lysates.

Full western blot of SorL1 at 250kDa in U87MG, 1321N1 and SVGp12 lysates (left to right). 10μg of protein was loaded.

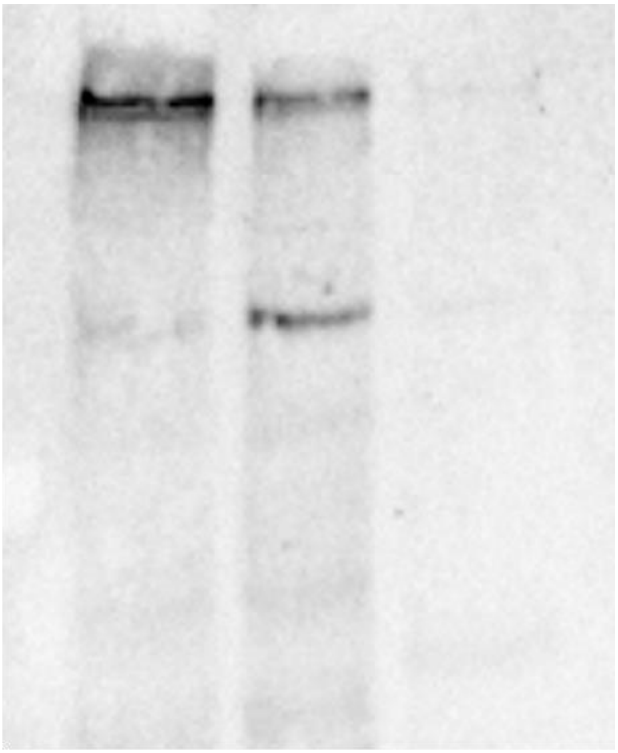

Figure A1.2 – SorL1 expression in PD301, PD304 and NHA lysates.

Full western blot of SorL1 at 250kDa in PD301, PD304 and NHA lysates (left to right). 10μg of protein was loaded.

Full western blots show specific binding to sSorL1 in medium from primary cell lines (Figure A1.3) from Chapter 4. Mouse serum western blots contained more background and grainy images (Figures A1.4 and Figure A1.5) from Chapter 4.

Figure A1.3 – Soluble SorL1 expression in PD301, PD304 and NHA cell medium.

Full western blot of sSorL1 at 240kDa in PD301, PD304 and NHA cell medium (left to right). Expression is not visible in lanes containing PD301 and PD304 medium. 10μg of protein was loaded.

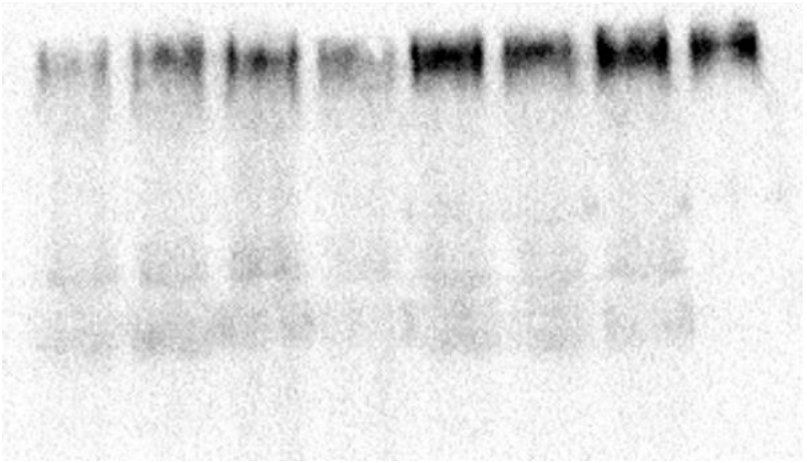

Figure A1.4 – Soluble SorL1 expression in mouse serum taken weekly from mice implanted with glioblastoma and sham mice.

Full western blot of sSorL1 at 240kDa from pre-bleed, week 1 bleed, week 2 bleed and week 3 bleed from a mouse implanted with U87MG cells, and pre-bleed, week 1 bleed, week 2 bleed and week 3 bleed from a mouse following sham surgery (left to right). 7.5μg of protein was loaded.

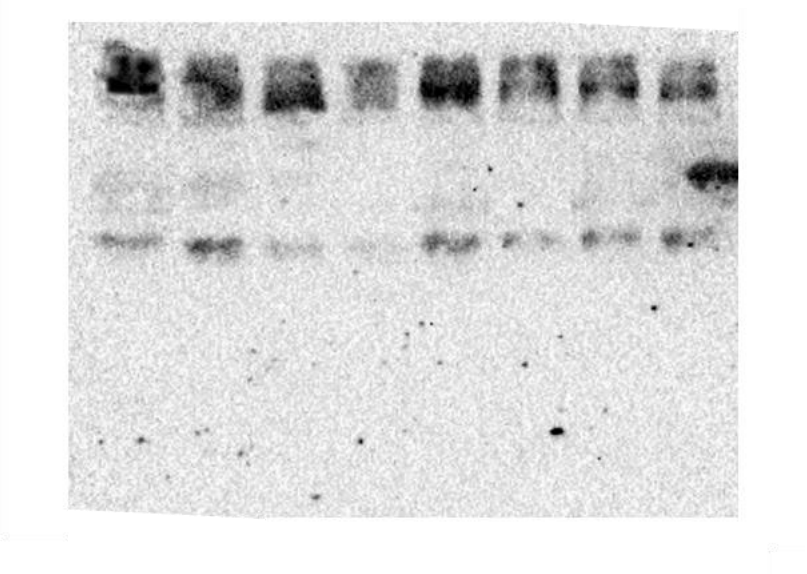

Figure A1.5 – Soluble SorL1 expression in mouse serum taken from terminal bleeds mice implanted with glioblastoma and sham mice.

Full western blot of sSorL1 at 240kDa from terminal bleeds from 4 mice implanted with U87MG cells, and 4 mice following sham surgery (left to right). 7.5μg of protein was loaded.

Full western blots show specific binding to SorL1 in PD301 cell conditions (Figure A1.6) and PD304 cell conditions (Figure A1.7) from Chapter 5. The second thinner band seen in the western blot underneath is likely an immature form of SorL1 that undergoes post-translational modifications to become the mature form seen as the thicker band above (Monti *et al.,* 2021; Rovelet-Lecrux *et al.,* 2021).

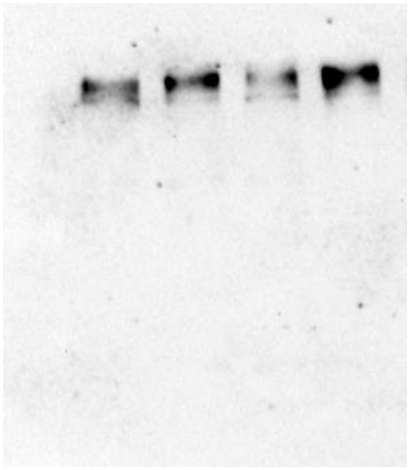

Figure A1.6 – SorL1 expression in PD301 cell conditions.

Full western blot of SorL1 at 250kDa in non-transfected PD301 cells, Lipofectamine only PD301 cells, PD301 cells transfected with SorL1 siRNA and PD301 cells transfected with scrambled (left to right). 10μg of protein was loaded.

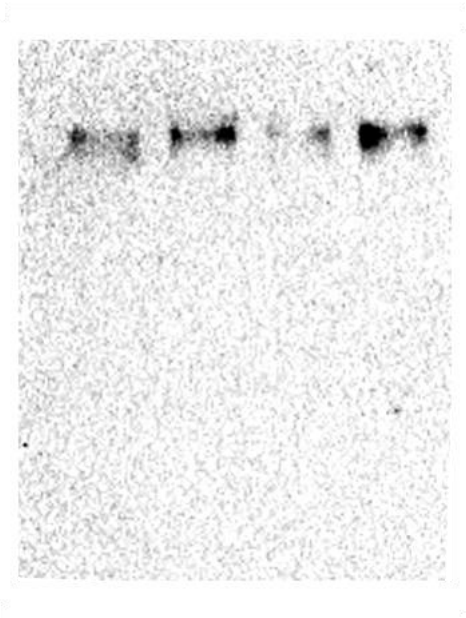

Figure A1.7 – SorL1 expression in PD304 cell conditions.

Full western blot of SorL1 at 250kDa in non-transfected PD304 cells, Lipofectamine only PD304 cells, PD304 cells transfected with SorL1 siRNA and PD304 cells transfected with scrambled (left to right). 10μg of protein was loaded.

8.2 Appendix 2 – Optimisation of Transfection

Initial optimisation of transiently transfecting PD301 and PD304 cells with SorL1 siRNA to knock down SorL1 protein using Lipofectamine 3000™. All siRNA required 1.5µl of Lipofectamine for optimal transection efficacy. SorL1 siRNA D had the best transfection efficiency, followed by siRNA B, siRNA C and siRNA A. Optimal scrambled siRNA conditions showed a third of PD301 cells were successfully transfected (Table A2.1).

Table A2.1 – Optimisation of ratio for transfection reagents for PD301 cells.

Optimised conditions of different siRNA with percentage of transfection efficacy for transient transfection of PD301 cells.

siRNA	***siRNA (µg)***	***P3000 (µl)***	***Lipofectamine (µl)***	***Transfection Efficacy (%)***
SorL1 siRNA A	*1µg*	*2µl*	*1.5µl*	*23.08%*
SorL1 siRNA B	*0.5µg*	*1µl*	*1.5µl*	*43.75%*
SorL1 siRNA C	*0.5µg*	*1µl*	*1.5µl*	*40.51%*
SorL1 siRNA D	*1µg*	*2µl*	*1.5µl*	*53.13%*
Scrambled siRNA	*1µg*	*2µl*	*1.5µl*	*33.33%*

Similar to PD301 cells, 1.5µl of Lipofectamine led to the highest transfection efficacy for all siRNA in transfected PD304 cells. All SorL1 siRNA had over 50% transfection efficacy, showing PD304 cells are more successfully transiently transfected than PD301 cells. However, optimal scrambled siRNA conditions only managed to transfect approximately half of what the SorL1 siRNA could transfect, nevertheless, is a very similar transfection efficacy to PD301 cells (Table A2.2).

Table A2.2 – Optimisation of ratio for transfection reagents for PD304 cells.

Optimised conditions of different siRNA with percentage of transfection efficacy for transient transfection of PD304 cells.

siRNA	***siRNA (µg)***	***P3000 (µl)***	***Lipofectamine (µl)***	***Transfection Efficacy (%)***
SorL1 siRNA A	*1µg*	*2µl*	*1.5µl*	*54.54%*
SorL1 siRNA B	*1µg*	*2µl*	*1.5µl*	*62.5%*
SorL1 siRNA C	*0.5µg*	*1µl*	*1.5µl*	*66.67%*
SorL1 siRNA D	*1µg*	*2µl*	*1.5µl*	*66.67%*
Scrambled siRNA	*1µg*	*2µl*	*1.5µl*	*31.33%*

8.3 Appendix 3 – Characterisation of Antibody for Aβ40 and Aβ42

The antibodies initially used in earlier studies became unavailable during the course of this project. Consequently, a new antibody against Aβ40 and Aβ42 had to be validated and was achieved in both PD301 and PD304 cells by omission of primary antibody. When primary antibody against either Aβ40 or Aβ42 was omitted, no fluorescence was seen in either PD301 or PD304 cells.

Punctate fluorescence corresponding to Aβ40 was seen in both PD301 (Figure A3.1) and PD304 (Figure A3.2) cells, however had visibly lower levels in PD301 cells. The labelling was predominantly confined to the cytoplasm with limited fluorescence seen in the nucleus, comparable to that seen previously (Chapter 3).

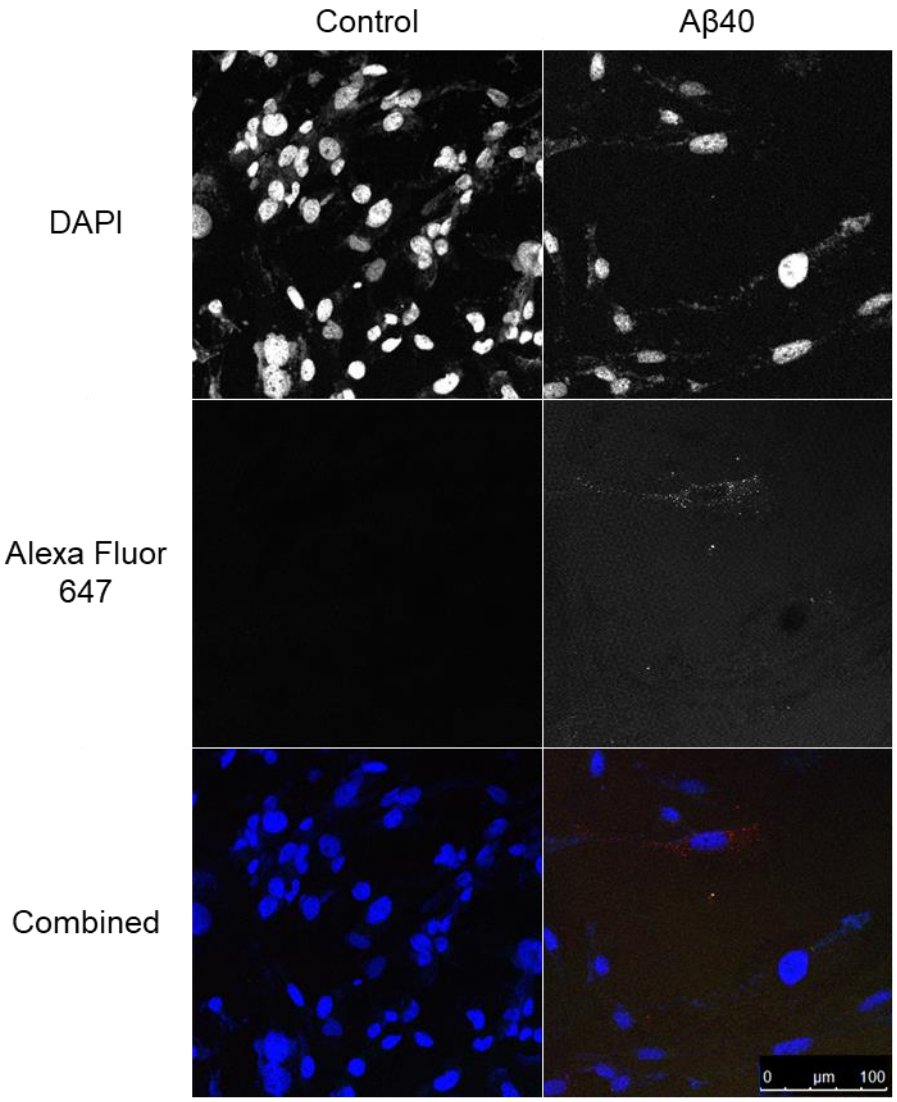

Figure A3.1 – Aβ40 expression in PD301 cells.

Fluorescence following incubation with (right) or without (left) antibody against Aβ40 (middle panel). Nuclei labelled with DAPI (top). Magnification = x20. Scale bar = 100µm.

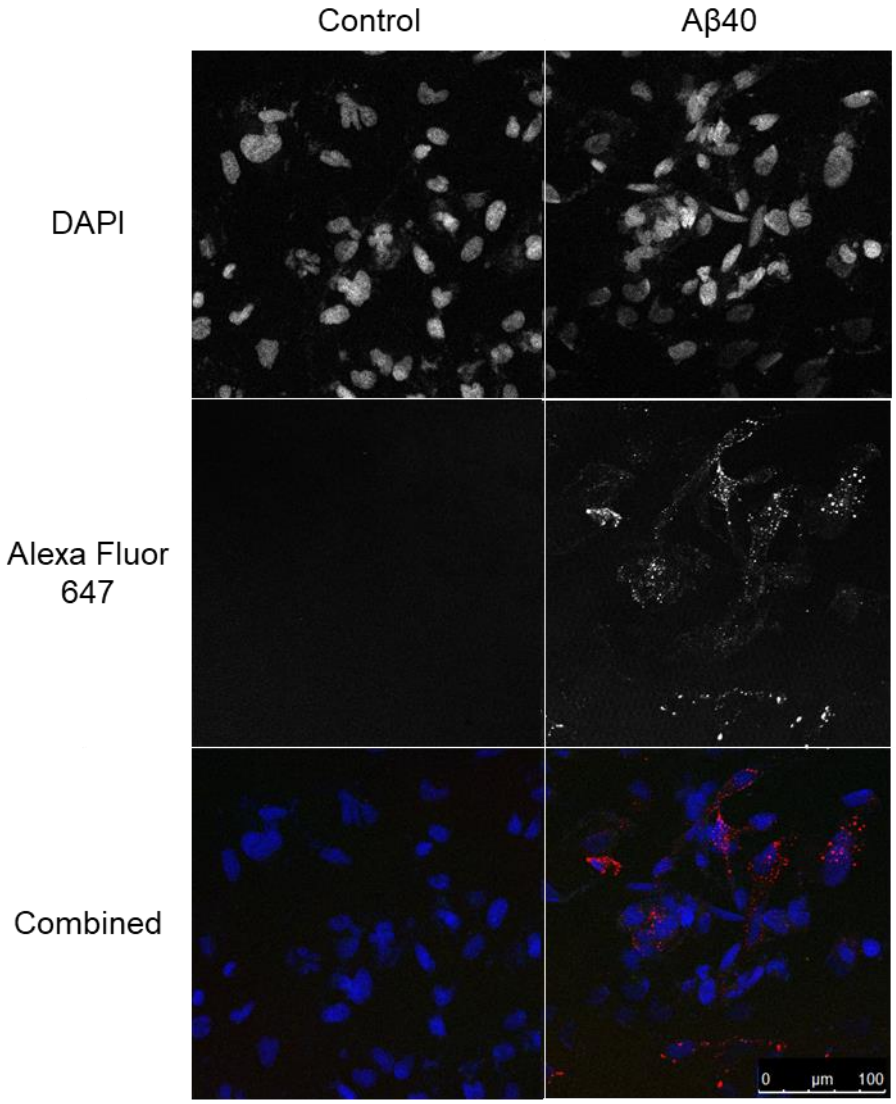

Figure A3.2 – Aβ40 expression in PD304 cells.

Fluorescence following incubation with (right) or without (left) antibody against Aβ40 (middle panel). Nuclei labelled with DAPI (top). Magnification = x20. Scale bar = 100µm.

Moderate fluorescence labelling of Aβ42 was seen evenly distributed throughout the cytoplasm of both PD301 and PD304 cells. The nucei was more heavily labelled than the cytoplasm (Figure A3.3 and Figure A3.4).

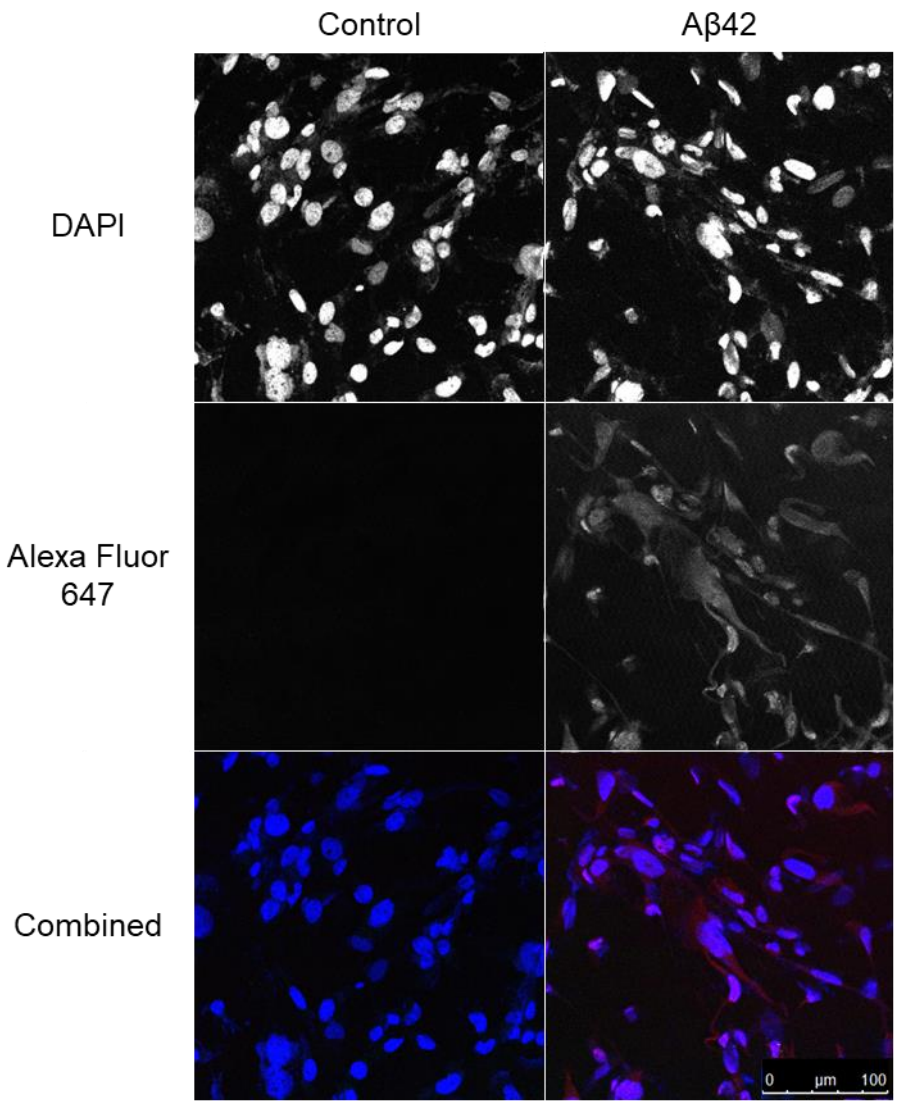

Figure A3.3 - Aβ42 expression in PD301 cells.

Fluorescence following incubation with (right) or without (left) antibody against Aβ42 (middle panel). Nuclei labelled with DAPI (top). Magnification = x20. Scale bar = 100µm

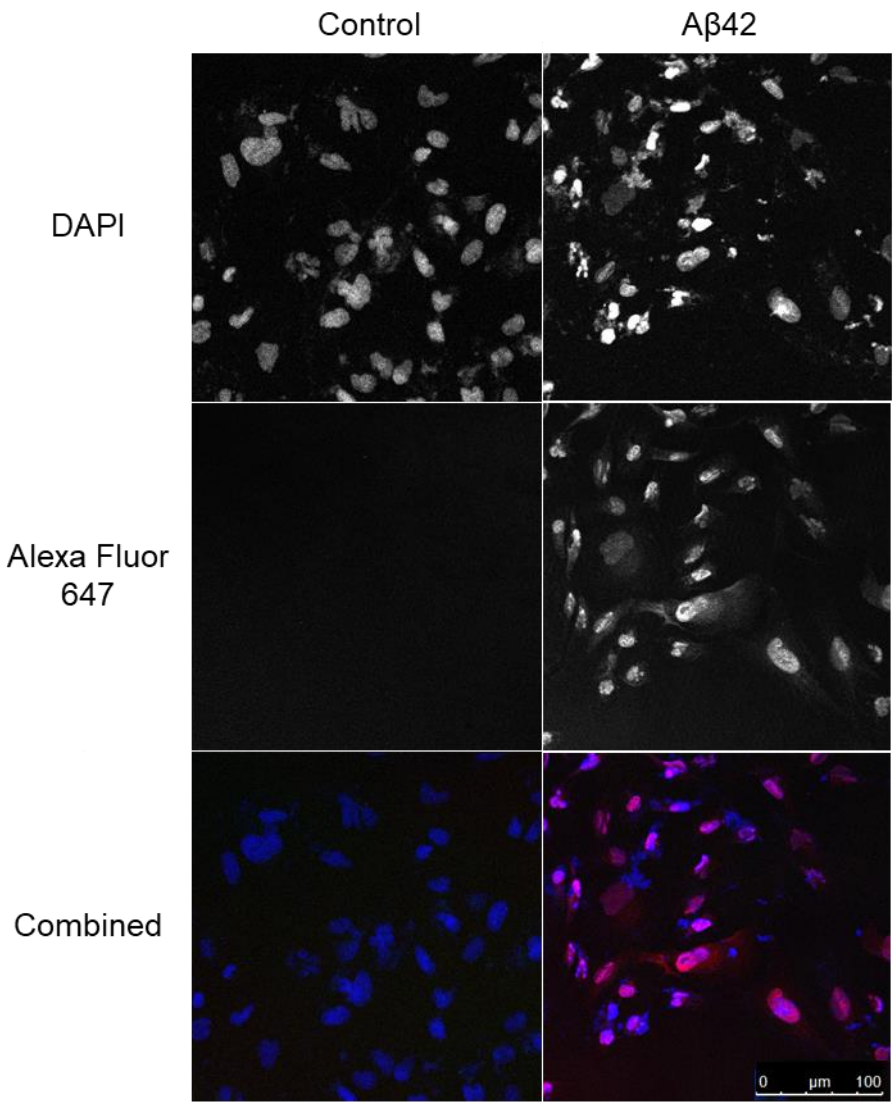

Figure A3.4 - Aβ42 expression in PD304 cells.

Fluorescence following incubation with (right) or without (left) antibody against Aβ40 (middle panel). Nuclei labelled with DAPI (top). Magnification = x20. Scale bar = 100µm

8.4 Appendix 4 – Standard Curves for ELISA

During ELISA experiments, standard curves were produced for both Aβ40 and Aβ42 kits. Known concentrations were plotted against their corrected absorbances to calculate the unknown concentrations of Aβ40 and Aβ42 within cell lysates using the graph's y=mx+c equation line.

Within the Aβ40 ELISA, lysates produced from PD301 and PD304 cells transfected with SorL1 siRNA or scrambled siRNA, treated with Lipofectamine only and those that were non-transfected were pushing the limit of detection towards the extreme lower end of the standard curve. All lysates had a concentration between 30 and 40 pg/ml of Aβ40 (Figure A4.1).

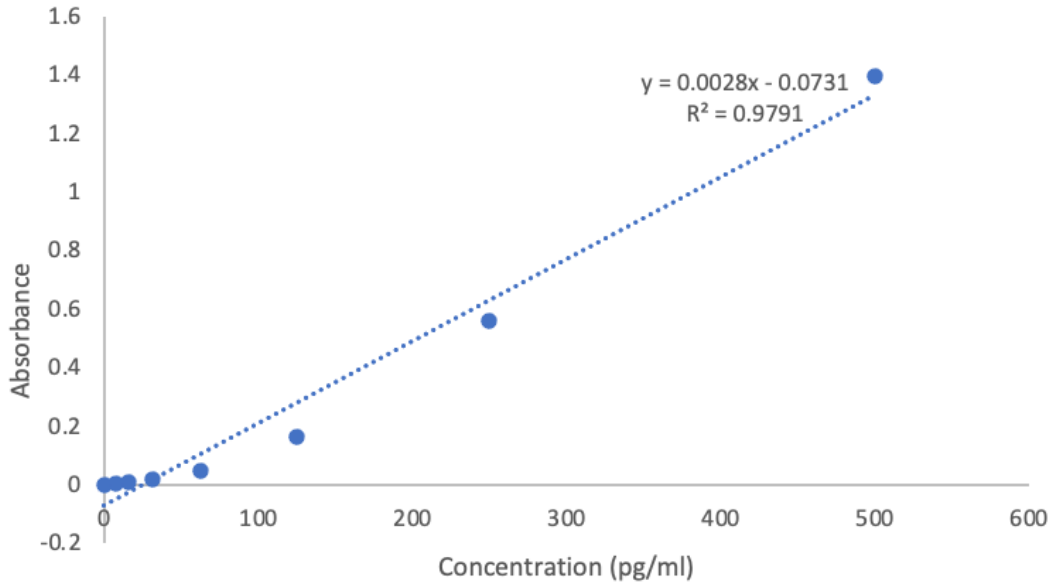

Figure A4.1 – Standard curve for Aβ40 ELISA.

The corrected absorbance levels of known Aβ40 concentrations: 0, 7.81, 15.63, 31.25, 62.5, 125, 250 and 500 pg/ml. Graph also provides the y=mx+c and the R^2 value.

Within the Aβ42 ELISA, lysates produced from PD301 and PD304 cells transfected with SorL1 siRNA or scrambled siRNA, treated with ipofectamine only and those that were non-transfected were pushing the limit of detection towards the extreme lower end of the standard curve. There was a large spread of data as all lysates had a concentration between 20 and 50 pg/ml of Aβ42 (Figure A4.2).

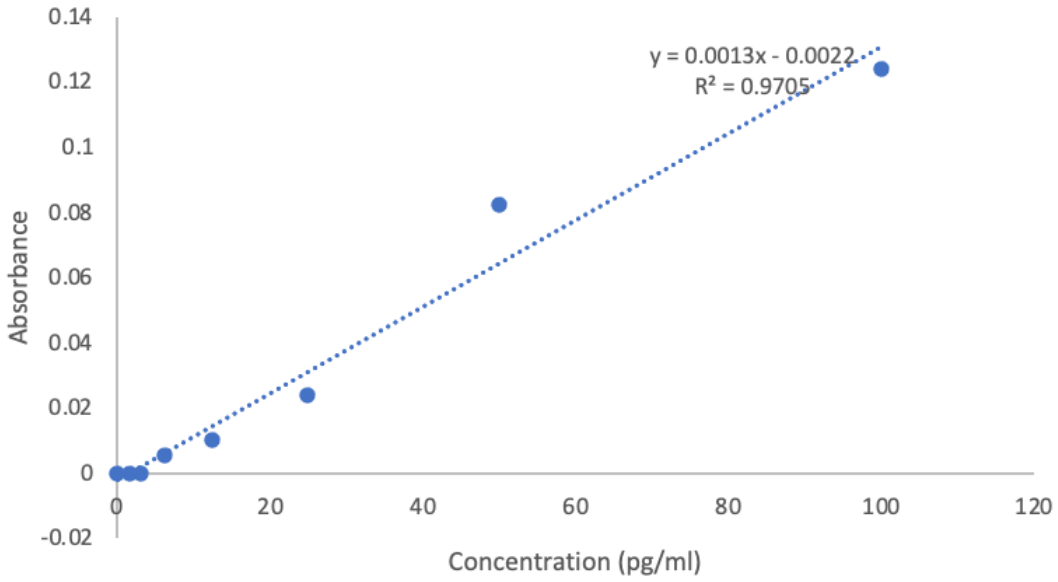

Figure A4.2 – Standard curve for Aβ42 ELISA.

The corrected absorbance levels of known Aβ42 concentrations: 0, 1.56, 3.13, 6.25, 12.5, 25, 50 and 100 pg/ml. Graph also provides the y=mx+c and the R^2 value.

References

9 References

Al-Akhrass, H., Conway, J.R.W., Poulsen, A.S.A., Paatero, I., Kaivola, J., Padzik, A., Andersen, O.M., Ivaska, J., 2021. A feed-forward loop between SorLA and HER3 determines heregulin response and neratinib resistance. Oncogene 40, 1300–1317. https://doi.org/10.1038/s41388-020-01604-5

Al-Akhrass, H., Pietilä, M., Lilja, J., Vesilahti, E.-M., Anttila, J.M., Haikala, H.M., Munne, P.M., Klefström, J., Peuhu, E., Ivaska, J., 2022. Sortilin-related receptor is a druggable therapeutic target in breast cancer. Mol Oncol 16, 116–129. https://doi.org/10.1002/1878-0261.13106

Alifieris, C., Trafalis, D.T., 2015. Glioblastoma multiforme: Pathogenesis and treatment. Pharmacology & Therapeutics 152, 63–82. https://doi.org/10.1016/j.pharmthera.2015.05.005

Allen, M., Bjerke, M., Edlund, H., Nelander, S., Westermark, B., 2016. Origin of the U87MG glioma cell line: Good news and bad news. Sci Transl Med 8, 354re3. https://doi.org/10.1126/scitranslmed.aaf6853

Alvarez-Mora, M.I., Blanco-Palmero, V.A., Quesada-Espinosa, J.F., Arteche-Lopez, A.R., Llamas-Velasco, S., Palma Milla, C., Lezana Rosales, J.M., Gomez-Manjon, I., Hernandez-Lain, A., Jimenez Almonacid, J., Gil-Fournier, B., Ramiro-León, S., González-Sánchez, M., Herrero-San Martín, A.O., Pérez-Martínez, D.A., Gómez-Tortosa, E., Carro, E., Bartolomé, F., Gomez-Rodriguez, M.J., Sanchez-Calvin, M.T., Villarejo-Galende, A., Moreno-Garcia, M., 2022. Heterozygous and Homozygous Variants in SORL1 Gene in Alzheimer's Disease Patients: Clinical, Neuroimaging and Neuropathological Findings. Int J Mol Sci 23, 4230. https://doi.org/10.3390/ijms23084230

Andersen, O.M., Bøgh, N., Landau, A.M., Pløen, G.G., Jensen, A.M.G., Monti, G., Ulhøi, B.P., Nyengaard, J.R., Jacobsen, K.R., Jørgensen, M.M., Holm, I.E., Kristensen, M.L., Alstrup, A.K.O., Hansen, E.S.S., Teunissen, C.E., Breidenbach, L., Droescher, M., Liu, Y., Pedersen, H.S., Callesen, H., Luo, Y., Bolund, L., Brooks, D.J., Laustsen, C., Small, S.A., Mikkelsen, L.F., Sørensen, C.B., 2022. A genetically modified minipig model for Alzheimer's

disease with SORL1 haploinsufficiency. Cell Reports Medicine 3, 100740. https://doi.org/10.1016/j.xcrm.2022.100740

Andersen, O.M., Reiche, J., Schmidt, V., Gotthardt, M., Spoelgen, R., Behlke, J., von Arnim, C.A.F., Breiderhoff, T., Jansen, P., Wu, X., Bales, K.R., Cappai, R., Masters, C.L., Gliemann, J., Mufson, E.J., Hyman, B.T., Paul, S.M., Nykjaer, A., Willnow, T.E., 2005. Neuronal sorting protein-related receptor sorLA/LR11 regulates processing of the amyloid precursor protein. Proc Natl Acad Sci U S A 102, 13461–13466. https://doi.org/10.1073/pnas.0503689102

Andersen, O.M., Rudolph, I.-M., Willnow, T.E., 2016. Risk factor SORL1: from genetic association to functional validation in Alzheimer's disease. Acta Neuropathol 132, 653–665. https://doi.org/10.1007/s00401-016-1615-4

Andrew, R.J., Kellett, K.A.B., Thinakaran, G., Hooper, N.M., 2016. A Greek Tragedy: The Growing Complexity of Alzheimer Amyloid Precursor Protein Proteolysis. J Biol Chem 291, 19235–19244. https://doi.org/10.1074/jbc.R116.746032

Annavarapu, S., Gogate, A., Pham, T., Davies, K., Singh, P., Robert, N., 2021. Treatment patterns and outcomes for patients with newly diagnosed glioblastoma multiforme: a retrospective cohort study. CNS Oncology 10, CNS76. https://doi.org/10.2217/cns-2021-0007

Arora, A., Somasundaram, K., 2019. Glioblastoma vs temozolomide: can the red queen race be won? Cancer Biol Ther 20, 1083–1090. https://doi.org/10.1080/15384047.2019.1599662

Asmamaw, M., Zawdie, B., 2021. Mechanism and Applications of CRISPR/Cas-9-Mediated Genome Editing. Biologics 15, 353–361. https://doi.org/10.2147/BTT.S326422

Atwood, C.S., Bowen, R.L., Smith, M.A., Perry, G., 2003. Cerebrovascular requirement for sealant, anti-coagulant and remodeling molecules that allow for the maintenance of vascular integrity and blood supply. Brain Res Brain Res Rev 43, 164–178. https://doi.org/10.1016/s0165-0173(03)00206-6

Awasthi, M., Singh, S., Pandey, V.P., Dwivedi, U.N., 2016. Alzheimer's disease: An overview of amyloid beta dependent pathogenesis and its therapeutic implications along with in silico approaches emphasizing the role of natural

products. J Neurol Sci 361, 256–271. https://doi.org/10.1016/j.jns.2016.01.008

Barthel, H., Gertz, H.-J., Dresel, S., Peters, O., Bartenstein, P., Buerger, K., Hiemeyer, F., Wittemer-Rump, S.M., Seibyl, J., Reininger, C., Sabri, O., Florbetaben Study Group, 2011. Cerebral amyloid-β PET with florbetaben (18F) in patients with Alzheimer's disease and healthy controls: a multicentre phase 2 diagnostic study. Lancet Neurol 10, 424–435. https://doi.org/10.1016/S1474-4422(11)70077-1

Barthelson, K., Newman, M., Lardelli, M., 2020. Sorting Out the Role of the Sortilin-Related Receptor 1 in Alzheimer's Disease. Journal of Alzheimer's Disease Reports 4, 123–140. https://doi.org/10.3233/ADR-200177

Behrens, M.I., Lendon, C., Roe, C.M., 2009. A common biological mechanism in cancer and Alzheimer's disease? Curr Alzheimer Res 6, 196–204. https://doi.org/10.2174/156720509788486608

Bellenguez, C., Charbonnier, C., Grenier-Boley, B., Quenez, O., Le Guennec, K., Nicolas, G., Chauhan, G., Wallon, D., Rousseau, S., Richard, A.C., Boland, A., Bourque, G., Munter, H.M., Olaso, R., Meyer, V., Rollin-Sillaire, A., Pasquier, F., Letenneur, L., Redon, R., Dartigues, Jean-François, Tzourio, C., Frebourg, T., Lathrop, M., Deleuze, J.-F., Hannequin, D., Genin, E., Amouyel, P., Debette, S., Lambert, J.-C., Campion, D., Hannequin, D., Campion, D., Wallon, D., Martinaud, O., Zarea, A., Nicolas, G., Rollin-Sillaire, A., Bombois, S., Mackowiak, M.-A., Deramecourt, V., Pasquier, F., Michon, A., Le Ber, I., Dubois, B., Godefroy, O., Etcharry-Bouyx, F., Chauviré, V., Chamard, L., Berger, E., Magnin, E., Dartigues, Jean-Francois, Auriacombe, S., Tison, F., Sayette, V. de la, Castan, D., Dionet, E., Sellal, F., Rouaud, O., Thauvin, C., Moreaud, O., Sauvée, M., Formaglio, M., Mollion, H., Roullet-Solignac, I., Vighetto, A., Croisile, B., Didic, M., Félician, O., Koric, L., Ceccaldi, M., Gabelle, A., Marelli, C., Labauge, P., Jonveaux, T., Vercelletto, M., Boutoleau-Bretonnière, C., Castelnovo, G., Paquet, C., Dumurgier, J., Hugon, J., De Boisgueheneuc, F., Belliard, S., Bakchine, S., Sarazin, M., Barrellon, M.-O., Laurent, B., Blanc, F., Pariente, J., Jurici, S., 2017. Contribution to Alzheimer's disease risk of rare variants in TREM2, SORL1, and ABCA7 in 1779 cases and 1273 controls.

Neurobiology of Aging 59, 220.e1-220.e9. https://doi.org/10.1016/j.neurobiolaging.2017.07.001

Belyaev, N.D., Kellett, K.A.B., Beckett, C., Makova, N.Z., Revett, T.J., Nalivaeva, N.N., Hooper, N.M., Turner, A.J., 2010. The transcriptionally active amyloid precursor protein (APP) intracellular domain is preferentially produced from the 695 isoform of APP in a {beta}-secretase-dependent pathway. J Biol Chem 285, 41443–41454. https://doi.org/10.1074/jbc.M110.141390

Berg, A.L., Rowson-Hodel, A., Hu, M., Keeling, M., Wu, H., VanderVorst, K., Chen, J.J., Hatakeyama, J., Jilek, J., Dreyer, C.A., Wheeler, M.R., Yu, A.-M., Li, Y., Carraway, K.L., 2022. The Cationic Amphiphilic Drug Hexamethylene Amiloride Eradicates Bulk Breast Cancer Cells and Therapy-Resistant Subpopulations with Similar Efficiencies. Cancers (Basel) 14, 949. https://doi.org/10.3390/cancers14040949

Binabaj, M.M., Bahrami, A., ShahidSales, S., Joodi, M., Joudi Mashhad, M., Hassanian, S.M., Anvari, K., Avan, A., 2018. The prognostic value of MGMT promoter methylation in glioblastoma: A meta-analysis of clinical trials. J Cell Physiol 233, 378–386. https://doi.org/10.1002/jcp.25896

Bishop, G.M., Robinson, S.R., 2002. The amyloid hypothesis: let sleeping dogmas lie? Neurobiology of Aging 23, 1101–1105. https://doi.org/10.1016/S0197-4580(02)00050-7

Bitting, L., Naidu, A., Cordell, B., Murphy, G.M., 1996. Beta-amyloid peptide secretion by a microglial cell line is induced by beta-amyloid-(25-35) and lipopolysaccharide. J Biol Chem 271, 16084–16089. https://doi.org/10.1074/jbc.271.27.16084

Black, R. A., 2002. Tumor necrosis factor-alpha converting enzyme. Int J Biochem Cell Biol 34, 1–5. https://doi.org/10.1016/s1357-2725(01)00097-8

Bogdanov, Alexey, Bogdanov, Andrey, Chubenko, V., Volkov, N., Moiseenko, F., Moiseyenko, V., 2022. Tumor acidity: From hallmark of cancer to target of treatment. Front Oncol 12, 979154. https://doi.org/10.3389/fonc.2022.979154

Böhm, C., Seibel, N.M., Henkel, B., Steiner, H., Haass, C., Hampe, W., 2006. SorLA signaling by regulated intramembrane proteolysis. J Biol Chem 281, 14547–14553. https://doi.org/10.1074/jbc.M601660200

Borrero, L.J.H., El-Deiry, W.S., 2021. Tumor Suppressor p53: Biology, Signaling Pathways, and Therapeutic Targeting. Biochim Biophys Acta Rev Cancer 1876, 188556. https://doi.org/10.1016/j.bbcan.2021.188556

Breijyeh, Z., Karaman, R., 2020. Comprehensive Review on Alzheimer's Disease: Causes and Treatment. Molecules 25, 5789. https://doi.org/10.3390/molecules25245789

Brothers, H.M., Gosztyla, M.L., Robinson, S.R., 2018. The Physiological Roles of Amyloid-β Peptide Hint at New Ways to Treat Alzheimer's Disease. Front Aging Neurosci 10, 118. https://doi.org/10.3389/fnagi.2018.00118

Caglayan, S., Takagi-Niidome, S., Liao, F., Carlo, A.-S., Schmidt, V., Burgert, T., Kitago, Y., Füchtbauer, E.-M., Füchtbauer, A., Holtzman, D.M., Takagi, J., Willnow, T.E., 2014. Lysosomal sorting of amyloid-β by the SORLA receptor is impaired by a familial Alzheimer's disease mutation. Sci Transl Med 6, 223ra20. https://doi.org/10.1126/scitranslmed.3007747

Cameron, D.J., Galvin, C., Alkam, T., Sidhu, H., Ellison, J., Luna, S., Ethell, D.W., 2012. Alzheimer's-related peptide amyloid-β plays a conserved role in angiogenesis. PLoS ONE 7, undefined-undefined. https://doi.org/10.1371/journal.pone.0039598

Campion, D., Charbonnier, C., Nicolas, G., 2019. SORL1 genetic variants and Alzheimer disease risk: a literature review and meta-analysis of sequencing data. Acta Neuropathol 138, 173–186. https://doi.org/10.1007/s00401-019-01991-4

Carter, M., Essner, R., Goldstein, N., Iyer, M., 2022. Chapter 13 - Cell Culture Techniques, in: Carter, M., Essner, R., Goldstein, N., Iyer, M. (Eds.), Guide to Research Techniques in Neuroscience (Third Edition). Academic Press, pp. 291–308. https://doi.org/10.1016/B978-0-12-818646-6.00015-4

Catalá-López, F., Suárez-Pinilla, M., Suárez-Pinilla, P., Valderas, J.M., Gómez-Beneyto, M., Martinez, S., Balanzá-Martínez, V., Climent, J., Valencia, A., McGrath, J., Crespo-Facorro, B., Sanchez-Moreno, J., Vieta, E., Tabarés-Seisdedos, R., 2014. Inverse and direct cancer comorbidity in people with central nervous system disorders: a meta-analysis of cancer incidence in 577,013 participants of 50 observational studies. Psychother Psychosom 83, 89–105. https://doi.org/10.1159/000356498

Chang, J.R., Ghafouri, M., Mukerjee, R., Bagashev, A., Chabrashvili, T., Sawaya, B.E., 2012. Role of p53 in Neurodegenerative Diseases. Neurodegener Dis 9, 68–80. https://doi.org/10.1159/000329999

Chasseigneaux, S., Allinquant, B., 2012. Functions of Aβ, sAPPα and sAPPβ : similarities and differences. J Neurochem 120 Suppl 1, 99–108. https://doi.org/10.1111/j.1471-4159.2011.07584.x

Chaudhry, A., Benson, L., Varshaver, M., Farber, O., Weinberg, U., Kirson, E., Palti, Y., 2015. NovoTTF™-100A System (Tumor Treating Fields) transducer array layout planning for glioblastoma: a NovoTAL™ system user study. World J Surg Oncol 13, 316. https://doi.org/10.1186/s12957-015-0722-3

Chen, G., Xu, T., Yan, Y., Zhou, Y., Jiang, Y., Melcher, K., Xu, H.E., 2017. Amyloid beta: structure, biology and structure-based therapeutic development. Acta Pharmacol Sin 38, 1205–1235. https://doi.org/10.1038/aps.2017.28

Cho, H.S., Huang, L.K., Lee, Y.T., Chan, L., Hong, C.T., 2018. Suboptimal Baseline Serum Vitamin B12 Is Associated With Cognitive Decline in People With Alzheimer's Disease Undergoing Cholinesterase Inhibitor Treatment. Front Neurol 9, 325. https://doi.org/10.3389/fneur.2018.00325

Chou, C.-T., Liao, Y.-C., Lee, W.-J., Wang, S.-J., Fuh, J.-L., 2016. SORL1 gene, plasma biomarkers, and the risk of Alzheimer's disease for the Han Chinese population in Taiwan. Alzheimers Res Ther 8, 53. https://doi.org/10.1186/s13195-016-0222-x

Christensen, A., Pike, C.J., 2020. Staining and Quantification of β-Amyloid Pathology in Transgenic Mouse Models of Alzheimer's Disease. Methods Mol Biol 2144, 211–221. https://doi.org/10.1007/978-1-0716-0592-9_19

Church, M.K., Church, D.S., 2013. Pharmacology of Antihistamines. Indian J Dermatol 58, 219–224. https://doi.org/10.4103/0019-5154.110832

Cong, L., Ran, F.A., Cox, D., Lin, S., Barretto, R., Habib, N., Hsu, P.D., Wu, X., Jiang, W., Marraffini, L.A., Zhang, F., 2013. Multiplex Genome Engineering Using CRISPR/Cas Systems. Science 339, 819–823. https://doi.org/10.1126/science.1231143

Copanaki, E., Chang, S., Vlachos, A., Tschäpe, J.-A., Müller, U.C., Kögel, D., Deller, T., 2010. sAPPα antagonizes dendritic degeneration and neuron

death triggered by proteasomal stress. Molecular and Cellular Neuroscience 44, 386–393. https://doi.org/10.1016/j.mcn.2010.04.007

Coric, V., Salloway, S., van Dyck, C.H., Dubois, B., Andreasen, N., Brody, M., Curtis, C., Soininen, H., Thein, S., Shiovitz, T., Pilcher, G., Ferris, S., Colby, S., Kerselaers, W., Dockens, R., Soares, H., Kaplita, S., Luo, F., Pachai, C., Bracoud, L., Mintun, M., Grill, J.D., Marek, K., Seibyl, J., Cedarbaum, J.M., Albright, C., Feldman, H.H., Berman, R.M., 2015. Targeting Prodromal Alzheimer Disease With Avagacestat: A Randomized Clinical Trial. JAMA Neurol 72, 1324–1333. https://doi.org/10.1001/jamaneurol.2015.0607

Cuccaro, M.L., Carney, R.M., Zhang, Y., Bohm, C., Kunkle, B.W., Vardarajan, B.N., Whitehead, P.L., Cukier, H.N., Mayeux, R., St. George-Hyslop, P., Pericak-Vance, M.A., 2016. SORL1 mutations in early- and late-onset Alzheimer disease. Neurol Genet 2, e116. https://doi.org/10.1212/NXG.0000000000000116

Culicchia, F., Cui, J.-G., Li, Y.Y., Lukiw, W.J., 2008. Upregulation of beta-amyloid precursor protein expression in glioblastoma multiforme. Neuroreport 19, 981–985. https://doi.org/10.1097/WNR.0b013e328302f139

Dana, H., Chalbatani, G.M., Mahmoodzadeh, H., Karimloo, R., Rezaiean, O., Moradzadeh, A., Mehmandoost, N., Moazzen, F., Mazraeh, A., Marmari, V., Ebrahimi, M., Rashno, M.M., Abadi, S.J., Gharagouzlo, E., 2017. Molecular Mechanisms and Biological Functions of siRNA. Int J Biomed Sci 13, 48–57.

Dang, L., Jin, S., Su, S.M., 2010. IDH mutations in glioma and acute myeloid leukemia. Trends in Molecular Medicine 16, 387–397. https://doi.org/10.1016/j.molmed.2010.07.002

Davis, M.E., 2016. Glioblastoma: Overview of Disease and Treatment. Clin J Oncol Nurs 20, S2–S8. https://doi.org/10.1188/16.CJON.S1.2-8

Dawkins, E., Small, D.H., 2014. Insights into the physiological function of the β-amyloid precursor protein: beyond Alzheimer's disease. J Neurochem 129, 756–769. https://doi.org/10.1111/jnc.12675

De-Paula, V.J., Radanovic, M., Diniz, B.S., Forlenza, O.V., 2012. Alzheimer's disease. Subcell Biochem 65, 329–352. https://doi.org/10.1007/978-94-007-5416-4_14

DiFrancesco, J.C., Longoni, M., Piazza, F., 2015. Anti-Aβ Autoantibodies in Amyloid Related Imaging Abnormalities (ARIA): Candidate Biomarker for Immunotherapy in Alzheimer's Disease and Cerebral Amyloid Angiopathy. Front Neurol 6, 207. https://doi.org/10.3389/fneur.2015.00207

Dodson, S.E., Andersen, O.M., Karmali, V., Fritz, J.J., Cheng, D., Peng, J., Levey, A.I., Willnow, T.E., Lah, J.J., 2008. Loss of LR11/SORLA enhances early pathology in a mouse model of amyloidosis: evidence for a proximal role in Alzheimer's disease. J Neurosci 28, 12877–12886. https://doi.org/10.1523/JNEUROSCI.4582-08.2008

Doody, R.S., Raman, R., Farlow, M., Iwatsubo, T., Vellas, B., Joffe, S., Kieburtz, K., He, F., Sun, X., Thomas, R.G., Aisen, P.S., Alzheimer's Disease Cooperative Study Steering Committee, Siemers, E., Sethuraman, G., Mohs, R., Semagacestat Study Group, 2013. A phase 3 trial of semagacestat for treatment of Alzheimer's disease. N Engl J Med 369, 341–350. https://doi.org/10.1056/NEJMoa1210951

Doody, R.S., Thomas, R.G., Farlow, M., Iwatsubo, T., Vellas, B., Joffe, S., Kieburtz, K., Raman, R., Sun, X., Aisen, P.S., Siemers, E., Liu-Seifert, H., Mohs, R., Alzheimer's Disease Cooperative Study Steering Committee, Solanezumab Study Group, 2014. Phase 3 trials of solanezumab for mild-to-moderate Alzheimer's disease. N Engl J Med 370, 311–321. https://doi.org/10.1056/NEJMoa1312889

Dorsey, J.F., Salinas, R.D., Dang, M., Alonso-Basanta, M., Judy, K.D., Maity, A., Lustig, R.A., Lee, J.Y.K., Phillips, P.C., Pruitt, A.A., 2020. 63 - Cancer of the Central Nervous System, in: Niederhuber, J.E., Armitage, J.O., Kastan, M.B., Doroshow, J.H., Tepper, J.E. (Eds.), Abeloff's Clinical Oncology (Sixth Edition). Elsevier, Philadelphia, pp. 906-967.e12. https://doi.org/10.1016/B978-0-323-47674-4.00063-3

Driver, J.A., 2014. Inverse association between cancer and neurodegenerative disease: review of the epidemiologic and biological evidence. Biogerontology 15, 547–557. https://doi.org/10.1007/s10522-014-9523-2

Driver, J.A., Beiser, A., Au, R., Kreger, B.E., Splansky, G.L., Kurth, T., Kiel, D.P., Lu, K.P., Seshadri, S., Wolf, P.A., 2012. Inverse association between cancer and Alzheimer's disease: results from the Framingham Heart Study. BMJ 344, e1442. https://doi.org/10.1136/bmj.e1442

Dubois, B., Hampel, H., Feldman, H.H., Scheltens, P., Aisen, P., Andrieu, S., Bakardjian, H., Benali, H., Bertram, L., Blennow, K., Broich, K., Cavedo, E., Crutch, S., Dartigues, J.-F., Duyckaerts, C., Epelbaum, S., Frisoni, G.B., Gauthier, S., Genthon, R., Gouw, A.A., Habert, M.-O., Holtzman, D.M., Kivipelto, M., Lista, S., Molinuevo, J.-L., O'Bryant, S.E., Rabinovici, G.D., Rowe, C., Salloway, S., Schneider, L.S., Sperling, R., Teichmann, M., Carrillo, M.C., Cummings, J., Jack, C.R., 2016. Preclinical Alzheimer's disease: Definition, natural history, and diagnostic criteria. Alzheimers Dement 12, 292–323. https://doi.org/10.1016/j.jalz.2016.02.002

Ellegaard, A.-M., Dehlendorff, C., Vind, A.C., Anand, A., Cederkvist, L., Petersen, N.H.T., Nylandsted, J., Stenvang, J., Mellemgaard, A., Østerlind, K., Friis, S., Jäättelä, M., 2016. Repurposing Cationic Amphiphilic Antihistamines for Cancer Treatment. EBioMedicine 9, 130–139. https://doi.org/10.1016/j.ebiom.2016.06.013

Elsner, C., Bohne, J., 2017. The retroviral vector family: something for everyone. Virus Genes 53, 714–722. https://doi.org/10.1007/s11262-017-1489-0

Farmer, K.M., Ghag, G., Puangmalai, N., Montalbano, M., Bhatt, N., Kayed, R., 2020. P53 aggregation, interactions with tau, and impaired DNA damage response in Alzheimer's disease. Acta Neuropathol Commun 8, 132. https://doi.org/10.1186/s40478-020-01012-6

Farrell, R.E., 2010. Chapter 23 - RNAi: Take a RISC – Role the Dicer, in: Farrell, R.E. (Ed.), RNA Methodologies (Fourth Edition). Academic Press, San Diego, pp. 539–560. https://doi.org/10.1016/B978-0-12-374727-3.00023-1

Fire, A., Xu, S., Montgomery, M.K., Kostas, S.A., Driver, S.E., Mello, C.C., 1998. Potent and specific genetic interference by double-stranded RNA in Caenorhabditis elegans. Nature 391, 806–811. https://doi.org/10.1038/35888

Fujimura, K., Ebinuma, H., Fukamachi, I., Ohwada, C., Kawaguchi, T., Shimizu, N., Takeuchi, M., Sakaida, E., Jiang, M., Nakaseko, C., Bujo, H., 2014. Circulating LR11 is a novel soluble-receptor marker for early-stage clinical conditions in patients with non-Hodgkin's lymphoma. Clin Chim Acta 430, 48–54. https://doi.org/10.1016/j.cca.2013.12.039

Fus-Kujawa, A., Prus, P., Bajdak-Rusinek, K., Teper, P., Gawron, K., Kowalczuk, A., Sieron, A.L., 2021. An Overview of Methods and Tools for Transfection

of Eukaryotic Cells in vitro. Frontiers in Bioengineering and Biotechnology 9.

GBD 2015 Mortality and Causes of Death Collaborators, 2016. Global, regional, and national life expectancy, all-cause mortality, and cause-specific mortality for 249 causes of death, 1980–2015: a systematic analysis for the Global Burden of Disease Study 2015. Lancet 388, 1459–1544. https://doi.org/10.1016/S0140-6736(16)31012-1

Gerson, S.L., 2004. MGMT: its role in cancer aetiology and cancer therapeutics. Nat Rev Cancer 4, 296–307. https://doi.org/10.1038/nrc1319

Goethe, E., Carter, B.Z., Rao, G., Pemmaraju, N., 2018. Glioblastoma and acute myeloid leukemia: malignancies with striking similarities. J Neurooncol 136, 223–231. https://doi.org/10.1007/s11060-017-2676-5

Gosztyla, M.L., Brothers, H.M., Robinson, S.R., 2018. Alzheimer's Amyloid-β is an Antimicrobial Peptide: A Review of the Evidence. J Alzheimers Dis 62, 1495–1506. https://doi.org/10.3233/JAD-171133

Graff-Radford, N.R., Crook, J.E., Lucas, J., Boeve, B.F., Knopman, D.S., Ivnik, R.J., Smith, G.E., Younkin, L.H., Petersen, R.C., Younkin, S.G., 2007. Association of low plasma Abeta42/Abeta40 ratios with increased imminent risk for mild cognitive impairment and Alzheimer disease. Arch Neurol 64, 354–362. https://doi.org/10.1001/archneur.64.3.354

Greenblatt, K., Khaddour, K., 2023. Trastuzumab, in: StatPearls. StatPearls Publishing, Treasure Island (FL).

Gresch, O., Altrogge, L., 2012. Transfection of difficult-to-transfect primary mammalian cells. Methods Mol Biol 801, 65–74. https://doi.org/10.1007/978-1-61779-352-3_5

Guerreiro, R., Wojtas, A., Bras, J., Carrasquillo, M., Rogaeva, E., Majounie, E., Cruchaga, C., Sassi, C., Kauwe, J.S.K., Younkin, S., Hazrati, L., Collinge, J., Pocock, J., Lashley, T., Williams, J., Lambert, J.-C., Amouyel, P., Goate, A., Rademakers, R., Morgan, K., Powell, J., St. George-Hyslop, P., Singleton, A., Hardy, J., 2013. TREM2 Variants in Alzheimer's Disease. N Engl J Med 368, 117–127. https://doi.org/10.1056/NEJMoa1211851

Guo, Q., Wang, Z., Li, H., Wiese, M., Zheng, H., 2012. APP physiological and pathophysiological functions: insights from animal models. Cell Res 22, 78–89. https://doi.org/10.1038/cr.2011.116

Gustaw-Rothenberg, K., Lerner, A., Bonda, D.J., Lee, H., Zhu, X., Perry, G., Smith, M.A., 2010. Biomarkers in Alzheimer's disease: past, present and future. Biomark Med 4, 15–26. https://doi.org/10.2217/bmm.09.86

Guthrie, J.W., 2012. 3.01 - General Considerations when Dealing with Biological Fluid Samples, in: Pawliszyn, J. (Ed.), Comprehensive Sampling and Sample Preparation. Academic Press, Oxford, pp. 1–19. https://doi.org/10.1016/B978-0-12-381373-2.00065-X

Halliwell, W.H., 1997. Cationic amphiphilic drug-induced phospholipidosis. Toxicol Pathol 25, 53–60. https://doi.org/10.1177/019262339702500111

Hampel, H., Bürger, K., Teipel, S.J., Bokde, A.L.W., Zetterberg, H., Blennow, K., 2008. Core candidate neurochemical and imaging biomarkers of Alzheimer's disease. Alzheimer's & Dementia 4, 38–48. https://doi.org/10.1016/j.jalz.2007.08.006

Hampel, H., Hardy, J., Blennow, K., Chen, C., Perry, G., Kim, S.H., Villemagne, V.L., Aisen, P., Vendruscolo, M., Iwatsubo, T., Masters, C.L., Cho, M., Lannfelt, L., Cummings, J.L., Vergallo, A., 2021. The Amyloid-β Pathway in Alzheimer's Disease. Mol Psychiatry 26, 5481–5503. https://doi.org/10.1038/s41380-021-01249-0

Hanahan, D., 2022. Hallmarks of Cancer: New Dimensions. Cancer Discovery 12, 31–46. https://doi.org/10.1158/2159-8290.CD-21-1059

Hanahan, D., Weinberg, R.A., 2011. Hallmarks of Cancer: The Next Generation. Cell 144, 646–674. https://doi.org/10.1016/j.cell.2011.02.013

Hansel, D.E., Rahman, A., Wehner, S., Herzog, V., Yeo, C.J., Maitra, A., 2003. Increased expression and processing of the Alzheimer amyloid precursor protein in pancreatic cancer may influence cellular proliferation. Cancer Res 63, 7032–7037.

Hardy, J.A., Higgins, G.A., 1992. Alzheimer's disease: the amyloid cascade hypothesis. Science 256, 184–185. https://doi.org/10.1126/science.1566067

Hashimoto, N., Nagano, H., Tanaka, T., 2019. The role of tumor suppressor p53 in metabolism and energy regulation, and its implication in cancer and lifestyle-related diseases. Endocr J 66, 485–496. https://doi.org/10.1507/endocrj.EJ18-0565

Haytural, H., Lundgren, J.L., Köse, T.B., Jordà-Siquier, T., Kalcheva, M., Seed Ahmed, M., Winblad, B., Sundström, E., Barthet, G., Tjernberg, L.O., Frykman, S., 2019. Non-specific Detection of a Major Western Blotting Band in Human Brain Homogenates by a Multitude of Amyloid Precursor Protein Antibodies. Frontiers in Aging Neuroscience 11.

Hermey, G., Sjøgaard, S.S., Petersen, C.M., Nykjær, A., Gliemann, J., 2006. Tumour necrosis factor α-converting enzyme mediates ectodomain shedding of Vps10p-domain receptor family members. Biochem J 395, 285–293. https://doi.org/10.1042/BJ20051364

Herskowitz, J.H., Offe, K., Deshpande, A., Kahn, R.A., Levey, A.I., Lah, J.J., 2012. GGA1-mediated endocytic traffic of LR11/SorLA alters APP intracellular distribution and amyloid-β production. Mol Biol Cell 23, 2645–2657. https://doi.org/10.1091/mbc.E12-01-0014

Herzog, V., Kirfel, G., Siemes, C., Schmitz, A., 2004. Biological roles of APP in the epidermis. Eur J Cell Biol 83, 613–624. https://doi.org/10.1078/0171-9335-00401

Hesse, R., von Einem, B., Wagner, F., Bott, P., Schwanzar, D., Jackson, R.J., Föhr, K.J., Lausser, L., Kroker, K.S., Proepper, C., Walther, P., Kestler, H.A., Spires-Jones, T.L., Boeckers, T., Rosenbrock, H., von Arnim, C.A.F., 2018. sAPPβ and sAPPα increase structural complexity and E/I input ratio in primary hippocampal neurons and alter Ca2+ homeostasis and CREB1-signaling. Experimental Neurology 304, 1–13. https://doi.org/10.1016/j.expneurol.2018.02.010

Hoadley, K.A., Yau, C., Hinoue, T., Wolf, D.M., Lazar, A.J., Drill, E., Shen, R., Taylor, A.M., Cherniack, A.D., Thorsson, Vésteinn, Akbani, R., Bowlby, R., Wong, C.K., Wiznerowicz, M., Sanchez-Vega, F., Robertson, A.G., Schneider, B.G., Lawrence, M.S., Noushmehr, H., Malta, T.M., Caesar-Johnson, S.J., Demchok, J.A., Felau, I., Kasapi, M., Ferguson, M.L., Hutter, C.M., Sofia, H.J., Tarnuzzer, R., Wang, Z., Yang, L., Zenklusen, J.C., Zhang, J. (Julia), Chudamani, S., Liu, J., Lolla, L., Naresh, R., Pihl, T., Sun, Q., Wan, Y., Wu, Y., Cho, J., DeFreitas, T., Frazer, S., Gehlenborg, N., Getz, G., Heiman, D.I., Kim, J., Lawrence, M.S., Lin, P., Meier, S., Noble, M.S., Saksena, G., Voet, D., Zhang, Hailei, Bernard, B., Chambwe, N., Dhankani, V., Knijnenburg, T., Kramer, R., Leinonen, K., Liu, Y., Miller, M.,

Reynolds, S., Shmulevich, I., Thorsson, Vesteinn, Zhang, W., Akbani, R., Broom, B.M., Hegde, A.M., Ju, Z., Kanchi, R.S., Korkut, A., Li, J., Liang, H., Ling, S., Liu, W., Lu, Y., Mills, G.B., Ng, K.-S., Rao, A., Ryan, M., Wang, Jing, Weinstein, J.N., Zhang, J., Abeshouse, A., Armenia, J., Chakravarty, D., Chatila, W.K., Bruijn, I. de, Gao, J., Gross, B.E., Heins, Z.J., Kundra, R., La, K., Ladanyi, M., Luna, A., Nissan, M.G., Ochoa, A., Phillips, S.M., Reznik, E., Sanchez-Vega, F., Sander, C., Schultz, N., Sheridan, R., Sumer, S.O., Sun, Y., Taylor, B.S., Wang, Jioajiao, Zhang, Hongxin, Anur, P., Peto, M., Spellman, P., Benz, C., Stuart, J.M., Wong, C.K., Yau, C., Hayes, D.N., Parker, J.S., Wilkerson, M.D., Ally, A., Balasundaram, M., Bowlby, R., Brooks, D., Carlsen, R., Chuah, E., Dhalla, N., Holt, R., Jones, S.J.M., Kasaian, K., Lee, D., Ma, Y., Marra, M.A., Mayo, M., Moore, R.A., Mungall, A.J., Mungall, K., Robertson, A.G., Sadeghi, S., Schein, J.E., Sipahimalani, P., Tam, A., Thiessen, N., Tse, K., Wong, T., Berger, A.C., Beroukhim, R., Cherniack, A.D., Cibulskis, C., Gabriel, S.B., Gao, G.F., Ha, G., Meyerson, M., Schumacher, S.E., Shih, J., Kucherlapati, M.H., Kucherlapati, R.S., Baylin, S., Cope, L., Danilova, L., Bootwalla, M.S., Lai, P.H., Maglinte, D.T., Berg, D.J.V.D., Weisenberger, D.J., Auman, J.T., Balu, S., Bodenheimer, T., Fan, C., Hoadley, K.A., Hoyle, A.P., Jefferys, S.R., Jones, C.D., Meng, S., Mieczkowski, P.A., Mose, L.E., Perou, A.H., Perou, C.M., Roach, J., Shi, Y., Simons, J.V., Skelly, T., Soloway, M.G., Tan, D., Veluvolu, U., Fan, H., Hinoue, T., Laird, P.W., Shen, H., Zhou, W., Bellair, M., Chang, K., Covington, K., Creighton, C.J., Dinh, H., Doddapaneni, H., Donehower, L.A., Drummond, J., Gibbs, R.A., Glenn, R., Hale, W., Han, Y., Hu, J., Korchina, V., Lee, S., Lewis, L., Li, W., Liu, X., Morgan, M., Morton, D., Muzny, D., Santibanez, J., Sheth, M., Shinbrot, E., Wang, L., Wang, M., Wheeler, D.A., Xi, L., Zhao, F., Hess, J., Appelbaum, E.L., Bailey, M., Cordes, M.G., Ding, L., Fronick, C.C., Fulton, L.A., Fulton, R.S., Kandoth, C., Mardis, E.R., McLellan, M.D., Miller, C.A., Schmidt, H.K., Wilson, R.K., Crain, D., Curley, E., Gardner, J., Lau, K., Mallery, D., Morris, S., Paulauskis, J., Penny, R., Shelton, C., Shelton, T., Sherman, M., Thompson, E., Yena, P., Bowen, J., Gastier-Foster, J.M., Gerken, M., Leraas, K.M., Lichtenberg, T.M., Ramirez, N.C., Wise, L., Zmuda, E., Corcoran, N., Costello, T., Hovens, C., Carvalho, A.L., Carvalho, A.C. de,

Fregnani, J.H., Longatto-Filho, A., Reis, R.M., Scapulatempo-Neto, C., Silveira, H.C.S., Vidal, D.O., Burnette, A., Eschbacher, J., Hermes, B., Noss, A., Singh, R., Anderson, M.L., Castro, P.D., Ittmann, M., Huntsman, D., Kohl, B., Le, X., Thorp, R., Andry, C., Duffy, E.R., Lyadov, V., Paklina, O., Setdikova, G., Shabunin, A., Tavobilov, M., McPherson, C., Warnick, R., Berkowitz, R., Cramer, D., Feltmate, C., Horowitz, N., Kibel, A., Muto, M., Raut, C.P., Malykh, A., Barnholtz-Sloan, J.S., Barrett, W., Devine, K., Fulop, J., Ostrom, Q.T., Shimmel, K., Wolinsky, Y., Sloan, A.E., Rose, A.D., Giuliante, F., Goodman, M., Karlan, B.Y., Hagedorn, C.H., Eckman, J., Harr, J., Myers, J., Tucker, K., Zach, L.A., Deyarmin, B., Hu, H., Kvecher, L., Larson, C., Mural, R.J., Somiari, S., Vicha, A., Zelinka, T., Bennett, J., Iacocca, M., Rabeno, B., Swanson, P., Latour, M., Lacombe, L., Têtu, B., Bergeron, A., McGraw, M., Staugaitis, S.M., Chabot, J., Hibshoosh, H., Sepulveda, A., Su, T., Wang, T., Potapova, O., Voronina, O., Desjardins, L., Mariani, O., Roman-Roman, S., Sastre, X., Stern, M.-H., Cheng, F., Signoretti, S., Berchuck, A., Bigner, D., Lipp, E., Marks, J., McCall, S., McLendon, R., Secord, A., Sharp, A., Behera, M., Brat, D.J., Chen, A., Delman, K., Force, S., Khuri, F., Magliocca, K., Maithel, S., Olson, J.J., Owonikoko, T., Pickens, A., Ramalingam, S., Shin, D.M., Sica, G., Meir, E.G.V., Zhang, Hongzheng, Eijckenboom, W., Gillis, A., Korpershoek, E., Looijenga, L., Oosterhuis, W., Stoop, H., Kessel, K.E. van, Zwarthoff, E.C., Calatozzolo, C., Cuppini, L., Cuzzubbo, S., DiMeco, F., Finocchiaro, G., Mattei, L., Perin, A., Pollo, B., Chen, C., Houck, J., Lohavanichbutr, P., Hartmann, A., Stoehr, C., Stoehr, R., Taubert, H., Wach, S., Wullich, B., Kycler, W., Murawa, D., Wiznerowicz, M., Chung, K., Edenfield, W.J., Martin, J., Baudin, E., Bubley, G., Bueno, R., Rienzo, A.D., Richards, W.G., Kalkanis, S., Mikkelsen, T., Noushmehr, H., Scarpace, L., Girard, N., Aymerich, M., Campo, E., Giné, E., Guillermo, A.L., Bang, N.V., Hanh, P.T., Phu, B.D., Tang, Y., Colman, H., Evason, K., Dottino, P.R., Martignetti, J.A., Gabra, H., Juhl, H., Akeredolu, T., Stepa, S., Hoon, D., Ahn, K., Kang, K.J., Beuschlein, F., Breggia, A., Birrer, M., Bell, D., Borad, M., Bryce, A.H., Castle, E., Chandan, V., Cheville, J., Copland, J.A., Farnell, M., Flotte, T., Giama, N., Ho, T., Kendrick, M., Kocher, J.-P., Kopp, K., Moser, C., Nagorney, D., O'Brien, D., O'Neill, B.P., Patel, T., Petersen, G., Que, F.,

Rivera, M., Roberts, L., Smallridge, R., Smyrk, T., Stanton, M., Thompson, R.H., Torbenson, M., Yang, J.D., Zhang, L., Brimo, F., Ajani, J.A., Gonzalez, A.M.A., Behrens, C., Bondaruk, O., Broaddus, R., Czerniak, B., Esmaeli, B., Fujimoto, J., Gershenwald, J., Guo, C., Lazar, A.J., Logothetis, C., Meric-Bernstam, F., Moran, C., Ramondetta, L., Rice, D., Sood, A., Tamboli, P., Thompson, T., Troncoso, P., Tsao, A., Wistuba, I., Carter, C., Haydu, L., Hersey, P., Jakrot, V., Kakavand, H., Kefford, R., Lee, K., Long, G., Mann, G., Quinn, M., Saw, R., Scolyer, R., Shannon, K., Spillane, A., Stretch, J., Synott, M., Thompson, J., Wilmott, J., Al-Ahmadie, H., Chan, T.A., Ghossein, R., Gopalan, A., Levine, D.A., Reuter, V., Singer, S., Singh, B., Tien, N.V., Broudy, T., Mirsaidi, C., Nair, P., Drwiega, P., Miller, J., Smith, J., Zaren, H., Park, J.-W., Hung, N.P., Kebebew, E., Linehan, W.M., Metwalli, A.R., Pacak, K., Pinto, P.A., Schiffman, M., Schmidt, L.S., Vocke, C.D., Wentzensen, N., Worrell, R., Yang, H., Moncrieff, M., Goparaju, C., Melamed, J., Pass, H., Botnariuc, N., Caraman, I., Cernat, M., Chemencedji, I., Clipca, A., Doruc, S., Gorincioi, G., Mura, S., Pirtac, M., Stancul, I., Tcaciuc, D., Albert, M., Alexopoulou, I., Arnaout, A., Bartlett, J., Engel, J., Gilbert, S., Parfitt, J., Sekhon, H., Thomas, G., Rassl, D.M., Rintoul, R.C., Bifulco, C., Tamakawa, R., Urba, W., Hayward, N., Timmers, H., Antenucci, A., Facciolo, F., Grazi, G., Marino, M., Merola, R., Krijger, R. de, Gimenez-Roqueplo, A.-P., Piché, A., Chevalier, S., McKercher, G., Birsoy, K., Barnett, G., Brewer, C., Farver, C., Naska, T., Pennell, N.A., Raymond, D., Schilero, C., Smolenski, K., Williams, F., Morrison, C., Borgia, J.A., Liptay, M.J., Pool, M., Seder, C.W., Junker, K., Omberg, L., Dinkin, M., Manikhas, G., Alvaro, D., Bragazzi, M.C., Cardinale, V., Carpino, G., Gaudio, E., Chesla, D., Cottingham, S., Dubina, M., Moiseenko, F., Dhanasekaran, R., Becker, K.-F., Janssen, K.-P., Slotta-Huspenina, J., Abdel-Rahman, M.H., Aziz, D., Bell, S., Cebulla, C.M., Davis, A., Duell, R., Elder, J.B., Hilty, J., Kumar, B., Lang, J., Lehman, N.L., Mandt, R., Nguyen, P., Pilarski, R., Rai, K., Schoenfield, L., Senecal, K., Wakely, P., Hansen, P., Lechan, R., Powers, J., Tischler, A., Grizzle, W.E., Sexton, K.C., Kastl, A., Henderson, J., Porten, S., Waldmann, J., Fassnacht, M., Asa, S.L., Schadendorf, D., Couce, M., Graefen, M., Huland, H., Sauter, G., Schlomm, T., Simon, R., Tennstedt, P., Olabode, O., Nelson, M., Bathe, O., Carroll,

P.R., Chan, J.M., Disaia, P., Glenn, P., Kelley, R.K., Landen, C.N., Phillips, J., Prados, M., Simko, J., Smith-McCune, K., VandenBerg, S., Roggin, K., Fehrenbach, A., Kendler, A., Sifri, S., Steele, R., Jimeno, A., Carey, F., Forgie, I., Mannelli, M., Carney, M., Hernandez, B., Campos, B., Herold-Mende, C., Jungk, C., Unterberg, A., Deimling, A. von, Bossler, A., Galbraith, J., Jacobus, L., Knudson, M., Knutson, T., Ma, D., Milhem, M., Sigmund, R., Godwin, A.K., Madan, R., Rosenthal, H.G., Adebamowo, C., Adebamowo, S.N., Boussioutas, A., Beer, D., Giordano, T., Mes-Masson, A.-M., Saad, F., Bocklage, T., Landrum, L., Mannel, R., Moore, K., Moxley, K., Postier, R., Walker, J., Zuna, R., Feldman, M., Valdivieso, F., Dhir, R., Luketich, J., Pinero, E.M.M., Quintero-Aguilo, M., Carlotti, C.G., Santos, J.S.D., Kemp, R., Sankarankuty, A., Tirapelli, D., Catto, J., Agnew, K., Swisher, E., Creaney, J., Robinson, B., Shelley, C.S., Godwin, E.M., Kendall, S., Shipman, C., Bradford, C., Carey, T., Haddad, A., Moyer, J., Peterson, L., Prince, M., Rozek, L., Wolf, G., Bowman, R., Fong, K.M., Yang, I., Korst, R., Rathmell, W.K., Fantacone-Campbell, J.L., Hooke, J.A., Kovatich, A.J., Shriver, C.D., DiPersio, J., Drake, B., Govindan, R., Heath, S., Ley, T., Tine, B.V., Westervelt, P., Rubin, M.A., Lee, J.I., Aredes, N.D., Mariamidze, A., Stuart, J.M., Benz, C.C., Laird, P.W., 2018. Cell-of-Origin Patterns Dominate the Molecular Classification of 10,000 Tumors from 33 Types of Cancer. Cell 173, 291-304.e6. https://doi.org/10.1016/j.cell.2018.03.022

Houck, A.L., Seddighi, S., Driver, J.A., 2018. At the Crossroads Between Neurodegeneration and Cancer: A Review of Overlapping Biology and Its Implications. Curr Aging Sci 11, 77–89. https://doi.org/10.2174/1874609811666180223154436

Huang, E.J., Reichardt, L.F., 2001. Neurotrophins: Roles in Neuronal Development and Function. Annu Rev Neurosci 24, 677–736. https://doi.org/10.1146/annurev.neuro.24.1.677

Huang, L.-K., Chao, S.-P., Hu, C.-J., 2020. Clinical trials of new drugs for Alzheimer disease. J Biomed Sci 27, 18. https://doi.org/10.1186/s12929-019-0609-7

Huang, T.Y., Zhao, Y., Li, X., Wang, X., Tseng, I.-C., Thompson, R., Tu, S., Willnow, T.E., Zhang, Y., Xu, H., 2016. SNX27 and SORLA Interact to

Reduce Amyloidogenic Subcellular Distribution and Processing of Amyloid Precursor Protein. J Neurosci 36, 7996–8011. https://doi.org/10.1523/JNEUROSCI.0206-16.2016

Hunsberger, H.C., Pinky, P.D., Smith, W., Suppiramaniam, V., Reed, M.N., 2019. The role of APOE4 in Alzheimer's disease: strategies for future therapeutic interventions. Neuronal Signal 3, NS20180203. https://doi.org/10.1042/NS20180203

Igoucheva, O., Alexeev, V., Yoon, K., 2006. Differential cellular responses to exogenous DNA in mammalian cells and its effect on oligonucleotide-directed gene modification. Gene Ther 13, 266–275. https://doi.org/10.1038/sj.gt.3302643

Ikeuchi, T., Hirayama, S., Miida, T., Fukamachi, I., Tokutake, T., Ebinuma, H., Takubo, K., Kaneko, H., Kasuga, K., Kakita, A., Takahashi, H., Bujo, H., Saito, Y., Nishizawa, M., 2010. Increased levels of soluble LR11 in cerebrospinal fluid of patients with Alzheimer disease. Dement Geriatr Cogn Disord 30, 28–32. https://doi.org/10.1159/000315539

Irizarry, M.C., 2004. Biomarkers of Alzheimer Disease in Plasma. NeuroRx 1, 226–234.

Ishino, Y., Shinagawa, H., Makino, K., Amemura, M., Nakata, A., 1987. Nucleotide sequence of the iap gene, responsible for alkaline phosphatase isozyme conversion in Escherichia coli, and identification of the gene product. J Bacteriol 169, 5429–5433.

Jacobsen, L., Madsen, P., Jacobsen, C., Nielsen, M.S., Gliemann, J., Petersen, C.M., 2001. Activation and Functional Characterization of the Mosaic Receptor SorLA/LR11 *. Journal of Biological Chemistry 276, 22788–22796. https://doi.org/10.1074/jbc.M100857200

Jain, A.K., Barton, M.C., 2018. p53: emerging roles in stem cells, development and beyond. Development 145, dev158360. https://doi.org/10.1242/dev.158360

Jarosz-Griffiths, H.H., Noble, E., Rushworth, J.V., Hooper, N.M., 2016. Amyloid-β Receptors: The Good, the Bad, and the Prion Protein. J Biol Chem 291, 3174–3183. https://doi.org/10.1074/jbc.R115.702704

Jatoi, S., Hafeez, A., Riaz, S.U., Ali, A., Ghauri, M.I., Zehra, M., 2020. Low Vitamin B12 Levels: An Underestimated Cause Of Minimal Cognitive Impairment And Dementia. Cureus 12, e6976. https://doi.org/10.7759/cureus.6976

Jin, C., Liu, X., Zhang, Fuquan, Wu, Y., Yuan, J., Zhu, J., Zhang, Feng, Wang, G., Cheng, Z., 2013. An updated meta-analysis of the association between SORL1 variants and the risk for sporadic Alzheimer's disease. J Alzheimers Dis 37, 429–437. https://doi.org/10.3233/JAD-130533

Jin, W.-S., Bu, X.-L., Liu, Y.-H., Shen, L.-L., Zhuang, Z.-Q., Jiao, S.-S., Zhu, C., Wang, Q.-H., Zhou, H.-D., Zhang, T., Wang, Y.-J., 2017. Plasma Amyloid-Beta Levels in Patients with Different Types of Cancer. Neurotox Res 31, 283–288. https://doi.org/10.1007/s12640-016-9682-9

Jin, W.-S., Bu, X.-L., Liu, Y.-H., Shen, L.-L., Zhuang, Z.-Q., Jiao, S.-S., Zhu, C., Wang, Q.-H., Zhou, H.-D., Zhang, T., Wang, Y.-J., 2016. Plasma Amyloid-Beta Levels in Patients with Different Types of Cancer. Neurotox Res 31, 283–288. https://doi.org/10.1007/s12640-016-9682-9

Johnson, D.R., Fogh, S.E., Giannini, C., Kaufmann, T.J., Raghunathan, A., Theodosopoulos, P.V., Clarke, J.L., 2015. Case-Based Review: newly diagnosed glioblastoma. Neuro-Oncology Practice 2, 106–121. https://doi.org/10.1093/nop/npv020

Kagan, B.L., Jang, H., Capone, R., Arce, F.T., Ramachandran, S., Lal, R., Nussinov, R., 2012. Antimicrobial Properties of Amyloid Peptides. Mol Pharm 9, 708–717. https://doi.org/10.1021/mp200419b

Kamenetz, F., Tomita, T., Hsieh, H., Seabrook, G., Borchelt, D., Iwatsubo, T., Sisodia, S., Malinow, R., 2003. APP Processing and Synaptic Function. Neuron 37, 925–937. https://doi.org/10.1016/S0896-6273(03)00124-7

Kanderi, T., Gupta, V., 2023. Glioblastoma Multiforme, in: StatPearls. StatPearls Publishing, Treasure Island (FL).

Kanekiyo, T., Xu, H., Bu, G., 2014. ApoE and Aβ in Alzheimer's disease: accidental encounters or partners? Neuron 81, 740–754. https://doi.org/10.1016/j.neuron.2014.01.045

Kang, H.S., Kim, J.H., Lim, H., Kim, J.-H., Noh, H.-M., Choi, H.G., Min, K.-W., Kim, N.Y., Kwon, M.J., 2023. Alzheimer's Disease and Different Types of Cancer Likelihood: Unveiling Disparities and Potential Protective Effects in a Korean Cohort Study. Cancers (Basel) 15, 4615. https://doi.org/10.3390/cancers15184615

Kim, D.-H., Behlke, M.A., Rose, S.D., Chang, M.-S., Choi, S., Rossi, J.J., 2005. Synthetic dsRNA Dicer substrates enhance RNAi potency and efficacy. Nat Biotechnol 23, 222–226. https://doi.org/10.1038/nbt1051

Kirson, E.D., Gurvich, Z., Schneiderman, R., Dekel, E., Itzhaki, A., Wasserman, Y., Schatzberger, R., Palti, Y., 2004. Disruption of Cancer Cell Replication by Alternating Electric Fields. Cancer Research 64, 3288–3295. https://doi.org/10.1158/0008-5472.CAN-04-0083

Kleffman, K., Levinson, G., Rose, I.V.L., Blumenberg, L.M., Shadaloey, S.A.A., Dhabaria, A., Wong, E., Galán-Echevarría, F., Karz, A., Argibay, D., Von Itter, R., Floristán, A., Baptiste, G., Eskow, N.M., Tranos, J.A., Chen, J., Vega y Saenz de Miera, E.C., Call, M., Rogers, R., Jour, G., Wadghiri, Y.Z., Osman, I., Li, Y.-M., Mathews, P., DeMattos, R., Ueberheide, B., Ruggles, K.V., Liddelow, S.A., Schneider, R.J., Hernando, E., 2022. Melanoma-secreted Amyloid Beta Suppresses Neuroinflammation and Promotes Brain Metastasis. Cancer Discov 12, 1314–1335. https://doi.org/10.1158/2159-8290.CD-21-1006

Knupp, A., Mishra, S., Martinez, R., Braggin, J.E., Szabo, M., Kinoshita, C., Hailey, D.W., Small, S.A., Jayadev, S., Young, J.E., 2020. Depletion of the AD Risk Gene SORL1 Selectively Impairs Neuronal Endosomal Traffic Independent of Amyloidogenic APP Processing. Cell Rep 31, 107719. https://doi.org/10.1016/j.celrep.2020.107719

Koppensteiner, P., Trinchese, F., Fà, M., Puzzo, D., Gulisano, W., Yan, S., Poussin, A., Liu, S., Orozco, I., Dale, E., Teich, A.F., Palmeri, A., Ninan, I., Boehm, S., Arancio, O., 2016. Time-dependent reversal of synaptic plasticity induced by physiological concentrations of oligomeric Aβ42: an early index of Alzheimer's disease. Sci Rep 6, 32553. https://doi.org/10.1038/srep32553

Kucheryavykh, L.Y., Ortiz-Rivera, J., Kucheryavykh, Y.V., Zayas-Santiago, A., Diaz-Garcia, A., Inyushin, M.Y., 2019. Accumulation of Innate Amyloid Beta Peptide in Glioblastoma Tumors. Int J Mol Sci 20, 2482. https://doi.org/10.3390/ijms20102482

Kumar, A., Sidhu, J., Goyal, A., Tsao, J.W., 2023. Alzheimer Disease, in: StatPearls. StatPearls Publishing, Treasure Island (FL).

Kwak, D., Hammarström, L.G.J., Haraldsson, M., Ernfors, P., 2021. Glioblastoma cytotoxicity conferred through dual disruption of endolysosomal homeostasis by Vacquinol-1. Neuro-Oncology Advances 3, vdab152. https://doi.org/10.1093/noajnl/vdab152

Lam, J.K.W., Chow, M.Y.T., Zhang, Y., Leung, S.W.S., 2015. siRNA Versus miRNA as Therapeutics for Gene Silencing. Mol Ther Nucleic Acids 4, e252. https://doi.org/10.1038/mtna.2015.23

Lane-Donovan, C.E., Philips, G.T., Herz, J., 2014. More Than Cholesterol Transporters: Lipoprotein Receptors in CNS Function and Neurodegeneration. Neuron 83, 771–787. https://doi.org/10.1016/j.neuron.2014.08.005

Lannfelt, L., Relkin, N.R., Siemers, E.R., 2014. Amyloid-ß-directed immunotherapy for Alzheimer's disease. J Intern Med 275, 284–295. https://doi.org/10.1111/joim.12168

Lanni, C., Masi, M., Racchi, M., Govoni, S., 2021. Cancer and Alzheimer's disease inverse relationship: an age-associated diverging derailment of shared pathways. Mol Psychiatry 26, 280–295. https://doi.org/10.1038/s41380-020-0760-2

Le Joncour, V., Filppu, P., Hyvönen, M., Holopainen, M., Turunen, S.P., Sihto, H., Burghardt, I., Joensuu, H., Tynninen, O., Jääskeläinen, J., Weller, M., Lehti, K., Käkelä, R., Laakkonen, P., 2019. Vulnerability of invasive glioblastoma cells to lysosomal membrane destabilization. EMBO Mol Med 11, e9034. https://doi.org/10.15252/emmm.201809034

LeBlanc, A.C., Gambetti, P., 1994. Production of Alzheimer 4kDa beta-amyloid peptide requires the C-terminal cytosolic domain of the amyloid precursor protein. Biochem Biophys Res Commun 204, 1371–1380. https://doi.org/10.1006/bbrc.1994.2615

Lee, J.H., Barral, S., Reitz, C., 2008. The Neuronal Sortilin-Related Receptor Gene SORL1 and Late-Onset Alzheimer's Disease. Curr Neurol Neurosci Rep 8, 384–391.

Lehrer, S., 2010. Glioblastoma and dementia may share a common cause. Med Hypotheses 75, 67–68. https://doi.org/10.1016/j.mehy.2010.01.031

Lewczuk, P., Riederer, P., O'Bryant, S.E., Verbeek, M.M., Dubois, B., Visser, P.J., Jellinger, K.A., Engelborghs, S., Ramirez, A., Parnetti, L., Jack, C.R.,

Teunissen, C.E., Hampel, H., Lleó, A., Jessen, F., Glodzik, L., de Leon, M.J., Fagan, A.M., Molinuevo, J.L., Jansen, W.J., Winblad, B., Shaw, L.M., Andreasson, U., Otto, M., Mollenhauer, B., Wiltfang, J., Turner, M.R., Zerr, I., Handels, R., Thompson, A.G., Johansson, G., Ermann, N., Trojanowski, J.Q., Karaca, I., Wagner, H., Oeckl, P., van Waalwijk van Doorn, L., Bjerke, M., Kapogiannis, D., Kuiperij, H.B., Farotti, L., Li, Y., Gordon, B.A., Epelbaum, S., Vos, S.J.B., Klijn, C.J.M., Van Nostrand, W.E., Minguillon, C., Schmitz, M., Gallo, C., Lopez Mato, A., Thibaut, F., Lista, S., Alcolea, D., Zetterberg, H., Blennow, K., Kornhuber, J., Members of the WFSBP Task Force Working on this Topic: Peter Riederer, Carla Gallo, Dimitrios Kapogiannis, Andrea Lopez Mato, Florence Thibaut, 2018. Cerebrospinal fluid and blood biomarkers for neurodegenerative dementias: An update of the Consensus of the Task Force on Biological Markers in Psychiatry of the World Federation of Societies of Biological Psychiatry. World J Biol Psychiatry 19, 244–328. https://doi.org/10.1080/15622975.2017.1375556

Liappas, A., Mourouzis, I., Zisakis, A., Economou, K., Lea, R.-W., Pantos, C., 2011. Cell-type-dependent thyroid hormone effects on glioma tumor cell lines. J Thyroid Res 2011, 856050. https://doi.org/10.4061/2011/856050

Lichtenthaler, S.F., 2012. Alpha-secretase cleavage of the amyloid precursor protein: proteolysis regulated by signaling pathways and protein trafficking. Curr Alzheimer Res 9, 165–177. https://doi.org/10.2174/156720512799361655

Ling, L., Yuan, X., Liu, X., Pei, W., Li, R., 2021. A novel peptide promotes human trophoblast proliferation and migration through PI3K/Akt/mTOR signaling pathway. Annals of Translational Medicine 9, 981–981. https://doi.org/10.21037/atm-21-2574

Louis, D.N., Ohgaki, H., Wiestler, O.D., Cavenee, W.K., Burger, P.C., Jouvet, A., Scheithauer, B.W., Kleihues, P., 2007. The 2007 WHO classification of tumours of the central nervous system. Acta Neuropathol 114, 97–109. https://doi.org/10.1007/s00401-007-0243-4

Louis, D.N., Perry, A., Reifenberger, G., von Deimling, A., Figarella-Branger, D., Cavenee, W.K., Ohgaki, H., Wiestler, O.D., Kleihues, P., Ellison, D.W., 2016. The 2016 World Health Organization Classification of Tumors of the

Central Nervous System: a summary. Acta Neuropathol 131, 803–820. https://doi.org/10.1007/s00401-016-1545-1

Louis, D.N., Perry, A., Wesseling, P., Brat, D.J., Cree, I.A., Figarella-Branger, D., Hawkins, C., Ng, H.K., Pfister, S.M., Reifenberger, G., Soffietti, R., von Deimling, A., Ellison, D.W., 2021. The 2021 WHO Classification of Tumors of the Central Nervous System: a summary. Neuro Oncol 23, 1231–1251. https://doi.org/10.1093/neuonc/noab106

Lu, M., Zhang, Q., Deng, M., Miao, J., Guo, Y., Gao, W., Cui, Q., 2008. An Analysis of Human MicroRNA and Disease Associations. PLoS One 3, e3420. https://doi.org/10.1371/journal.pone.0003420

Luo, J., Wärmländer, S.K.T.S., Gräslund, A., Abrahams, J.P., 2016. Cross-interactions between the Alzheimer Disease Amyloid-β Peptide and Other Amyloid Proteins: A Further Aspect of the Amyloid Cascade Hypothesis. J Biol Chem 291, 16485–16493. https://doi.org/10.1074/jbc.R116.714576

Ma, Q.-L., Galasko, D.R., Ringman, J.M., Vinters, H.V., Edland, S.D., Pomakian, J., Ubeda, O.J., Rosario, E.R., Teter, B., Frautschy, S.A., Cole, G.M., 2009. Sorla/LR11, A Sorting Protein Limiting Abeta Production, Is Reduced In Alzheimer's Disease CSF. Arch Neurol 66, 448–457. https://doi.org/10.1001/archneurol.2009.22

Mahley, R.W., 1988. Apolipoprotein E: cholesterol transport protein with expanding role in cell biology. Science 240, 622–630. https://doi.org/10.1126/science.3283935

Mansouri, A., Hachem, L.D., Mansouri, S., Nassiri, F., Laperriere, N.J., Xia, D., Lindeman, N.I., Wen, P.Y., Chakravarti, A., Mehta, M.P., Hegi, M.E., Stupp, R., Aldape, K.D., Zadeh, G., 2019. MGMT promoter methylation status testing to guide therapy for glioblastoma: refining the approach based on emerging evidence and current challenges. Neuro Oncol 21, 167–178. https://doi.org/10.1093/neuonc/noy132

Maple-Grødem, J., Chung, J., Lunde, K.A., Tzoulis, C., Tysnes, O.-B., Pedersen, K.F., Alves, G., 2018. Alzheimer disease associated variants in SORL1 accelerate dementia development in Parkinson disease. Neuroscience Letters 674, 123–126. https://doi.org/10.1016/j.neulet.2018.03.036

Mayeux, R., Honig, L.S., Tang, M.-X., Manly, J., Stern, Y., Schupf, N., Mehta, P.D., 2003. Plasma A[beta]40 and A[beta]42 and Alzheimer's disease: relation to

age, mortality, and risk. Neurology 61, 1185–1190. https://doi.org/10.1212/01.wnl.0000091890.32140.8f

McCabe, C., Claxton, K., Culyer, A.J., 2008. The NICE cost-effectiveness threshold: what it is and what that means. Pharmacoeconomics 26, 733–744. https://doi.org/10.2165/00019053-200826090-00004

McDonald, P.C., Chafe, S.C., Dedhar, S., 2016. Overcoming Hypoxia-Mediated Tumor Progression: Combinatorial Approaches Targeting pH Regulation, Angiogenesis and Immune Dysfunction. Front Cell Dev Biol 4, 27. https://doi.org/10.3389/fcell.2016.00027

McNab, F., Mayer-Barber, K., Sher, A., Wack, A., O'Garra, A., 2015. Type I interferons in infectious disease. Nat Rev Immunol 15, 87–103. https://doi.org/10.1038/nri3787

Mehmedbasic, A., Christensen, S.K., Nilsson, J., Rüetschi, U., Gustafsen, C., Poulsen, A.S.A., Rasmussen, R.W., Fjorback, A.N., Larson, G., Andersen, O.M., 2015. SorLA Complement-type Repeat Domains Protect the Amyloid Precursor Protein against Processing*. Journal of Biological Chemistry 290, 3359–3376. https://doi.org/10.1074/jbc.M114.619940

Meng, J.Y., Kataoka, H., Itoh, H., Koono, M., 2001. Amyloid beta protein precursor is involved in the growth of human colon carcinoma cell in vitro and in vivo. Int J Cancer 92, 31–39.

Michael, I.P., Saghafinia, S., Hanahan, D., 2019. A set of microRNAs coordinately controls tumorigenesis, invasion, and metastasis. Proc Natl Acad Sci U S A 116, 24184–24195. https://doi.org/10.1073/pnas.1913307116

Milone, M.C., O'Doherty, U., 2018. Clinical use of lentiviral vectors. Leukemia 32, 1529–1541. https://doi.org/10.1038/s41375-018-0106-0

Montagne, A., Barnes, S.R., Sweeney, M.D., Halliday, M.R., Sagare, A.P., Zhao, Z., Toga, A.W., Jacobs, R.E., Liu, C.Y., Amezcua, L., Harrington, M.G., Chui, H.C., Law, M., Zlokovic, B.V., 2015. Blood-Brain Barrier Breakdown in the Aging Human Hippocampus. Neuron 85, 296–302. https://doi.org/10.1016/j.neuron.2014.12.032

Monti, G., Andersen, O.M., 2017. 20 Years Anniversary for SORLA/SORL1 (1996-2016). Receptor Clin Invest 4. https://doi.org/10.14800/rci.1611

Monti, G., Kjolby, M., Jensen, A.M.G., Allen, M., Reiche, J., Møller, P.L., Comaposada-Baró, R., Zolkowski, B.E., Vieira, C., Jørgensen, M.M., Holm,

I.E., Valdmanis, P.N., Wellner, N., Vægter, C.B., Lincoln, S.J., Nykjær, A., Ertekin-Taner, N., Young, J.E., Nyegaard, M., Andersen, O.M., 2021. Expression of an alternatively spliced variant of SORL1 in neuronal dendrites is decreased in patients with Alzheimer's disease. Acta Neuropathologica Communications 9, 43. https://doi.org/10.1186/s40478-021-01140-7

Montuori, N., Pesapane, A., Rossi, F.W., Giudice, V., De Paulis, A., Selleri, C., Ragno, P., 2016. Urokinase type plasminogen activator receptor (uPAR) as a new therapeutic target in cancer. Transl Med UniSa 15, 15–21.

Morato, E., Mayor, F., 1993. Production of the Alzheimer's beta-amyloid peptide by C6 glioma cells. FEBS Lett 336, 275–278. https://doi.org/10.1016/0014-5793(93)80819-g

Moreno, J.A.T., Lanau, A.V., Zapata, L.M., Pineda, A.Y.B., Hernandez, J.V., Nieto, O.C., Ospina, A.S., Marín, P.A., Rishishwar, L., Norris, E.T., Chande, A.T., Jordan, I.K., Berrio, G.B., 2022. Mutations in SORL1 and MTHFDL1 possibly contribute to the development of Alzheimer's disease in a multigenerational Colombian Family. PLOS ONE 17, e0269955. https://doi.org/10.1371/journal.pone.0269955

Morris, G.P., Clark, I.A., Vissel, B., 2014. Inconsistencies and Controversies Surrounding the Amyloid Hypothesis of Alzheimer's Disease. Acta Neuropathologica Communications 2, 135. https://doi.org/10.1186/s40478-014-0135-5

Motoi, Y., Aizawa, T., Haga, S., Nakamura, S., Namba, Y., Ikeda, K., 1999. Neuronal localization of a novel mosaic apolipoprotein E receptor, LR11, in rat and human brain. Brain Research 833, 209–215. https://doi.org/10.1016/S0006-8993(99)01542-5

Munir, H., Jones, J.O., Janowitz, T., Hoffmann, M., Euler, M., Martins, C.P., Welsh, S.J., Shields, J.D., 2021. Stromal-driven and Amyloid β-dependent induction of neutrophil extracellular traps modulates tumor growth. Nat Commun 12, 683. https://doi.org/10.1038/s41467-021-20982-2

Munter, L.-M., Voigt, P., Harmeier, A., Kaden, D., Gottschalk, K.E., Weise, C., Pipkorn, R., Schaefer, M., Langosch, D., Multhaup, G., 2007. GxxxG motifs within the amyloid precursor protein transmembrane sequence are critical

for the etiology of Aβ42. EMBO J 26, 1702–1712. https://doi.org/10.1038/sj.emboj.7601616

Murira, A., Lamarre, A., 2016. Type-I Interferon Responses: From Friend to Foe in the Battle against Chronic Viral Infection. Frontiers in Immunology 7.

Murphy, M.P., LeVine, H., 2010. Alzheimer's disease and the amyloid-beta peptide. J Alzheimers Dis 19, 311–323. https://doi.org/10.3233/JAD-2010-1221

Musicco, M., Adorni, F., Di Santo, S., Prinelli, F., Pettenati, C., Caltagirone, C., Palmer, K., Russo, A., 2013. Inverse occurrence of cancer and Alzheimer disease: a population-based incidence study. Neurology 81, 322–328. https://doi.org/10.1212/WNL.0b013e31829c5ec1

Musiek, E.S., Holtzman, D.M., 2015. Three dimensions of the amyloid hypothesis: time, space and "wingmen." Nat Neurosci 18, 800–806. https://doi.org/10.1038/nn.4018

Naghavi, M., Abajobir, A.A., Abbafati, C., Abbas, K.M., Abd-Allah, F., Abera, S.F., Aboyans, V., Adetokunboh, O., Afshin, A., Agrawal, A., Ahmadi, A., Ahmed, M.B., Aichour, A.N., Aichour, M.T.E., Aichour, I., Aiyar, S., Alahdab, F., Al-Aly, Z., Alam, K., Alam, N., Alam, T., Alene, K.A., Al-Eyadhy, A., Ali, S.D., Alizadeh-Navaei, R., Alkaabi, J.M., Alkerwi, A., Alla, F., Allebeck, P., Allen, C., Al-Raddadi, R., Alsharif, U., Altirkawi, K.A., Alvis-Guzman, N., Amare, A.T., Amini, E., Ammar, W., Amoako, Y.A., Anber, N., Andersen, H.H., Andrei, C.L., Androudi, S., Ansari, H., Antonio, C.A.T., Anwari, P., Ärnlöv, J., Arora, M., Artaman, A., Aryal, K.K., Asayesh, H., Asgedom, S.W., Atey, T.M., Avila-Burgos, L., Avokpaho, E.F.G., Awasthi, A., Babalola, T.K., Bacha, U., Balakrishnan, K., Barac, A., Barboza, M.A., Barker-Collo, S.L., Barquera, S., Barregard, L., Barrero, L.H., Baune, B.T., Bedi, N., Beghi, E., Béjot, Y., Bekele, B.B., Bell, M.L., Bennett, J.R., Bensenor, I.M., Berhane, A., Bernabé, E., Betsu, B.D., Beuran, M., Bhatt, S., Biadgilign, S., Bienhoff, K., Bikbov, B., Bisanzio, D., Bourne, R.R.A., Breitborde, N.J.K., Bulto, L.N.B., Bumgarner, B.R., Butt, Z.A., Cahuana-Hurtado, L., Cameron, E., Campuzano, J.C., Car, J., Cárdenas, R., Carrero, J.J., Carter, A., Casey, D.C., Castañeda-Orjuela, C.A., Catalá-López, F., Charlson, F.J., Chibueze, C.E., Chimed-Ochir, O., Chisumpa, V.H., Chitheer, A.A., Christopher, D.J., Ciobanu, L.G., Cirillo, M., Cohen, A.J., Colombara, D., Cooper, C., Cowie,

B.C., Criqui, M.H., Dandona, L., Dandona, R., Dargan, P.I., Das Neves, J., Davitoiu, D.V., Davletov, K., De Courten, B., Defo, B.K., Degenhardt, L., Deiparine, S., Deribe, K., Deribew, A., Dey, S., Dicker, D., Ding, E.L., Djalalinia, S., Do, H.P., Doku, D.T., Douwes-Schultz, D., Driscoll, T.R., Dubey, M., Duncan, B.B., Echko, M., El-Khatib, Z.Z., Ellingsen, C.L., Enayati, A., Ermakov, S.P., Erskine, H.E., Eskandarieh, S., Esteghamati, A., Estep, K., Farinha, C.S.E.S., Faro, A., Farzadfar, F., Feigin, V.L., Fereshtehnejad, S.-M., Fernandes, J.C., Ferrari, A.J., Feyissa, T.R., Filip, I., Finegold, S., Fischer, F., Fitzmaurice, C., Flaxman, A.D., Foigt, N., Frank, T., Fraser, M., Fullman, N., Fürst, T., Furtado, J.M., Gakidou, E., Garcia-Basteiro, A.L., Gebre, T., Gebregergs, G.B., Gebrehiwot, T.T., Gebremichael, D.Y., Geleijnse, J.M., Genova-Maleras, R., Gesesew, H.A., Gething, P.W., Gillum, R.F., Giref, A.Z., Giroud, M., Giussani, G., Godwin, W.W., Gold, A.L., Goldberg, E.M., Gona, P.N., Gopalani, S.V., Gouda, H.N., Goulart, A.C., Griswold, M., Gupta, R., Gupta, T., Gupta, V., Gupta, P.C., Haagsma, J.A., Hafezi-Nejad, N., Hailu, A.D., Hailu, G.B., Hamadeh, R.R., Hambisa, M.T., Hamidi, S., Hammami, M., Hancock, J., Handal, A.J., Hankey, G.J., Hao, Y., Harb, H.L., Hareri, H.A., Hassanvand, M.S., Havmoeller, R., Hay, S.I., He, F., Hedayati, M.T., Henry, N.J., Heredia-Pi, I.B., Herteliu, C., Hoek, H.W., Horino, M., Horita, N., Hosgood, H.D., Hostiuc, S., Hotez, P.J., Hoy, D.G., Huynh, C., Iburg, K.M., Ikeda, C., Ileanu, B.V., Irenso, A.A., Irvine, C.M.S., Islam, S.M.S., Jacobsen, K.H., Jahanmehr, N., Jakovljevic, M.B., Javanbakht, M., Jayaraman, S.P., Jeemon, P., Jha, V., John, D., Johnson, C.O., Johnson, S.C., Jonas, J.B., Jürisson, M., Kabir, Z., Kadel, R., Kahsay, A., Kamal, R., Karch, A., Karimi, S.M., Karimkhani, C., Kasaeian, A., Kassaw, N.A., Kassebaum, N.J., Katikireddi, S.V., Kawakami, N., Keiyoro, P.N., Kemmer, L., Kesavachandran, C.N., Khader, Y.S., Khan, E.A., Khang, Y.-H., Khoja, A.T.A., Khosravi, M.H., Khosravi, A., Khubchandani, J., Kiadaliri, A.A., Kieling, C., Kievlan, D., Kim, Y.J., Kim, D., Kimokoti, R.W., Kinfu, Y., Kissoon, N., Kivimaki, M., Knudsen, A.K., Kopec, J.A., Kosen, S., Koul, P.A., Koyanagi, A., Kulikoff, X.R., Kumar, G.A., Kumar, P., Kutz, M., Kyu, H.H., Lal, D.K., Lalloo, R., Lambert, T.L.N., Lan, Q., Lansingh, V.C., Larsson, A., Lee, P.H., Leigh, J., Leung, J., Levi, M., Li, Y., Li Kappe, D.,

Liang, X., Liben, M.L., Lim, S.S., Liu, P.Y., Liu, A., Liu, Y., Lodha, R., Logroscino, G., Lorkowski, S., Lotufo, P.A., Lozano, R., Lucas, T.C.D., Ma, S., Macarayan, E.R.K., Maddison, E.R., Magdy Abd El Razek, M., Majdan, M., Majdzadeh, R., Majeed, A., Malekzadeh, R., Malhotra, R., Malta, D.C., Manguerra, H., Manyazewal, T., Mapoma, C.C., Marczak, L.B., Markos, D., Martinez-Raga, J., Martins-Melo, F.R., Martopullo, I., McAlinden, C., McGaughey, M., McGrath, J.J., Mehata, S., Meier, T., Meles, K.G., Memiah, P., Memish, Z.A., Mengesha, M.M., Mengistu, D.T., Menota, B.G., Mensah, G.A., Meretoja, T.J., Meretoja, A., Millear, A., Miller, T.R., Minnig, S., Mirarefin, M., Mirrakhimov, E.M., Misganaw, A., Mishra, S.R., Mohamed, I.A., Mohammad, K.A., Mohammadi, A., Mohammed, S., Mokdad, A.H., Mola, G.L.D., Mollenkopf, S.K., Molokhia, M., Monasta, L., Montañez, J.C., Montico, M., Mooney, M.D., Moradi-Lakeh, M., Moraga, P., Morawska, L., Morozoff, C., Morrison, S.D., Mountjoy-Venning, C., Mruts, K.B., Muller, K., Murthy, G.V.S., Musa, K.I., Nachega, J.B., Naheed, A., Naldi, L., Nangia, V., Nascimento, B.R., Nasher, J.T., Natarajan, G., Negoi, I., Ngunjiri, J.W., Nguyen, C.T., Nguyen, Q.L., Nguyen, T.H., Nguyen, G., Nguyen, M., Nichols, E., Ningrum, D.N.A., Nong, V.M., Noubiap, J.J.N., Ogbo, F.A., Oh, I.-H., Okoro, A., Olagunju, A.T., Olsen, H.E., Olusanya, B.O., Olusanya, J.O., Ong, K., Opio, J.N., Oren, E., Ortiz, A., Osman, M., Ota, E., Pa, M., Pacella, R.E., Pakhale, S., Pana, A., Panda, B.K., Panda-Jonas, S., Papachristou, C., Park, E.-K., Patten, S.B., Patton, G.C., Paudel, D., Paulson, K., Pereira, D.M., Perez-Ruiz, F., Perico, N., Pervaiz, A., Petzold, M., Phillips, M.R., Pigott, D.M., Pinho, C., Plass, D., Pletcher, M.A., Polinder, S., Postma, M.J., Pourmalek, F., Purcell, C., Qorbani, M., Quintanilla, B.P.A., Radfar, A., Rafay, A., Rahimi-Movaghar, V., Rahman, M.H.U., Rahman, M., Rai, R.K., Ranabhat, C.L., Rankin, Z., Rao, P.C., Rath, G.K., Rawaf, S., Ray, S.E., Rehm, J., Reiner, R.C., Reitsma, M.B., Remuzzi, G., Rezaei, S., Rezai, M.S., Rokni, M.B., Ronfani, L., Roshandel, G., Roth, G.A., Rothenbacher, D., Ruhago, G.M., Sa, R., Saadat, S., Sachdev, P.S., Sadat, N., Safdarian, M., Safi, S., Safiri, S., Sagar, R., Sahathevan, R., Salama, J., Salamati, P., Salomon, J.A., Samy, A.M., Sanabria, J.R., Sanchez-Niño, M.D., Santomauro, D., Santos, I.S., Santric Milicevic, M.M., Sartorius, B., Satpathy, M., Schmidt, M.I., Schneider, I.J.C.,

Schulhofer-Wohl, S., Schutte, A.E., Schwebel, D.C., Schwendicke, F., Sepanlou, S.G., Servan-Mori, E.E., Shackelford, K.A., Shahraz, S., Shaikh, M.A., Shamsipour, M., Shamsizadeh, M., Sharma, J., Sharma, R., She, J., Sheikhbahaei, S., Shey, M., Shi, P., Shields, C., Shigematsu, M., Shiri, R., Shirude, S., Shiue, I., Shoman, H., Shrime, M.G., Sigfusdottir, I.D., Silpakit, N., Silva, J.P., Singh, J.A., Singh, A., Skiadaresi, E., Sligar, A., Smith, D.L., Smith, A., Smith, M., Sobaih, B.H.A., Soneji, S., Sorensen, R.J.D., Soriano, J.B., Sreeramareddy, C.T., Srinivasan, V., Stanaway, J.D., Stathopoulou, V., Steel, N., Stein, D.J., Steiner, C., Steinke, S., Stokes, M.A., Strong, M., Strub, B., Subart, M., Sufiyan, M.B., Sunguya, B.F., Sur, P.J., Swaminathan, S., Sykes, B.L., Tabarés-Seisdedos, R., Tadakamadla, S.K., Takahashi, K., Takala, J.S., Talongwa, R.T., Tarawneh, M.R., Tavakkoli, M., Taveira, N., Tegegne, T.K., Tehrani-Banihashemi, A., Temsah, M.-H., Terkawi, A.S., Thakur, J.S., Thamsuwan, O., Thankappan, K.R., Thomas, K.E., Thompson, A.H., Thomson, A.J., Thrift, A.G., Tobe-Gai, R., Topor-Madry, R., Torre, A., Tortajada, M., Towbin, J.A., Tran, B.X., Troeger, C., Truelsen, T., Tsoi, D., Tuzcu, E.M., Tyrovolas, S., Ukwaja, K.N., Undurraga, E.A., Updike, R., Uthman, O.A., Uzochukwu, B.S.C., Van Boven, J.F.M., Vasankari, T., Venketasubramanian, N., Violante, F.S., Vlassov, V.V., Vollset, S.E., Vos, T., Wakayo, T., Wallin, M.T., Wang, Y.-P., Weiderpass, E., Weintraub, R.G., Weiss, D.J., Werdecker, A., Westerman, R., Whetter, B., Whiteford, H.A., Wijeratne, T., Wiysonge, C.S., Woldeyes, B.G., Wolfe, C.D.A., Woodbrook, R., Workicho, A., Xavier, D., Xiao, Q., Xu, G., Yaghoubi, M., Yakob, B., Yano, Y., Yaseri, M., Yimam, H.H., Yonemoto, N., Yoon, S.-J., Yotebieng, M., Younis, M.Z., Zaidi, Z., Zaki, M.E.S., Zegeye, E.A., Zenebe, Z.M., Zerfu, T.A., Zhang, A.L., Zhang, X., Zipkin, B., Zodpey, S., Lopez, A.D., Murray, C.J.L., 2017. Global, regional, and national age-sex specific mortality for 264 causes of death, 1980–2016: a systematic analysis for the Global Burden of Disease Study 2016. The Lancet 390, 1151–1210. https://doi.org/10.1016/S0140-6736(17)32152-9

Napoli, C., Lemieux, C., Jorgensen, R., 1990. Introduction of a Chimeric Chalcone Synthase Gene into Petunia Results in Reversible Co-Suppression of Homologous Genes in trans. Plant Cell 2, 279–289. https://doi.org/10.1105/tpc.2.4.279

Nelson, J.S., 2002. Alzheimer pathology in elderly patients with glioblastoma multiforme. Arch Pathol Lab Med 126, 1515–1517. https://doi.org/10.5858/2002-126-1515-APIEPW

Nelson, T.J., Xu, Y., 2023. Sting and p53 DNA repair pathways are compromised in Alzheimer's disease. Sci Rep 13, 8304. https://doi.org/10.1038/s41598-023-35533-6

Nicolas, Gaël, Charbonnier, C., Campion, D., 2016. From Common to Rare Variants: The Genetic Component of Alzheimer Disease. Hum Hered 81, 129–141. https://doi.org/10.1159/000452256

Nicolas, G., Charbonnier, C., Wallon, D., Quenez, O., Bellenguez, C., Grenier-Boley, B., Rousseau, S., Richard, A.-C., Rovelet-Lecrux, A., Le Guennec, K., Bacq, D., Garnier, J.-G., Olaso, R., Boland, A., Meyer, V., Deleuze, J.-F., Amouyel, P., Munter, H.M., Bourque, G., Lathrop, M., Frebourg, T., Redon, R., Letenneur, L., Dartigues, J.-F., Génin, E., Lambert, J.-C., Hannequin, D., Campion, D., 2016. SORL1 rare variants: a major risk factor for familial early-onset Alzheimer's disease. Mol Psychiatry 21, 831–836. https://doi.org/10.1038/mp.2015.121

Nielsen, M.S., Gustafsen, C., Madsen, P., Nyengaard, J.R., Hermey, G., Bakke, O., Mari, M., Schu, P., Pohlmann, R., Dennes, A., Petersen, C.M., 2007. Sorting by the Cytoplasmic Domain of the Amyloid Precursor Protein Binding Receptor SorLA. Mol Cell Biol 27, 6842–6851. https://doi.org/10.1128/MCB.00815-07

Nikolaev, A., McLaughlin, T., O'Leary, D., Tessier-Lavigne, M., 2009. N-APP binds DR6 to cause axon pruning and neuron death via distinct caspases. Nature 457, 981–989. https://doi.org/10.1038/nature07767

O'Brien, R.J., Wong, P.C., 2011. Amyloid precursor protein processing and Alzheimer's disease. Annu Rev Neurosci 34, 185–204. https://doi.org/10.1146/annurev-neuro-061010-113613

Offe, K., Dodson, S.E., Shoemaker, J.T., Fritz, J.J., Gearing, M., Levey, A.I., Lah, J.J., 2006. The Lipoprotein Receptor LR11 Regulates Amyloid β Production and Amyloid Precursor Protein Traffic in Endosomal Compartments. J Neurosci 26, 1596–1603. https://doi.org/10.1523/JNEUROSCI.4946-05.2006

O'Reilly, S.M., Newlands, E.S., Glaser, M.G., Brampton, M., Rice-Edwards, J.M., Illingworth, R.D., Richards, P.G., Kennard, C., Colquhoun, I.R., Lewis, P., 1993. Temozolomide: a new oral cytotoxic chemotherapeutic agent with promising activity against primary brain tumours. Eur J Cancer 29A, 940–942. https://doi.org/10.1016/s0959-8049(05)80198-4

Ostrom, Q.T., Bauchet, L., Davis, F.G., Deltour, I., Fisher, J.L., Langer, C.E., Pekmezci, M., Schwartzbaum, J.A., Turner, M.C., Walsh, K.M., Wrensch, M.R., Barnholtz-Sloan, J.S., 2014. The epidemiology of glioma in adults: a "state of the science" review. Neuro Oncol 16, 896–913. https://doi.org/10.1093/neuonc/nou087

Ou, S.-M., Lee, Y.-J., Hu, Y.-W., Liu, C.-J., Chen, T.-J., Fuh, J.-L., Wang, S.-J., 2013. Does Alzheimer's disease protect against cancers? A nationwide population-based study. Neuroepidemiology 40, 42–49. https://doi.org/10.1159/000341411

Pan, C., Kumar, C., Bohl, S., Klingmueller, U., Mann, M., 2009. Comparative Proteomic Phenotyping of Cell Lines and Primary Cells to Assess Preservation of Cell Type-specific Functions. Mol Cell Proteomics 8, 443–450. https://doi.org/10.1074/mcp.M800258-MCP200

Pan, E., Prados, M.D., 2003. Glioblastoma Multiforme and Anaplastic Astrocytoma, in: Holland-Frei Cancer Medicine. 6th Edition. BC Decker.

Paris, D., Ganey, N., Banasiak, M., Laporte, V., Patel, N., Mullan, Myles, Murphy, S.F., Yee, G.-T., Bachmeier, C., Ganey, C., Beaulieu-Abdelahad, D., Mathura, V.S., Brem, S., Mullan, Michael, 2010a. Impaired Orthotopic Glioma Growth and Vascularization in Transgenic Mouse Models of Alzheimer's Disease. J. Neurosci. 30, 11251–11258. https://doi.org/10.1523/JNEUROSCI.2586-10.2010

Paris, D., Patel, N., Ganey, N.J., Laporte, V., Quadros, A., Mullan, M.J., 2010b. Anti-Tumoral Activity of a Short Decapeptide Fragment of the Alzheimer's Aβ Peptide. Int J Pept Res Ther 16, 23–30. https://doi.org/10.1007/s10989-010-9198-8

Paris, D., Townsend, K., Quadros, A., Humphrey, J., Sun, J., Brem, S., Wotoczek-Obadia, M., DelleDonne, A., Patel, N., Obregon, D.F., Crescentini, R., Abdullah, L., Coppola, D., Rojiani, A.M., Crawford, F., Sebti, S.M., Mullan,

M., 2004. Inhibition of angiogenesis by Abeta peptides. Angiogenesis 7, 75–85. https://doi.org/10.1023/B:AGEN.0000037335.17717.bf

Park, Y.W., Vollmuth, P., Foltyn-Dumitru, M., Sahm, F., Ahn, S.S., Chang, J.H., Kim, S.H., 2023. The 2021 WHO Classification for Gliomas and Implications on Imaging Diagnosis: Part 1—Key Points of the Fifth Edition and Summary of Imaging Findings on Adult-Type Diffuse Gliomas. Journal of Magnetic Resonance Imaging 58, 677–689. https://doi.org/10.1002/jmri.28743

Pavliukeviciene, B., Zentelyte, A., Jankunec, M., Valiuliene, G., Talaikis, M., Navakauskiene, R., Niaura, G., Valincius, G., 2019. Amyloid β oligomers inhibit growth of human cancer cells. PLoS One 14, e0221563. https://doi.org/10.1371/journal.pone.0221563

Pedrero-Prieto, C.M., Flores-Cuadrado, A., Saiz-Sánchez, D., Úbeda-Bañón, I., Frontiñán-Rubio, J., Alcaín, F.J., Mateos-Hernández, L., de la Fuente, J., Durán-Prado, M., Villar, M., Martínez-Marcos, A., Peinado, J.R., 2019. Human amyloid-β enriched extracts: evaluation of in vitro and in vivo internalization and molecular characterization. Alzheimer's Research & Therapy 11, 56. https://doi.org/10.1186/s13195-019-0513-0

Penninkilampi, R., Brothers, H.M., Eslick, G.D., 2016. Pharmacological Agents Targeting γ-Secretase Increase Risk of Cancer and Cognitive Decline in Alzheimer's Disease Patients: A Systematic Review and Meta-Analysis. J Alzheimers Dis 53, 1395–1404. https://doi.org/10.3233/JAD-160275

Perl, D.P., 2010. Neuropathology of Alzheimer's disease. Mt Sinai J Med 77, 32–42. https://doi.org/10.1002/msj.20157

Perry, J., Zinman, L., Chambers, A., Spithoff, K., Lloyd, N., Laperriere, N., 2006. The use of prophylactic anticonvulsants in patients with brain tumours—a systematic review. Curr Oncol 13, 222–229.

Petersen, N.H.T., Olsen, O.D., Groth-Pedersen, L., Ellegaard, A.-M., Bilgin, M., Redmer, S., Ostenfeld, M.S., Ulanet, D., Dovmark, T.H., Lønborg, A., Vindeløv, S.D., Hanahan, D., Arenz, C., Ejsing, C.S., Kirkegaard, T., Rohde, M., Nylandsted, J., Jäättelä, M., 2013. Transformation-associated changes in sphingolipid metabolism sensitize cells to lysosomal cell death induced by inhibitors of acid sphingomyelinase. Cancer Cell 24, 379–393. https://doi.org/10.1016/j.ccr.2013.08.003

Pietilä, M., Sahgal, P., Peuhu, E., Jäntti, N.Z., Paatero, I., Närvä, E., Al-Akhrass, H., Lilja, J., Georgiadou, M., Andersen, O.M., Padzik, A., Sihto, H., Joensuu, H., Blomqvist, M., Saarinen, I., Boström, P.J., Taimen, P., Ivaska, J., 2019. SORLA regulates endosomal trafficking and oncogenic fitness of HER2. Nat Commun 10, 2340. https://doi.org/10.1038/s41467-019-10275-0

Plun-Favreau, H., Lewis, P.A., Hardy, J., Martins, L.M., Wood, N.W., 2010. Cancer and Neurodegeneration: Between the Devil and the Deep Blue Sea. PLoS Genet 6, e1001257. https://doi.org/10.1371/journal.pgen.1001257

Pomara, N., Willoughby, L.M., Sidtis, J.J., Mehta, P.D., 2005. Selective reductions in plasma Abeta 1-42 in healthy elderly subjects during longitudinal follow-up: a preliminary report. Am J Geriatr Psychiatry 13, 914–917. https://doi.org/10.1176/appi.ajgp.13.10.914

Portelius, E., Mattsson, N., Andreasson, U., Blennow, K., Zetterberg, H., 2011. Novel aβ isoforms in Alzheimer's disease - their role in diagnosis and treatment. Curr Pharm Des 17, 2594–2602. https://doi.org/10.2174/138161211797416039

Puig, K.L., Combs, C.K., 2013. Expression and Function of APP and its Metabolites Outside the Central Nervous System. Exp Gerontol 48, 608–611. https://doi.org/10.1016/j.exger.2012.07.009

Puig, K.L., Swigost, A.J., Zhou, X., Sens, M.A., Combs, C.K., 2012. Amyloid precursor protein expression modulates intestine immune phenotype. J Neuroimmune Pharmacol 7, 215–230. https://doi.org/10.1007/s11481-011-9327-y

Puzzo, D., Arancio, O., 2013. Amyloid-β peptide: Dr. Jekyll or Mr. Hyde? J Alzheimers Dis 33 Suppl 1, S111-120. https://doi.org/10.3233/JAD-2012-129033

Puzzo, D., Gulisano, W., Arancio, O., Palmeri, A., 2015. THE KEYSTONE OF ALZHEIMER PATHOGENESIS MIGHT BE SOUGHT IN Aβ PHYSIOLOGY. Neuroscience 307, 26–36. https://doi.org/10.1016/j.neuroscience.2015.08.039

Puzzo, D., Privitera, L., Leznik, E., Fà, M., Staniszewski, A., Palmeri, A., Arancio, O., 2008. Picomolar Amyloid-β Positively Modulates Synaptic Plasticity and Memory in Hippocampus. J Neurosci 28, 14537–14545. https://doi.org/10.1523/JNEUROSCI.2692-08.2008

Puzzo, D., Privitera, L., Palmeri, A., 2012. Hormetic effect of amyloid-β peptide in synaptic plasticity and memory. Neurobiol Aging 33, 1484.e15–24. https://doi.org/10.1016/j.neurobiolaging.2011.12.020

Raghavan, N.S., Brickman, A.M., Andrews, H., Manly, J.J., Schupf, N., Lantigua, R., Wolock, C.J., Kamalakaran, S., Petrovski, S., Tosto, G., Vardarajan, B.N., Goldstein, D.B., Mayeux, R., 2018. Whole-exome sequencing in 20,197 persons for rare variants in Alzheimer's disease. Ann Clin Transl Neurol 5, 832–842. https://doi.org/10.1002/acn3.582

Rajendran, L., Honsho, M., Zahn, T.R., Keller, P., Geiger, K.D., Verkade, P., Simons, K., 2006. Alzheimer's disease beta-amyloid peptides are released in association with exosomes. Proc Natl Acad Sci U S A 103, 11172–11177. https://doi.org/10.1073/pnas.0603838103

Rao, D.D., Vorhies, J.S., Senzer, N., Nemunaitis, J., 2009. siRNA vs. shRNA: Similarities and differences. Advanced Drug Delivery Reviews, Towards Therapeutic Application of RNA-Mediated Gene Regulation 61, 746–759. https://doi.org/10.1016/j.addr.2009.04.004

Reitz, C., Cheng, R., Rogaeva, E., Lee, J.H., Tokuhiro, S., Zou, F., Bettens, K., Sleegers, K., Tan, E.K., Kimura, R., Shibata, N., Arai, H., Kamboh, M.I., Prince, J.A., Maier, W., Riemenschneider, M., Owen, M., Harold, D., Hollingworth, P., Cellini, E., Sorbi, S., Nacmias, B., Takeda, M., Pericak-Vance, M.A., Haines, J.L., Younkin, S., Williams, J., van Broeckhoven, C., Farrer, L.A., St George–Hyslop, P.H., Mayeux, R., 2011. Meta-analysis of the Association Between Variants in SORL1 and Alzheimer Disease. Arch Neurol 68, 99–106. https://doi.org/10.1001/archneurol.2010.346

Ricciarelli, R., Fedele, E., 2017. The Amyloid Cascade Hypothesis in Alzheimer's Disease: It's Time to Change Our Mind. Curr Neuropharmacol 15, 926–935. https://doi.org/10.2174/1570159X15666170116143743

Robinson, S.R., Bishop, G.M., 2002. Aβ as a bioflocculant: implications for the amyloid hypothesis of Alzheimer's disease. Neurobiology of Aging 23, 1051–1072. https://doi.org/10.1016/S0197-4580(01)00342-6

Roe, C.M., Behrens, M.I., Xiong, C., Miller, J.P., Morris, J.C., 2005. Alzheimer disease and cancer. Neurology 64, 895–898. https://doi.org/10.1212/01.WNL.0000152889.94785.51

Roe, C.M., Fitzpatrick, A.L., Xiong, C., Sieh, W., Kuller, L., Miller, J.P., Williams, M.M., Kopan, R., Behrens, M.I., Morris, J.C., 2010. Cancer linked to Alzheimer disease but not vascular dementia. Neurology 74, 106–112. https://doi.org/10.1212/WNL.0b013e3181c91873

Rogaeva, E., Meng, Y., Lee, J.H., Gu, Y., Kawarai, T., Zou, F., Katayama, T., Baldwin, C.T., Cheng, R., Hasegawa, H., Chen, F., Shibata, N., Lunetta, K.L., Pardossi-Piquard, R., Bohm, C., Wakutani, Y., Cupples, L.A., Cuenco, K.T., Green, R.C., Pinessi, L., Rainero, I., Sorbi, S., Bruni, A., Duara, R., Friedland, R.P., Inzelberg, R., Hampe, W., Bujo, H., Song, Y.-Q., Andersen, O.M., Willnow, T.E., Graff-Radford, N., Petersen, R.C., Dickson, D., Der, S.D., Fraser, P.E., Schmitt-Ulms, G., Younkin, S., Mayeux, R., Farrer, L.A., St George-Hyslop, P., 2007. The neuronal sortilin-related receptor SORL1 is genetically associated with Alzheimer disease. Nat Genet 39, 168–177. https://doi.org/10.1038/ng1943

Rohe, M., Carlo, A.-S., Breyhan, H., Sporbert, A., Militz, D., Schmidt, V., Wozny, C., Harmeier, A., Erdmann, B., Bales, K.R., Wolf, S., Kempermann, G., Paul, S.M., Schmitz, D., Bayer, T.A., Willnow, T.E., Andersen, O.M., 2008. Sortilin-related receptor with A-type repeats (SORLA) affects the amyloid precursor protein-dependent stimulation of ERK signaling and adult neurogenesis. J Biol Chem 283, 14826–14834. https://doi.org/10.1074/jbc.M710574200

Rohe, M., Synowitz, M., Glass, R., Paul, S.M., Nykjaer, A., Willnow, T.E., 2009. Brain-Derived Neurotrophic Factor Reduces Amyloidogenic Processing through Control of SORLA Gene Expression. The Journal of Neuroscience 29, 15472. https://doi.org/10.1523/JNEUROSCI.3960-09.2009

Rominiyi, O., Vanderlinden, A., Clenton, S.J., Bridgewater, C., Al-Tamimi, Y., Collis, S.J., 2021. Tumour treating fields therapy for glioblastoma: current advances and future directions. Br J Cancer 124, 697–709. https://doi.org/10.1038/s41416-020-01136-5

Rovelet-Lecrux, A., Feuillette, S., Miguel, L., Schramm, C., Pernet, S., Quenez, O., Ségalas-Milazzo, I., Guilhaudis, L., Rousseau, S., Riou, G., Frébourg, T., Campion, D., Nicolas, G., Lecourtois, M., 2021. Impaired SorLA maturation and trafficking as a new mechanism for SORL1 missense variants in

Alzheimer disease. Acta Neuropathologica Communications 9, 196. https://doi.org/10.1186/s40478-021-01294-4

Sabbagh, M.N., Lue, L.-F., Fayard, D., Shi, J., 2017. Increasing Precision of Clinical Diagnosis of Alzheimer's Disease Using a Combined Algorithm Incorporating Clinical and Novel Biomarker Data. Neurol Ther 6, 83–95. https://doi.org/10.1007/s40120-017-0069-5

Sakai, S., Nakaseko, C., Takeuchi, M., Ohwada, C., Shimizu, N., Tsukamoto, S., Kawaguchi, T., Jiang, M., Sato, Y., Ebinuma, H., Yokote, K., Iwama, A., Fukamachi, I., Schneider, W.J., Saito, Y., Bujo, H., 2012. Circulating soluble LR11/SorLA levels are highly increased and ameliorated by chemotherapy in acute leukemias. Clin Chim Acta 413, 1542–1548. https://doi.org/10.1016/j.cca.2012.06.025

Sánchez-Valle, J., Tejero, H., Ibáñez, K., Portero, J.L., Krallinger, M., Al-Shahrour, F., Tabarés-Seisdedos, R., Baudot, A., Valencia, A., 2017. A molecular hypothesis to explain direct and inverse co-morbidities between Alzheimer's Disease, Glioblastoma and Lung cancer. Sci Rep 7, 4474. https://doi.org/10.1038/s41598-017-04400-6

Sandebring, A., Welander, H., Winblad, B., Graff, C., Tjernberg, L.O., 2013. The Pathogenic Aβ43 Is Enriched in Familial and Sporadic Alzheimer Disease. PLoS ONE 8, e55847. https://doi.org/10.1371/journal.pone.0055847

Scheuermann, S., Hambsch, B., Hesse, L., Stumm, J., Schmidt, C., Beher, D., Bayer, T.A., Beyreuther, K., Multhaup, G., 2001. Homodimerization of amyloid precursor protein and its implication in the amyloidogenic pathway of Alzheimer's disease. J Biol Chem 276, 33923–33929. https://doi.org/10.1074/jbc.M105410200

Schiff, D., Lee, E.Q., Nayak, L., Norden, A.D., Reardon, D.A., Wen, P.Y., 2015. Medical management of brain tumors and the sequelae of treatment. Neuro Oncol 17, 488–504. https://doi.org/10.1093/neuonc/nou304

Schmidt, S.D., Mazzella, M.J., Nixon, R.A., Mathews, P.M., 2012. Aβ Measurement by Enzyme-Linked Immunosorbent Assay, in: Sigurdsson, E.M., Calero, M., Gasset, M. (Eds.), Amyloid Proteins: Methods and Protocols, Methods in Molecular Biology. Humana Press, Totowa, NJ, pp. 507–527. https://doi.org/10.1007/978-1-61779-551-0_34

Schmidt, V., Baum, K., Lao, A., Rateitschak, K., Schmitz, Y., Teichmann, A., Wiesner, B., Petersen, C.M., Nykjaer, A., Wolf, J., Wolkenhauer, O., Willnow, T.E., 2012. Quantitative modelling of amyloidogenic processing and its influence by SORLA in Alzheimer's disease. EMBO J 31, 187–200. https://doi.org/10.1038/emboj.2011.352

Schmidt, V., Sporbert, A., Rohe, M., Reimer, T., Rehm, A., Andersen, O.M., Willnow, T.E., 2007. SorLA/LR11 Regulates Processing of Amyloid Precursor Protein via Interaction with Adaptors GGA and PACS-1*. Journal of Biological Chemistry 282, 32956–32964. https://doi.org/10.1074/jbc.M705073200

Schmidt, V., Subkhangulova, A., Willnow, T.E., 2017. Sorting receptor SORLA: cellular mechanisms and implications for disease. Cell Mol Life Sci 74, 1475–1483. https://doi.org/10.1007/s00018-016-2410-z

Selkoe, Dennis J, Hardy, J., 2016. The amyloid hypothesis of Alzheimer's disease at 25 years. EMBO Mol Med 8, 595–608. https://doi.org/10.15252/emmm.201606210

Sharma, N., Singh, A.N., 2016. Exploring Biomarkers for Alzheimer's Disease. J Clin Diagn Res 10, KE01–KE06. https://doi.org/10.7860/JCDR/2016/18828.8166

Shimizu, N., Nakaseko, C., Takeuchi, M., Ohwada, C., Tsukamoto, S., Kawaguchi, T., Nishii, K., Jiang, M., Yokote, K., Fukamachi, I., Bujo, H., 2011. Soluble LR11/SorLA, a Potential Circulating Marker Indicating the G-CSF-Induced Mobilization of Hematopoietic Stem Cells, Is a Modulator of G-CSF-Mediated Migration of HL-60 Cells,. Blood 118, 3210. https://doi.org/10.1182/blood.V118.21.3210.3210

Simoes, S., Neufeld, J.L., Triana-Baltzer, G., Moughadam, S., Chen, E.I., Kothiya, M., Qureshi, Y.H., Patel, V., Honig, L.S., Kolb, H., Small, S.A., 2020. Tau and other proteins found in Alzheimer's disease spinal fluid are linked to retromer-mediated endosomal traffic in mice and humans. Sci Transl Med 12, eaba6334. https://doi.org/10.1126/scitranslmed.aba6334

Singh, N., Miner, A., Hennis, L., Mittal, S., 2021. Mechanisms of temozolomide resistance in glioblastoma - a comprehensive review. Cancer Drug Resist 4, 17–43. https://doi.org/10.20517/cdr.2020.79

Spitzer, P., Herrmann, M., Klafki, H.-W., Smirnov, A., Lewczuk, P., Kornhuber, J., Wiltfang, J., Maler, J.M., 2010. Phagocytosis and LPS alter the maturation state of β-amyloid precursor protein and induce different Aβ peptide release signatures in human mononuclear phagocytes. J Neuroinflammation 7, 59. https://doi.org/10.1186/1742-2094-7-59

Steinberg, S., Stefansson, H., Jonsson, T., Johannsdottir, H., Ingason, A., Helgason, H., Sulem, P., Magnusson, O.T., Gudjonsson, S.A., Unnsteinsdottir, U., Kong, A., Helisalmi, S., Soininen, H., Lah, J.J., Aarsland, D., Fladby, T., Ulstein, I.D., Djurovic, S., Sando, S.B., White, L.R., Knudsen, G.-P., Westlye, L.T., Selbæk, G., Giegling, I., Hampel, H., Hiltunen, M., Levey, A.I., Andreassen, O.A., Rujescu, D., Jonsson, P.V., Bjornsson, S., Snaedal, J., Stefansson, K., 2015. Loss-of-function variants in ABCA7 confer risk of Alzheimer's disease. Nat Genet 47, 445–447. https://doi.org/10.1038/ng.3246

Stone, J., 2008. What initiates the formation of senile plaques? The origin of Alzheimer-like dementias in capillary haemorrhages. Med Hypotheses 71, 347–359. https://doi.org/10.1016/j.mehy.2008.04.007

Sung, H., Ferlay, J., Siegel, R.L., Laversanne, M., Soerjomataram, I., Jemal, A., Bray, F., 2021. Global Cancer Statistics 2020: GLOBOCAN Estimates of Incidence and Mortality Worldwide for 36 Cancers in 185 Countries. CA: A Cancer Journal for Clinicians 71, 209–249. https://doi.org/10.3322/caac.21660

Szylberg, M., Sokal, P., Śledzińska, P., Bebyn, M., Krajewski, S., Szylberg, Ł., Szylberg, A., Szylberg, T., Krystkiewicz, K., Birski, M., Harat, M., Włodarski, R., Furtak, J., 2022. MGMT Promoter Methylation as a Prognostic Factor in Primary Glioblastoma: A Single-Institution Observational Study. Biomedicines 10, 2030. https://doi.org/10.3390/biomedicines10082030

Tang, Y., Zhang, D., Robinson, S., Zheng, J., 2023. Inhibition of Pancreatic Cancer Cells by Different Amyloid Proteins Reveals an Inverse Relationship between Neurodegenerative Diseases and Cancer. Advanced Biology 7, 2300070. https://doi.org/10.1002/adbi.202300070

Tapia, M., Hernando, C., Martínez, M.T., Burgués, O., Tebar-Sánchez, C., Lameirinhas, A., Ágreda-Roca, A., Torres-Ruiz, S., Garrido-Cano, I., Lluch, A., Bermejo, B., Eroles, P., 2023. Clinical Impact of New Treatment

Strategies for HER2-Positive Metastatic Breast Cancer Patients with Resistance to Classical Anti-HER Therapies. Cancers (Basel) 15, 4522. https://doi.org/10.3390/cancers15184522

Terai, K., Jiang, M., Tokuyama, W., Murano, T., Takada, N., Fujimura, K., Ebinuma, H., Kishimoto, T., Hiruta, N., Schneider, W.J., Bujo, H., 2016. Levels of soluble LR11/SorLA are highly increased in the bile of patients with biliary tract and pancreatic cancers. Clin Chim Acta 457, 130–136. https://doi.org/10.1016/j.cca.2016.04.010

Thakkar, J.P., Dolecek, T.A., Horbinski, C., Ostrom, Q.T., Lightner, D.D., Barnholtz-Sloan, J.S., Villano, J.L., 2014. Epidemiologic and molecular prognostic review of glioblastoma. Cancer Epidemiol Biomarkers Prev 23, 1985–1996. https://doi.org/10.1158/1055-9965.EPI-14-0275

Tharp, W.G., Sarkar, I.N., 2013. Origins of amyloid-β. BMC Genomics 14, 290. https://doi.org/10.1186/1471-2164-14-290

Thorpe, J., Widman, L.P., Wallin, A., Beiswanger, J., Herman, T., 1994. Comorbidity of other chronic age-dependent diseases in dementia. Aging Clin Exp Res 6, 159–166. https://doi.org/10.1007/BF03324233

Tirumalasetti, F., Han, L., Birkett, D.P., 1991. The relationship between cancer and Alzheimer's disease. J Am Geriatr Soc 39, 840. https://doi.org/10.1111/j.1532-5415.1991.tb02713.x

Toms, S.A., Kim, C.Y., Nicholas, G., Ram, Z., 2019. Increased compliance with tumor treating fields therapy is prognostic for improved survival in the treatment of glioblastoma: a subgroup analysis of the EF-14 phase III trial. J Neurooncol 141, 467–473. https://doi.org/10.1007/s11060-018-03057-z

Troy, C.M., Rabacchi, S.A., Friedman, W.J., Frappier, T.F., Brown, K., Shelanski, M.L., 2000. Caspase-2 Mediates Neuronal Cell Death Induced by β-Amyloid. J Neurosci 20, 1386–1392. https://doi.org/10.1523/JNEUROSCI.20-04-01386.2000

Tsang, J.Y.S., Lee, M.A., Ni, Y., Chan, S., Cheung, S., Chan, W., Lau, K., Tse, G.M.K., 2018. Amyloid Precursor Protein Is Associated with Aggressive Behavior in Nonluminal Breast Cancers. Oncologist 23, 1273–1281. https://doi.org/10.1634/theoncologist.2018-0012

Tschuch, C., Schulz, A., Pscherer, A., Werft, W., Benner, A., Hotz-Wagenblatt, A., Barrionuevo, L.S., Lichter, P., Mertens, D., 2008. Off-target effects of siRNA

specific for GFP. BMC Molecular Biology 9, 60. https://doi.org/10.1186/1471-2199-9-60

van der Horst, G., van de Merbel, A.F., Ruigrok, E., van der Mark, M.H., Ploeg, E., Appelman, L., Tvingsholm, S., Jäätelä, M., van Uhm, J., Kruithof-de Julio, M., Thalmann, G.N., Pelger, R.C.M., Bangma, C.H., Boormans, J.L., van der Pluijm, G., Zwarthoff, E.C., 2020. Cationic amphiphilic drugs as potential anticancer therapy for bladder cancer. Mol Oncol 14, 3121–3134. https://doi.org/10.1002/1878-0261.12793

van Oijen, M., Hofman, A., Soares, H.D., Koudstaal, P.J., Breteler, M.M.B., 2006. Plasma Abeta(1-40) and Abeta(1-42) and the risk of dementia: a prospective case-cohort study. Lancet Neurol 5, 655–660. https://doi.org/10.1016/S1474-4422(06)70501-4

Vardarajan, B.N., Zhang, Y., Lee, J.H., Cheng, R., Bohm, C., Ghani, M., Reitz, C., Reyes-Dumeyer, D., Shen, Y., Rogaeva, E., St George-Hyslop, P., Mayeux, R., 2015. Coding mutations in SORL1 and Alzheimer's disease. Ann Neurol 77, 215–227. https://doi.org/10.1002/ana.24305

Verdoodt, F., Dehlendorff, C., Jäättelä, M., Strauss, R., Pottegård, A., Hallas, J., Friis, S., Kjaer, S.K., 2020. Antihistamines and Ovarian Cancer Survival: Nationwide Cohort Study and in Vitro Cell Viability Assay. J Natl Cancer Inst 112, 964–967. https://doi.org/10.1093/jnci/djz217

Vincent, B., Govitrapong, P., 2011. Activation of the α-secretase processing of AβPP as a therapeutic approach in Alzheimer's disease. J Alzheimers Dis 24 Suppl 2, 75–94. https://doi.org/10.3233/JAD-2011-110218

Wang, B., Liu, F., Li, Y., Chen, N., 2023. Role of Single Nucleotide Polymorphism-Related Genes in Tumour Immune Cell Infiltration and Prognosis of Cutaneous Melanoma. Biomed Res Int 2023, 3754094. https://doi.org/10.1155/2023/3754094

Wasco, W., Gurubhagavatula, S., Paradis, M.D., Romano, D.M., Sisodia, S.S., Hyman, B.T., Neve, R.L., Tanzi, R.E., 1993. Isolation and characterization of APLP2 encoding a homologue of the Alzheimer's associated amyloid beta protein precursor. Nat Genet 5, 95–100. https://doi.org/10.1038/ng0993-95

Wattmo, C., Minthon, L., Wallin, Å.K., 2016. Mild versus moderate stages of Alzheimer's disease: three-year outcomes in a routine clinical setting of

cholinesterase inhibitor therapy. Alzheimers Res Ther 8, 7. https://doi.org/10.1186/s13195-016-0174-1

Weaver, A.M., Hussaini, I.M., Mazar, A., Henkin, J., Gonias, S.L., 1997. Embryonic Fibroblasts That Are Genetically Deficient in Low Density Lipoprotein Receptor-related Protein Demonstrate Increased Activity of the Urokinase Receptor System and Accelerated Migration on Vitronectin *. Journal of Biological Chemistry 272, 14372–14379. https://doi.org/10.1074/jbc.272.22.14372

Williams, M.H., 2019. SorLA and Amyloid Beta Expression in Glioma (masters). University of Central Lancashire.

Willnow, T.E., Andersen, O.M., 2013. Sorting receptor SORLA--a trafficking path to avoid Alzheimer disease. J Cell Sci 126, 2751–2760. https://doi.org/10.1242/jcs.125393

Wirsching, H.-G., Galanis, E., Weller, M., 2016. Glioblastoma. Handb Clin Neurol 134, 381–397. https://doi.org/10.1016/B978-0-12-802997-8.00023-2

Wiseman, L.R., Faulds, D., 1996. Ebastine. a review of its pharmacological properties and clinical efficacy in the treatment of allergic disorders. Drugs 51, 260–277. https://doi.org/10.2165/00003495-199651020-00006

Woehrer, A., Bauchet, L., Barnholtz-Sloan, J.S., 2014. Glioblastoma survival: has it improved? Evidence from population-based studies. Curr Opin Neurol 27, 666–674. https://doi.org/10.1097/WCO.0000000000000144

Wolfrum, P., Fietz, A., Schnichels, S., Hurst, J., 2022. The function of p53 and its role in Alzheimer's and Parkinson's disease compared to age-related macular degeneration. Front. Neurosci. 16. https://doi.org/10.3389/fnins.2022.1029473

Wong, E., Cohen, T., Romi, E., Levin, M., Peleg, Y., Arad, U., Yaron, A., Milla, M.E., Sagi, I., 2016. Harnessing the natural inhibitory domain to control TNFα Converting Enzyme (TACE) activity in vivo. Sci Rep 6, 35598. https://doi.org/10.1038/srep35598

Xia, S., Chen, H., Tang, T., 2023. Risk of Death from Alzheimer's Disease Associated with Brain Tumor, Glioma, and Glioblastoma. J Alzheimers Dis 96, 623–631. https://doi.org/10.3233/JAD-230554

Xiromerisiou, G., Bourinaris, T., Houlden, H., Lewis, P.A., Senkevich, K., Hammer, M., Federoff, M., Khan, A., Spanaki, C., Hadjigeorgiou, G.M.,

Bonstanjopoulou, S., Fidani, L., Ermolaev, A., Gan-Or, Z., Singleton, A., Vandrovcova, J., Hardy, J., 2021. SORL1 mutation in a Greek family with Parkinson's disease and dementia. Ann Clin Transl Neurol 8, 1961–1969. https://doi.org/10.1002/acn3.51433

Xu, W., Jiang, X., Huang, L., 2019. RNA Interference Technology. Comprehensive Biotechnology 560–575. https://doi.org/10.1016/B978-0-444-64046-8.00282-2

Yang, J.-T., Lee, I.-N., Huang, C., Huang, H.-C., Wu, Y.-P., Chong, Z.-Y., Chen, J.-C., 2023. ADAM17 Confers Temozolomide Resistance in Human Glioblastoma Cells and miR-145 Regulates Its Expression. Int J Mol Sci 24, 7703. https://doi.org/10.3390/ijms24097703

Yin, R.-H., Yu, J.-T., Tan, L., 2014. The Role of SORL1 in Alzheimer's Disease. Mol Neurobiol 51, 909–918. https://doi.org/10.1007/s12035-014-8742-5

Youn, P., Chen, Y., Furgeson, D.Y., 2015. Cytoprotection against beta-amyloid (Aβ) peptide-mediated oxidative damage and autophagy by Keap1 RNAi in human glioma U87mg cells. Neurosci Res 94, 70–78. https://doi.org/10.1016/j.neures.2014.12.015

Yuan, G., Niu, L., Zhang, Y., Wang, X., Ma, K., Yin, H., Dai, J., Zhou, W., Pan, Y., 2017. Defining optimal cutoff value of MGMT promoter methylation by ROC analysis for clinical setting in glioblastoma patients. J Neurooncol 133, 193–201. https://doi.org/10.1007/s11060-017-2433-9

Zayas-Santiago, A., Díaz-García, A., Nuñez-Rodríguez, R., Inyushin, M., 2020. Accumulation of amyloid beta in human glioblastomas. Clin Exp Immunol 202, 325–334. https://doi.org/10.1111/cei.13493

Zayas-Santiago, A., Martínez-Montemayor, M.M., Colón-Vázquez, J., Ortiz-Soto, G., Cirino-Simonet, J.G., Inyushin, M., 2021. Accumulation of amyloid beta (Aβ) and amyloid precursor protein (APP) in tumors formed by a mouse xenograft model of inflammatory breast cancer. FEBS Open Bio 12, 95–105. https://doi.org/10.1002/2211-5463.13308

Zhai, B.-T., Tian, H., Sun, J., Zou, J.-B., Zhang, X.-F., Cheng, J.-X., Shi, Y.-J., Fan, Y., Guo, D.-Y., 2022. Urokinase-type plasminogen activator receptor (uPAR) as a therapeutic target in cancer. Journal of Translational Medicine 20, 135. https://doi.org/10.1186/s12967-022-03329-3

Zhang, H., Ma, Q., Zhang, Y.-W., Xu, H., 2012. Proteolytic processing of Alzheimer's β-amyloid precursor protein. J Neurochem 120 Suppl 1, 9–21. https://doi.org/10.1111/j.1471-4159.2011.07519.x

Zhao, H., Zhu, J., Cui, K., Xu, X., O'Brien, M., Wong, K.K., Kesari, S., Xia, W., Wong, S.T.C., 2009. Bioluminescence imaging reveals inhibition of tumor cell proliferation by Alzheimer's amyloid beta protein. Cancer Cell Int 9, 15. https://doi.org/10.1186/1475-2867-9-15

Zheng, H., Koo, E.H., 2011. Biology and pathophysiology of the amyloid precursor protein. Mol Neurodegener 6, 27. https://doi.org/10.1186/1750-1326-6-27

Zheng, X., Jiang, F., Katakowski, M., Kalkanis, S.N., Hong, X., Zhang, X., Zhang, Z.G., Yang, H., Chopp, M., 2007. Inhibition of ADAM17 reduces hypoxia-induced brain tumor cell invasiveness. Cancer Science 98, 674–684. https://doi.org/10.1111/j.1349-7006.2007.00440.x

Zhou, X.-F., Wang, Y.-J., 2011. The p75NTR extracellular domain: a potential molecule regulating the solubility and removal of amyloid-β. Prion 5, 161–163. https://doi.org/10.4161/pri.5.3.16896

Zhu, Y., Bujo, H., Yamazaki, H., Hirayama, S., Kanaki, T., Takahashi, K., Shibasaki, M., Schneider, W.J., Saito, Y., 2002. Enhanced Expression of the LDL Receptor Family Member LR11 Increases Migration of Smooth Muscle Cells In Vitro. Circulation 105, 1830–1836. https://doi.org/10.1161/01.CIR.0000014413.91312.EF

Zhu, Y., Bujo, H., Yamazaki, H., Ohwaki, K., Jiang, M., Hirayama, S., Kanaki, T., Shibasaki, M., Takahashi, K., Schneider, W.J., Saito, Y., 2004. LR11, an LDL Receptor Gene Family Member, Is a Novel Regulator of Smooth Muscle Cell Migration. Circulation Research 94, 752–758. https://doi.org/10.1161/01.RES.0000120862.79154.0F

Zuccato, C., Marullo, M., Conforti, P., MacDonald, M.E., Tartari, M., Cattaneo, E., 2008. RESEARCH ARTICLE: Systematic Assessment of BDNF and Its Receptor Levels in Human Cortices Affected by Huntington's Disease. Brain Pathol 18, 225–238. https://doi.org/10.1111/j.1750-3639.2007.00111.x